

T-3343

USE OF THE HOLLOW ELECTRODE IN GTA
WELDING AND ITS EFFECTS ON BEAD
MORPHOLOGY IN STAINLESS STEEL
WELDMENTS

by

KENNETH PATRICK MARTS

ARTHUR LAMPS LIBRARY
COLORADO SCHOOL of MINES
GOLDEN, COLORADO 80401

ProQuest Number: 10782890

All rights reserved

INFORMATION TO ALL USERS

The quality of this reproduction is dependent upon the quality of the copy submitted.

In the unlikely event that the author did not send a complete manuscript and there are missing pages, these will be noted. Also, if material had to be removed, a note will indicate the deletion.



ProQuest 10782890

Published by ProQuest LLC (2018). Copyright of the Dissertation is held by the Author.

All rights reserved.

This work is protected against unauthorized copying under Title 17, United States Code
Microform Edition © ProQuest LLC.

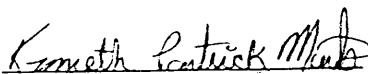
ProQuest LLC.
789 East Eisenhower Parkway
P.O. Box 1346
Ann Arbor, MI 48106 – 1346

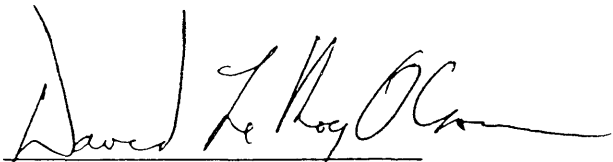
T-3343

A thesis submitted to the Faculty and the Board
of Trustees of the Colorado School of Mines in partial
fulfillment of the requirements for the degree of Master
of Science (Metallurgical Engineering).

Golden, Colorado

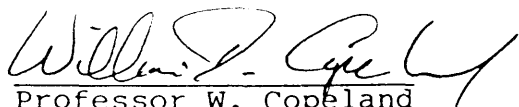
Date: 29 December 1986

Signed: 
Kenneth P. Marts

Approved: 
Professor D. L. Olson,
Thesis Advisor

Golden, Colorado

Date: January 9, 1987


Professor W. Copeland
Head, Department of
Metallurgical Engineering

ABSTRACT

Welding by the Gas Tungsten Arc Welding (GTAW) process is normally limited to about 300 Amperes. At higher currents, the welding arc has been found to be unstable due to excessive arc pressure. It has been reported that GTAW hollow electrode improves bead morphology and arc voltage stability at currents as high as 700 to 800 Amperes.

This work characterizes the effect on bead morphology and arc stability while utilizing a hollow two-percent thoriated tungsten electrode in GTAW. Bead-on-plate welds on 17-4PH stainless steel were analyzed. Shaped (150 and 90 degree blunt tip and 150 and 90 degree hollow tip) and unshaped (180 degree tip) electrodes were used in argon, 75ArHe, and 25ArHe shield gas atmospheres. Current was varied between 100 and 500 Amperes DC while maintaining a constant travel speed of 10 ipm (4.2 mm/sec).

In addition, welding under constant heat input conditions was also performed in the three shield gases. Unshaped (180 degree) hollow electrodes were used in DC from 150 to 300 Amperes and in AC from 100 to 230 Amperes. Finally, for comparison purposes, solid electrodes were utilized under conditions similar to those for hollow electrodes to get a direct comparison between data parameters for each welding

condition. The electrodes used in this study were 5/32 inch (4 mm) diameter with 3/32 inch (2.3 mm) holes to make the hollow electrode or 3/32 inch (2.3 mm) blunt end diameters for the shaped solid electrodes.

Arc potential stability, as measured with a high-speed strip chart recorder was, in general, not found to be better with hollow electrodes (both shaped and unshaped) than with solid electrodes in DC (no measurements were made in AC). This was found to be true for all welding currents (high and low). Shield gas was found to have a minor effect on arc stability. Arc potential stability improved with decreased helium content in the shield gas (going from 25ArHe to 75ArHe) for solid electrode GTAW.

DC hollow electrodes produced improvements in bead morphology at higher currents (above 400 Amperes). Penetration, melt efficiency, and p/w (penetration depth divided by bead width) were all improved; again, under limited conditions. The penetration and melt area behavior as a function of welding current showed evidence of the transition from the fluid flow dominated region to the arc dominant parameter control region as suggested by the literature. This improvement was more pronounced when using a higher helium content shield gas and when shaped electrodes were used.

Transitional behavior was seen under both conditions above held true for both conditions of constant heat input and constant travel speed. AC GTAW hollow electrode showed the opposite phenomenon at all currents investigated (i.e. bead morphology and melt efficiency were better with solid electrode GTAW).

Little difference was seen in the operating arc voltage between hollow and solid electrodes although the arc stability varied as previously mentioned.

Correlations of bead morphology measurements with existing bead morphology prediction equations was moderately successful and was possible only at currents above 300 Amperes in the present study. This high current region corresponds with the parameter control zone region seen in previous experiments. Measured penetration was found to match the prediction equations well. The prediction equations were not found accurate for melt area. The results in this investigation are compared with the results and models of GTAW behavior from literature.

TABLE OF CONTENTS

ABSTRACT	- - - - -	iii
TABLE OF CONTENTS	- - - - -	vi
LIST OF FIGURES	- - - - -	ix
LIST OF TABLES	- - - - -	xvii
ACKNOWLEDGMENTS	- - - - -	xviii
INTRODUCTION	- - - - -	1
CHAPTER		
I HISTORY	- - - - -	32
A. Stainless Steel Welding	- - - - -	32
B. Variation In Electrode Shape	- - - - -	32
C. Penetration	- - - - -	34
1. Studies	- - - - -	34
2. Equations To Predict	- - - - -	40
D. Effect of GTAW Parameters On Weld Bead Morphology	-	43
1. Fusion Zone Width	- - - - -	44
2. Bead Melt Area	- - - - -	44
3. Equations To Predict	- - - - -	44
E. Use of Hollow Electrodes/Cathodes	- - - - -	45
F. Shield Gases	- - - - -	47
G. Arc Stability/Appearance	- - - - -	48
II EXPERIMENTAL PROCEDURE	- - - - -	51
A. Material Selection	- - - - -	51
B. Equipment and Set-Up	- - - - -	51

C. Arc Characterization	- - - - -	54
D. Weld Procedure	- - - - -	54
E. Metallographic Procedure	- - - - -	57
F. Test Matrix	- - - - -	62
G. Weld Cross-Section Measurements	- - - - -	65
H. Arc Characterization	- - - - -	65
III. RESULTS	- - - - -	66
A. Constant Heat Input	- - - - -	66
1. DC Constant Heat Input	- - - - -	66
a. arc characteristic curves	- - - - -	67
b. penetration	- - - - -	70
c. p/w	- - - - -	72
d. melt area	- - - - -	72
2. AC Constant Heat Input	- - - - -	75
a. arc characteristic curves	- - - - -	75
b. penetration	- - - - -	75
c. p/w	- - - - -	78
d. melt area	- - - - -	78
B. Constant Travel Speed	- - - - -	81
1. Unshaped electrodes	- - - - -	81
a. arc characteristic curves	- - - - -	81
b. penetration	- - - - -	85
c. p/w	- - - - -	85
d. melt area	- - - - -	85
2. Shaped electrodes 150 degree	- - - - -	88
a. arc characteristic curves	- - - - -	88
b. penetration	- - - - -	91
c. p/w	- - - - -	93
d. melt area	- - - - -	93
3. Shaped electrodes 90 degree	- - - - -	93
a. arc characteristic curves	- - - - -	93
b. penetration	- - - - -	97
c. p/w	- - - - -	97
d. melt area	- - - - -	100

IV DISCUSSION	- - - - -	102
A. Shield Gas Effects	- - - - -	103
B. Electrode Shape Effects	- - - - -	104
C. Current Effects	- - - - -	105
D. Arc Stability	- - - - -	106
E. General Discussion	- - - - -	107
F. Prediction Equations	- - - - -	107
1. Penetration	- - - - -	126
V FUTURE WORK IMPLICATIONS	- - - - -	129
VI CONCLUSIONS	- - - - -	131
REFERENCES	- - - - -	132
APPENDIX	- - - - -	137
I Constant Heat Input (DC and AC)	- - - - -	137
a. raw data		
b. graphs		
II Constant Travel Speed Unshaped and Shaped Electrodes (150 and 90 Degree Tip)	- - - - -	164
a. raw data		
b. graphs		
III Melt Area Prediction Model	- - - - -	198
IV Arc Stability Data for Constant Travel Speed Weldments	- - - - -	206

LIST OF FIGURES

<u>FIGURE</u>	<u>DESCRIPTION</u>	<u>PAGE</u>
1	Illustration of GTAW Process	2
2	Characteristic GTAW Arc Potential-Current Curve	5
3	Typical Weld Pool Flows For High and Low Arc Pressure Welds (deep and shallow penetration)	8
4	GTAW Arc Regions	9
5	Typical Modes of GTAW Operation	13
6	Typical GTAW Arc Length Arc Potential plot	19
7	Effect of Shield Gas On Arc Potential-Current Characteristic Curves	20
8	Arc Pressure Distribution Curves	25
9	Proposed Regimes In Current versus Bead Morphology Plot	36
10	Proposed Model For Two Regimes In Current versus Bead Morphology Plots	37
11	Plot of Arc Stability	49
12	Electrode Configurations Used	53
13	Sample Weld Bead Orientation	61
14	Typical Weld Profiles for DC Constant Heat Input Welds	67
15	Typical Weld Profiles for AC Constant Heat Input Welds	68
16	Arc Potential-Current Characteristic Curves for DC Constant Heat Input Welds	69
17	Current Versus Penetration For DC Constant Heat Input Welds	71

18	Current versus p/w For DC Constant Heat Input welds	73
19	Current versus Melt Area For DC Constant Heat Input Welds	74
20	Arc Potential-Current Characteristic Curves for AC Constant Heat Input Welds	76
21	Current Versus Penetration For AC Constant Heat Input Welds	77
22	Current versus p/w For AC Constant Heat Input Welds	79
23	Current versus Melt Area For AC Constant Heat Input Welds	80
24	Typical Weld Profiles for DC Constant Travel Speed Welds	82
25	Arc Potential-Current Characteristic Curves for Constant Travel Speed Welds Unshaped Electrode	84
26	Current Versus Penetration For Constant Travel Speed Welds Unshaped Electrode	86
27	Current versus p/w For Constant Travel Speed Welds Unshaped Electrode	87
28	Current versus Melt Area For Constant Travel Speed Welds Unshaped Electrode	89
29	Arc Potential-Current Characteristic Curves for Constant Travel Speed Welds 150 Degree Tip Angle	90
30	Current Versus Penetration For Constant Travel Speed Welds 150 Degree Tip Angle	92
31	Current versus p/w For Constant Travel Speed Welds 150 Degree Tip Angle	94

32	Current versus Melt Area For Constant Travel Speed Welds 150 Degree Tip Angle	95
33	Arc Potential-Current Characteristic Curves for Constant Travel Speed Welds 90 Degree Tip Angle	96
34	Current Versus Penetration For Constant Travel Speed Welds 90 Degree Tip Angle	98
35	Current versus p/w For Constant Travel Speed Welds 90 Degree Tip Angle	99
36	Current versus Melt Area For Constant Travel Speed Welds 90 Degree Tip Angle	101
37	Results of Two Penetration Models Used In Predicting Weld Penetration	109
38	Measured versus Predicted Penetration For Constant Travel Speed Welds Unshaped Electrode In 75ArHe	111
39	Measured versus Predicted Penetration For Constant Travel Speed Welds Unshaped Electrode In 25ArHe	113
40	Measured versus Predicted Penetration For Constant Travel Speed Welds 150 Degree Electrode Tip In 75ArHe	115
41	Measured versus Predicted Penetration For Constant Travel Speed Welds 150 Degree Electrode Tip In 25ArHe	117
42	Measured versus Predicted Penetration For Constant Travel Speed Welds 90 Degree Electrode Tip In Argon	120
43	Measured versus Predicted Penetration For Constant Travel Speed Welds 90 Degree Electrode Tip In 75ArHe	122
44	Measured versus Predicted Penetration For Constant Travel Speed Welds 90 Degree Electrode Tip In 25ArHe	124

45	Effect of Shield Gas and Electrode Shape On "k" In Jackson Penetration Prediction Equation	127
----	--	-----

APPENDIX

Al-1	Arc Potential-Current Characteristic Curve for DC Constant Heat Input Welds In Argon	140
Al-2	Arc Potential-Current Characteristic Curve for DC Constant Heat Input Welds In 75ArHe	141
Al-3	Arc Potential-Current Characteristic Curve for DC Constant Heat Input Welds In 25ArHe	142
Al-4	Current Versus Penetration For DC Constant Heat Input Welds In Argon	143
Al-5	Current Versus Penetration For DC Constant Heat Input Welds In 75ArHe	144
Al-6	Current Versus Penetration For DC Constant Heat Input Welds In 25ArHe	145
Al-7	Current versus p/w For DC Constant Heat Input Welds In Argon	146
Al-8	Current versus p/w For DC Constant Heat Input Welds In 75ArHe	147
Al-9	Current versus p/w For DC Constant Heat Input Welds In 25ArHe	148
Al-10	Current versus Melt Area For DC Constant Heat Input Welds In Argon	149
Al-11	Current versus Melt Area For DC Constant Heat Input Welds In 75ArHe	150
Al-12	Current versus Melt Area For DC Constant Heat Input Welds In 25ArHe	151

Al-13	Arc Potential-Current Characteristic Curves for AC Constant Heat Input Welds In Argon	152
Al-14	Arc Potential-Current Characteristic Curves for AC Constant Heat Input Welds In 75ArHe	153
Al-15	Arc Potential-Current Characteristic Curves for AC Constant Heat Input Welds In 25ArHe	154
Al-16	Current Versus Penetration For AC Constant Heat Input Welds In Argon	155
Al-17	Current Versus Penetration For AC Constant Heat Input Welds In 75ArHe	156
Al-18	Current Versus Penetration For AC Constant Heat Input Welds In 25ArHe	157
Al-19	Current versus p/w For AC Constant Heat Input Welds In Argon	158
Al-20	Current versus p/w For AC Constant Heat Input Welds In 75ArHe	159
Al-21	Current versus p/w For AC Constant Heat Input Welds In 25ArHe	160
Al-22	Current versus Melt Area For AC Constant Heat Input Welds In Argon	161
Al-23	Current versus Melt Area For AC Constant Heat Input Welds In 75ArHe	162
Al-24	Current versus Melt Area For AC Constant Heat Input Welds In 25ArHe	163
A2-1	Arc Potential-Current Characteristic Curves for Constant Travel Speed Welds Unshaped Electrode In 75ArHe	169
A2-2	Arc Potential-Current Characteristic Curves for Constant Travel Speed Welds Unshaped Electrode In 25ArHe	170

A2-3	Current Versus Penetration For Constant Travel Speed Welds Unshaped Electrode In 75ArHe	171
A2-4	Current Versus Penetration For Constant Travel Speed Welds Unshaped Electrode In 25ArHe	172
A2-5	Current versus p/w For Constant Travel Speed Welds Unshaped Elec- trode In 75ArHe	173
A2-6	Current versus p/w For Constant Travel Speed Welds Unshaped Elec- trode In 25ArHe	174
A2-7	Current versus Melt Area For Constant Travel Speed Welds Unshaped Electrode In 75ArHe	175
A2-8	Current versus Melt Area For Constant Travel Speed Welds Unshaped Electrode In 25ArHe	176
A2-9	Arc Potential-Current Characteristic Curves for Constant Travel Speed Welds 150 Degree Tip Angle In 75ArHe	177
A2-10	Arc Potential-Current Characteristic Curves for Constant Travel Speed Welds 150 Degree Tip Angle In 25ArHe	178
A2-11	Current Versus Penetration For Constant Travel Speed Welds 150 Degree Tip Angle In 75ArHe	179
A2-12	Current Versus Penetration For Constant Travel Speed Welds 150 Degree Tip Angle In 25ArHe	180
A2-13	Current versus p/w For Constant Travel Speed Welds 150 Degree Tip Angle In 75ArHe	181
A2-14	Current versus p/w For Constant Travel Speed Welds 150 Degree Tip Angle In 25ArHe	182

A2-15	Current versus Melt Area For Constant Travel Speed Welds 150 Degree Tip Angle In 75ArHe	183
A2-16	Current versus Melt Area For Constant Travel Speed Welds 150 Degree Tip Angle In 25ArHe	184
A2-17	Arc Potential-Current Characteristic Curves for Constant Travel Speed Welds 90 Degree Tip Angle In Argon	185
A2-18	Arc Potential-Current Characteristic Curves for Constant Travel Speed Welds 90 Degree Tip Angle In 75ArHe	186
A2-19	Arc Potential-Current Characteristic Curves for Constant Travel Speed Welds 90 Degree Tip Angle In 25ArHe	187
A2-20	Current Versus Penetration For Constant Travel Speed Welds 90 Degree Tip Angle In Argon	188
A2-21	Current Versus Penetration For Constant Travel Speed Welds 90 Degree Tip Angle In 75ArHe	189
A2-22	Current Versus Penetration For Constant Travel Speed Welds 90 Degree Tip Angle In 25ArHe	190
A2-23	Current versus p/w For Constant Travel Speed Welds 90 Degree Tip Angle In Argon	191
A2-24	Current versus p/w For Constant Travel Speed Welds 90 Degree Tip Angle In 75ArHe	192
A2-25	Current versus p/w For Constant Travel Speed Welds 90 Degree Tip Angle In 25ArHe	193
A2-26	Current versus Melt Area For Constant Travel Speed Welds 90 Degree Tip Angle In Argon	194

A2-27	Current versus Melt Area For Constant Travel Speed Welds 90 Degree Tip Angle In 75ArHe	195
A2-28	Current versus Melt Area For Constant Travel Speed Welds 90 Degree Tip Angle In 25ArHe	196
A2-29	Effect of Shield Gas and Electrode Shape On "k" In Jackson and Shrubbsall Penetration Prediction Equation	197
A3-1	Measured versus Predicted Melt Area For Constant Travel Speed Welds Unshaped Electrode In 75ArHe	199
A3-2	Measured versus Predicted Melt Area For Constant Travel Speed Welds Unshaped Electrode In 25ArHe	200
A3-3	Measured versus Predicted Melt Area For Constant Travel Speed Welds 150 Degree Electrode Tip In 75ArHe	201
A3-4	Measured versus Predicted Melt Area For Constant Travel Speed Welds 150 Degree Electrode Tip In 25ArHe	202
A3-5	Measured versus Predicted Melt Area For Constant Travel Speed Welds 90 Degree Electrode Tip In Argon	203
A3-6	Measured versus Predicted Melt Area For Constant Travel Speed Welds 90 Degree Electrode Tip In 75ArHe	204
A3-7	Measured versus Predicted Melt Area For Constant Travel Speed Welds 90 Degree Electrode Tip In 25ArHe	205

LIST OF TABLES

<u>TABLE</u>	<u>DESCRIPTION</u>	<u>PAGE</u>
1	Prediction Equations Used To Match Data	41
2	Chemical Analysis of Raw Material	49
3	Constant Heat Input Weld Parameters Used In This Study	55
4	Constant Travel Speed Weld Parameters Used In This Study	58

APPENDIX

AI-1	Arc Characteristic and Bead Morphology Data For Constant Heat Input Welds	139
AII-1	Arc Characteristic and Bead Morphology Data For Constant Travel Speed Welds	164
AIV-1	Arc Stability Measurements	206

ACKNOWLEDGMENTS

To my wife Cheryl for her support and motivation during all those dismal late nights of testing and writing of what is now this thesis. A feat to be extremely proud of.

The help, consultation, and prodding of Dr. Dave Olson is also greatly appreciated in his role as my advisor.

Thanks also to Mr. Ron Blake for help in welding and Mr. Richard Herzog for his motivation and help when the going got tough!

I would also like to express appreciation for the numerous consultations with Dr. Paul Burgardt.

The Custom 630 raw material for this study was supplied by Carpenter Technology Corporation.

The author would like to acknowledge the support of the United States Army Research Center and Martin Marietta Denver Aerospace.

INTRODUCTION

Gas Tungsten Arc Welding

Gas Tungsten Arc Welding (GTAW), also known as tungsten inert gas (TIG) welding is an electric arc welding process which fuses materials together by heating them with an arc between a non-consumable tungsten electrode and the material itself. Filler material may or may not be used. Shielding of the weld is obtained from either a pure inert gas (argon or helium) or a mixture of inert gases (argon-helium mixes are typically used). GTAW can be either a manual or automatic welding process that may be used on both ferrous and nonferrous metals. Figure 1 illustrates, and a later section describes the details of this process.

The advantages of GTAW over other welding techniques includes the ability to make high quality welds in almost all metals and alloys. GTAW is typically used in the welding of stainless steels, aluminum, titanium, and some of the more exotic metals used in the nuclear and defense industries. Welding may also be performed in all positions. Other advantages include the fact that both the weld pool and arc are visible to the welder, post-weld cleanup is minimized since no surface slag is produced and typically no filler metal is carried across the arc which could lead to weld splatter (it is possible to use filler metal with the GTAW process).

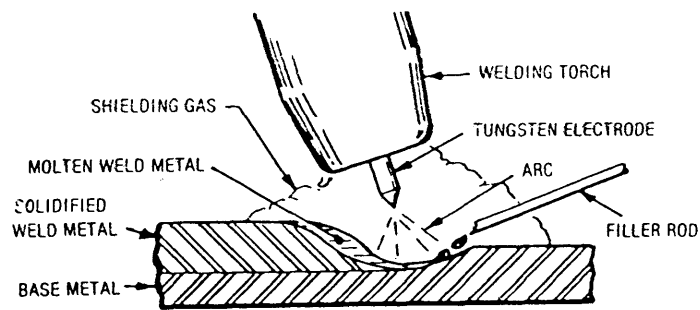


FIGURE 1 Illustration of Gas Tungsten Arc Weld Process Showing Parent Material, Electrode, and Shield Gas. Filler Wire May Be Added When Required (1)

The major disadvantage to GTAW is its low productivity. The deposition rate of GTAW is much lower than that for other processes. Its initial cost can also be a disadvantage. The power source and torch are more expensive than those used in gas metal arc welding. Welding must be controlled under a generous flow of shield gas to prevent oxidation of the weld and welders require significantly more training than those in other gas arc welding processes. Another disadvantage that can be avoided if precautions are taken during welding are tungsten inclusions from the electrode breaking off during welding. One last disadvantage is electrode tip contamination. This may occur when high currents, lengthy welds, and/or large mismatch weld conditions are used or exist. It may also occur (as is obvious) if small electrode working gaps are used where the electrode may actually dip into and physically contact the molten weld pool.

Constant current power supplies are commonly used for gas tungsten arc welding. They are generally characterized by a drooping Volt-Ampere curve. Its advantage lies in the fact that small variations in voltage do not adversely affect the current output and subsequently the deposition rate (for wire feed applications). These voltage fluctuations arise from small changes in the arc length or arc gap.

With this in mind, it is obvious that the steeper the current-potential characteristic curve, the more stable the arc is (ref figure 2). This is because fluctuations in arc voltage will lead to very small changes in the welding current. The electrode is typically negative in the Direct Current Straight Polarity (DCSP) GTAW process. This polarity allows 70 percent of the heat to be generated at the workpiece (2) and lets the energy be expended in melting the workpiece. This also allows the tungsten electrode to carry the maximum current. It is extremely important to utilize the correct shielding gas atmosphere as this can determine the welding penetration, efficiency of operation, and arc stability.

Alternating current (AC) may also be used in GTAW. This is especially true when welding aluminum where the tenacious aluminum oxide is continually removed by the alternating current pulses.

Pulsed DCSP has recently been used with favorable results (3). A high rate of current rise and decay and a high or low pulse repetition rate are achieved with pulsed arcs. The advantages of pulsations are as follows:

1. Increased depth-to-width ratios for weld beads. A short duration, high current weld pulse (as well as the use of a small blunt thoriated tungsten electrode) has produced depth-to-width ratios approaching 2:1 in

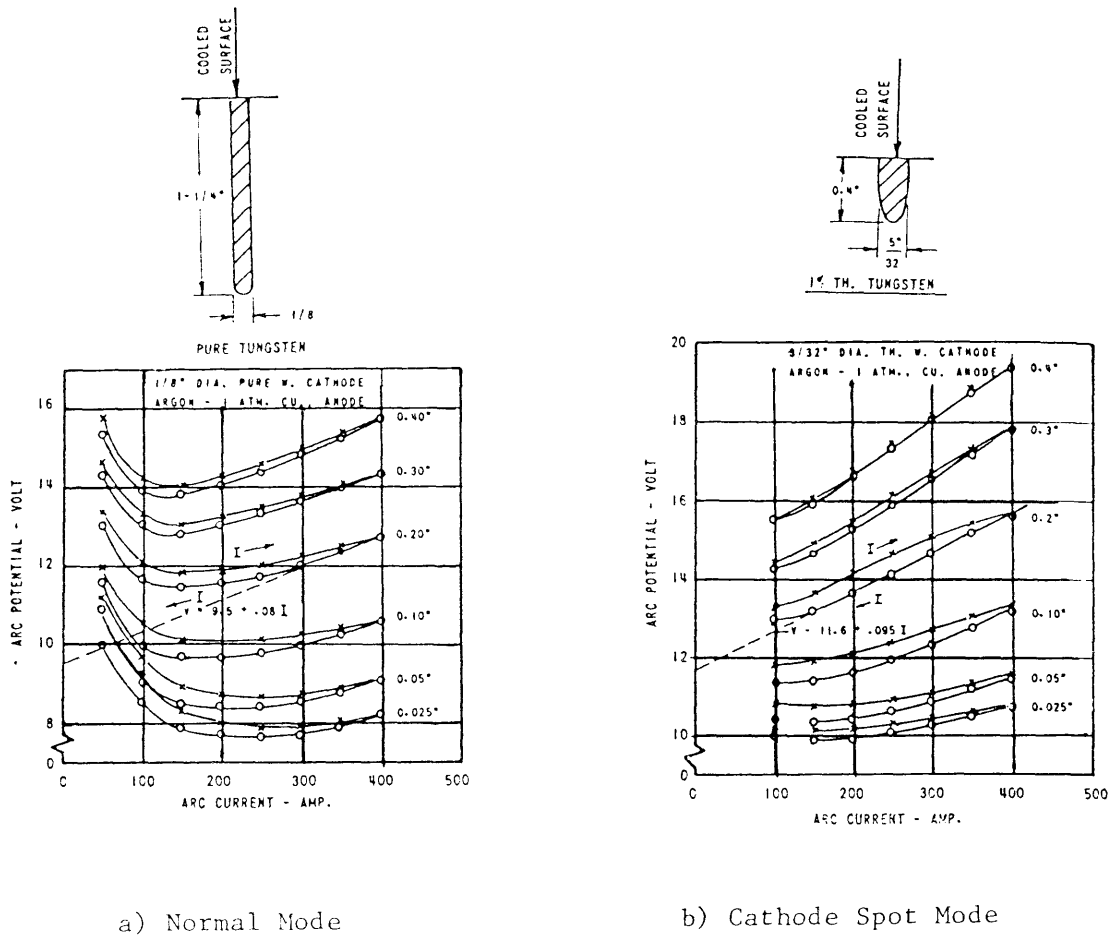


Figure 2 Typical Arc Potential-Current Characteristic Curve For Different Electrode Gaps a) Normal mode and b) Cathode Spot Mode. (2)

stainless steel. This arises because of an increase in the arc force. Increased arc force can lead to deeper penetration due to the flow of the molten weld pool as shown in figure 3. This is discussed in farther detail in a later section due to conflicting theories which say penetration decreases when arc pressure is too high.

2. Drop-through can be eliminated. The use of high current, short duration pulses melt through the root pass and solidify before the weld pool sags.
3. Minimal heat-affect zone. By proper proportioning of the pulse height and on-time, the extent of the heat-affected zone is minimized.
4. Stirring of the weld pool. Arc and electromagnetic forces are developed by the high current of the pulse. These forces which are greater than those developed by constant current, agitate the weld pool, resulting in a reduction of weld porosity and lack of fusion at the bottom of the weld pool (reference figure 3).

B. Arc Physics

Jackson (2) has described the GTAW process as "an electrical conduction in the arc occurs through a gaseous column (inert gas) possessing a high electrical conductivity to provide an electrical circuit between the positive anode (workpiece) and the negative tungsten electrode. This gaseous column; also, known as the arc plasma; radiates a mixture of free electrons, positive ions, and excited neutral atoms. The plasma conductivity is maintained by thermal ionization meaning the plasma temperature is extremely high. Some temperature measurements (4) indicate it to be as high

as 10,000 to 20,000°F (5540 to 11090°C).

The nature of the plasma sets up a thermal gradient between the two regions of electrical contact. These two regions are the plasma/anode interface and the plasma/electrode interface. Because of this, there are three regions representing the arc: 1) the cathode region, 2) the anode region, and 3) the plasma region. These areas in a typical gas tungsten arc can be seen in figure 4. A "space charge" is also associated with the plasma region where high electric field strengths exist. These in turn produce magnetic fields which act to compress the "plasma."

Goldman (5) farther states that the nature of the plasma is dependent on the electrode material, arc atmosphere, arc gap, arc mode, and the efficiency of electrode cooling. He also found that small current increases at low current caused a sharp drop in potential. It is estimated (6,7) that approximately 70 percent of the energy generated by the arc reaches the anode and contributes to forming the weld bead. Heat energy is dissipated at the anode in the following manner (8):

- 1) Normal heat conduction- heat supplied to the work piece and used to heat the material directly under the arc as well as the heat dissipated through the material away from the arc. This is also the heat used to melt the parent material and has one of the greatest

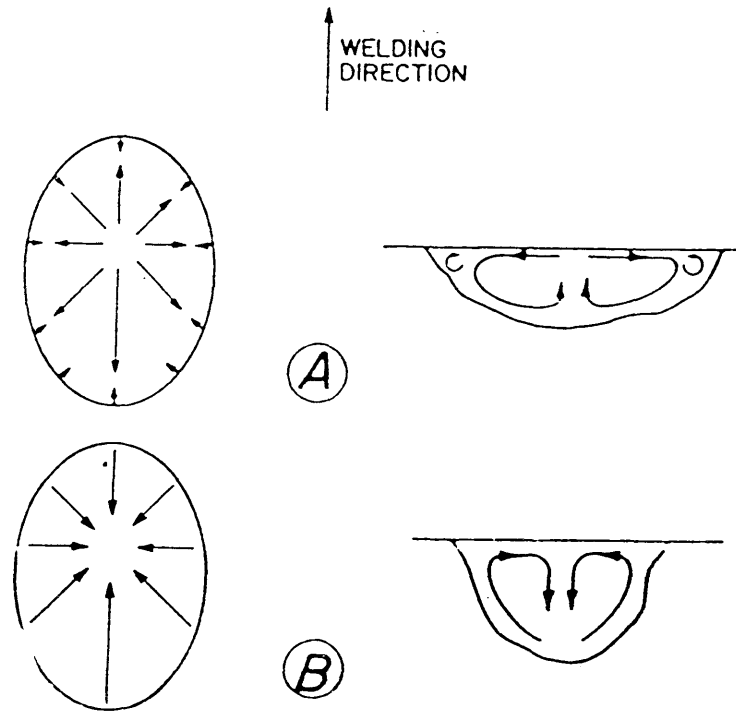


FIGURE 3 Typical Weld Pool Fluid Flow With a) Negative Surface Tension Temperature Coefficient or low arc pressure and b) Positive Surface Tension Temperature Coefficient or low arc pressure (9)

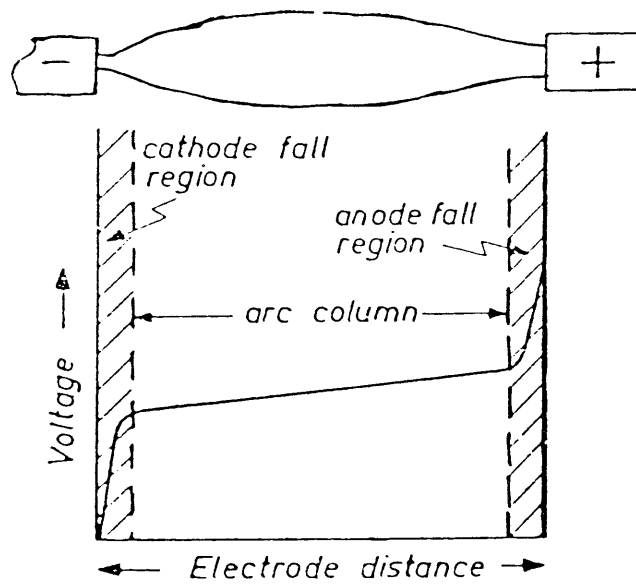


FIGURE 4 Schematic Representation of the Three Regions Seen In the Gas Tungsten Arc (5)

affects on weld bead penetration.

- 2) Vaporization of the boiling anode- heat supplied to the workpiece causing vaporization of the parent material and may lead to electrode buildup (due to condensation of the vaporized material on the electrode surface) or weld splatter. This is a reasonably small contributor to the heat loss except at currents near the upper extremes of the electrodes capability where electron cooling occurs.
- 3) radiation- of heat to the outside environment as well as to the shield gas.
- 4) anode melting- this occurs under the arc and is utilized to fuse the two materials together at the joint interface which upon solidification becomes the weld bead.
- 5) convection, and
- 6) anode ion emission.

As stated previously, the arc is considered to be composed of three distinct areas. The first area is the cathode region (reference figure 4) or the tungsten electrode. This region is very small, extending outward approximately 10^{-5} mm out from the cathode (8). The cathode supplies electrons; removed from the electrode by thermionic emission to the arc plasma. The ease by which thermionic emission occurs is determined by the work function of the electrode. The work function may be lowered (thus allowing more electrons to be transferred) by adding thoria or zirconia to the electrode. Typically one or two percent of these materials is added to the electrode surface.

The cathode spot refers to the area on the cathode where electrons are emitted and transferred to the plasma. This may sometimes represent a restricted condition of the arc when a cathode spot mode is encountered. When the operating conditions of the arc are more diffuse, the normal mode is seen. Both normal and cathode spot mode arcs are discussed in detail in a later section. The thermal characteristics of the arc plasma plumes exert a substantial influence on the penetrating power of the arc (7).

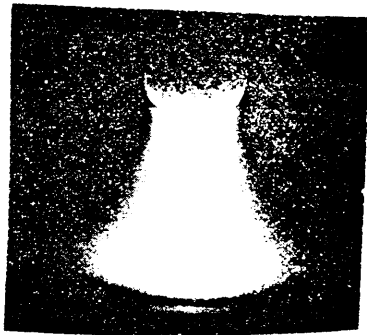
The cathode spot is defined as the spot on the tungsten electrode at which electron emission (field or thermionic) is generated. As the current increases, the cathode spot has a tendency to climb the electrode (for shaped electrodes) to an area of larger diameter which will support the current density and maintain a stable arc. The reason for this movement of the cathode spot is related to a phenomena known as electrode cooling. Thermionic emission allows the electrons to escape the electrode. As current increases, so does the emission of electrons. Heat is lost in the electrode with each electron lost and the more electrons which are lost due to emission, the more heat that will be lost from the electrode surface. This forces the cathode spot up the electrode to an area with a higher temperature where electron emission

will occur more efficiently.

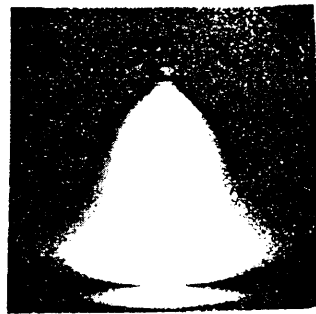
The normal spot mode is the most stable and easily obtained welding arc. This mode of operation is characterized by a broad luminous plasma extending around the cathode tip. This is the typical mode of operation when using a blunt tipped pure tungsten electrode in a pure argon atmosphere.

Typically, the normal mode arc is more prevalent than the cathode spot arc at currents up to about 200 Amperes when using a large vertex angle electrode. This can be as low as 150 Amperes if a small vertex angle (sharp point) electrode is used.

Operation in the cathode spot mode represents a constriction of the arc plasma at the cathode and exhibits a higher potential for a given arc length than the normal spot mode. It is characterized by a dark circular spot on the cathode tip which is coaxial with a deep-blue cone of radiation extending into the plasma, with its apex toward the anode (reference figure 5). This mode of operation is typically obtained when using a sharp tipped pure tungsten electrode in an argon atmosphere (may or may not be pure) at relatively high welding currents. It may also be seen at high currents using any shaped electrode or at relatively low currents when using sharp pointed electrodes.



a) Normal Mode



b) Cathode Spot Mode

FIGURE 5 Typical Electric Arc Operating Modes and Their Respective Arc Appearance. Refer to Figure 2 for the Arc Potential-Current Characteristic Curve for Each.
(2)

Goldman (5) in his studies of electric arcs in argon found three other arc mode types which are derivatives of the normal and cathode spot modes. These three additional types are as follows: 1) Unspotted bell shaped arc which is the cathode spot mode arc without the dark spot, 2) a coneless bell-shaped arc which is the cathode spot mode without the characteristic blue cone or dark spot, and 3) a normal mode arc characterized by an axe-shaped envelope with no spot. This last mode is found between the transition from the unspotted bell-shaped arc to the normal mode. Goldman found the above characteristics present at overlapping conditions of current and voltage.

The second area is the plasma region in which the electrons emitted from the cathode are ionized in the shield gas to supply the necessary energy to melt the base metal. Plasma jets emanating from both the cathode and anode also convey energy to the workpiece and are considered a part of the arc plasma. The cathode jet is typically the most dominant force of the two.

It has been reported (10) that both the temperature and electrical conductivity of the plasma near the anode surface increases with increasing current. This has been verified in tests where both temperature and electrical

conductivity at and near the vicinity of the arc were measured (10).

A very rapid temperature reduction (11) in this area results in poor thermal ionization and insufficient ion generation to maintain the ion flow or plasma stream. If the plasma temperature near the anode is low, ion generation will be dominant and accomplished by field ionization rather than thermal ionization. A high anode fall voltage will also be characteristic of this condition. As the anode temperature increases, the amount of thermal ionization generated ions will also increase. Those generated by field emission will conversely decrease as will the anode fall voltage.

The third area is the anode region (the workpiece). Energy transported through the arc plasma from the cathode melts the workpiece material and allows the weld to be accomplished. Like the cathode, the anode also has a "spot". Though not always visible, electrons (energy) enter the workpiece at the anode spot. This phenomena has been seen by Dinulescu (12), Jones (13), Kouwenhaven (14) and Ludwig (15). Each of these papers looked at single spots which were formed rather than typical weld beads comprised of many overlapping spots. However, it is at the anode spot where anode melting occurs and depending on weld conditions may be non-existent

(no melting occurs) to rather large in size.

The anode spot is analogous to the cathode spot in that this is the area on the anode in which the emitted electrons from the cathode are absorbed. Numerous authors (12-15) have studied the anode spot portion of the welding arc. It is in this area that the weld bead is formed.

Jones, et. al. (13) studied the heat effects in anode spots of high current arcs using a steel tape moving at a fast rate across the surface of an electrode. It is in the anode area where the effectiveness of the expended arc energy is seen. The smaller the anode spot area, the greater the current density and the smaller the weld bead (although penetration may or may not be increased). This can be detrimental if too high a current density is achieved as excessive arc splatter and an unstable arc may occur.

Kouwenhaven (14) performed a similar study and found the same results. Both studies used single spots which were evenly, but distantly spaced. This differs from the common weld bead where a large number of individual anode spots overlap to form a continuous pattern known as the weld bead.

In another study, Ludwig (15) studied current density

and anode spot size in GTAW. This study was similar to many recent studies (16-18) where the effects of surface impurities on arc stability and appearance and penetration were studied. Ludwig (15) This study was similar to many already completed; and, some which were in progress, found that surface impurities could have either relatively small or large effects on the weld bead parameters including arc stability and weld penetration depending on the relative location, concentration, and nature of the impurities. The impurities affected the surface-tension temperature coefficient in either a positive or negative manner (reference figure 3). Anode impurity effects on bead morphology have been discussed by a number of other investigators (9, 16-18).

Energy distribution in the welding arc can be significantly changed by variations in the current, travel speed, arc gap and shield gas. These same factors affect GTA welding efficiency (i.e. efficiency decreases as current increases and travel speed decreases). An increase in either travel speed or current (to a defined limit for a given set of welding parameters) increases the arc efficiency. Arc efficiency being defined as: the heat required and used to melt the anode and form the weld bead divided by the total heat input (18).

Niles (19) states the potential drop is proportional

to the arc length. The larger the arc column the larger the total potential drop as well as a greater electrode climb for electrodes with small vertex angle tips (reference figure 6). Chihoski (20) also studied potential drops and found that higher potential drops occur with sharper cone tip electrodes than with broader cone tips.

Gordon, et. al. (21) studied the effects of current and shield gas on arc temperatures. In their studies they also investigated the potential drop across the electrode under constant conditions for each experiment. They found that argon had the lowest and helium the highest potential drop under similar welding conditions. This is to be expected since helium has a higher ionization potential than argon (reference figure 7).

Jackson (2) concluded that the potential drop near the anode in both arc modes (cathode spot and normal) is independent of arc current for currents above 200 Amperes. However, potential drops in the system at currents above 200 Amperes must be attributed to the cathode and probably result from a change in the cathode tip configuration. Potential drop was found to increase slightly with increasing current between 200 and 500 Amperes in the current study with no change in the electrode tip configuration.

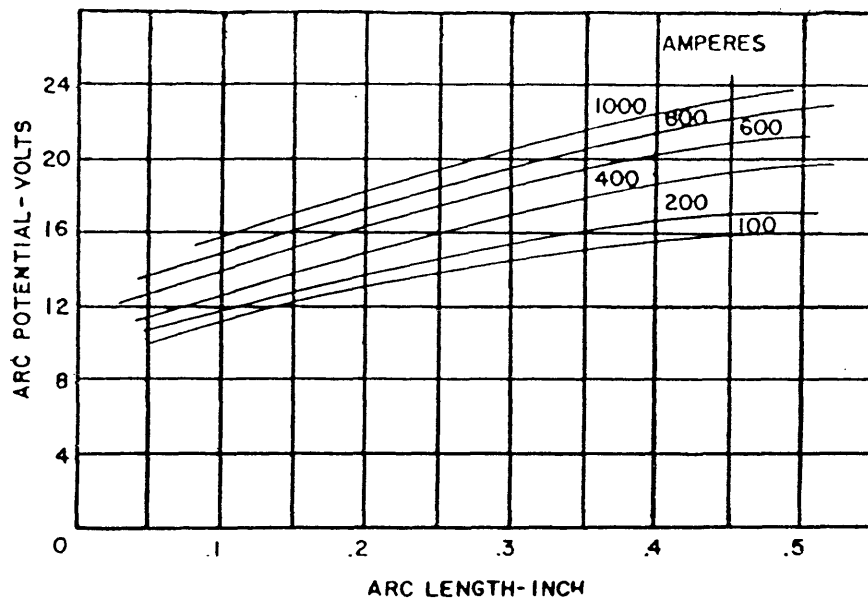
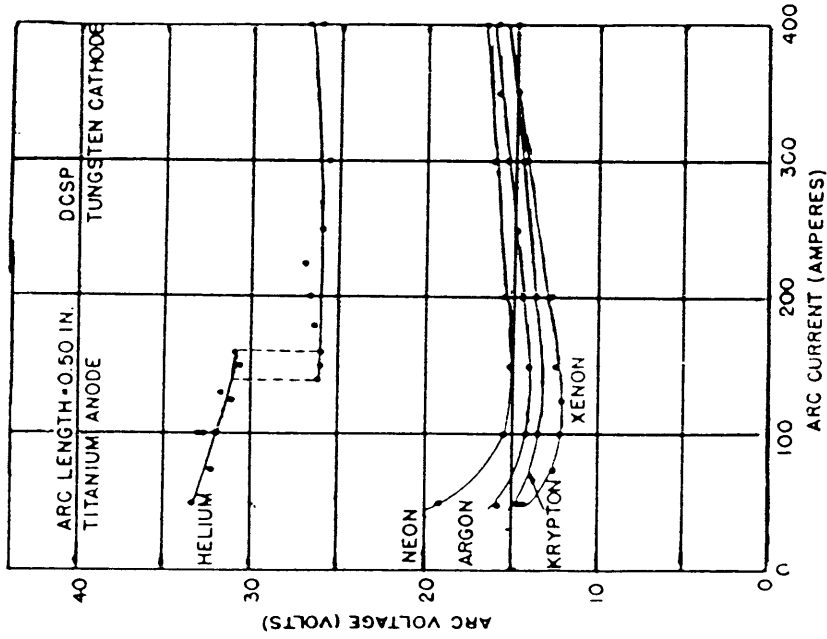
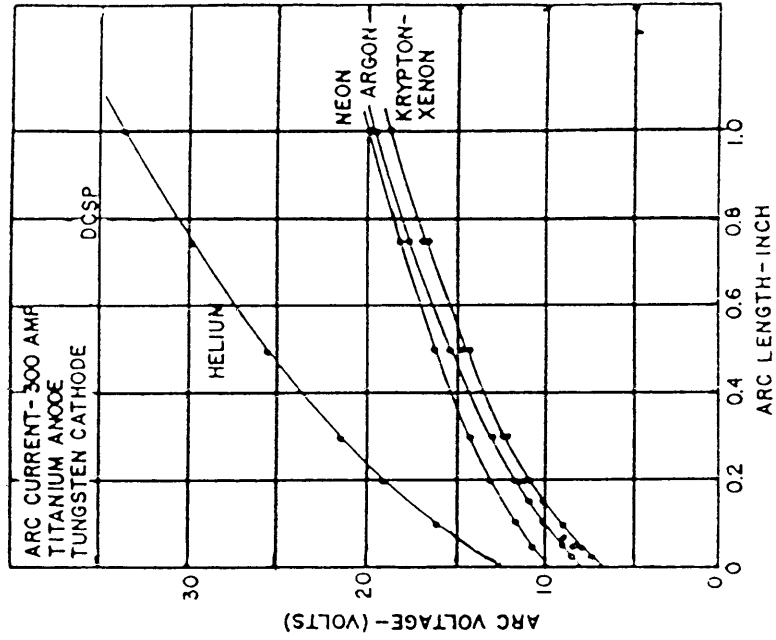


FIGURE 6 Typical Arc Potential-Arc Length Curves at Low, Moderate, and High Currents. (2)



a) V-I Characteristic Curves



b) V-L Characteristic Curves

FIGURE 7 Typical Arc Potential-Current and Arc Potential-Arc Length Curves Under Different Shield Gases. (2)

The potential drop is caused by the arc gap between the cathode and anode or workpiece. It is more dependent on the current type (AC vs DC), shield gas (helium, argon, or a mix), arc gap spacing, and electrode type (pure, thoriated, or zirconated tungsten) than on anode material (aluminum, steel, stainless steel, etc.).

The potential drop, as mentioned above, may be controlled by varying the weld parameters to obtain the optimum weld conditions. By controlling the potential drop to a minimum value, one improves the weld efficiency and the energy required to produce a weld becomes more cost-effective.

The cathode drop is independent of and the anode drop a function of arc length. As arc length is increases, the anode drop also increases.

Fett (22) defined the cathode drop as the difference in potential between the cathode and a point in the arc very near the cathode; the potential gradient over the intervening space between the cathode and this point is very high (approaching many thousands of volts per centimeter).

Lancaster (23) later analyzed this same region and derived a heat balance for the cathode drop region. In this region, there are two main sources of heat loss; 1) heat loss

to the environment and 2) heat loss due to the cooling effect of electrons evaporating from the anode or metal surface. Heat loss to the environment occurs through the electrode by conduction.

Lancaster (23) also analyzed the anode area and derived formulas for the anode heat balance (the anode drop area). The anode potential drop results from a deficiency of positive ions near the metal surface giving rise to a negative space charge.

Measurements of the anode drop by Nestor (10) over a distance of 1 mm from the electrode indicate that the potential drop decreases with increasing current and decreasing arc length. Equations also exist to measure the anode drop distance. It is from these equations that the distance was derived to be in the order of one electron free path, meaning each electron would arrive at the anode surface with a kinetic energy approximately equal to the sum of the anode drop potential times the electron unit charge plus its own kinetic energy at the top of the anode drop region.

Many investigators (2, 6, 7, 9, 16-18, and 20) have found that gas composition, welding parameters (electrode gap, current, voltage, etc.), anode material and impurity content in the anode can all greatly affect the weld pool

configuration, and subsequently bead morphology (penetration, width, and melt area) and arc characteristics. In particular, the effect of anode impurities on weldability and penetration in a variety of materials has been studied (16-18).

A previous investigation (24) has found that very large arc pressures exist when attempts are made to weld at high (above 350-400 Amperes) currents. This high arc pressure is set up due to the Lorentz forces in the plasma. Undercutting, intermittent weld beads (weld bead is characterized by severe instability as characterized by blowholes and other indications of poor welding), porosity, and arc instability are all symptoms of excessive arc pressure. Some of the side effects include tungsten inclusions (in the weld material) and unnecessary electrode tip erosion.

Within limits, increased penetration may be achieved at higher currents and arc pressures though parameters must be tightly controlled to avoid the undercut problems which have been seen in many welds to date.

Arc pressure may be lowered in the following manner: 1) use a hollow electrode (as shown in figure 8), 2) use an electrode with a dull vertex angle (this may lead to an unstable arc and current densities of approximately 120 amperes per mm² are required to stabilize the arc), or 3) use

either helium or hydrogen shield gas. However, using a hollow electrode in argon shield gas serves the same purpose as changing shield gas to hydrogen or helium. This is evidenced by the results of Yamauchi, et. al. (24) as shown in figure 8.

A drawback to the use of the hollow electrode is the undercut which can occur as the travel speed is increased. Undercut was seen on both sides of the weld beads of Yamauchi, et. al. (24) as well as some of the welds in the current study using the hollow electrode. However, this same phenomenon has also been seen when conventional welding methods and electrodes are used and low arc pressure is encountered. Yamauchi, et. al. (24) did not report the travel speeds in their studies. The travel speed used in this current study was 10 ipm (4.2 mm/sec) and undercut was typically seen in hollow electrode GTAW above 300 Amperes.

Bukarov, et. al. (25) looked at constricted arcs and the effects (force effects) on the weld metal. The effects of the arc pressure of a constricted arc on penetration were studied. As previously stated, penetration is primarily determined by the thermal and mechanical properties of the arc. A constricted arc produces more pronounced effects on the mechanical properties of the arc rather than on its thermal properties. The arc pressure of a constricted arc is approximately six to seven times that of a free arc with

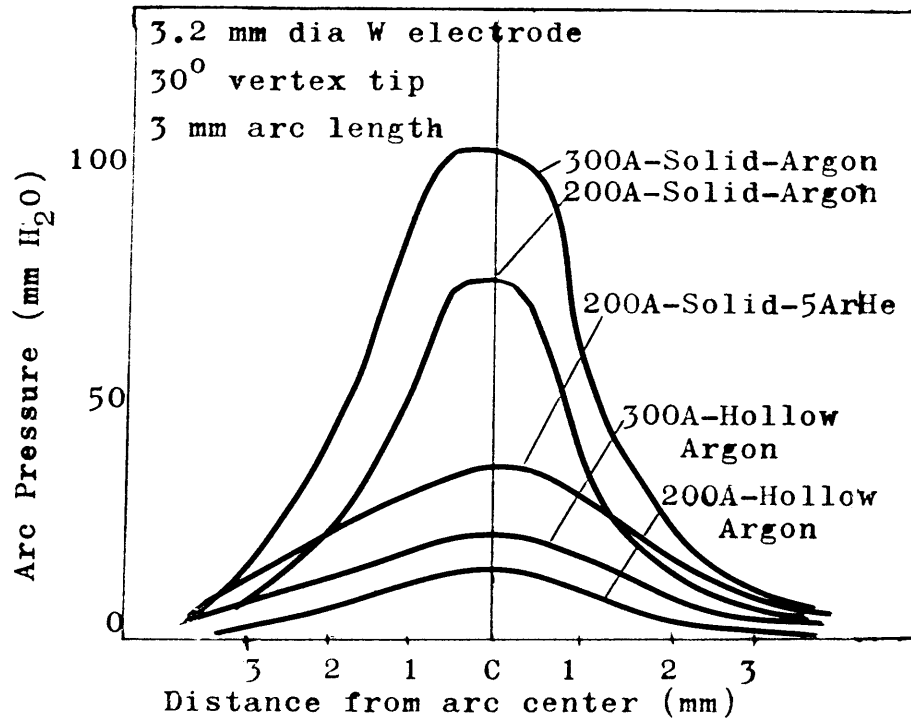


FIGURE 8 Arc Pressure Distribution Curves Indicating Advantage of Hollow Electrode In Argon versus Solid Electrode In Helium. (24)

no constriction.

Jackson (2) went farther and developed a formula to determine the arc force acting toward the weld crater as

$$F = KI^2 \log(r_1/r_2) \quad \text{eq. (1)}$$

where F is the arc force in question, K is a constant, I is current in Amperes, r_1 is the arc radius at the center of the arc, and r_2 is the arc radius at the electrode.

From this equation, it can be seen that an increase in current with a given electrode, or a decrease in the electrode diameter for a given current, will lead to an increase in the arc force.

Numerous other investigators (24-26) have also measured the arc force in a variety of ways. Most have found its dependence on current was quadratic in nature (i.e. $P_{\text{arc}} = kI^2$). Two main forces contribute to the arc force. These are 1) the dynamic pressure of the shielding gas flow, and 2) the electrodynamic forces caused by the interaction of the molten metal pools with the arcs inherent magnetic field. The dynamic pressure is formed as a result of constriction at the cathode. The greater the constriction,

the greater the dynamic pressure.

Selyanenkov, et. al. (26, 27) found in their studies that the magnitude of the arc pressure is determined primarily by the angle of the tip and the truncation angle of the tungsten electrode.

Yamauchi, et. al. (24) in the Sumitomo Hollow Tungsten Arc (SHOLTA) process found that arc pressure at high currents could be greatly reduced by using a hollow electrode rather than the standard solid electrode (at currents above 250 Amperes). The arc pressure is reduced by decreasing the current density at the arc striking point. The larger the electrode hole, the lower the arc pressure. As seen in figure 8 the arc pressure distribution curves are relatively flat for hollow electrodes in both argon and helium shield gases which is similar to solid electrodes when using helium shield gas. The arc pressure distribution curve for solid electrodes in argon is shown for comparison. It can be seen that high arc pressure does exist above 250 Amperes when welding in pure argon using a solid electrode. The arc pressure obtained for a given set of welding conditions is dependent on the electrode hole diameter.

In GTAW, the arc characteristics are very sensitive

to changes in cathode geometry and material, and the different modes of arc operation (normal or cathode spot), making it nearly impossible to derive a mathematical formula which truly expresses the current-potential characteristics. Figure 2 illustrates the different current-potential curves which were obtained in a variety of experiments. A fixed electrode gap of 0.2 inch (5mm) and the potential drop along the cathode were taken into account in the curves. The differences in operating potentials for the same current observed with different cathodes is due partially to the changes in potential drop in the immediate vicinity of the electrodes. In all cases, the anode material was the same, indicating the anode drop was independent of cathode changes for a given current. The figure also illustrates that the location of the most stable arc happened to occur at the lowest possible potential. This condition was reported to occur most readily with a relatively long cathode extension and a blunt tipped electrode. The characteristic curves are sensitive to slight changes in electrode geometry and material as well as to the cathode mechanism (normal or cathode-spot mode), but more drastically due to changes in shield gas.

The difference in the arc-potential characteristic curves between normal and cathode spot operating modes is also illustrated in figure 2. Comparing the curves, it can

be seen that cathode spot mode arcs exhibit a much greater potential increase than arcs operating in the normal mode.

Figure 6 illustrates the effect arc length has on the arc potential of a given weld. When working with low current and low pressure welds, the plasma potential gradient can be determined from the slope of the potential-arc length curve (1). It can be seen from the figure that small changes in the arc length produce rather large increases in the operating potential. Electrode separation also affects the radial current density of the electrode and hence the energy available to the anode.

Jackson (2) also noted that the higher the current, the greater the minimum potential required to maintain the arc at a given arc length. For any given potential the arc length decreased with an increase in current in his studies.

Figure 7 illustrates the effect shield gas has on the arc potential-current characteristic curve. For the example shown, it can be seen that the use of helium rather than argon as the shield gas gives you a much higher arc potential. This is also the case with increasing arc length as shown in figure 7. It can also be seen that the arc potential is much higher in helium than in argon as arc length increases.

Winsor and Turk (28) studied electrode material

effects in both argon and helium atmospheres using pure, thoriated, and zirconiated electrodes. The thoriated tungsten electrodes exhibited superior starting performance during DCSP welding of stainless steel, while pure tungsten exhibited the worst performance. This same trend was seen when initiating an arc and maintaining it at low potential settings. The minimum starting potential for both thoriated and zirconiated electrodes was seen to be more constant while that for pure tungsten was random. The increasing work functions of the thoriated and zirconiated electrodes corresponded to an increasing starting potential.

The choice of shield gas will also greatly affect the arc potential, with helium having a greater ionization potential than argon. Thus, thoria or zirconia additions to the tungsten electrode tend to yield a better, more stable arc at most current settings (high and low). Winsor and Turk (24) also found that the electrode temperature was slightly higher in helium than in argon.

The current has a much smaller effect on the arc potential causing the potential to gradually increase with increasing currents (above 150 Amperes in this current study).

The electrode material (pure, thoriated, or zirconiated) influences the manner and ability of the electrode to

generate electrons for the arc plasma. Thermionic emission is the means by which the electrode supplies electrons to the arc. This effect is known as the electrode materials work function. The work function is a measure of the materials ability (energy necessary) to lose (emit) electrons from its surface through thermionic emission. In scientific terms, it is the energy that must be imparted to an electron near the Fermi energy level (maximum energy that an electron in a solid may reach and still be stable) of a solid to get the electron out of the solid into the plasma. Zirconia and thoria additions to tungsten lower the work function making the release or emission of electrons from the electrode surface to the arc much easier.

Lowering the work function by even one volt can have a relatively substantial effect on the arc characteristics. Thus, work began to examine how the work function of the tungsten electrode could be lowered to improve the effectiveness of the electrode during welding. Decreasing the work function of the electrode improves both the ease of arc initiation and the maintenance of the arc after initiation. As previously mentioned, both thoria and zirconia additions (ThO_2 and ZrO_2 respectively) were found to lower the tungsten electrode work function and improve the arc stability at higher currents.

HISTORY

Stainless Steel Welding

Many studies (9, 16, 18) have been initiated to determine the weldability of stainless steels. These studies (9, 16, 18) have concentrated on the effects that minor element additions (to the anode) have on bead morphology, namely penetration. These studies did not treat the bead morphology of the base material with changes in weld parameters. The conclusion of the studies (9, 16, 18) was that minor element additions to the stainless steel anode can and do affect bead morphology. The effect can be either positive or negative in nature depending on the affect the addition has on the molten weld pool surface tension (reference figure 3). Both penetration and the p/w ratio (penetration divided by the surface bead width) were affected.

Variation In Electrode Shape

Studies have also been initiated to determine the effect that electrode shape has on arc and weld bead characteristics. The conclusion reached by many of the studies (20, 29-31) was that both arc stability and bead morphology (penetration, bead width, p/w, and melt area) were influenced and could be optimized by altering the electrode tip configuration.

Savage, et. al. (31) initiated one of the first

studies in this area of improving penetration by altering the tungsten electrode geometry. Many other studies to date have expanded on his work to study the effects the tungsten electrode has on bead morphology. The conclusions reached by Savage in his study were as follows:

- 1) In the cathode spot operating mode, the arc potential-current characteristics, penetration, and bead characteristics (bead morphology), and temperature distribution along the arc length and the electrode are all affected by the electrode tip geometry.
- 2) Bead width decreased by half, and penetration increased approximately fifty percent while melt area remained relatively constant by increasing the electrode vertex angle from 30 to 120 degrees when using two-percent thoriated tungsten electrodes. This equates to a threefold increase in melt efficiency.

Chihoski (29) found that better penetration (and a narrower weld bead) could be achieved at lower currents by using a fine tipped electrode. Higher currents were required to achieve the same results when the electrode vertex angle increased. In addition, Chihoski (29) surmised that finer electrode tips produced better penetration because of increased arc pressure. No further studies were found that pursued this idea, although if we take it to its conclusion, it would suggest that by ever increasing arc pressure and hence a finer and sharper tipped electrode one could expect very good penetration and p/w ratios at moderate current levels. The error in this thinking is that as the electrode

tip becomes sharper, the arc has a tendency to move up or "climb" the electrode to find a stable point on the electrode. due to the electron cooling effect described in a previous section. Penetration and p/w are affected, but may or may not increase.

In general, bead width and penetration are improved (decreased bead width and increased penetration) with an increase in the electrode included vertex angle. The weld cross-sectional area remains nearly the same with the decreased vertex angle and the arc potential is also decreased (30).

Arc characteristics are also greatly affected by electrode configuration. As the electrode tip becomes finer (smaller vertex angle), the cathode spot has a tendency to climb to a higher point on the electrode as the operating current is increased. This occurs because the cathode spot is finding the point on the electrode of maximum temperature where thermionic emission will occur more efficiently.

Penetration

A number of studies (compiled in (34)) have also attempted to derive equations to predict bead morphology; namely penetration, although bead width and melt area have also been predicted. These studies have been used with good

success in submerged arc welding (SAW) and one investigator (32) used them with GTAW and had fair success. We will now look at these equations and how they apply to this current study.

Variation of one or more of a combination of welding variables usually has an effect on bead morphology. Potential, weld current, travel speed, and electrode shape, size, and composition must be considered when determining weld bead morphology prediction equations. This study was mainly interested in the effects and improvements a hollow electrode had over the use of a solid electrode on weld bead morphology. In particular, penetration, p/w, and melt area were examined.

A recent study by Burgardt and Heiple (33) has indicated that the proposed models based on welding parameters for GTA weldment bead morphology has limitations. These limitations are that the models hold only in the "parameter control region" of the plots. Figure 9 illustrates this phenomena. At lower currents, "fluid flow" controls the weld pool; at higher currents the weld pool is in the parameter control region and is modelled well by the existing equations.

The reason for the two zones (fluid flow and parameter control) is shown in figure 3 and 10. In particular; for a

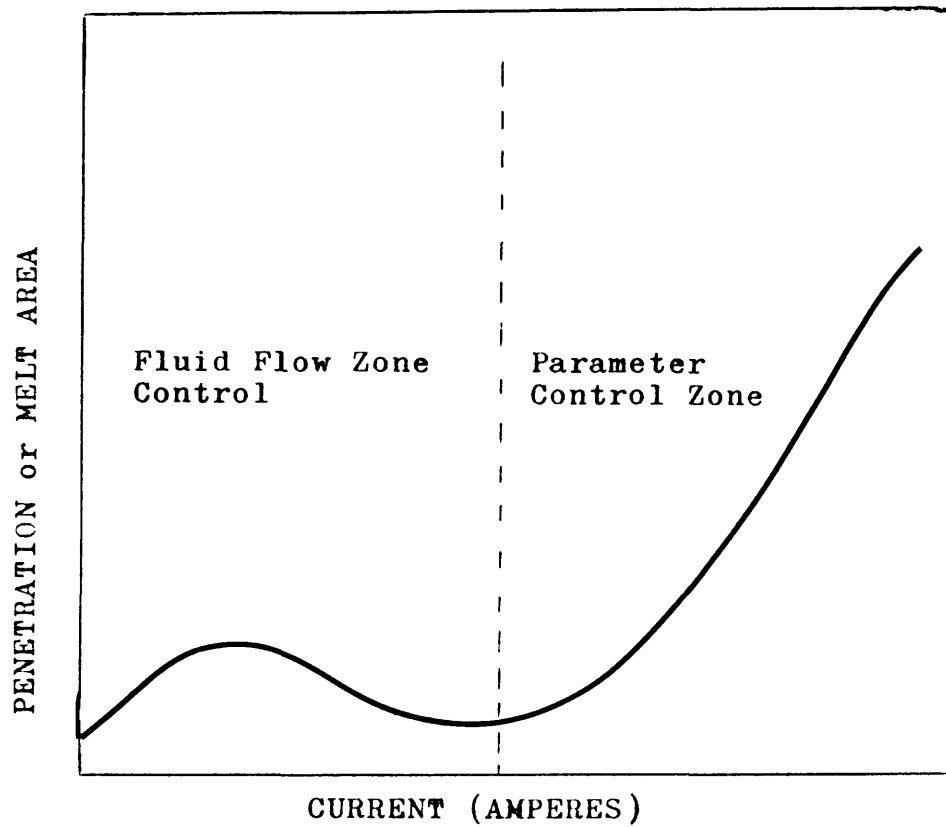


Figure 9 Proposed Regimes In Current versus Bead Morphology Plot Indicating Two Regions Seen, Fluid Flow Zone at Low Currents and Parameter Control Zone at High Currents. (33)

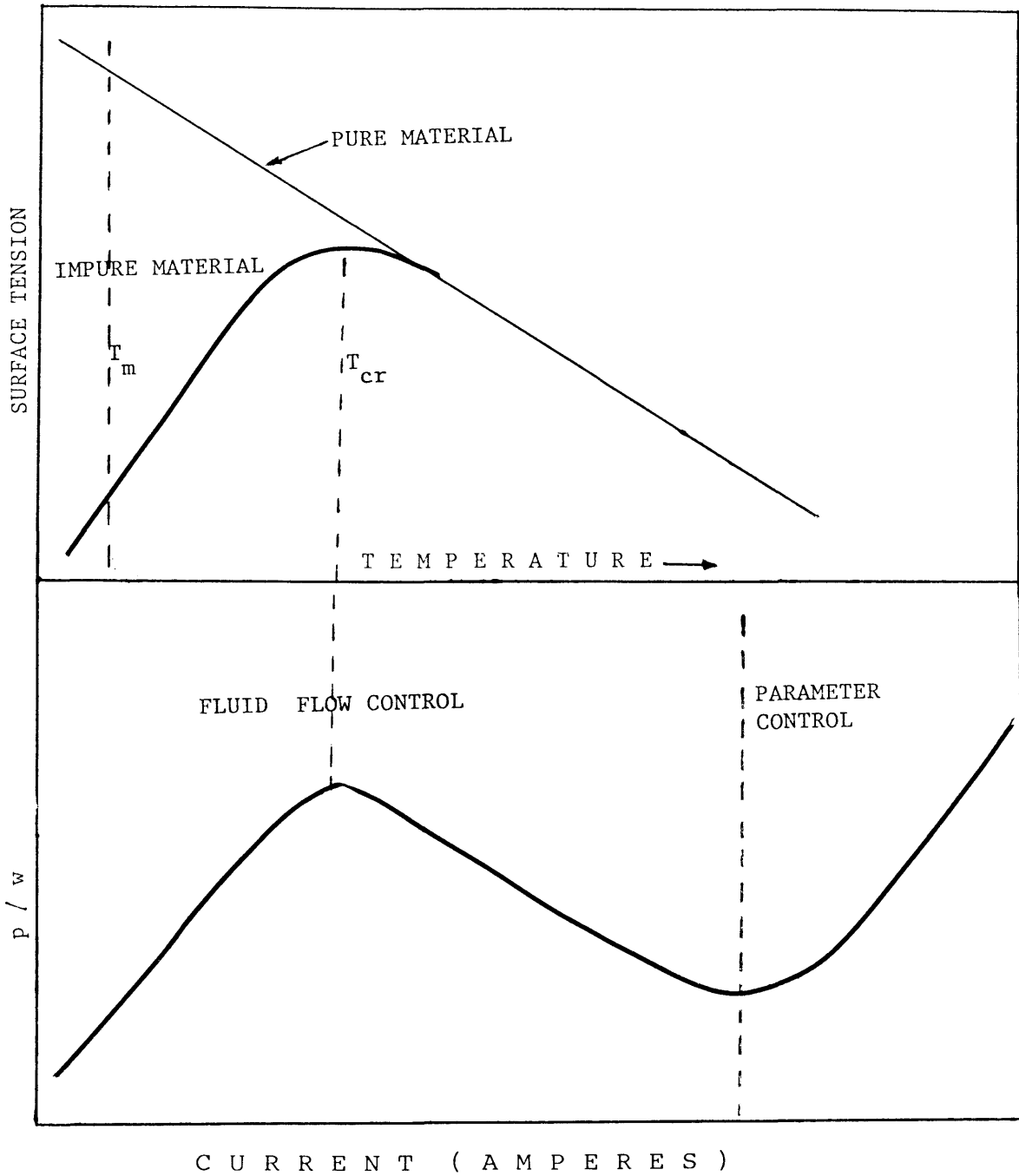


Figure 10 Schematic Showing Effects of Surface Tension versus Weld Pool Temperature For Pure and Impure Materials On p/w Ratio versus Current Curve (From 9)

pure material, as weld pool temperature increases, the surface tension decreases. Referring to figure 3, it can be seen that the temperature in the middle of the pool is hotter than at the edge of the pool which is limited to the melting point of the material (T_m). Under these circumstances, weld pool flow will occur as shown in figure 3a or outward from the middle of the pool (leading to a wide, shallow pool and a low p/w ratio).

For an impure material (comparably larger Sulfur amounts) the opposite will occur. Surface tension increases with increasing temperature (up to a maximum or critical temperature). This is shown in figure 3b where weld pool flow occurs from the outside weld pool surface inward due to the higher temperature in the middle of the pool. This in turn leads to a narrower, deeper pool and a larger p/w ratio. With increasing temperature, the driving force of the surface tension difference between the middle of the pool and the edge increases leading to an increased p/w until a critical temperature is reached where p/w begins decreasing because of the smaller driving force (γ decreases with increasing temperature) above this critical temperature (the weld pool becomes wider and shallower). This continues until fluid flow from surface tension is no longer the dominant force. Above this point in figure 10, the parameter control region

is encountered and p/w increases with current.

Custom 630 with its impurity constituents (including Sulfur) follows the trends of the impure material just discussed. The results of this study using hollow and solid electrodes followed this pattern seen in the two regions. Namely penetration and p/w ratio were modelled well at higher currents in the parameter control zone, but this relationship broke down in the fluid flow zone.

Use of a hollow electrode in place of the standard solid electrode has been promoted by the Japanese (24) as a means of improving penetration at higher currents (above 300 Amperes). The effects of shield gas, current type (AC or DC) and level, and electrode shape and type (solid or hollow) on melt area in addition to p/w and penetration were examined in this current study.

A compilation of the studies to date (compiled in (34)) have derived complex equations interrelating current, travel speed, and potential. In general, increasing current leads to increased bead width, melt area, and penetration. Most studies (compiled in (34)) have shown that both penetration and melt area are inversely related to travel speed.

A study by Jackson and Shrubbsall (35) found that

penetration could be predicted as follows:

$$P = k[I^4/(SV^2)]^{1/3} \quad \text{eq. (2)}$$

where P is penetration (inch), I is current (Amperes), V is potential (volts), k is a constant determined by type of flux or shield gas, and S is travel speed (ipm).

In this study, k represents a constant determined by shield gas, anode material and welding process, and is the slope of the plot of measured penetration versus the functionality of the Jackson and Shrubbsall (35) equation (eq. 2).

A study by Schwemmer and Olson (36) further defined k as being dependent on the surface tension between the solid parent metal/liquid weld pool interface. This equation is listed in Table I.

A study by Savage, et. al. (37) proposed that penetration was a function of current, potential, travel speed, and material thickness as follows:

$$P = 3.35 \times 10^{-2} I^{0.338} V^{0.057} S^{-0.449} b^{-0.037} \quad \text{eq. (3)}$$

where P is penetration (inch), S is travel speed (ipm) and b is material thickness (inch).

TABLE I PREDICTION EQUATIONS USED TO MATCH DATA IN CURRENT STUDY

<u>PENETRATION</u>	<u>INVESTIGATOR</u>	<u>EQUATION</u>
	*Jackson, et.al.	(35) $P_{mm} = k [I^4 / S_{cm} V^2]^{1/3}$
	Jackson, et.al.	(35) $P = k [I^4 / SV^2]^{1/3}$
	*Schwemmer, et.al.	(36) $P = k [I^4 / SV^2]^{1/3}$ where $k = k_0 N (\sqrt{1 - \gamma} f_m) (V - \Delta V)^n$
	*Savage, et.al.	(37) $P = 3.35 \times 10^{-2} I^{0.338} V^{0.057} S^{-0.449} b^{-0.037}$
	*Erokhin, et.al.	(38) $P = 3.55 \times 10^{-3} [(1.27 \times 10^{-5} I^2) + (6 \times 10^{-6} q^2 / S_{cm})]$
	*Watanabe, et.al	(39) $P_{cm} / T_{cm} = (S_3 I / T_{cm}) / (S_{cm} / T_{cm})^{1/2}$
	*Shinoda, et.al.	(34) $P_{mm} = T^2 / (6.05 V^2 D_{mm} S_m^{0.4})$
	*ZIS	(40) $P_{mm} = [(19.2 \times 10^{-4} I^2) / DV^{0.5} S^{0.4}] + 0.8G$

Another study (38), considering surface tension and static equilibrium conditions, suggested an expression for penetration as follows:

$$P_{cm} = 0.00355[(1.27 \times 10^{-5} I^2) + (6 \times 10^{-6} q^2 / S_{cm})] \quad \text{eq. (4)}$$

where P_{cm} is penetration (centimeters), S_{cm} is travel speed (centimeters per minute), q is effective heat input (cal/sec) equal to the product of $0.024nIV$, and n is arc efficiency (energy) and was assumed to be 0.6 for these studies. This equation was found to be satisfactory when the root side of the weld is not oxidized. If the root side is oxidized, there is a decrease in the surface tension in the molten weld pool. The root side is not oxidized provided penetration does not exceed about seventy-five percent of the material thickness.

Watanabe (39) predicted penetration as follows:

$$P_{cm}/T_{cm} = (S_3 I / T_{cm}) / (S_{cm} / T_{cm})^{1/2} \quad \text{eq. (5)}$$

where S_3 is a constant dependent on electrode or flux type, and T_{cm} is material thickness (cm)

Another study, by Shinoda (34) predicts penetration with the following equation:

$$P_{\text{mm}} = I^2/[6.05V^{0.5}D_{\text{mm}}S_{\text{m}}^{0.4}] \quad \text{eq. (6)}$$

where D_{mm} is electrode diameter (millimeters), and S_{m} is travel speed (meters per hour). This equation may be used when filler wire is added to the pool.

Lastly, a computer determination of welding parameters from ZIS (German Democratic Republic Welding Institute (40)) derived the following equation for penetration:

$$P_{\text{mm}} = [(19.2 \times 10^{-4} I^2)/DV^{0.5}S^{0.4}] + 0.8G \quad \text{eq. (7)}$$

where G is root gap (mm). Many of the of these penetration prediction equations were derived for the submerged arc welding process (SAW) but are considered valid for use in GTAW because the arc and heat flow characteristics between the two processes are similiar. Table I is a compilation of these equations.

Effect of GTAW Weld Parameters on Bead Morphology

The previous section discussed how increased current and travel speed, as well as electrode shape influenced penetration. Bead width (and hence p/w) and melt area are also affected by variations in GTAW parameters. Bead width and melt area (like penetration) are all affected by the molten

weld pool flow. Any GTAW parameter which affects the pool fluid flow will in turn affect bead width and melt area. Melt area measurement has an additional advantage in that it is a good measure of the arcs melt efficiency.

Sharapov (4) predicted bead morphology using a dimensionless Peclet number. The equation is as follows:

$$P_o = [(q/kT_f) ((S_{mm}/\alpha T_{cm})^{1/2})] \quad \text{eq. (8)}$$

where k is the thermal conductivity (cal/centi- $^{\circ}$ C-sec), T_f is weld pool melting temperature ($^{\circ}$ C), α is the thermal diffusivity (cm² per second), T_{cm} is plate thickness (cm), and S_{mm} is travel speed (millimeters per minute)

ZIS (40) also derived an equation for bead width as follows:

$$W_{mm} = (0.38V^{1.05}D^{0.44}) / (I^{0.02}S_m^{0.48}) \quad \text{eq. (9)}$$

where W_{mm} is bead width (mm), S_m is travel speed (meters per hour).

Jackson and Shruballs (30) also predicted bead melt area with the following expression:

$$\text{Log } A_{\text{mm}} = 0.903 \log(I^{0.716}/S_{\text{cm}}) - 0.78 \quad \text{eq. (10)}$$

where A_{mm} is the fused area (mm). Jackson and Shrubbsall (35) also found that the melt area was relatively unaffected by normal changes in the operating potential and is more greatly influenced by travel speed and current. The results of the melt area predictions can be found in Appendix III.

Hollow Electrodes/Cathodes

As previously mentioned, the Japanese (24) have pursued the use of hollow electrodes to improve penetration at higher currents with success. They relate this improvement (and success) to the decreased arc pressure which has been measured and is shown in figure 9.

Soviet experimenters have also pursued the use of hollow electrodes (42-46). Their applications have all been in vacuum type environments. The mentioned references deal mainly with the electrical characteristics of the weld and do not address penetration or bead morphology affects. Other studies with Vanadium (47) and type 304 stainless steel (48) all report increased penetration and arc performance using hollow electrodes in place of the standard solid electrodes.

Very little work has been performed in the United States except for that accomplished by Key, et. al. (49).

These studies have also indicated improved d/w and penetration for hollow electrodes over the standard solid electrode during welding.

Numerous Soviet investigators (42-46) have utilized hollow electrodes, but their applications have been in vacuum (similar to a space-type environment or a pressure vessel welding chamber). They found that hollow electrodes provided excellent arc stability (compared with solid electrodes), lower sensitivity to changes in penetration depth at considerable fluctuations in arc length, and higher weld quality (all compared to the results obtained when utilizing standard solid electrodes). The hollow electrodes used were actually tungsten (or in some cases tantalum foil) tube utilizing argon as the shielding gas which was passed through the hollow. Flow rates as low as 0.31 liters per hour were found to allow relatively easy initiation of the arc (using a high frequency start system). Once initiated flow rates as low as 0.14 liters per hour allowed stable welding arcs to be used. They also found that the electrode wall thickness should be about half the hollow diameter to ensure long service lives with little electrode buildup problems. Currents up to 200 Amperes were analyzed.

In summary, the purported advantages of hollow electrode GTA welding (over solid electrode GTA welding include

the following:

- 1) lower arc pressure (and hence better arc stability)
- 2) improved penetration at constant heat inputs
- 3) the ability to arc weld in a vacuum with relatively low shield gas flows (compared with regular gas shielded welding where the gas is quickly removed from the welding arc preventing ionization from occurring)
- 4) improved arc control with smaller sensitivities to arc length and little effect on penetration

Shield Gases

The shielding gas utilized in GTAW also has an effect on arc characteristics and to a lesser extent bead morphology. However, it may affect penetration based on the flow rates and compositions of the shielding gases involved. Each gas/gas combination has its own unique advantages and disadvantages which warrant their use for specific applications.

In general, higher arc potentials are obtained as the percent helium is increased. Pure helium produces arc potentials higher than those in pure argon at the same current levels. This is due to the higher ionization potential of helium than of argon producing a hotter arc. It has also been seen that arcs at lower currents start much more readily in pure argon atmospheres and it generally produces weldments with deeper penetration and narrower widths than when using

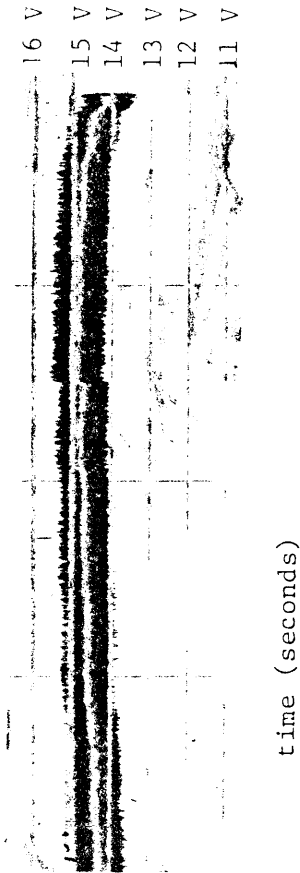
helium. Helium also permits higher travel speeds to be utilized before weld undercutting is seen.

Argon-helium gas mixtures tend to retain the properties of the argon gas up to about a 25ArHe mix. Mixes at this ratio have the advantages of both helium and argon making it the optimum gas composition (generally).

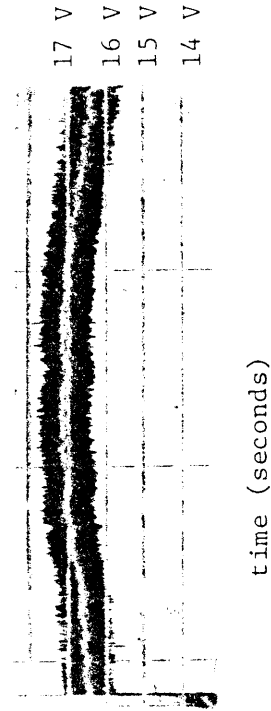
Arc Stability/Appearance

Arc stability has been typically measured using an oscillograph type feedback equipment monitoring system which analyzes the current and potential fluctuations as a function of time. Another equally acceptable measurement technique is the use of a high speed strip chart recorder (visicorder). Figure 10 illustrates a typical example for both electrode types at the same current.

As current and potential increase (at a predetermined travel speed), an optimum point is reached whereby there exists a small fluctuation in the arc stability plot. Above this point the arc stability decreases. Travel speed will also have an affect on arc stability; therefore, as travel speed is altered, the optimum current/potential point for the most stable arc will also change. The arc stability results for this study can be found in Appendix IV.



SOLID ELECTRODE



HOLLOW ELECTRODE

FIGURE 11 Typical Arc Stability Measurement Outputs From Visicorder For Shaped Solid and Hollow Electrode GTAW in 75ArHe at 500 Amperes, 150 degree tip.

TABLE II Nominal Chemical Analysis of Raw Material

Cr	Ni	C	Cu	Cb + Ta	Mn	Si	Fe
17.0	4.0	0.07	4.0	0.15-0.45	1.0	1.0	rem.

The intent of the present work was to verify the increased penetration results of the Japanese (24) using argon and argon-heliumk gas mixtures in the welding of stainless steels. In addition, if improvements were found, an understanding of the physical reasons for these observations was attempted.

EXPERIMENTAL PROCEDURE

Material Selection

Stainless steel (Custom 630) was selected for use in this study because of its known weldability with the GTAW process and it was believed that the nugget and heat-affected-zone would be readily discernible from the parent material. The material was supplied by Carpenter Technology in 0.5 (12.7 mm) inch thick by 3 inch (76 mm) wide bars which were cut into nine inch (230 mm) lengths. The material came from heat lot 57029 and is in the H1165 condition. Chemical analysis of the material is given in Table II (it can be seen that the material matches 17-4PH stainless steel).

Equipment and Set-up

Argon and argon-helium mixtures (75ArHe and 25ArHe) were used in this study to aid in determining the effect of shield gas on penetration and bead morphology while utilizing both solid and hollow electrodes. The advantages and disadvantages of each shield gas are well known and were discussed in an earlier section.

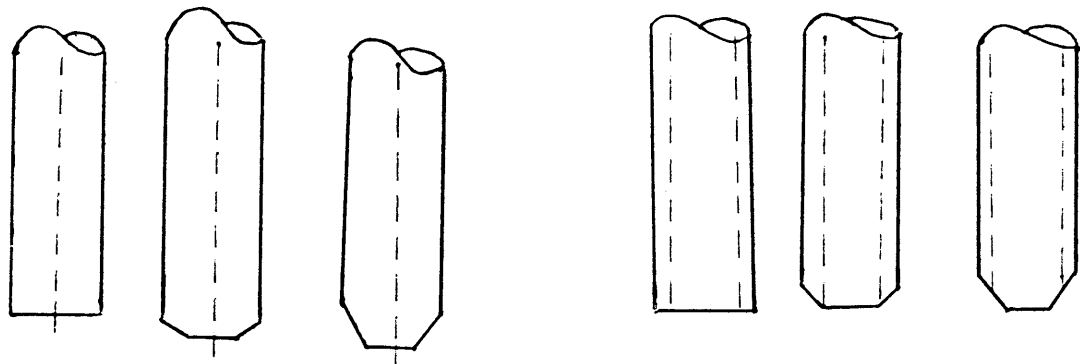
Two percent thoriated solid, hollow, and unshaped and shaped solid and hollow electrodes were used in this study to determine the validity of increased penetration by utilizing hollow over solid electrodes. The electrode diameter

was 5/32 inch (4mm) to allow for boring of the hollow electrodes. Hollow electrodes were made by using a carbide-tip bit to drill a 3/32 (2.3mm) inch diameter hole 1/2 inch (12.7mm) deep into the solid electrodes. The electrode shapes used are shown in figure 12.

Three vertex angle electrodes were utilized in this study; namely, 180 (unshaped), 150, and 90 degree included angles. The solid electrodes with 150 and 90 degree vertex angles were blunted to a 3/32 inch (2.3mm) diameter (representing the hole diameter in the hollow electrode), while the hollow electrodes were ground to a point at the hole center (shown in figure 12).

Electrode preparation was done using a standard electrode grinder. A relatively smooth finish (better than 32 RMS) was obtained with the 150 and 90 degree blunt tipped solid and 150 and 90 degree tapered hollow electrodes.

The power supply utilized for the lower currents (100 to 290 Amperes DC and 100 to 230 Amperes AC) for constant heat input welding was a Hobart Cyber TIG 300 series machine. The remaining welds at constant travel speed were done using a Merrick power supply controlled with an Amptrak Micro I-B controller.



180°

150°

90°

180°

150°

90°

a) Solid Electrode 3/32 inch
(2.3mm) blunt end

b) Hollow Electrode 3/32 inch
(2.3mm) hollow

FIGURE 12 Electrode Configurations Used In the Present Study.
All Electrodes Were 5/32 inch (4mm) diameter, two-
percent thoriated tungsten.

Arc Characterization

A high speed strip chart recorder (visicorder) was used to monitor arc stability. Figure 11 illustrates what was obtained using a visicorder for the arc stability measurements.

The arc was observed visually to discern differences with the varied welding parameters (current, potential shield-gas, etc.). The effects of electrode type (solid, hollow, or shaped solid or hollow) were also examined. The results of these observations are discussed in more detail in the results section.

Weld Procedure

Two welding approaches were taken in this work. The first, maintaining constant heat input utilized at lower currents to determine what affect increasing current under constant heat input had on puddle formation (and subsequently bead morphology). Using both solid and hollow electrodes in argon and argon-helium mixtures, weldments were made to determine these effects on bead morphology. Weld parameters are listed in Table III and electrode configurations are shown in figure 12.

The second approach, maintaining constant travel speed, was used at low and high current ranges to determine what

TABLE III Constant Heat Input Weld Parameters

<u>CURRENT</u> <u>(AMPERES)</u>	<u>TYPE</u>	<u>SHIELD GAS</u>	<u>ELECTRODE</u>
100	DC	ARGON	SOLID
150	DC	ARGON	SOLID
175	DC	ARGON	SOLID
200	DC	ARGON	SOLID
225	DC	ARGON	SOLID
250	DC	ARGON	SOLID
275	DC	ARGON	SOLID
300	DC	ARGON	SOLID
100	DC	ARGON	HOLLOW
150	DC	ARGON	HOLLOW
175	DC	ARGON	HOLLOW
200	DC	ARGON	HOLLOW
225	DC	ARGON	HOLLOW
250	DC	ARGON	HOLLOW
275	DC	ARGON	HOLLOW
300	DC	ARGON	HOLLOW
150	DC	75ArHe	SOLID
200	DC	75ArHe	SOLID
250	DC	75ArHe	SOLID
300	DC	75ArHe	SOLID
150	DC	75ArHe	HOLLOW
200	DC	75ArHe	HOLLOW
250	DC	75ArHe	HOLLOW
300	DC	75ArHe	HOLLOW
150	DC	25ArHe	HOLLOW
200	DC	25ArHe	HOLLOW
250	DC	25ArHe	HOLLOW
300	DC	25ArHe	HOLLOW
100	AC	ARGON	SOLID
150	AC	ARGON	SOLID
200	AC	ARGON	SOLID
250	AC	ARGON	SOLID
100	AC	ARGON	HOLLOW
150	AC	ARGON	HOLLOW
200	AC	ARGON	HOLLOW
250	AC	ARGON	HOLLOW

TABLE III (continued)

<u>CURRENT</u> <u>(AMPERES)</u>	<u>TYPE</u>	<u>SHIELD GAS</u>	<u>ELECTRODE</u>
100	AC	75ArHe	SOLID
150	AC	75ArHe	SOLID
200	AC	75ArHe	SOLID
250	AC	75ArHe	SOLID
100	AC	75ArHe	HOLLOW
150	AC	75ArHe	HOLLOW
200	AC	75ArHe	HOLLOW
100	AC	25ArHe	HOLLOW
150	AC	25ArHe	HOLLOW
200	AC	25ArHe	HOLLOW

effect increasing current at constant travel speed had on puddle formation and arc stability. Shaped and unshaped electrodes were used in the previously mentioned gases. Weld parameters used are listed in Table IV and figure 12 shows the electrode configurations used.

Standard GTAW procedures were followed in this study to make "bead-on-bar" welds. The weld samples were grit blasted to remove all evidence of the surface oxide present on the samples at receipt. In addition, the samples were solvent cleaned using acetone until a clean wipe resulted from wiping the surface. The samples were then placed into position for welding.

The power supply and water were turned on, the electrode gap and stickout were adjusted, and the shield gas flow and type were adjusted to yield a flow of 40 cfh (1.13 cmh). Shield gas was flower in the normal manner (through a shield cup) and not through the electrode hollow. Electrode gap and stickout were set at 5/32 inch (4mm) for all welds completed in this study.

Metallographic Procedure

Metallographic preparation of the welds was accomplished using standard practice. Each test bar was sectioned in three places (yielding four data points per weld measurement

TABLE IV Constant Travel Speed Weld Parameters

<u>CURRENT</u> <u>(AMPERES)</u>	<u>TYPE</u>	<u>T. SPEED</u>	<u>SHIELD GAS</u>	<u>ELECTRODE</u>
100	DC	10 ipm	75ArHe	SOLID
150	DC	10	75ArHe	SOLID
200	DC	10	75ArHe	SOLID
250	DC	10	75ArHe	SOLID
300	DC	10	75ArHe	SOLID
350	DC	10	75ArHe	SOLID
400	DC	10	75ArHe	SOLID
450	DC	10	75ArHe	SOLID
500	DC	10	75ArHe	SOLID
100	DC	10	75ArHe	HOLLOW
150	DC	10	75ArHe	HOLLOW
200	DC	10	75ArHe	HOLLOW
250	DC	10	75ArHe	HOLLOW
300	DC	10	75ArHe	HOLLOW
350	DC	10	75ArHe	HOLLOW
400	DC	10	75ArHe	HOLLOW
450	DC	10	75ArHe	HOLLOW
500	DC	10	75ArHe	HOLLOW
100	DC	10	25ArHe	SOLID
150	DC	10	25ArHe	SOLID
200	DC	10	25ArHe	SOLID
250	DC	10	25ArHe	SOLID
300	DC	10	25ArHe	SOLID
350	DC	10	25ArHe	SOLID
400	DC	10	25ArHe	SOLID
450	DC	10	25ArHe	SOLID
500	DC	10	25ArHe	SOLID
100	DC	10	25ArHe	HOLLOW
150	DC	10	25ArHe	HOLLOW
200	DC	10	25ArHe	HOLLOW
250	DC	10	25ArHe	HOLLOW
300	DC	10	25ArHe	HOLLOW
350	DC	10	25ArHe	HOLLOW
400	DC	10	25ArHe	HOLLOW
450	DC	10	25ArHe	HOLLOW
500	DC	10	25ArHe	HOLLOW
100	DC	10	ARGON	90 SBLUNT
150	DC	10	ARGON	90 SBLUNT
200	DC	10	ARGON	90 SBLUNT
250	DC	10	ARGON	90 SBLUNT
300	DC	10	ARGON	90 SBLUNT

TABLE IV (continued)

CURRENT (AMPERES)	TYPE	T. SPEED	SHIELD GAS	ELECTRODE
350	DC	10 ipm	ARGON	90 SBLUNT
400	DC	10	ARGON	90 SBLUNT
450	DC	10	ARGON	90 SBLUNT
500	DC	10	ARGON	90 SBLUNT
100	DC	10	ARGON	90 HOLLOW
150	DC	10	ARGON	90 HOLLOW
200	DC	10	ARGON	90 HOLLOW
250	DC	10	ARGON	90 HOLLOW
300	DC	10	ARGON	90 HOLLOW
350	DC	10	ARGON	90 HOLLOW
400	DC	10	ARGON	90 HOLLOW
450	DC	10	ARGON	90 HOLLOW
500	DC	10	ARGON	90 HOLLOW
100	DC	10	75ArHe	150SBLUNT
150	DC	10	75ArHe	150SBLUNT
200	DC	10	75ArHe	150SBLUNT
250	DC	10	75ArHe	150SBLUNT
300	DC	10	75ArHe	150SBLUNT
350	DC	10	75ArHe	150SBLUNT
400	DC	10	75ArHe	150SBLUNT
450	DC	10	75ArHe	150SBLUNT
500	DC	10	75ArHe	150SBLUNT
100	DC	10	75ArHe	150HOLLOW
150	DC	10	75ArHe	150HOLLOW
200	DC	10	75ArHe	150HOLLOW
250	DC	10	75ArHe	150HOLLOW
300	DC	10	75ArHe	150HOLLOW
350	DC	10	75ArHe	150HOLLOW
400	DC	10	75ArHe	150HOLLOW
450	DC	10	75ArHe	150HOLLOW
500	DC	10	75ArHe	150HOLLOW
100	DC	10	25ArHe	150SBLUNT
150	DC	10	25ArHe	150SBLUNT
200	DC	10	25ArHe	150SBLUNT
250	DC	10	25ArHe	150SBLUNT
300	DC	10	25ArHe	150SBLUNT
350	DC	10	25ArHe	150SBLUNT
400	DC	10	25ArHe	150SBLUNT
450	DC	10	25ArHe	150SBLUNT
500	DC	10	25ArHe	150SBLUNT

TABLE IV (continued)

<u>CURRENT</u> (AMPERES)	<u>TYPE</u>	<u>T. SPEED</u>	<u>SHIELD GAS</u>	<u>ELECTRODE</u>
100	DC	10 ipm	25ArHe	150HOLLOW
150	DC	10	25ArHe	150HOLLOW
200	DC	10	25ArHe	150HOLLOW
250	DC	10	25ArHe	150HOLLOW
300	DC	10	25ArHe	150HOLLOW
350	DC	10	25ArHe	150HOLLOW
400	DC	10	25ArHe	150HOLLOW
450	DC	10	25ArHe	150HOLLOW
500	DC	10	25ArHe	150HOLLOW
100	DC	10	75ArHe	90 SBLUNT
150	DC	10	75ArHe	90 SBLUNT
200	DC	10	75ArHe	90 SBLUNT
250	DC	10	75ArHe	90 SBLUNT
300	DC	10	75ArHe	90 SBLUNT
350	DC	10	75ArHe	90 SBLUNT
400	DC	10	75AAHe	90 SBLUNT
450	DC	10	75AAHe	90 SBLUNT
500	DC	10	75ArHe	90 SBLUNT
100	DC	10	75ArHe	90 HOLLOW
150	DC	10	75ArHe	90 HOLLOW
200	DC	10	75ArHe	90 HOLLOW
250	DC	10	75ArHe	90 HOLLOW
300	DC	10	75ArHe	90 HOLLOW
350	DC	10	75ArHe	90 HOLLOW
400	DC	10	75ArHe	90 HOLLOW
450	DC	10	75ArHe	90 HOLLOW
500	DC	10	75ArHe	90 HOLLOW
100	DC	10	25ArHe	90 SBLUNT
150	DC	10	25ArHe	90 SBLUNT
200	DC	10	25ArHe	90 SBLUNT
250	DC	10	25ArHe	90 SBLUNT
300	DC	10	25ArHe	90 SBLUNT
350	DC	10	25ArHe	90 SBLUNT
400	DC	10	25ArHe	90 SBLUNT
450	DC	10	25ArHe	90 SBLUNT
500	DC	10	25ArHe	90 SBLUNT
100	DC	10	25ArHe	90 HOLLOW
150	DC	10	25ArHe	90 HOLLOW
200	DC	10	25ArHe	90 HOLLOW
250	DC	10	25ArHe	90 HOLLOW
300	DC	10	25ArHe	90 HOLLOW

TABLE IV (continued)

<u>CURRENT</u> <u>(AMPERES)</u>	<u>TYPE</u>	<u>T. SPEED</u>	<u>SHIELD GAS</u>	<u>ELECTRODE</u>
350	DC	10 ipm	25ArHe	90 HOLLOW
400	DC	10	25ArHe	90 HOLLOW
450	DC	10	25ArHe	90 HOLLOW
500	DC	10	25ArHe	90 HOLLOW

listed in Table A1-1 or A1-2) and ground successively through 80, 120, 320, and 600 grit paper. The samples were then etched in heated (approximately 160°F (71°C)) Marbles reagent and were etched for 20 to 30 seconds. This brought the weld nugget and heat affected zone out for measurements of the bead morphology.

Test Matrix

Phase I Constant Heat Input

Arc potential-current characteristic curves were obtained for currents ranging from 100 to 300 Amperes in AC and 150 to 300 Amperes for DC. The arc potential-current plots describe the nature of the arc behavior. This data was used in determining the travel speed to be used for each of the current settings to obtain welds produced with the same heat input per the equation, $\text{heat input} = I \times V/S$; where I is the current in Amperes, V is the potential, and S is the travel speed in inches per second. Data was obtained for all welding conditions including each electrode configuration (solid or hollow) and shield gas combination as noted in Table III.

Phase II Constant Travel Speed- Unshaped Electrodes

Arc potential/current characteristic curves were obtained for currents ranging from 100 to 500 Amperes for DC

welding. Data was obtained for all welding conditions including each electrode configuration (solid or hollow) and shield gas combination. Unshaped (180 degree) solid and hollow electrodes were used in this phase. The weld parameters used are listed in Table IV.

Phase III Constant Travel Speed- Shaped Electrodes

Arc potential-current characteristic curves were obtained for currents ranging from 100 to 500 Amperes for DC welding. Two different electrode shapes were used (90 and 150 degree included angle) for both solid and hollow. The shaped solid electrodes had a 3/32 inch (2.3mm) truncation on the tip.

Using the above (all three phases), welds were made on each of the nine inch bar samples making attempts to keep the heat input constant at about 24,000 joules/inch (for constant heat input welds) or constant travel speed (10 ipm (4.2 mm/sec)). Three welds were made on each piece as shown in figure 12 (at currents above 400 Amperes, two welds per bar were made) per side of bar.

Arc potential-current characteristic data was gathered in all three phases and is presented in the Results section. In addition, arc characteristic changes (normal to cathode spot mode) and bead morphology (penetration, bead width, p/w,

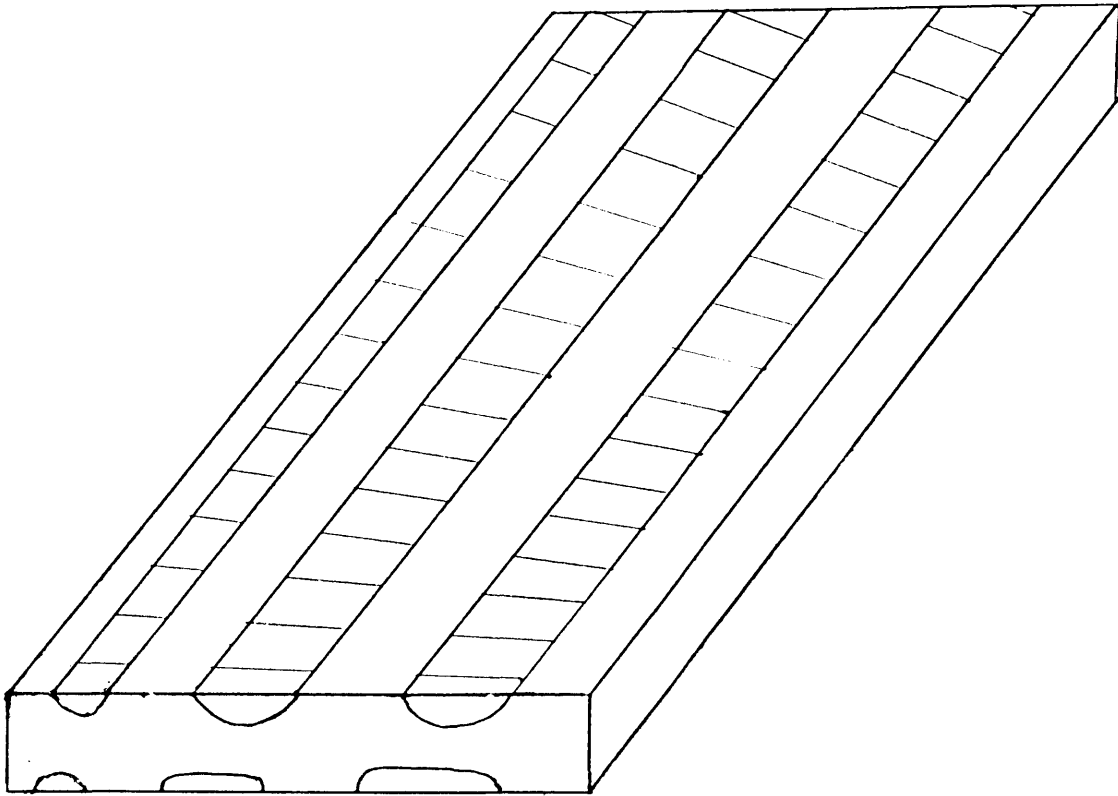


FIGURE 13 Orientation of "Bead-on Plate" Weldments

and melt area) were recorded/measured for each of the completed welds. The weld parameters used in all three phases are listed in Table III and IV.

Weld Cross-Section Measurements

Weld bead morphology (penetration, melt area, bead width, and p/w) was measured by sectioning each weld; in a stable weld area, and preparing each sample as previously outlined. Photographs at 4 to 20X were taken of each weld to aid in making the required measurements. The data obtained was an average of four data points. Melt area was determined by cutting the weld nugget out of each picture and weighing it. Knowing the weight of the weld nugget and dividing it by the weight of a given area of photo yields the melt area.

Arc Characterization

Arc characterization has been investigated by many investigators (2,5,12,13,29). The arc operating mode (normal or cathode spot) as well as the arc stability were determined. It is generally determined visually, visually with the aid of a high-speed camera, or with the use of an oscilloscope. A high speed strip chart recorder (visicorder) was utilized in the present study. All arcs for the various conditions were visually characterized and the observations are described in the Results section.

RESULTS

Constant Heat Input

Constant heat input was utilized initially during the tests as it provides a good understanding of the weld under conditions conducive to a constant weld pool size.

Measurements were made on each weldment to determine penetration, bead width, penetration to bead width ratio (p/w), and melt area for each of the forty-six welds. These measurements are listed in Table A1-1. Figure 14 and 15 show the typical weld profiles seen under DC and AC conditions with pure argon as the shield gas. The two argon-helium gas mixtures yielded similiar profiles but are not shown.

Bead-on-plate welds were made on Custom 630 stainless steel bar with variations in current and shield gas. Travel speed was also varied to maintain constant heat input conditions for each weld.

DC Constant Heat Input

The arc potential-current characteristic curves for weldments made using unshaped solid and hollow two-percent thoriated tungsten electrodes, in two argon-helium shield gas mixtures, under DC conditions are shown in figure 16.

Examination of this figure indicates that increasing



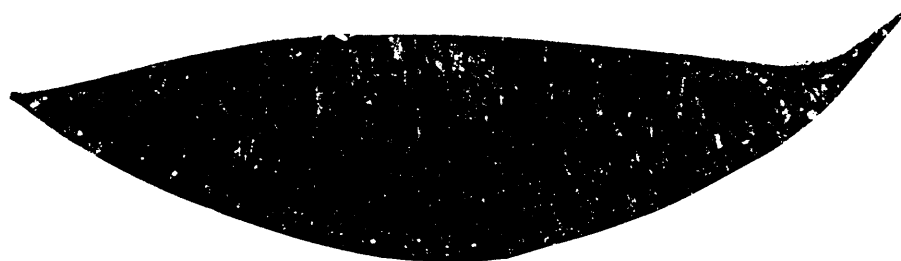
150 Amperes



200 Amperes



250 Amperes



290 Amperes

FIGURE 14 Weld Profiles For DC Constant Heat
Input Welds With Solid Electrode
in Argon 11.4X



100 Amperes



150 Amperes



200 Amperes



230 Amperes

FIGURE 15 Weld Profiles For AC Constant Heat Input Welds With Solid Electrode in Argon 11.4X

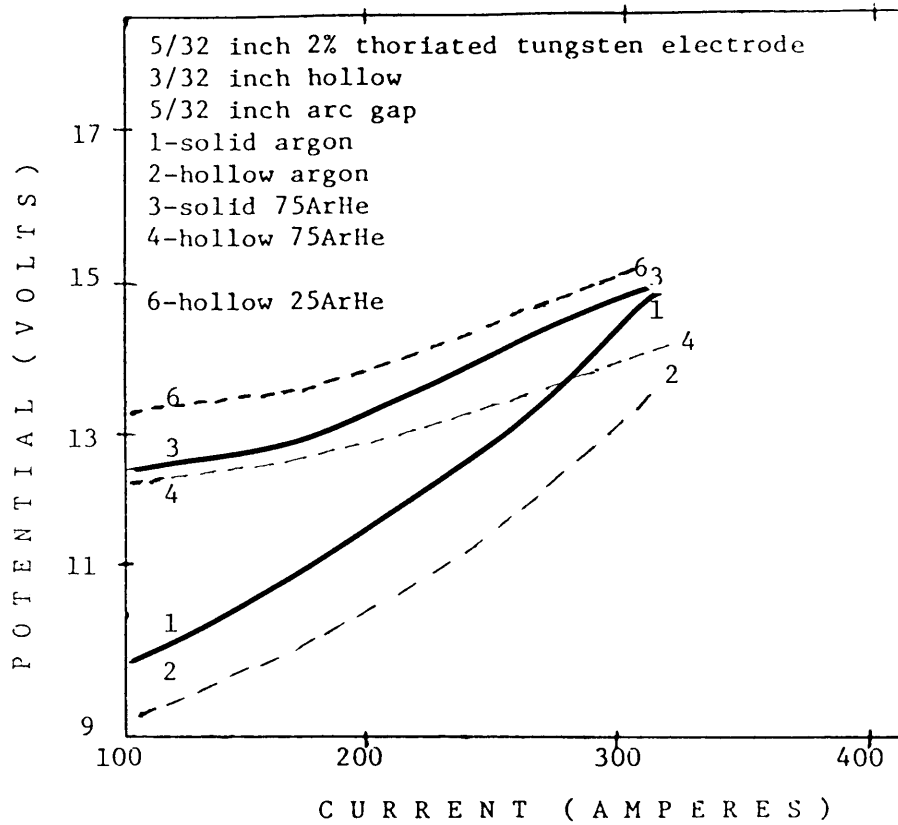


FIGURE 16 Arc Potential-Current Characteristic Curve DC Constant Heat Input Welds.

helium content in the shield gas increases the arc potential for a given current as well as decreasing the slope of the curve. It is also seen that the arc potential using a solid electrode is greater than that for a hollow electrode at comparable current levels in pure argon. This difference is much smaller between the two electrodes in 75ArHe gas mixtures and is expected to be nearly identical in 25ArHe.

Examination of the weld cross-sections yielded the current-penetration curves for the above conditions as seen in figure 17. No benefits were seen when utilizing the hollow electrode over the solid electrode in terms of penetration up to 300 Amperes. Penetration for both electrodes decreased at a rapid rate in argon below 200 Amperes while the other two argon-helium gas mixtures did not show this trend.

It is also interesting to note the characteristic shape of the curve. Penetration increased to a maximum, decreased to a minimum and began increasing again with increasing current. Both electrodes exhibited this phenomenon and electrode type (solid or hollow) had no affect on the location of the maxima/minima points. Shield gas did have an affect on the location of these characteristic points. Increasing helium content shifted the maxima/minima points to the left for hollow electrode GTA and had no affect on solid

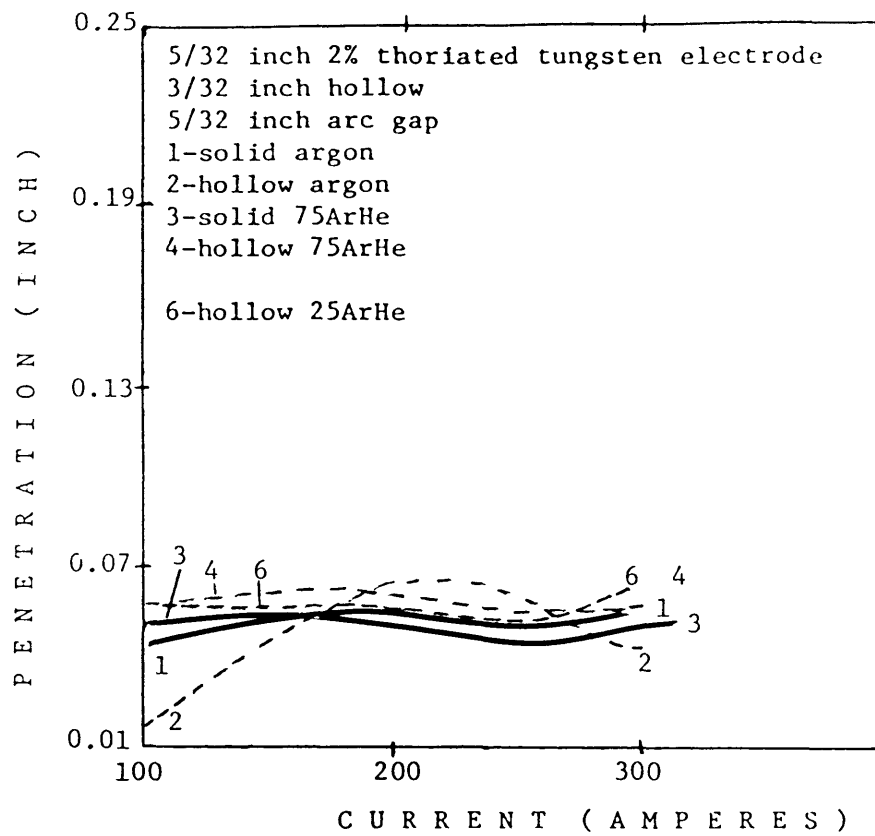


FIGURE 17 Current versus Penetration for DC Constant Heat Input Welds

electrode GTA.

Cross-sectional measurements of the weldments also yielded penetration to bead width ratio (p/w) and melt area measurements. Melt area measurements are a good approximate measure of the arcs melt efficiency. As was seen in the penetration plots discussed earlier, the current versus penetration to bead width ratio (p/w) also showed the characteristic maxima/minima points as seen in figure 18. Again, shield gas had the greater affect than electrode type on the location of these maxima/minima points. Increased helium spread the curves such that the initial maxima was shifted to the left and the minima was shifted to the right of the points seen in pure argon. Increased helium content also had the tendency to decrease p/w for electrodes at currents above 200 Amperes (and to 300 Amperes), although p/w was relatively unaffected by electrode type.

Melt area was not affected by either shield gas composition or electrode type utilized up to 300 Amperes as seen in figure 19. Maxima/minima points were also seen, but not to the degree seen in the earlier plots. The hollow electrode exhibited a stronger tendency towards maxima/minima points than the solid electrode.

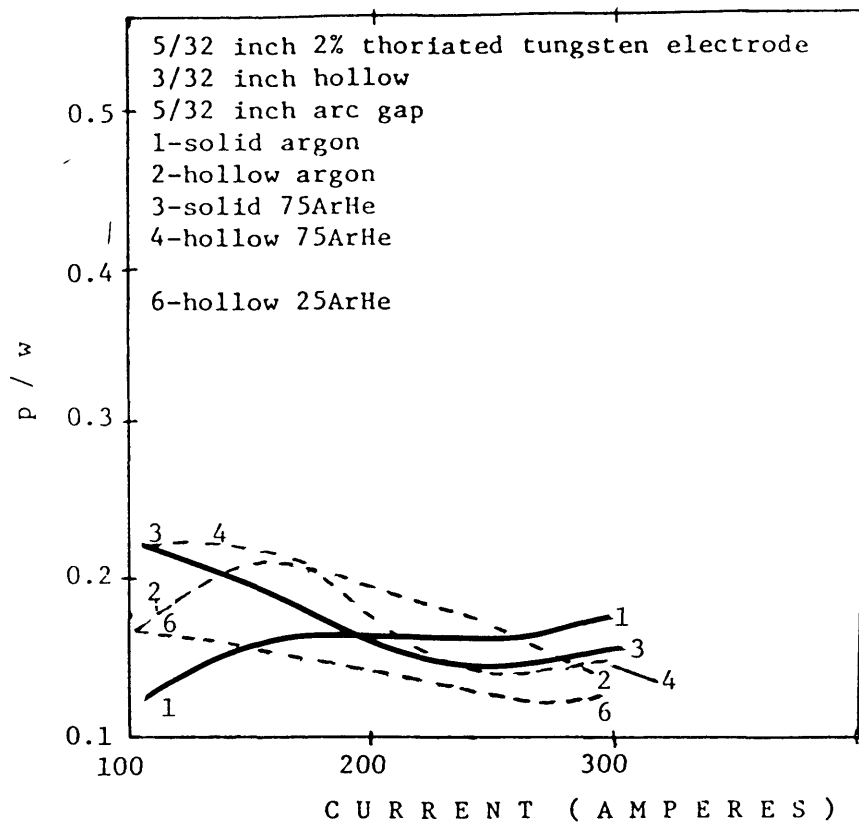


FIGURE 18 Current versus p/w for DC Constant Heat Input Welds

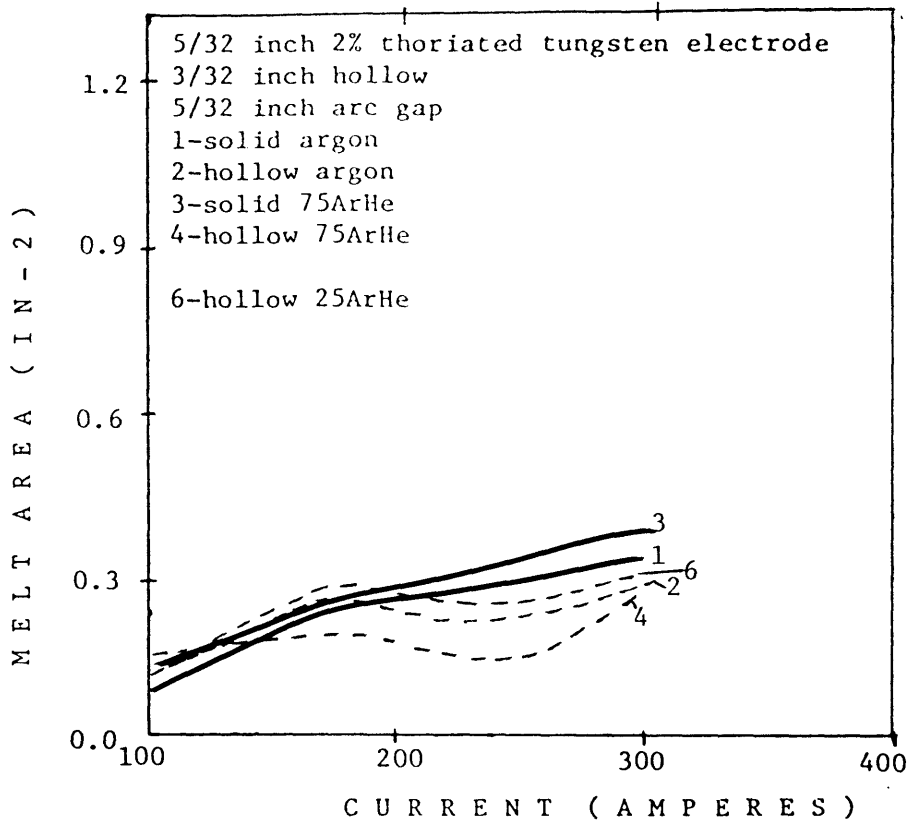


Figure 19 Current versus Melt Area for DC Constant Heat Input Welds

AC Constant Heat Input

The arc potential-current characteristic curves for weldments made using unshaped solid and hollow two-percent thoriated tungsten electrodes, in argon and two argon-helium shield gas mixtures, under AC weld conditions are shown in figure 20.

The arc potential for both electrodes under AC was significantly greater than that seen in DC welding. Examination of this figure indicates that increasing helium content in the shield gas increases the arc potential for a given current. Increased helium content in the shield gas and current lead to a greater arc potential difference between the hollow and solid electrodes. Little difference can be seen in the arc potential between the two electrode types in pure argon.

Examination of the weld cross-sections yielded the current-penetration curves for the above conditions as seen in figure 21. No benefits were seen when utilizing the hollow electrode over the solid electrode in terms of penetration up to 250 Amperes.

It is also interesting to note the characteristic shape of the curve. Penetration increased to a maximum, decreased to a minimum and began increasing again with increasing current. Both electrodes exhibited this phenomenon

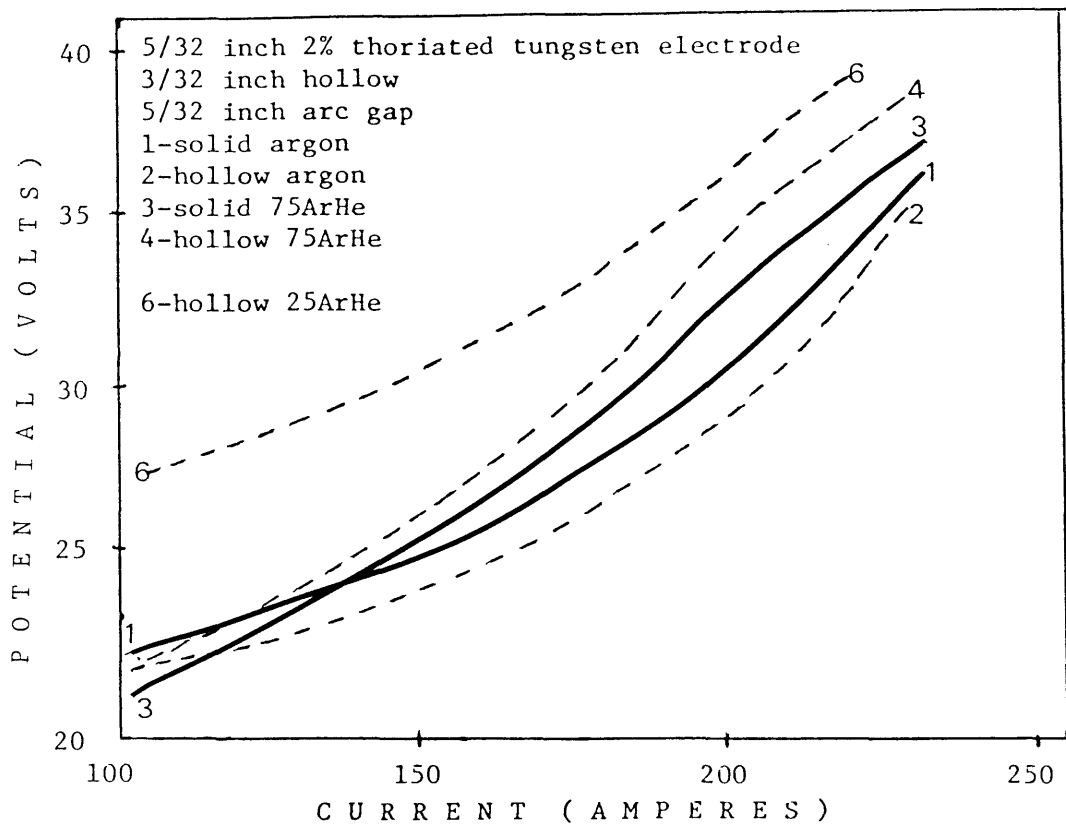


FIGURE 20 Arc Potential-Current Characteristic Curve AC Constant Heat Input Welds.

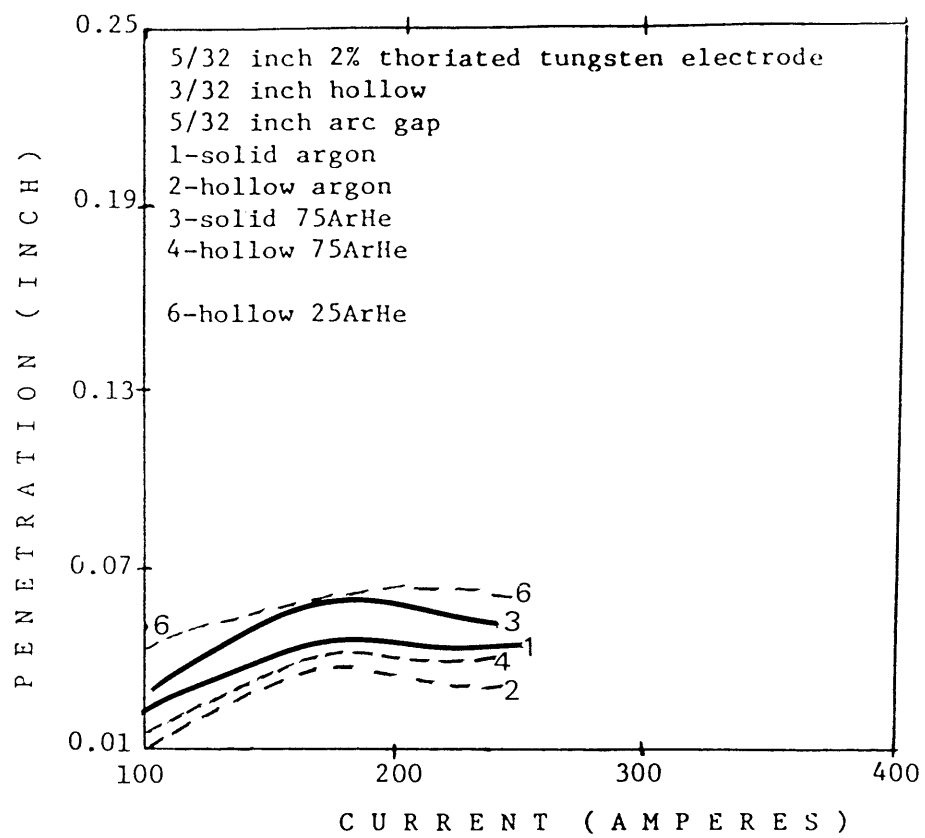


FIGURE 21 Current versus Penetration for AC Constant Heat Input Welds

and electrode type (solid or hollow) had no effect on the location of the maxima/minima points. Shield gas did have an affect on their location. Increasing helium content shifted the maxima/minima points to the left for hollow electrode GTA and had no affect on solid electrode GTA.

Weld cross-section measurements also yielded penetration to bead width ratio (p/w) and melt area measurements. As was seen in the penetration plots discussed earlier, the current versus penetration to bead width ratio (p/w) also showed the characteristic maxima/minima points as seen in figure 22. This characteristic was not as prominent under AC weld conditions as was seen under DC conditions. Again, shield gas had the greater affect than electrode type on the location of these maxima/minima points although neither had a significant influence on p/w for currents up to 250 Amperes. Increased helium spread the curves such that the initial maxima was shifted to the left and the minima was shifted to the right of the points seen in pure argon. Increased helium content also had the tendency to decrease p/w for electrodes at currents above 200 Amperes although p/w was relatively unaffected by electrode type.

Melt area was not affected by electrode type, but shield gas did have an affect up to 250 Amperes as can be seen in figure 23. Increased helium led to increased melt

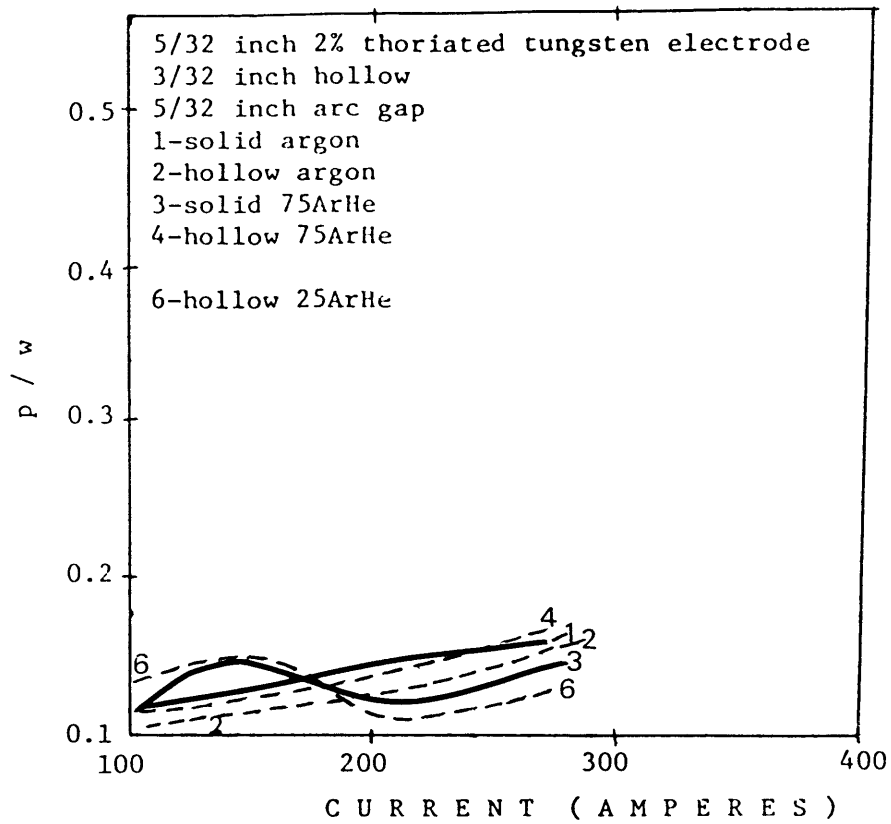


FIGURE 22 Current versus p/w for AC Constant Heat Input Welds

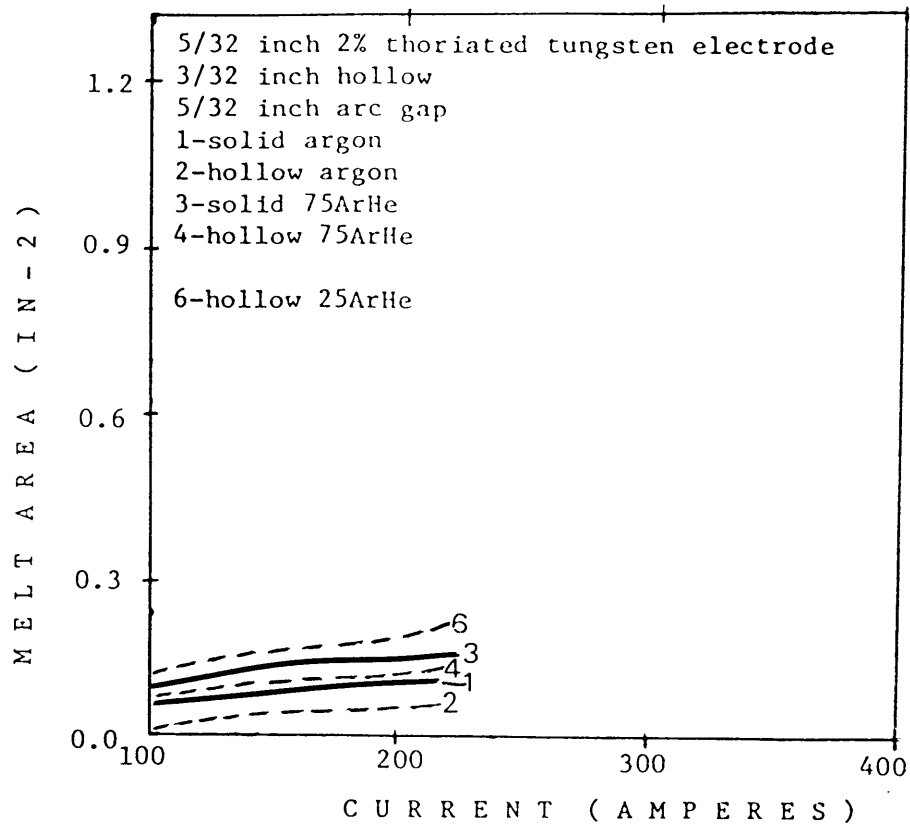


Figure 23 Current versus Melt Area for AC Constant Heat Input Welds

area or melt efficiency. However, maxima/minima points were not seen.

Constant Travel Speed

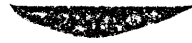
Constant travel speed was utilized in the second set of welds using both shaped and unshaped (180 degree) electrodes because it was believed that increasing weld pool size would also yield an accurate assessment of the effectiveness while utilizing a hollow, rather than a solid tungsten electrode.

Bead-on-plate welds were made on Custom 630 stainless steel bar with variations in current and shield gas. Travel speed was maintained constant at 10 ipm (4.2mm/sec).

Measurements were made on each of the weldments determine penetration, bead width, penetration to bead width ratio (p/w) and melt area for each of the welds. These measurements are listed in Table A2-1. Figure 24 shows the typical weld bead profiles in 25ArHe DC weld condition using unshaped (180) solid electrodes. The other argon-helium shield gas mixture showed a similiar profiles, but these welds are not shown.

Unshaped Electrode

The arc potential-current characteristic curves for weldments made using unshaped (180) solid and hollow two-percent thoriated tungsten electrodes, in two argon-helium



100 Amperes



150 Amperes



200 Amperes



250 Amperes



300 Amperes

FIGURE 24 Typical Weld Profile for DC Constant Travel Speed Welds in 25ArHe Using Shaped Solid Electrode GTAW With 150 Degree Electrode Tip. 4X



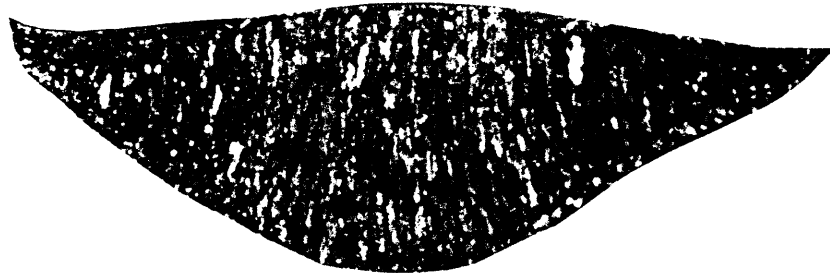
350 Amperes



400 Amperes



450 Amperes



500 Amperes

FIGURE 24 con.

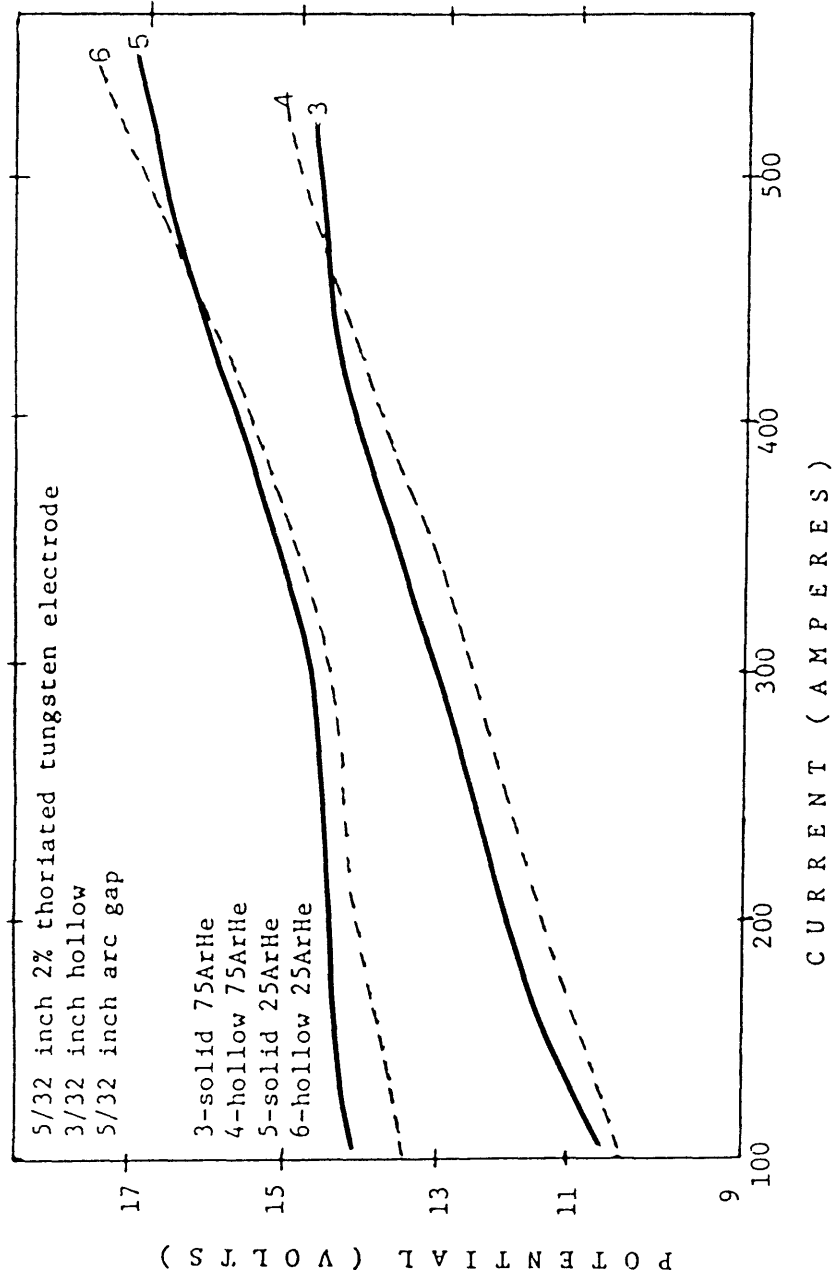


FIGURE 25 Arc Potential-Current Characteristic Curve DC Constant Travel Speed Welds Using Unshaped Electrode.

shield gas mixtures, under DC weld conditions are shown in figure 25. It can be seen that arc potential increases with increasing current and increased helium content in the shield gas. The slopes of the curves are approximately equal with the 25ArHe being raised 2.5 to 3.0 volts above that of the 75ArHe. Both electrode types exhibited similar arc potentials in their respective gas mixtures between 100 and 500 Amperes.

Examination of the weld cross-sections yielded the penetration-current curves for the above conditions as seen in figure 26. Increased helium in the shield gas yields a slight increase in penetration. This is particularly true at low currents (100 to 200 Amperes) and high currents (400 to 500 Amperes). Little difference in penetration existed between the two electrode types in the current range studied.

As previously noted, the characteristic maxima, minima, steady rise in penetration with increasing current can also be seen in these plots. Increased helium content in the shield gas shifts these maxima/minima points to the right and leads to a greater penetration difference between the maxima and minima seen in the 75ArHe mixture.

Weld cross-section measurements also yielded penetration to bead width ratio (p/w) and melt area measurements. Examining figure 27, it can be seen that p/w goes through a

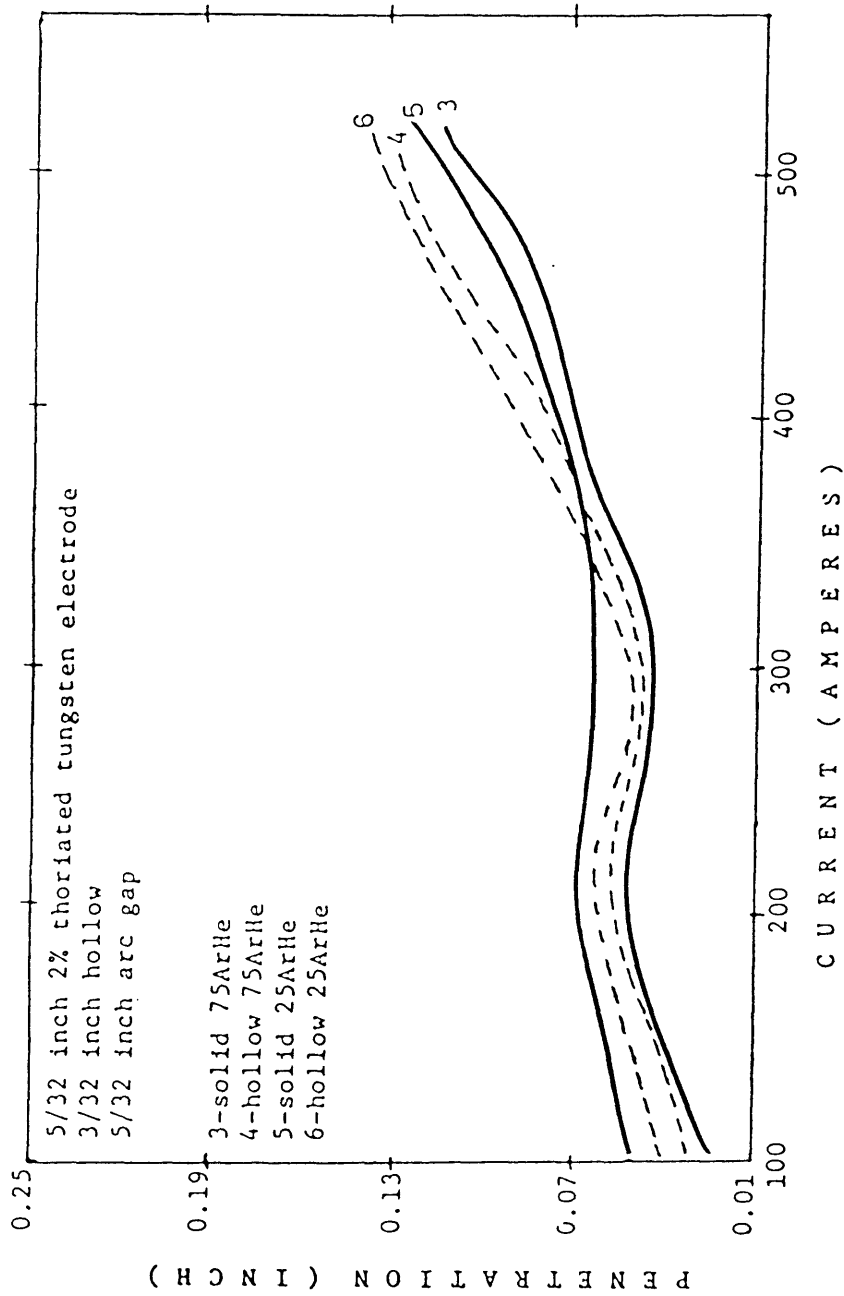


FIGURE 26 Current versus Penetration for DC Constant Travel Speed Welds Using Unshaped Electrodes.

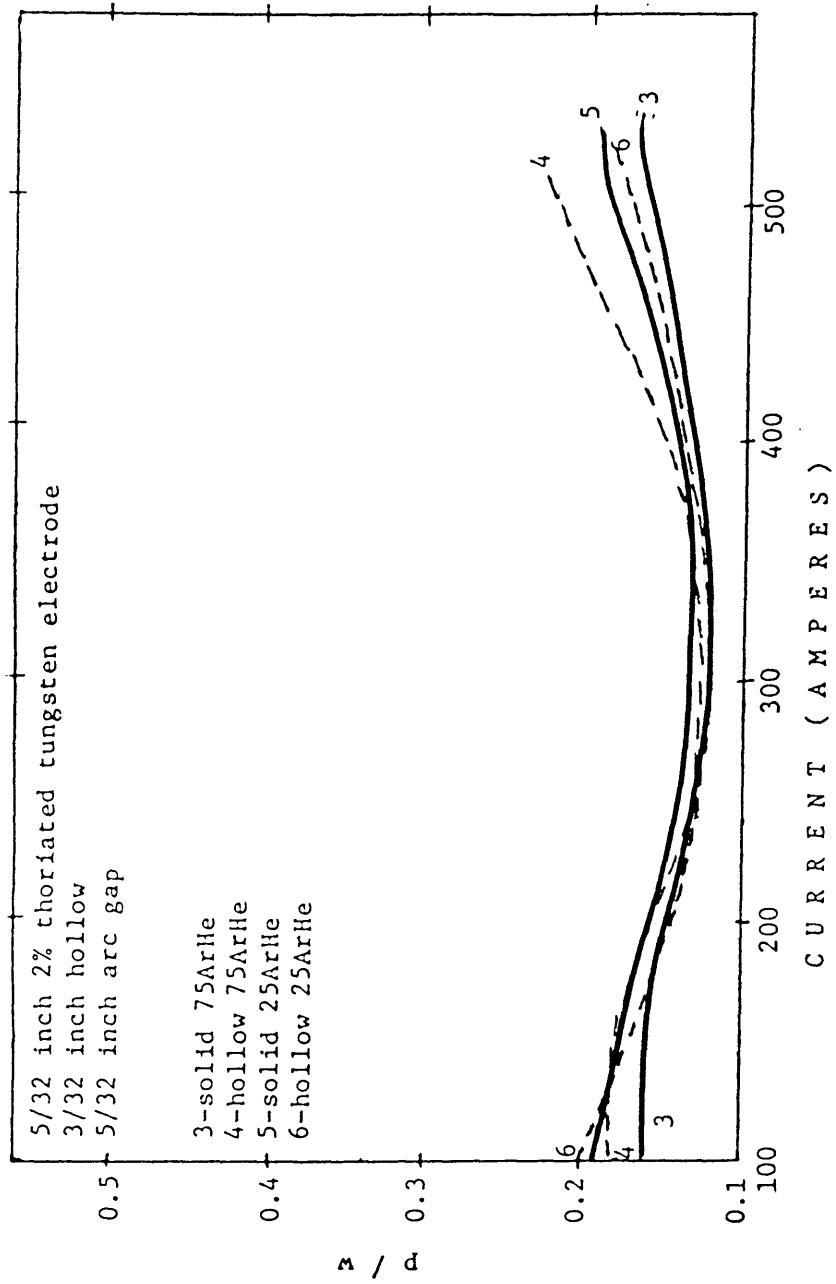


FIGURE 27 Current versus p/w for DC Constant Travel Speed Welds Using Unshaped Electrodes.

minima near the minima seen in the current-penetration plot (figure 26). It can also be seen that p/w is similar for both electrode types in both shield gas mixtures up to 400 Amperes. Above this, little difference in p/w is seen for welds in 25ArHe, but 75ArHe produces substantially better (and gradually increasing) p/w for hollow electrode GTAW.

Looking at figure 28, it can be seen that melt area for all conditions (both shield gas mixtures and electrode types) are the same for any given current up to 400 Amperes. Above 400 Amperes, shield gas tends to play a more important role in increased melt efficiency than electrode type. Hollow electrode GTAW melt efficiency is seen to be slightly better than that seen for solid electrode GTAW. The data to support each of the above figures can be seen in Table A1-2.

Shaped Electrode 150 Degree Tip

The current-arc potential characteristic curves for welds made using shaped solid and hollow two percent thoriated tungsten electrodes in argon and argon-helium gas mixtures under DC weld conditions are shown in figure 29. Two shapes were used, namely 150 and 90 degree included tip angles. A later section discusses weldments made utilizing 90 degree included tip angle electrodes.

It can be seen that arc potential increases with

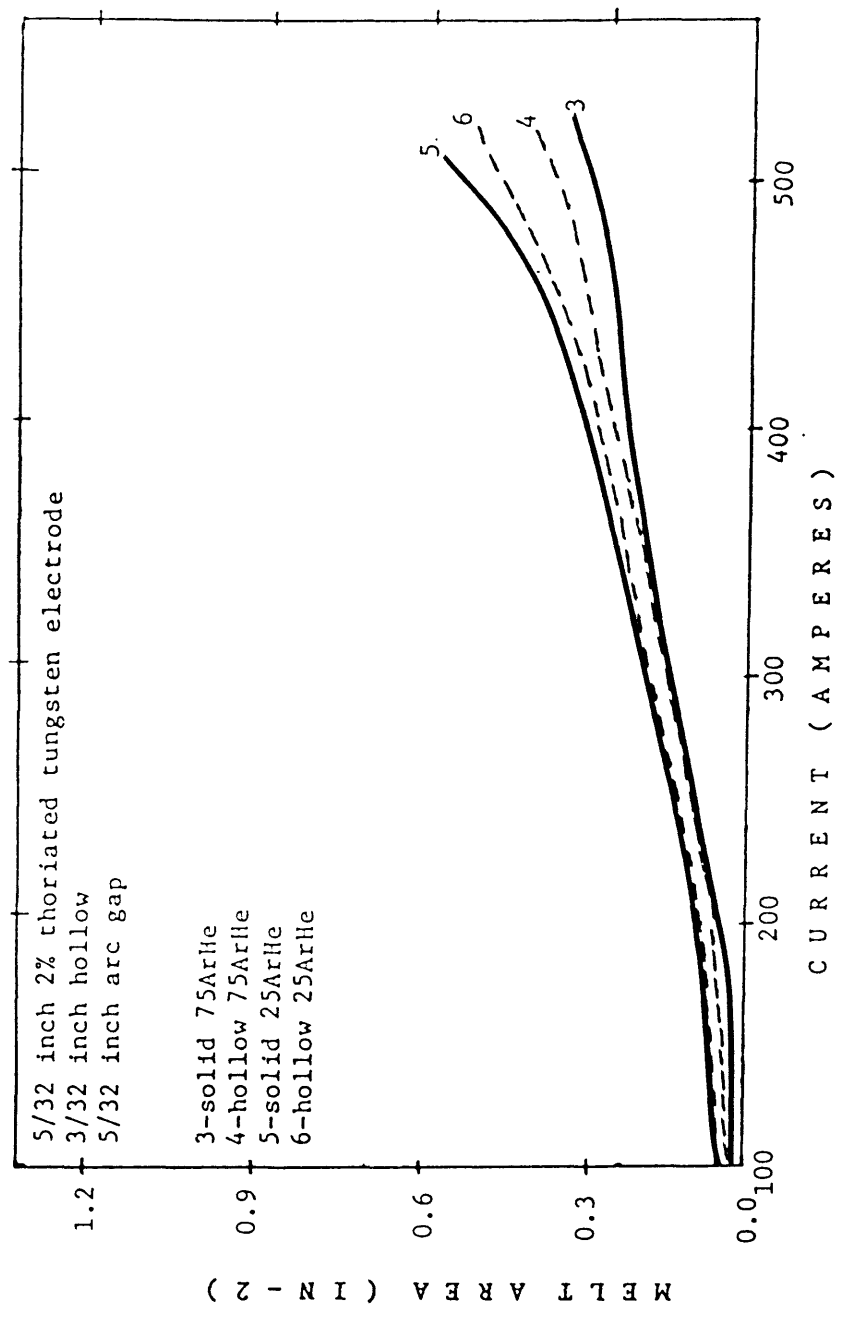


Figure 28 Current versus Melt Area for DC Constant Travel Speed Welds Using Unshaped Electrodes

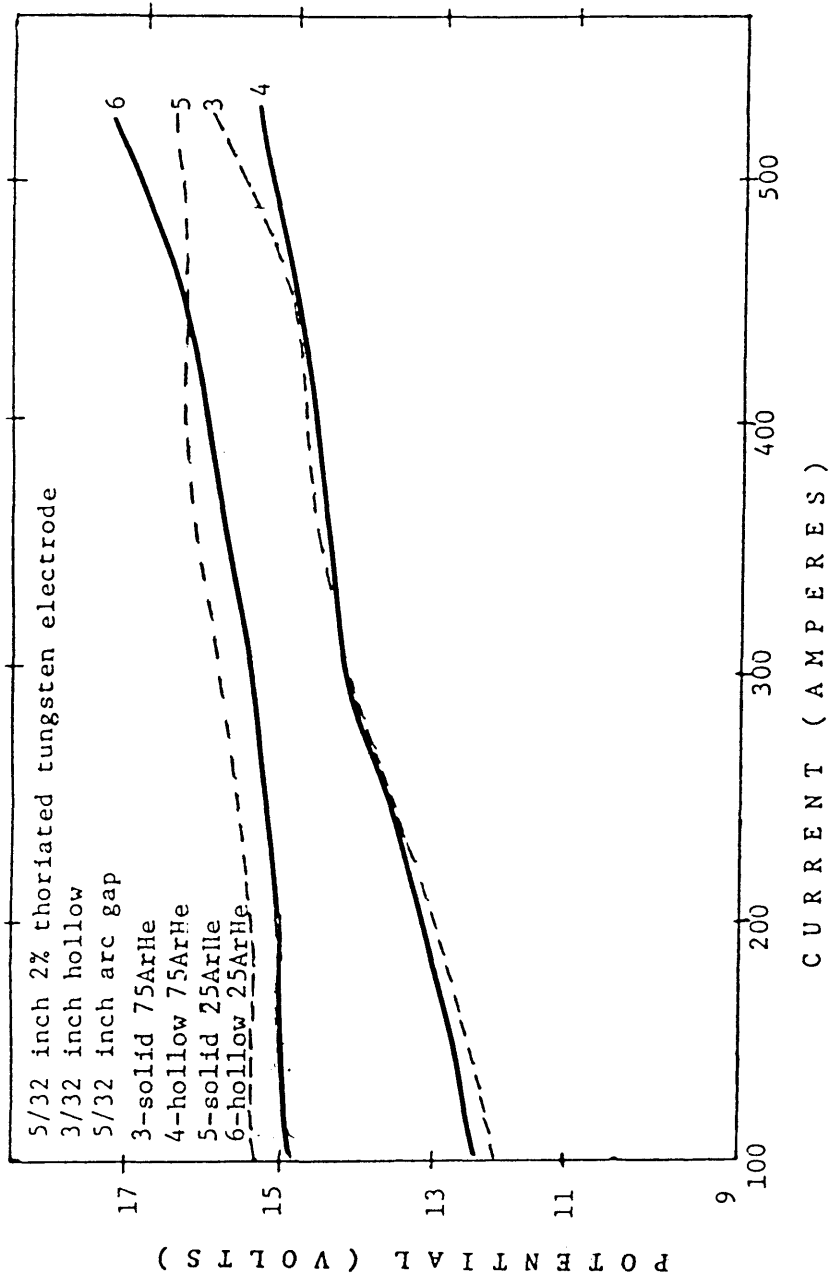


FIGURE 29 Arc Potential-Current Characteristic Curve DC Constant Travel Speed Welds Using 150 Degree Tip Electrodes.

increasing current and increased helium content in the shield gas. The slopes of the curves are approximately equal with the 25ArHe curve being raised 2.5 to 3.0 volts above that of the 75ArHe. Both electrode types exhibited similar arc potentials in their respective gas mixtures between 100 and 450 Amperes. At higher currents with the hollow electrode, the 75ArHe curve appears to converge with the 25ArHe curve. In addition, opposite trends are seen with the two electrodes. In 75ArHe, the hollow electrode arc potential begins increasing at a faster rate than that for the solid electrode. In 25ArHe, the opposite trend is seen. This penetration-current behavior is similar to that suggested by the Japanese (24).

Examination of the weld cross-sections yielded the penetration-current curves for the above conditions as seen in figure 30. Penetration increased with increasing current, except as noted when using solid and hollow electrodes with 150 degree included tip angle. Both shield gas and electrode type had little effect on penetration between 100 and 500 Amperes. The exception to this was the penetration data for hollow electrode GTAW using 75ArHe and no explanation is available for this vast improvement in penetration with the hollow electrode over weldments made with the solid electrode. The characteristic maxima/minima points were seen and increasing helium content led to a shift in the location of these

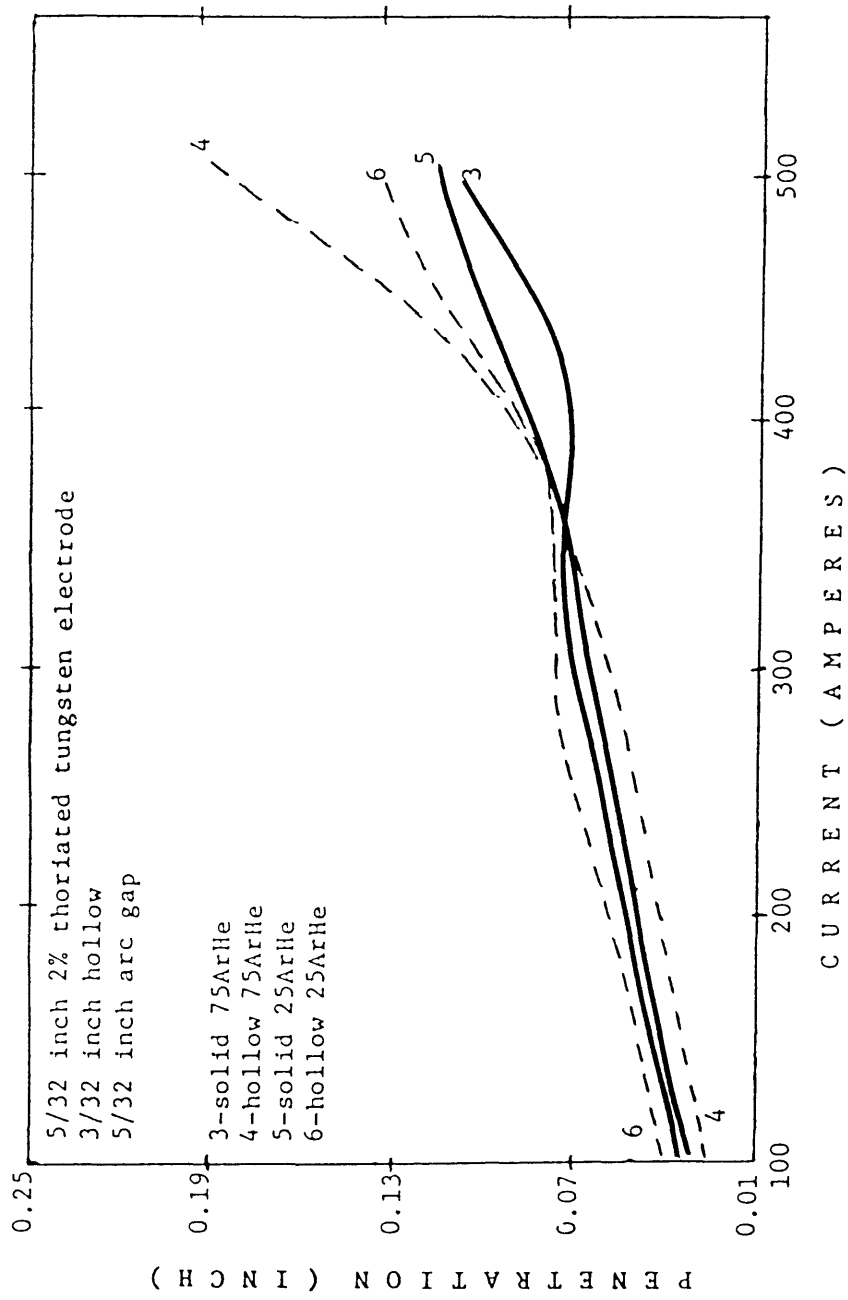


FIGURE 30 Current versus Penetration for DC Constant Travel Speed Welds Using 150 Degree Tip Electrodes.

points to the right for both electrodes.

Weld cross-section measurements also yielded penetration to bead width ratio (p/w) and melt area measurements. p/w remained nearly constant with increasing current except as noted when using solid and hollow electrodes with 150 degree included tip angle as shown in figure 31. Both shield gas and electrode type had little affect on p/w between 100 and 500 Amperes. The exception to this was the p/w data for hollow electrode GTAW using 75ArHe and no explanation is available for this behavior. No characteristic maxima/minima points were seen.

Figure 32 shows the melt area-current curve for 150 degree included tip angle electrodes. Shield gas had no affect on melt efficiency up to 300 Amperes, above this, shield gas had a significant affect on the melt efficiency. Melt efficiency increased with increasing current in 25ArHe at a faster rate than in 75ArHe. Electrode type had a minor affect on melt efficiency, but this trend rapidly decreased with increasing helium in the shield gas.

Shaped Electrode 90 Degree Tip

It can be seen in figure 33 that arc potential increases with increasing current and increased helium content in the shield gas. The slopes of the curves are nearly

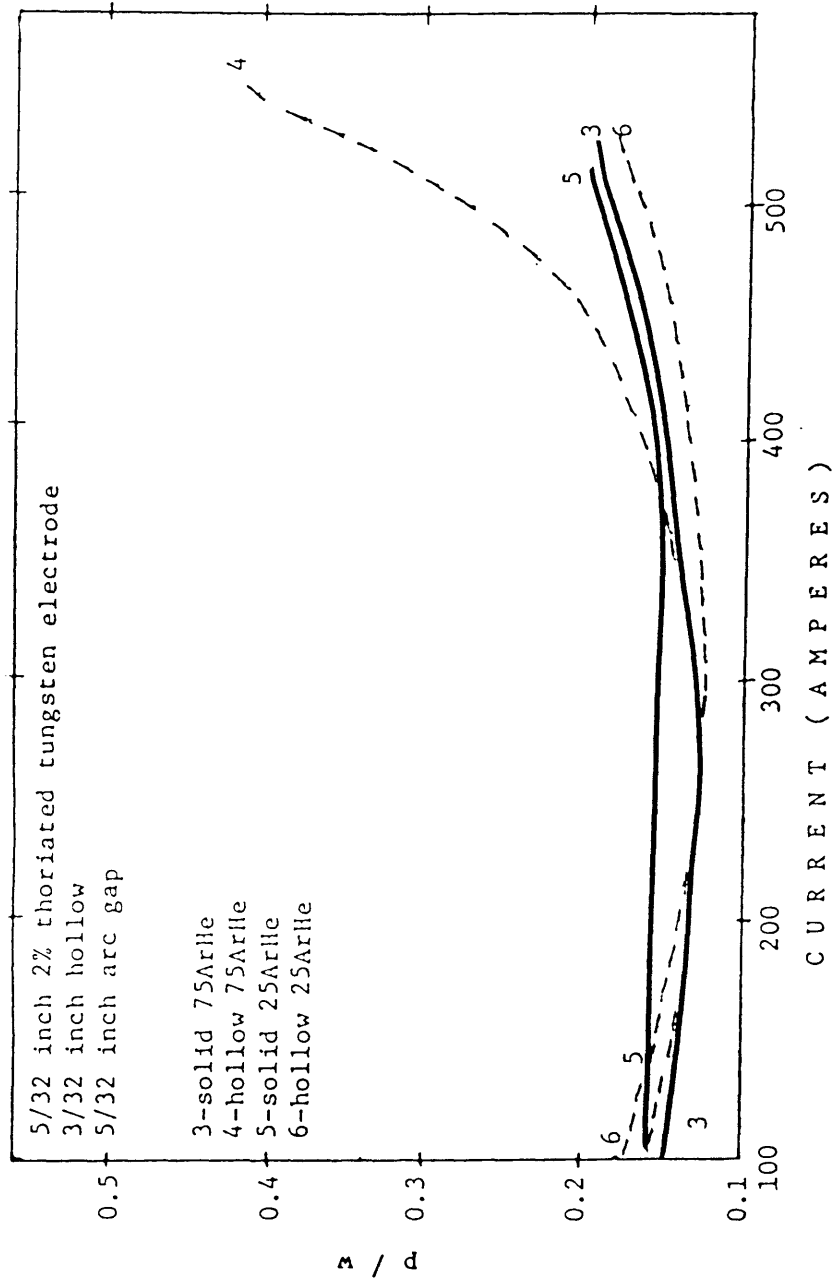


FIGURE 31 Current versus p/w for DC Constant Travel Speed Welds Using 150 Degree Tip Electrodes.

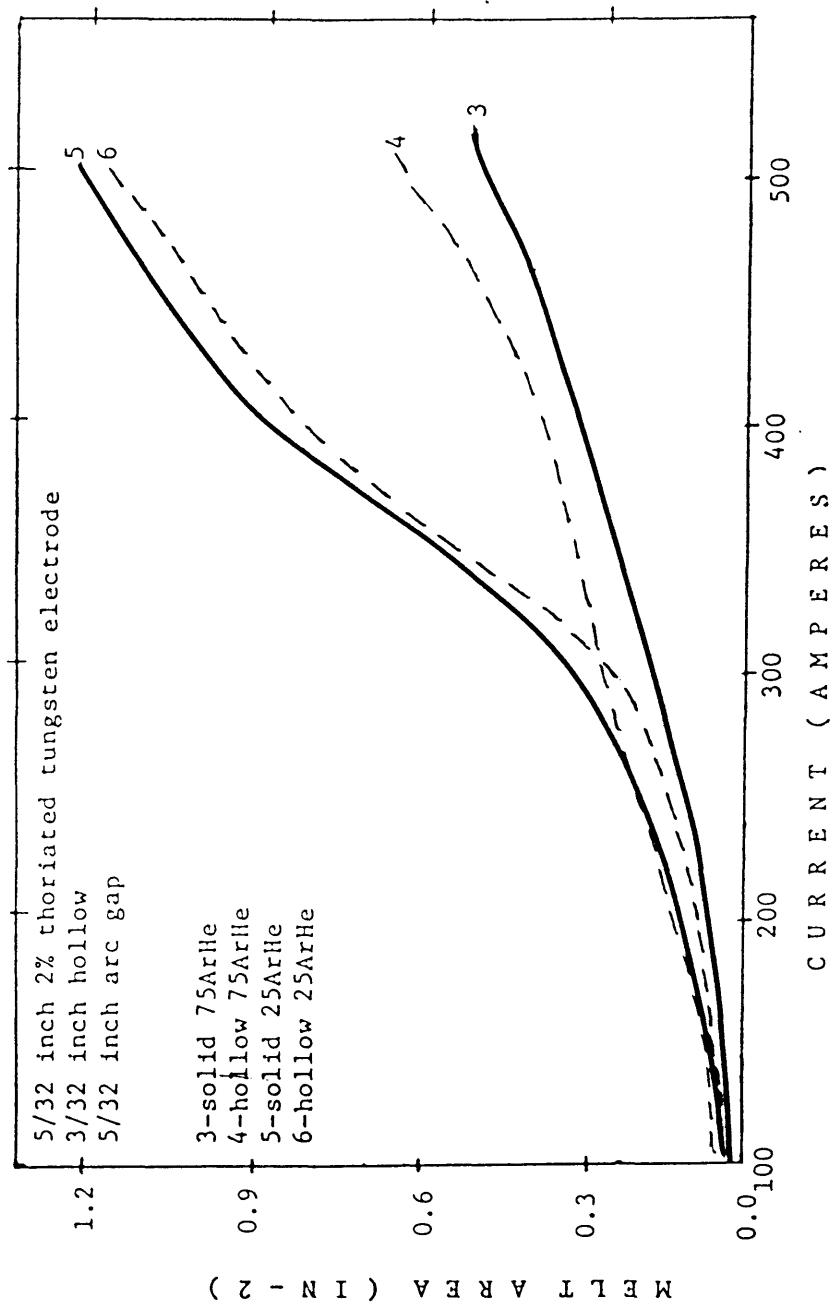


FIGURE 32 Current versus Melt Area for DC Constant Travel Speed Welds Using 150 Degree Tip Electrodes.

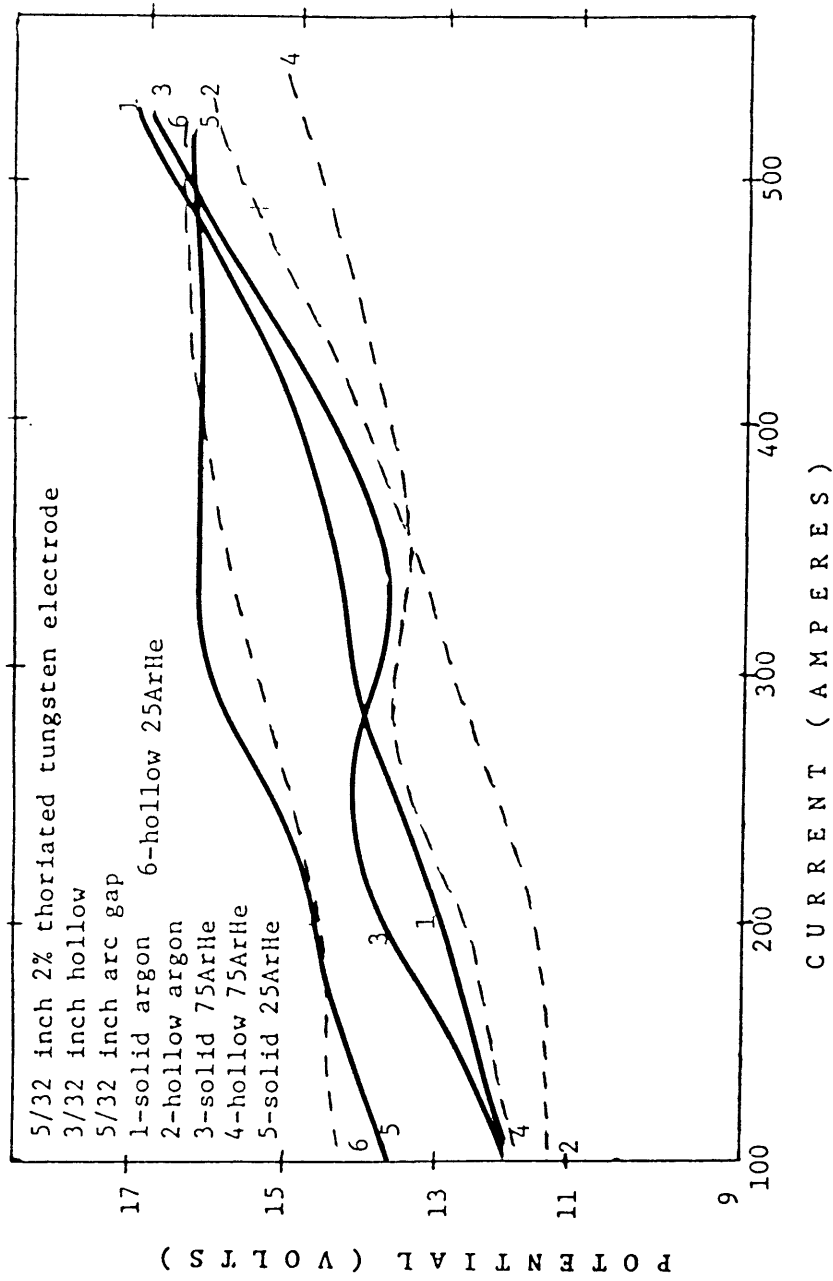


FIGURE 33 Arc Potential-Current Characteristic Curves for DC Constant Travel Speed Welds Using 90 Degree Tip Electrodes.

equal with the 25ArHe being raised 2.5 to 3.0 volts above that of the 75ArHe. Both electrode types exhibited similar arc potentials in their respective gas mixtures between 100 and 450 Amperes when helium was added to the shield gas. At higher currents, arc potential increasingly diverged with decreasing helium content, with the hollow electrode exhibiting a lower arc potential than seen for the solid electrode at similar currents. In pure argon, the arc potential for solid electrode GTAW was greater than that seen for hollow electrode GTAW at all currents.

Penetration increased with increasing current, except as noted when using solid and hollow electrodes with 90 degree included tip angles as shown in figure 34. Both shield gas and electrode type had little influence on penetration. As noted many previous times, the characteristic maxima/minima points were seen. These points were shifted to the right with increasing helium content in the shield gas.

p/w remained nearly constant with increasing current, except as noted when using solid and hollow electrodes with 90 degree included tip angles as shown in figure 35. Both shield gas and electrode type had little influence on p/w. As noted previously, the characteristic maxima/minima points were seen. These points were shifted to the right with increasing helium content in the shield gas.

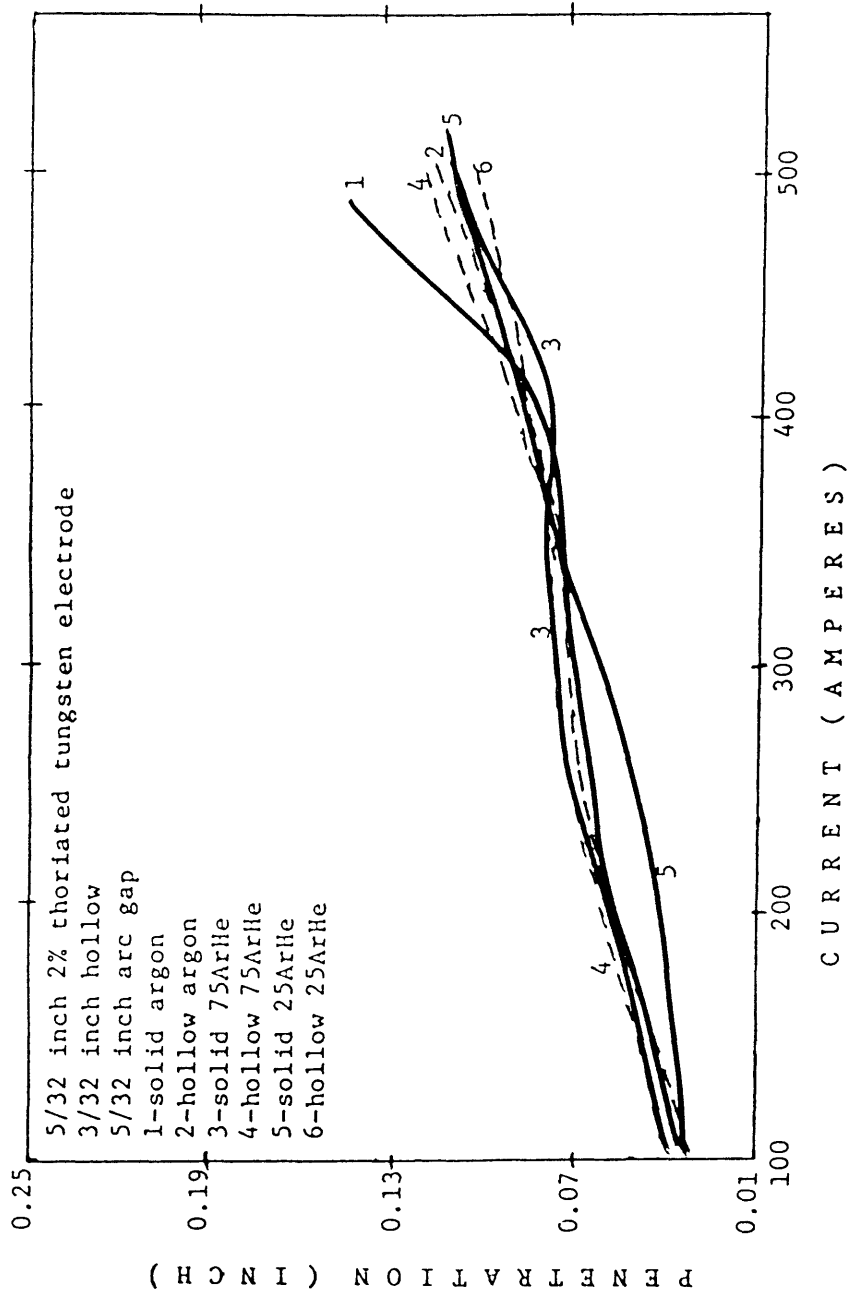


FIGURE 34 Current versus Penetration for DC Constant Travel Speed Welds Using 90 Degree Tip Electrodes.

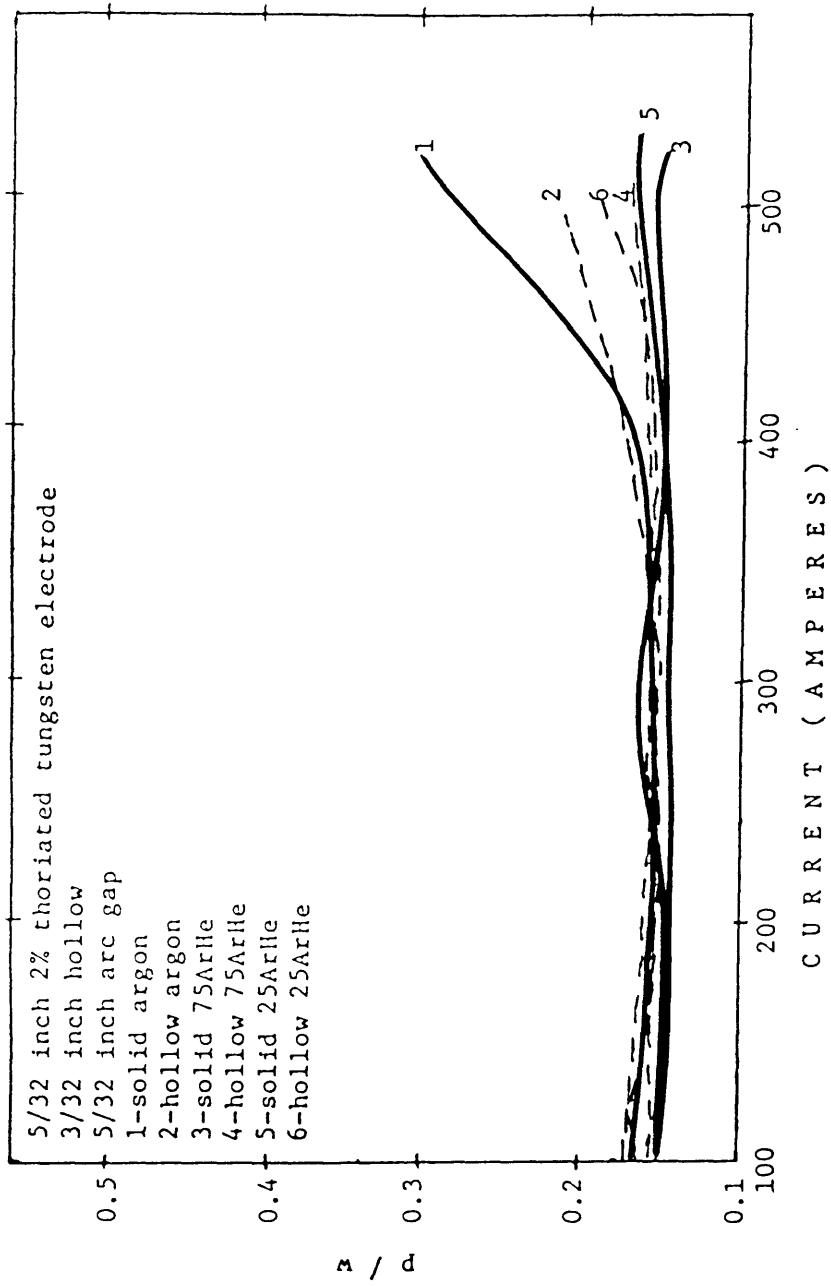


FIGURE 35 Current versus p/w for DC Constant Travel Speed Welds Using 90 Degree Tip Electrodes.

Melt area for 90 degree included tip angle electrodes increased with increasing current as shown in figure 36, and up to 300 Amperes, melt area was independent of shield gas composition and electrode type. Above this, increasing helium content generally led to an increase in melt area. This was more readily apparent for small additions (25 percent) of helium rather than larger additions (75 percent).

Electrode type played a much smaller role in determining melt area and mixed results were obtained with both electrode types. Hollow electrode GTAW produced larger melt areas when using 75ArHe, but smaller melt areas were seen in both pure argon and 25ArHe than found when using solid electrode GTAW. No explanation is available for the large increase in melt area seen with solid electrode GTAW in 25ArHe. The data to support each of the above figures can be seen in Table A1-2.

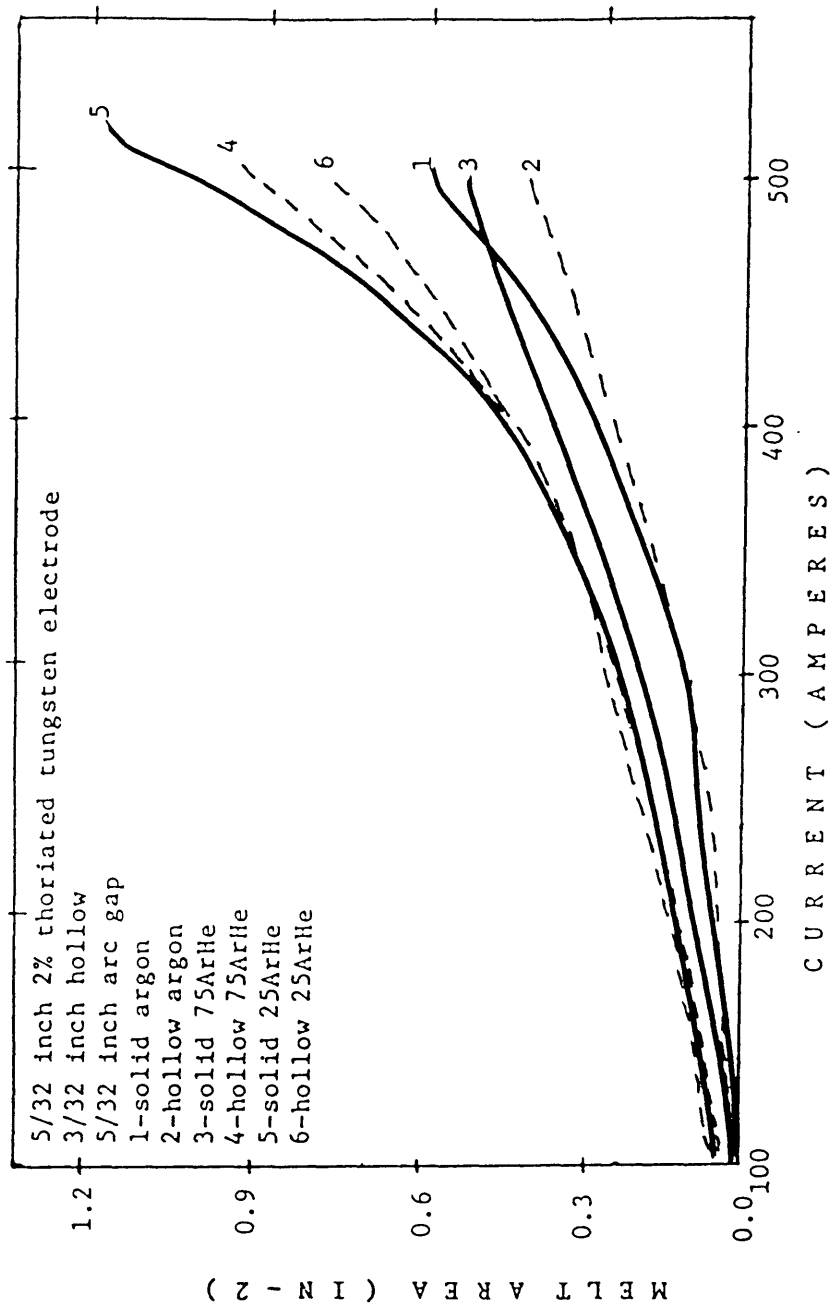


FIGURE 36 Current versus Melt Area for DC Constant Travel Speed Welds Using 90 Degree Tip Electrodes.

DISCUSSION

The reported observations of hollow electrode GTAW over solid electrode GTAW predicts improvements in the following areas:

- 1) Improved penetration in argon at high currents
- 2) Decreased arc pressure in pure argon cover gases
- 3) Increased arc stability again in pure argon cover gases.

In this investigation, the effect of shield gas, electrode shape (unshaped (180) or 150 or 90 degree included tip angle), and current on penetration, p/w, and melt area as well as arc stability using solid and hollow electrode GTAW was investigated. Previous studies (24,42-46) with the hollow electrode have not dealt with bead morphology in as sufficient depth as discussed herein.

This investigation was not able to substantiate the suggested improvements when utilizing hollow electrode as a generally accepted fact. The improvements were typically seen at either high (greater than 450 Amperes) or low (less than 150 Amperes) currents and then only under special conditions for the welding parameters. Shield gas composition (helium versus argon) played a more significant role in parameter improvements than electrode type or the other parameters studied.

Shield Gas Effects

As expected, increased helium in the shield gas led to a hotter arc due to the ionization potential of helium being greater than that for argon. This was true for both AC and DC weld conditions and constant heat input/travel speed weldments. Arc potential for solid and hollow electrode GTAW were similar under similar welding conditions at all currents investigated. Shield gas had a more pronounced effect on arc potential than electrode type.

Also, as expected, increased helium in the shield gas led to improved penetration. Electrode type had a minor affect which was more pronounced in pure argon than the two argon-helium gas mixtures. The hollow electrode showed occasional unpredictable excursions (usually at high current) of vastly improved penetration over solid electrode GTAW. The general trend indicated shield gas had a substantially greater role in penetration than did electrode type.

Shield gas and electrode type had relatively no effect on the p/w ratio. This ratio was nominally between 0.14 and 0.18 (considered low) and helium additions to the shield gas tended to slightly lower the ratio. p/w decreased slightly with helium additions because the weld puddle was wider than that seen when using argon as the cover gas.

Melt area was affected by increasing helium in the shield gas. As the figures indicate, melt area improved with increasing helium content and this trend was more pronounced with decreasing electrode included angle (from 180 to 150 to 90 degree) tip. Little difference was noted between the two electrode types.

Electrode Shape Effects

A slight increase in electrode angle (150 degrees) increased the arc potential approximately one to two volts. A farther increase in tip angle (to 90 degrees) had little effect. Again, shield gas had a greater effect on arc potential than either electrode shape or type.

Electrode shape did have an effect (greater than that seen for shield gas) on penetration at medium to high current (300 to 500 Amperes). At low current (less than 200 Amperes), penetration was better with an unshaped electrode than a shaped electrode. This phenomena at low currents contradicts the work of Chihoski (29) where increased penetration occurred with increased electrode tip (sharper). The explanation for this lies in the electrode size used. Chihoski used a 1/8 inch (3.2mm) diameter electrode sharpened to a point while the current study used a 5/32 inch (4mm) diameter electrode ground to a blunt 3/32 inch (2.3mm) end (solid

electrode).

Although penetration was improved by electrode shape, p/w remained unchanged regardless of electrode shape. This was due to bead width increasing at the same rate penetration was increasing. p/w remained between 0.14 and 0.18. Electrode shape did have a "flattening" effect at all currents studied up to 400 Amperes. The transition from fluid flow zone control to arc welding parameter control with increasing current became less prominent with decreasing tip angle.

Melt area was improved with increasing tip angle and the effect was further improved with increasing helium in the shield gas. Once again, shield gas had a substantially greater effect on melt area than either electrode shape or type.

Current Effects

Increased current led to a phenomena seen in penetration, p/w, and melt area plots. This same phenomena has been seen by other investigators (16,33) and was present in this study under both constant heat input and constant travel speed conditions. This phenomenon represents a transition from the fluid flow zone at lower currents to the parameter control zone at higher currents. It is characterized by an increase in a specific fusion zone to a maximum between 200

and 250 Amperes followed by a decrease in this same measure to a minimum between 250 and 300 Amperes. Above this, the measure (penetration or p/w) steadily increases with increasing current and follows the predicted parameter zone. The trend was more pronounced in the constant heat input welds where the pool size is maintained (more or less) constant. Once again, as has been previously stated, shield gas had a much greater effect on bead morphology than the other varied welding parameters.

Arc Stability

Arc stability was measured on all welds at currents above 300 Amperes while utilizing shaped electrodes. The actual data can be seen in the appendix (Table A1-3), but little difference was seen in arc stability between the two electrode types. Figure 11 shows the arc stability results for solid and hollow electrode GTA welding at 500 Amperes in 75ArHe while using a 150 degree electrode tip angle.

Shield gas did have an effect on arc stability. Increased helium in the shield gas led to a less stable arc. This is not surprising since helium typically gives a higher arc potential than argon under similiar welding conditions.

General Discussion

The transitional behavior phenomena mentioned earlier seen in the majority of the data gathered in this study and plotted as a function of current is described as the transition from fluid flow zone control to parameter zone control. This transition occurs at different currents and is determined by shield gas, electrode type, and to a lesser degree electrode shape. The transition occurred between 250 and 300 Amperes in the present study.

Hollow electrode GTAW did not show the major increase in penetration expected as seen by the Japanese investigators (24). It was seen under optimum conditions only and could not be predicted. Shield gas had a much greater effect on penetration (and p/w and melt area) than any other parameter which was varied. In addition, the increased penetration seen at 250 Amperes in pure argon using hollow electrode GTAW occurred because the transition (going from maximum parameter to a minimum value) had not occurred as it had for solid electrode GTAW. The arc pressure measured by Yamauchi (24) was lower in argon for the hollow electrode than for the solid electrode in this condition. The fallacy in this measurement, at least at this current level, is that at these low currents, arc pressure has a minor role compared with shield gas in affecting the weld pool. At higher currents,

the arc force does play a substantial role in affecting penetration.

Jackson and Shrubbsall (35) derived two equations to predict penetration and melt area in submerged arc welds. These same equations apply equally well to gas tungsten arc welds for the reasons given in an earlier section. The application applies only to the parameter control zone and not to the fluid flow zone.

Two other penetration prediction equations were used to model the data obtained. The two equations were Erokhin (38) and Savage (37) but they were found to not accurately model the data. For this reason, the Jackson and Shrubbsall (35) model was used and presented in the next set of figures. Figure 37 shows the result of using both the Erokhin (38) and Savage (37) models to predict penetration. It can be seen that the Erokhin (38) equation is off by an order of magnitude while the Savage (37) model is off by about fifteen percent. The reason offered for these two models being inaccurate is that they were developed for SAW with specific welding conditions while the Jackson and Shrubbsall (34) model contains a constant (k) which accounts for shield gas and electrode shape in GTA welding.

A constant could be developed for the Savage (37)

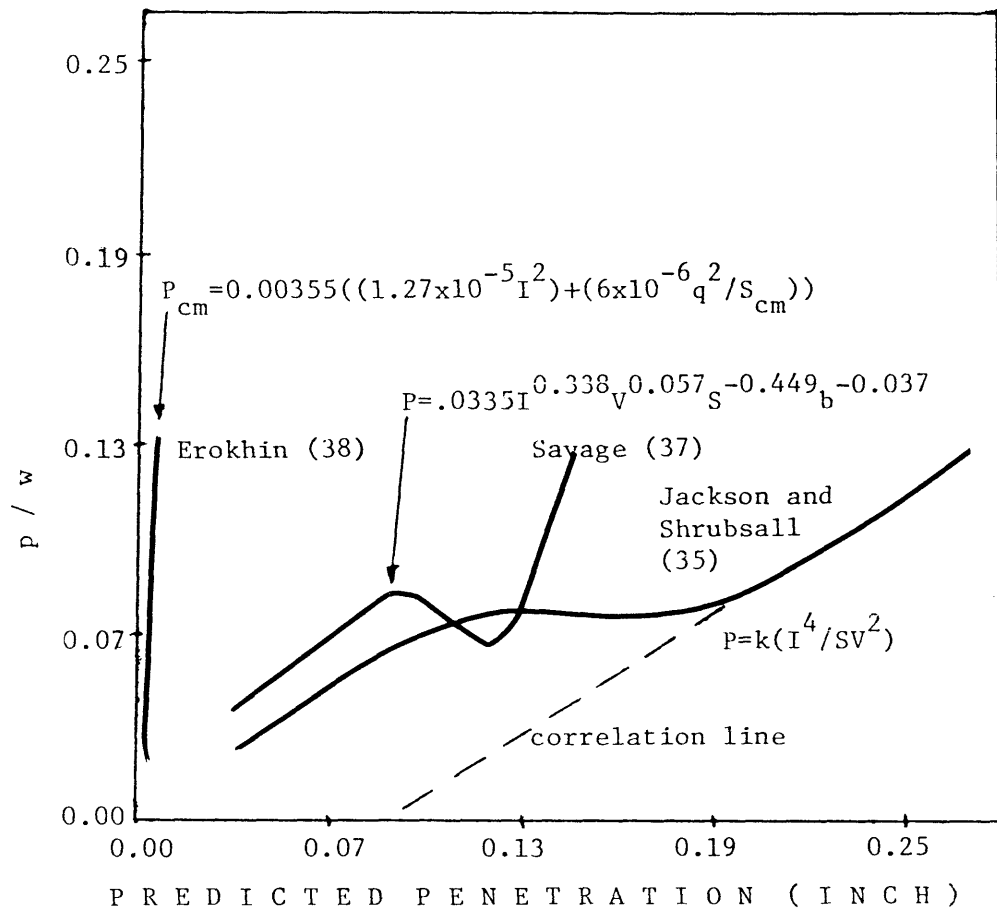


Figure 37 Comparison of Penetration Prediction Equations of Savage (37) and Erokhin (38). Comparison is shown for data from weldments using 150 Degree Electrode Tip In 75ArHe.

model which would work for the current study, but the Jackson and Shrubbsall (35) model was used. With the correct constant, it would be expected that both the Jackson and Shrubbsall (35) and Savage (37) penetration models would be similar.

Bead Morphology Prediction Equations

Bead morphology prediction equations were investigated for the constant travel speed weldments utilizing both shaped and unshaped (180) electrodes. Penetration, and melt area for each of the three weld conditions were compared with the values predicted by the equations noted in Table I. These equations were originally derived for submerged arc welds; but, because of the nature of the arc (as discussed previously), and the fact that a number of other authors have utilized them for GTAW it has been shown that they may be used with reasonable accuracy in predicting bead morphology.

The results of plotting actual penetration versus that predicted by the Jackson and Shrubbsall (35) equation are shown in figures 38 and 39 for unshaped (180 degree) electrodes, in 75ArHe and 25ArHe respectively.

Figures 40 and 41 show the results of plotting predicted versus measured penetration, respectively for weldments using 150 degree tip electrodes in 75ArHe and 25ArHe.

Figures 42, 43, and 44 show the results of plotting

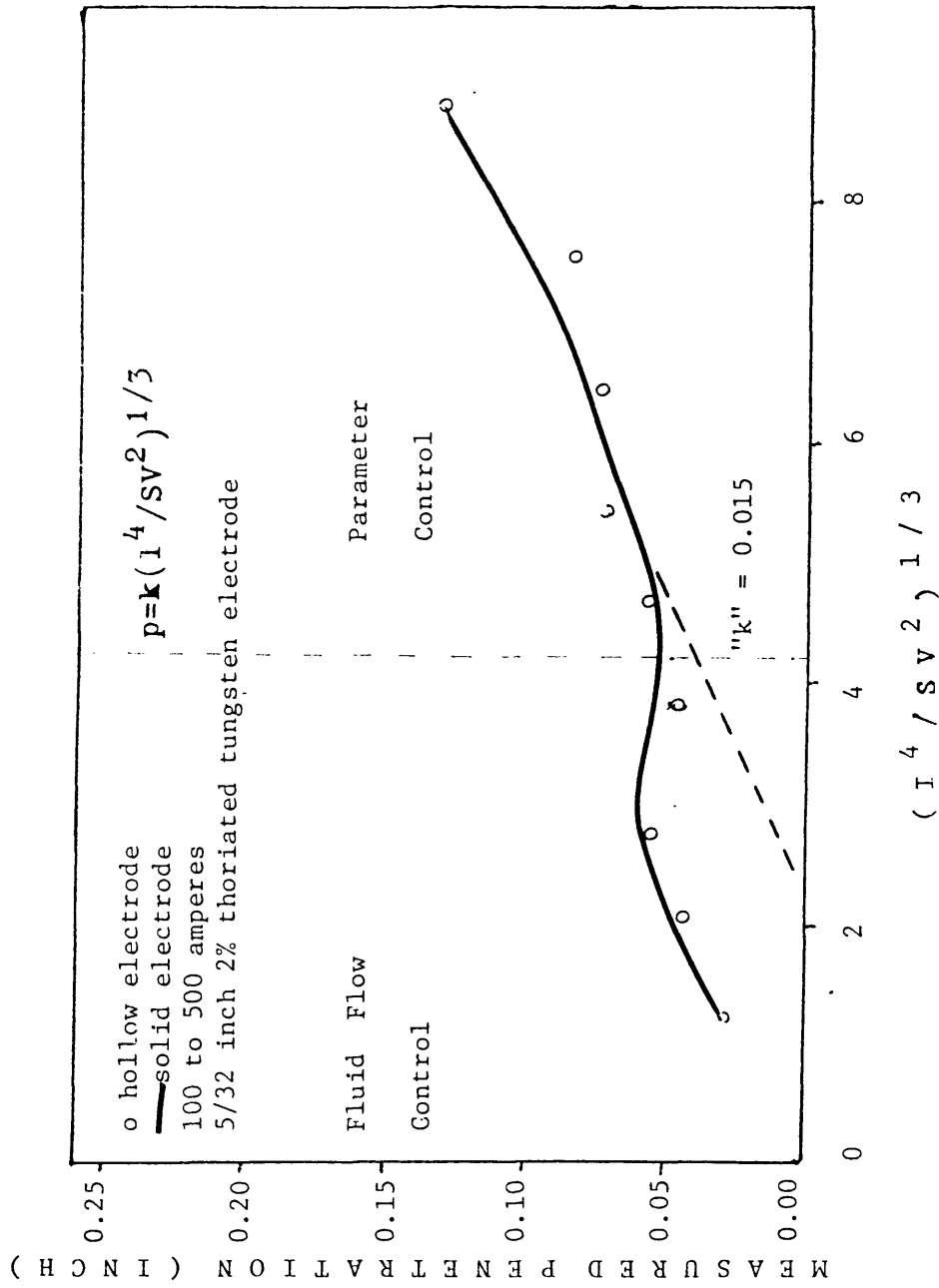


Figure 38a Measured penetration versus Jackson and Shrubbsall Functionality (35) for constant travel speed weldments utilizing unshaped electrodes in 75ArHe.

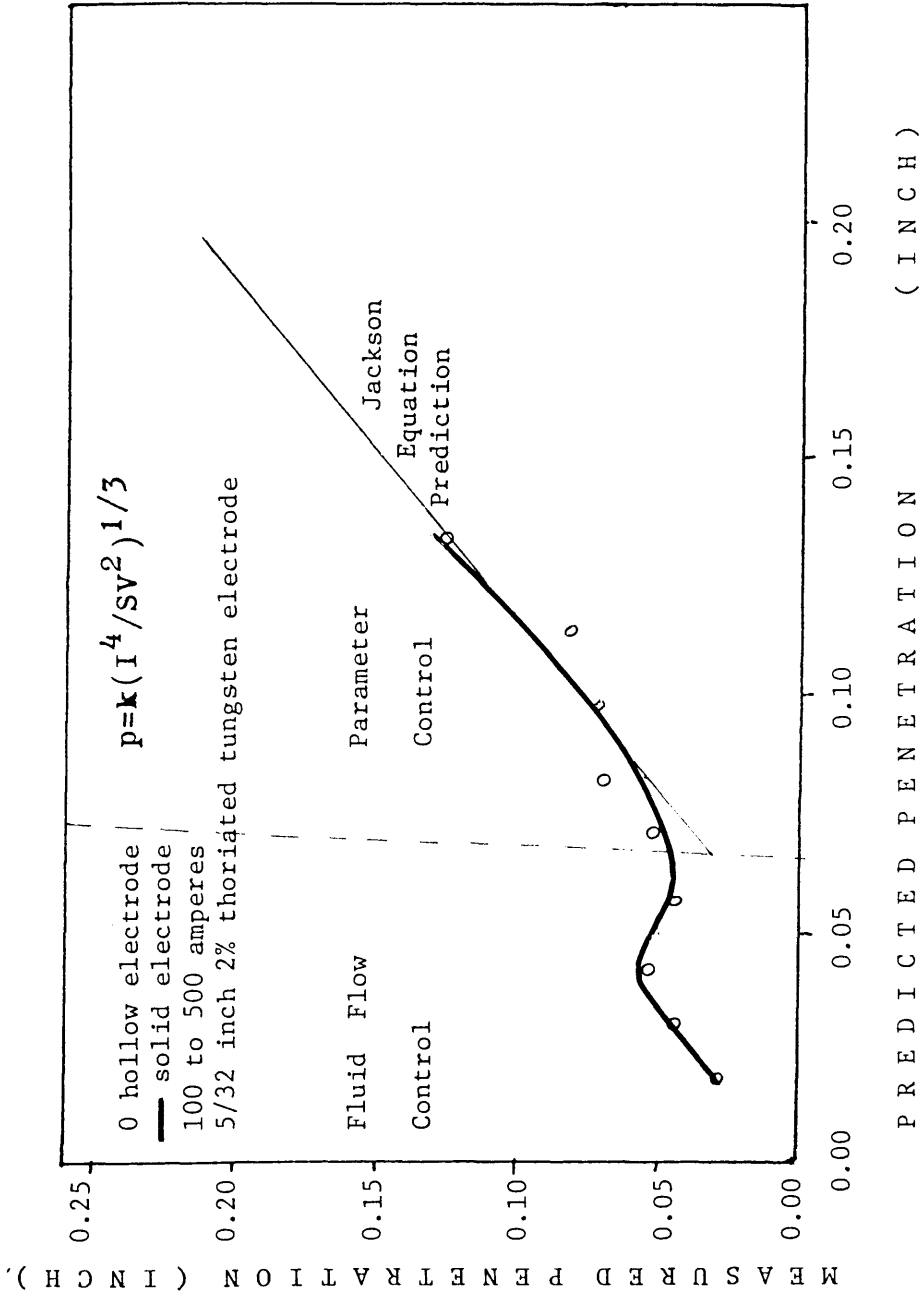


Figure 38b Predicted versus measured penetration for constant travel speed weldments utilizing unshaped electrodes in 75ArHe.

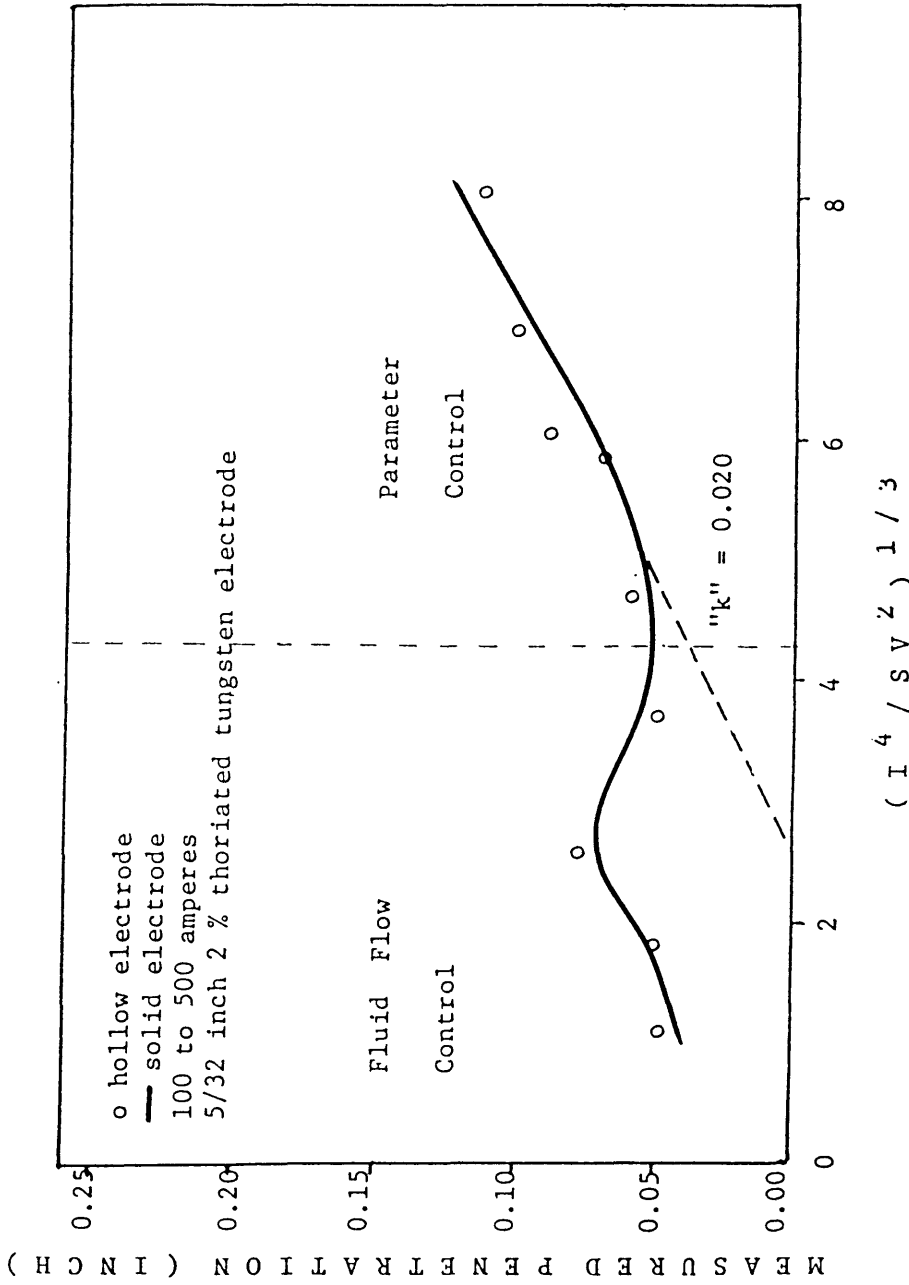


Figure 39a Measured penetration versus Jackson and Shrubshell Functionality (35) for constant travel speed weldments utilizing unshaped electrodes in 25ArHe.

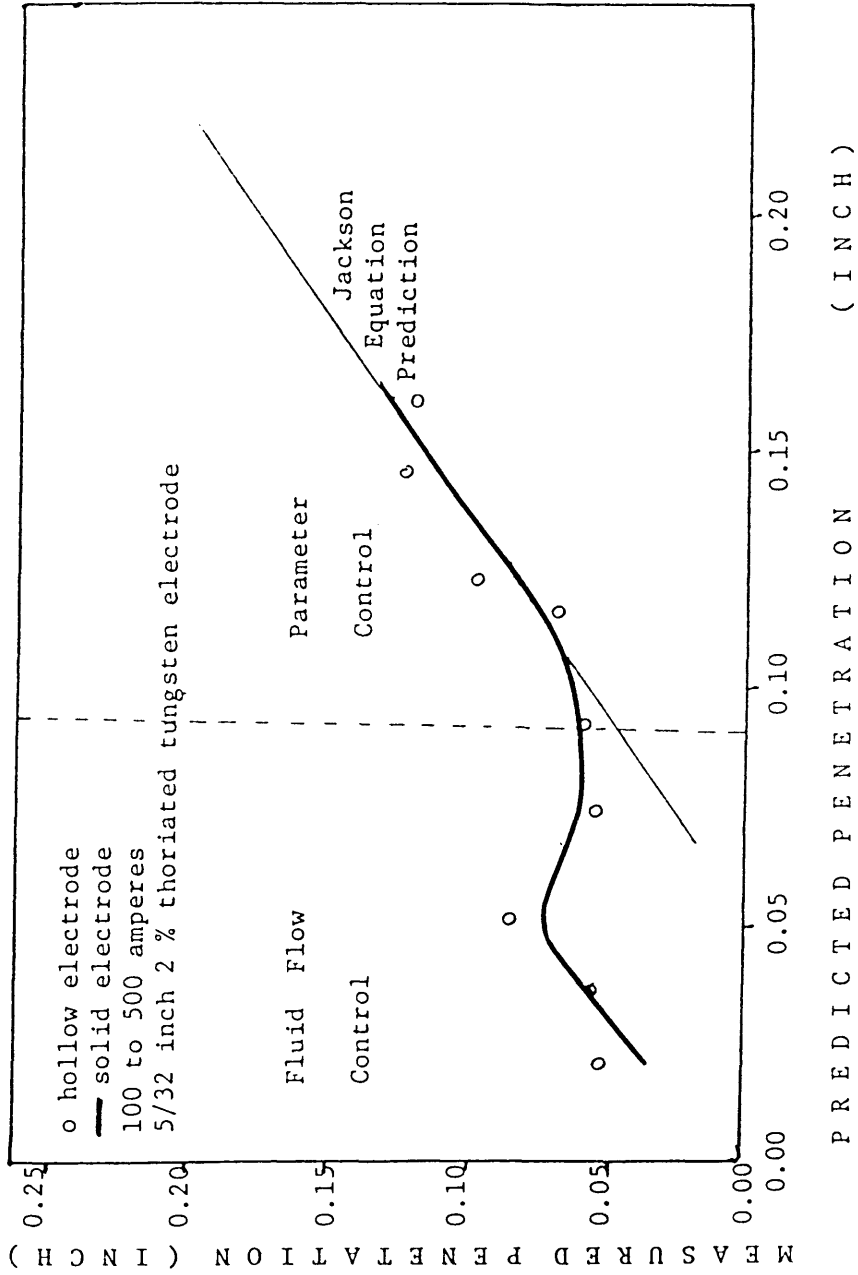


Figure 39b Predicted versus measured penetration for constant travel speed weldments utilizing unshaped electrodes in 25ArHe.

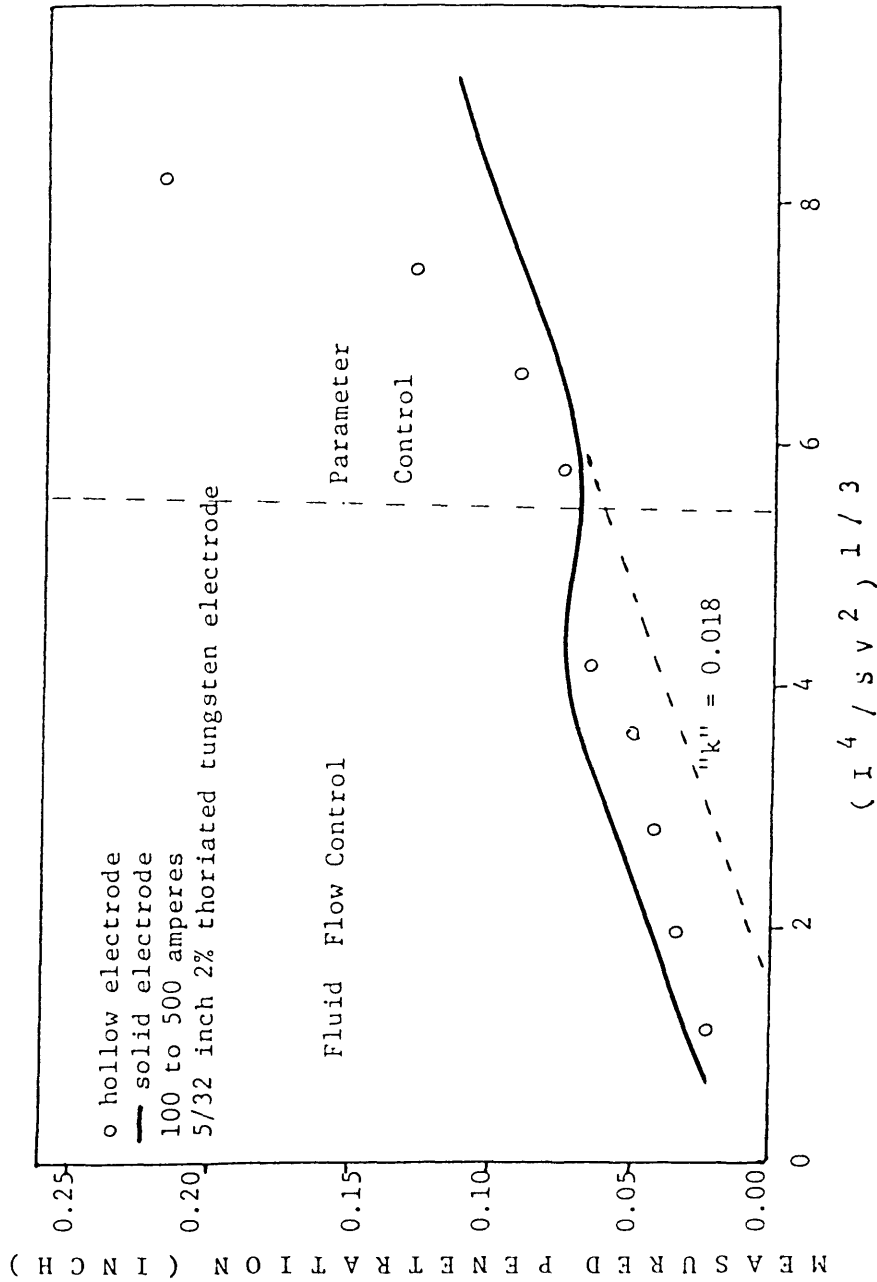


Figure 40a Measured penetration versus Jackson and Shrubbsall Functionality (35) for constant travel speed weldments utilizing 150 degree tip electrodes in 75ArHe.

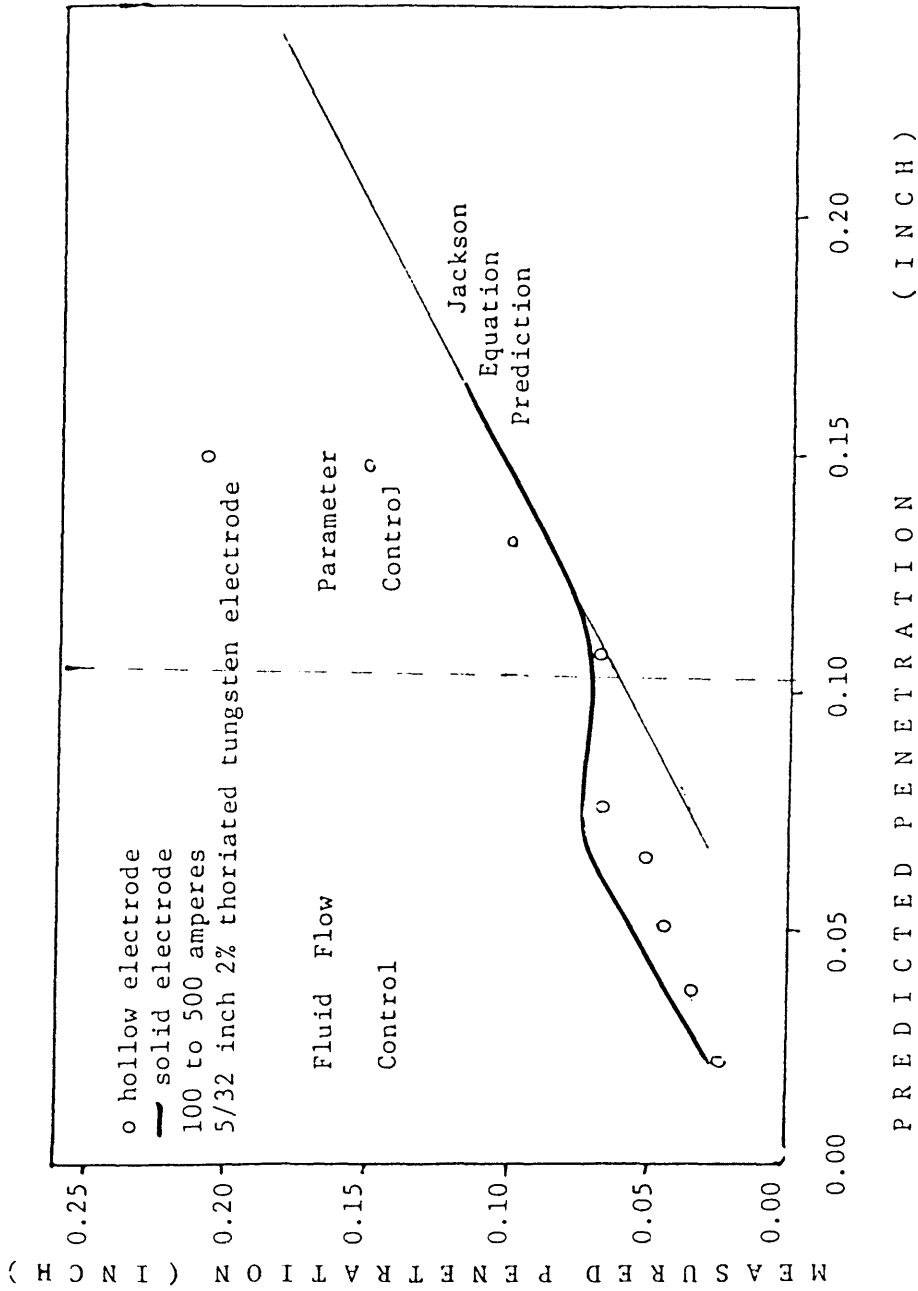


Figure 40b Predicted versus measured penetration for constant travel speed weldments utilizing 150 degree tip electrodes in 75ArHe.

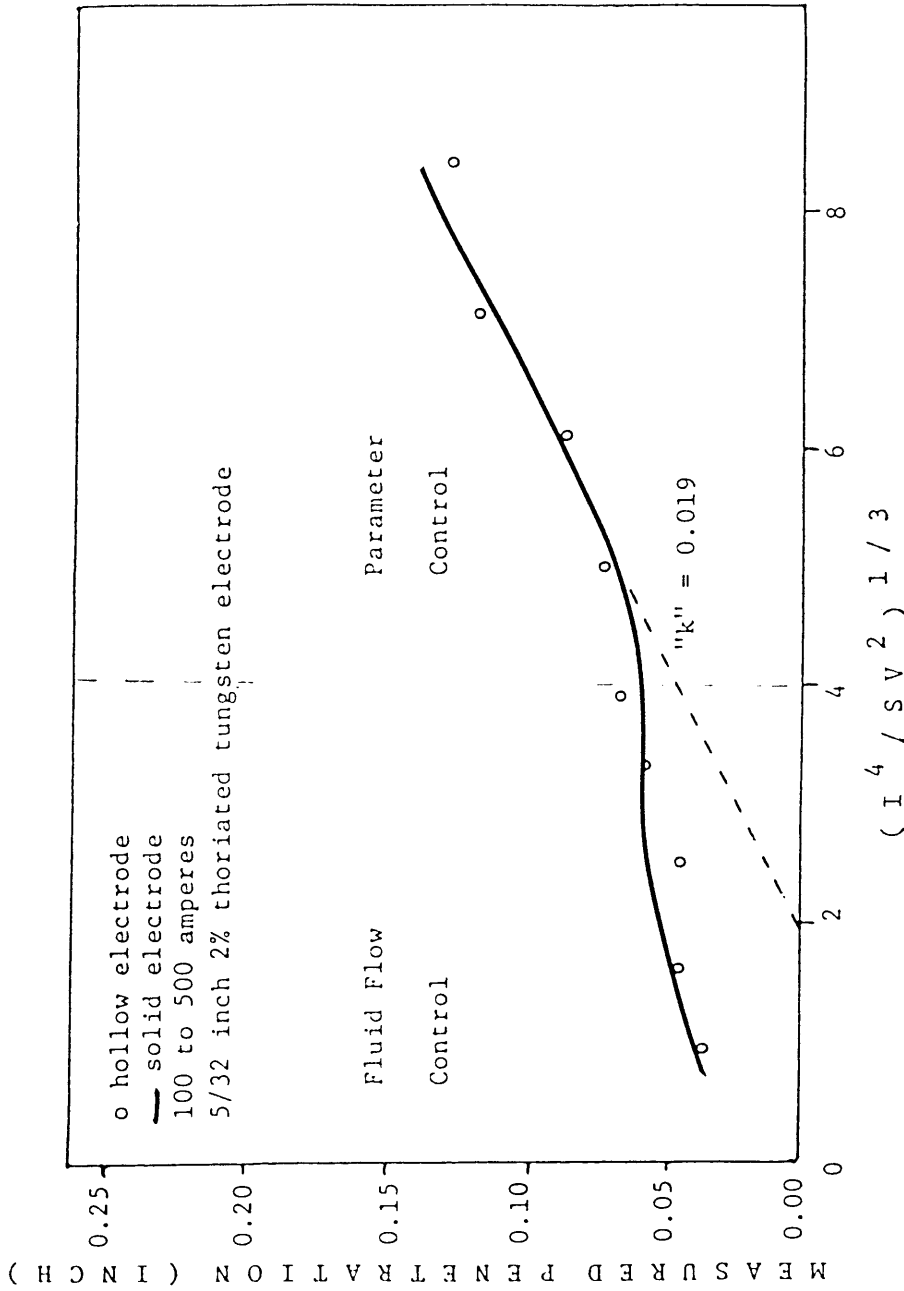


Figure 41a Measured penetration versus Jackson and Shrubbsall Functionality (35) for constant travel speed weldments utilizing 150 degree tip electrodes in 25ArHe.

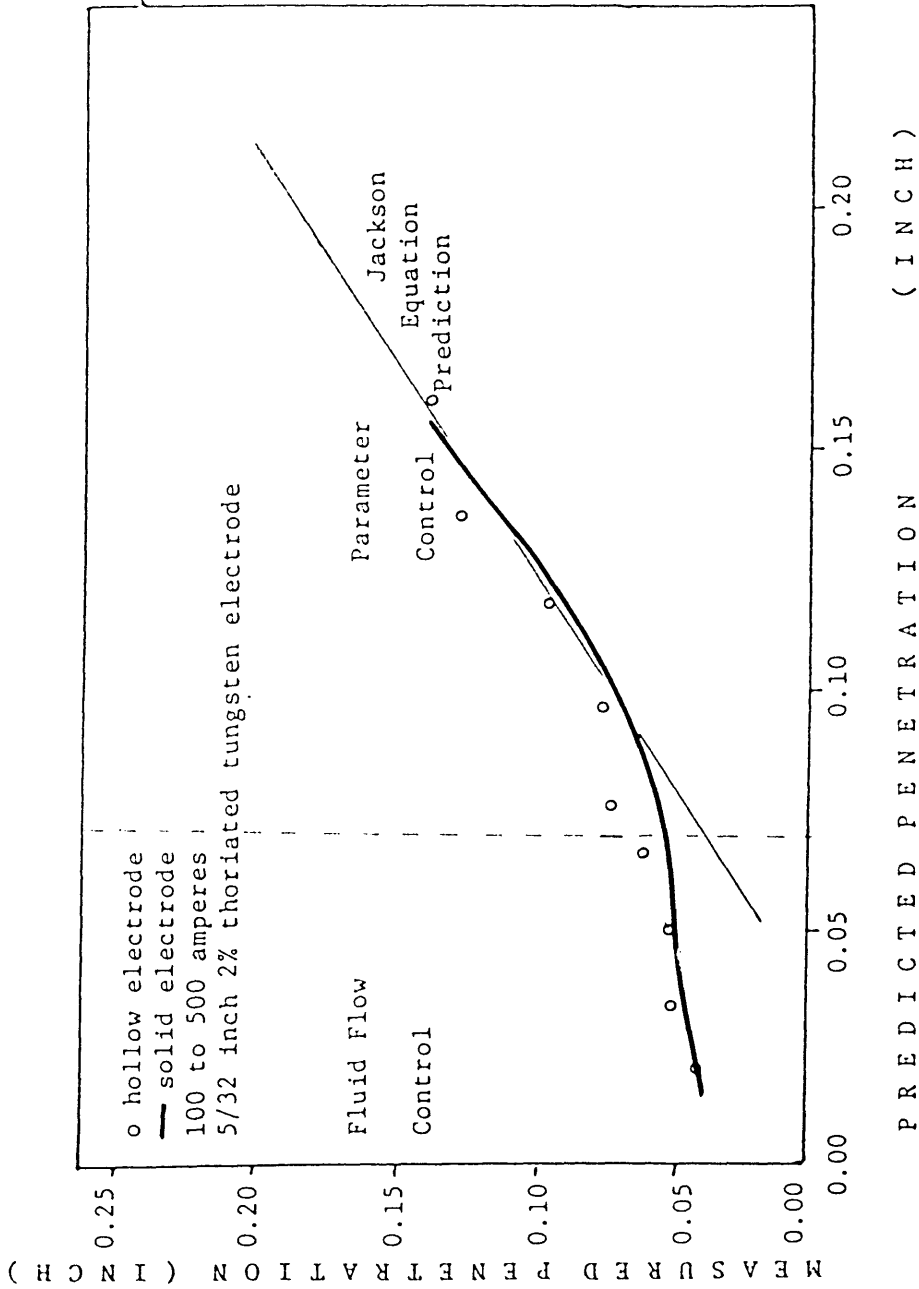


Figure 41b Predicted versus measured penetration for constant travel speed weldments utilizing 150 degree tip electrodes in 25ArHe.

predicted versus measured penetration, respectively for weldments using 90 degree tip electrodes in argon, 75ArHe, and 25ArHe.

The Jackson and Shrubbsall (35) equation for predicting penetration contains a constant "k". This constant is determined by taking the slope of the linear portion of the plot of measured penetration versus the model functionality. This constant is noted on each of the above figures for reference ("a" figure in each figure). Multiplying the model functionality by "k" and plotting these values against actual penetration yields the figures shown as "b" in each case. It is readily apparent that this equation is fairly accurate in predicting penetration in the parameter control zone of the figure at higher current, but does not apply at lower currents in the fluid flow zone region. These two areas are noted on the figures.

It is interesting to note in "b" of each figure, when plotting predicted penetration multiplied by "k" versus actual penetration, that penetration in the fluid flow control region is not predicted well and penetration in the parameter control region is predicted well by the equation. This is shown graphically by the line running from left to right at approximately 35 degrees.

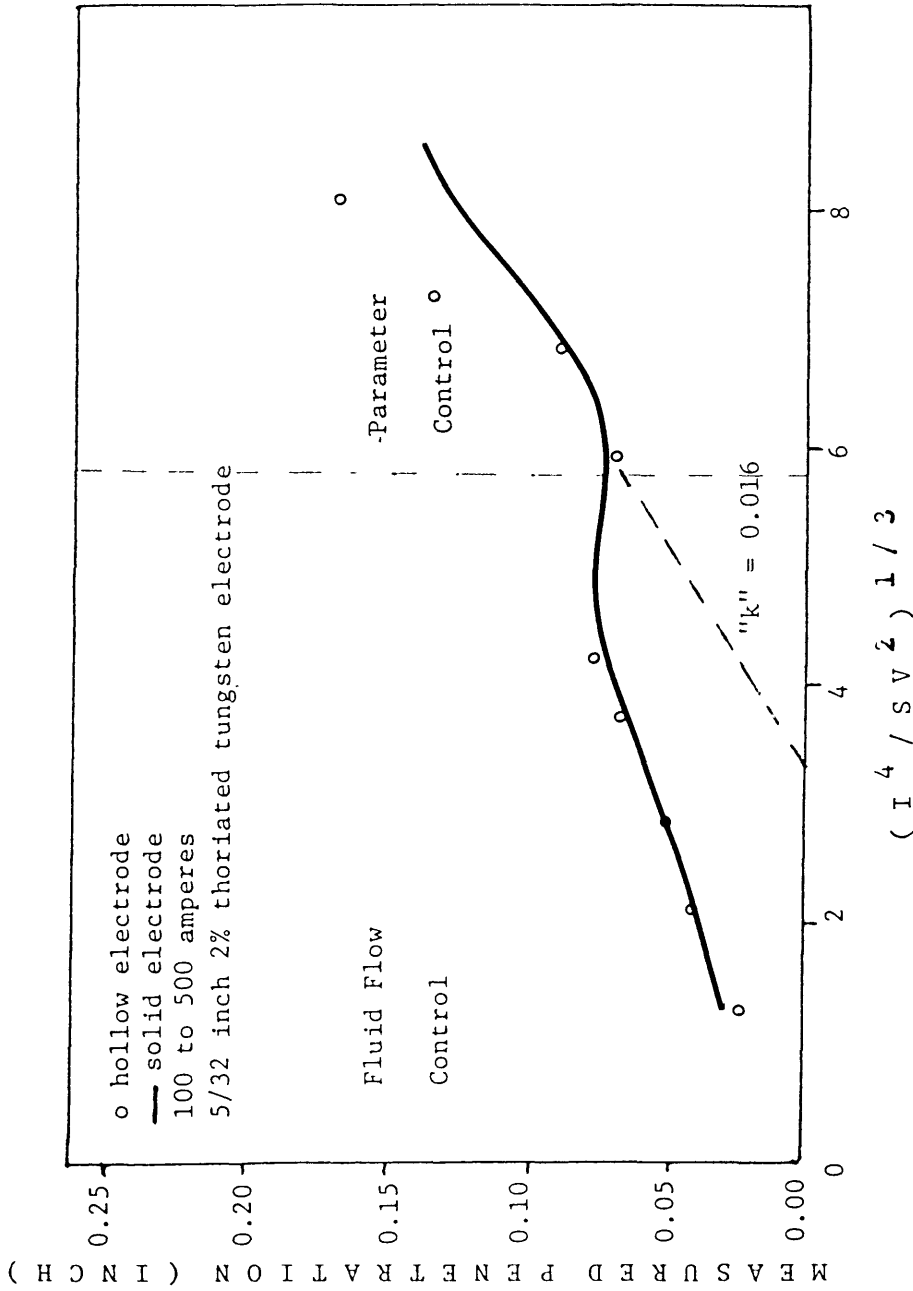


Figure 42a Measured penetration versus Jackson and Shrubbsall Functionality (35) for constant travel speed weldments utilizing 90 degree tip electrodes in argon.

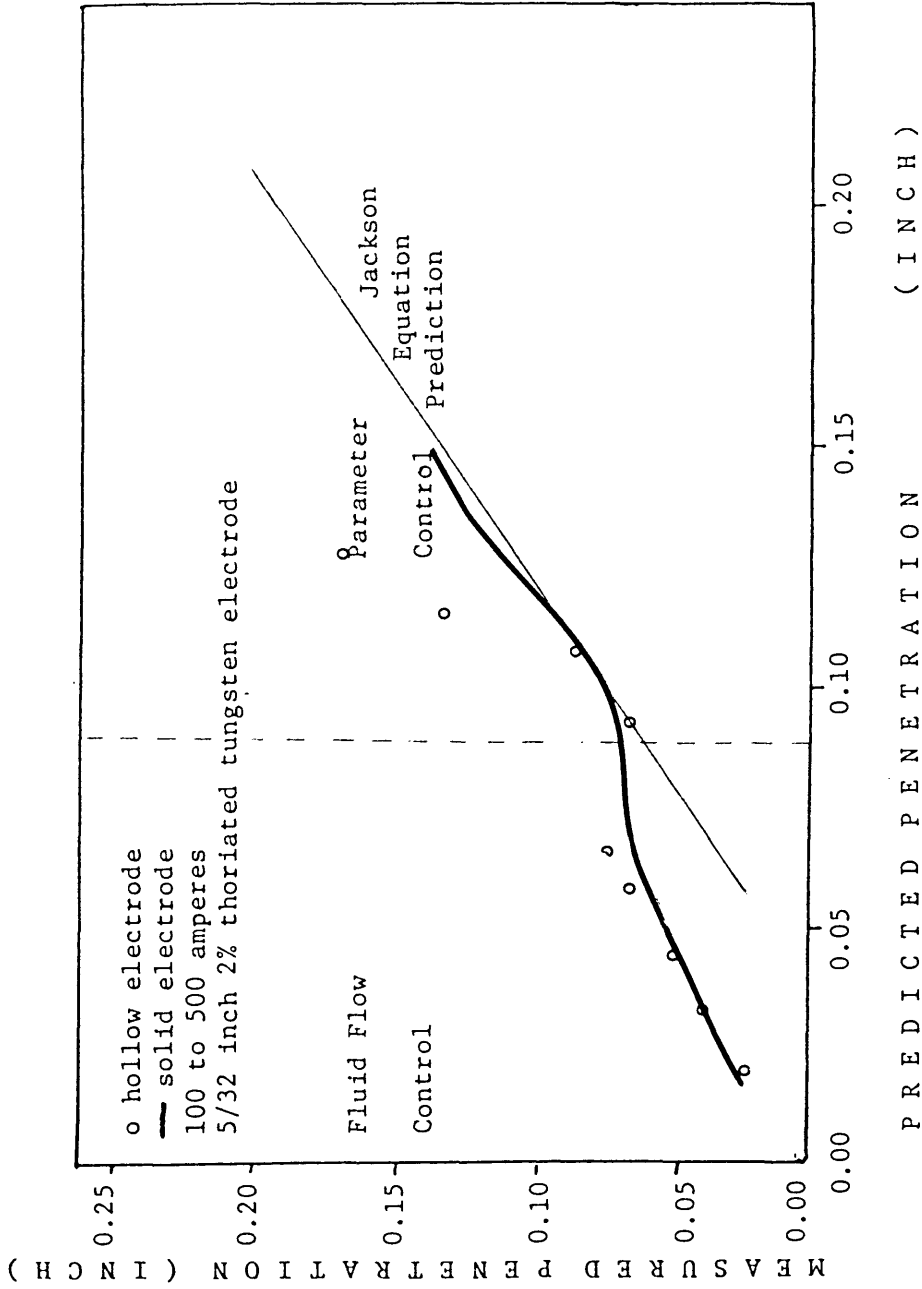


Figure 43b Predicted versus measured penetration for constant travel speed weldments utilizing 90 degree tip electrodes in argon.

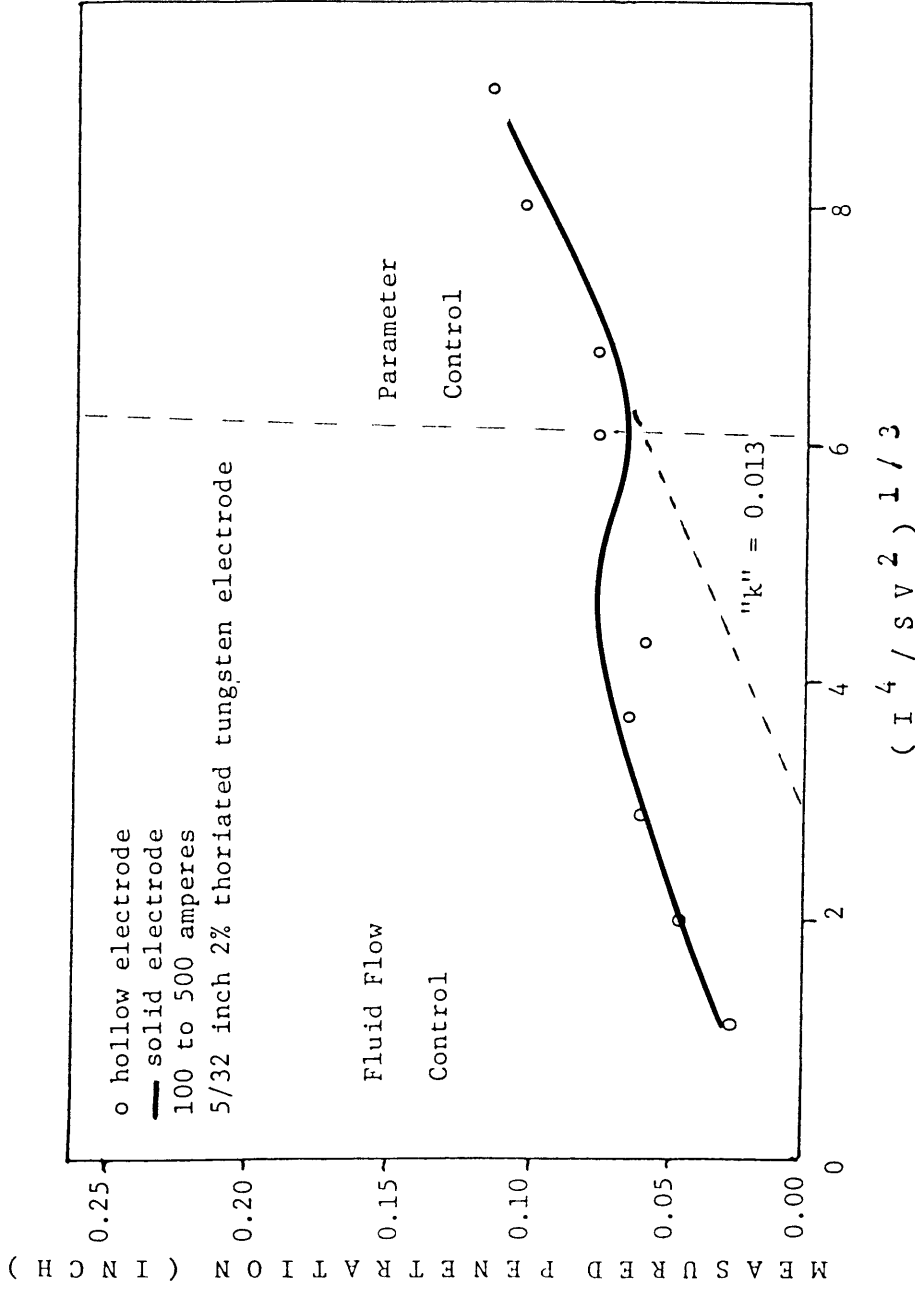


Figure 43a Measured penetration versus Jackson and Shrubbsall Functionality (35) for constant travel speed weldments utilizing 90 degree tip electrodes in 75ArHe.

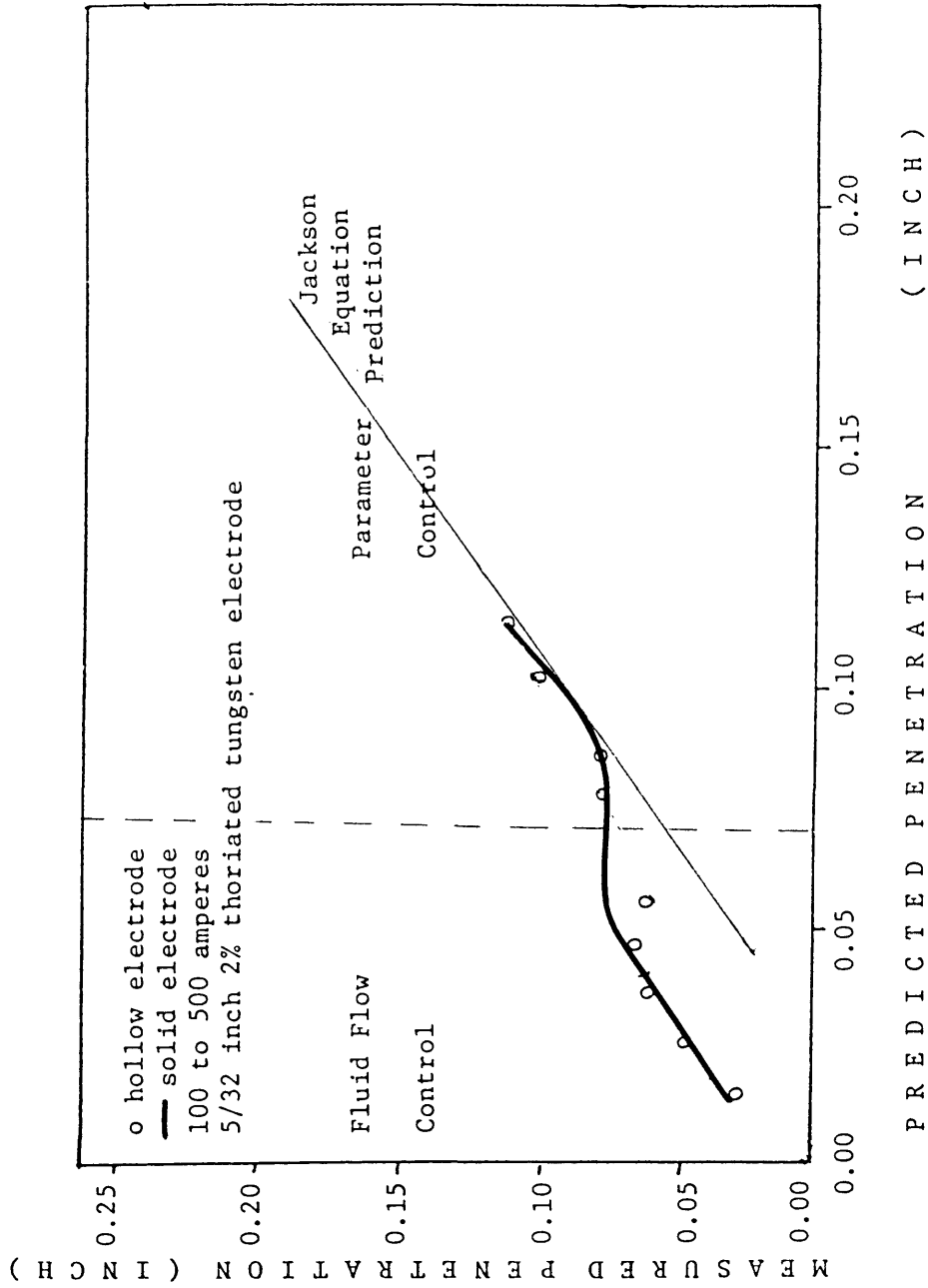


Figure 43b Predicted versus measured penetration for constant travel speed weldments utilizing 90 degree tip electrodes in 75ArHe.

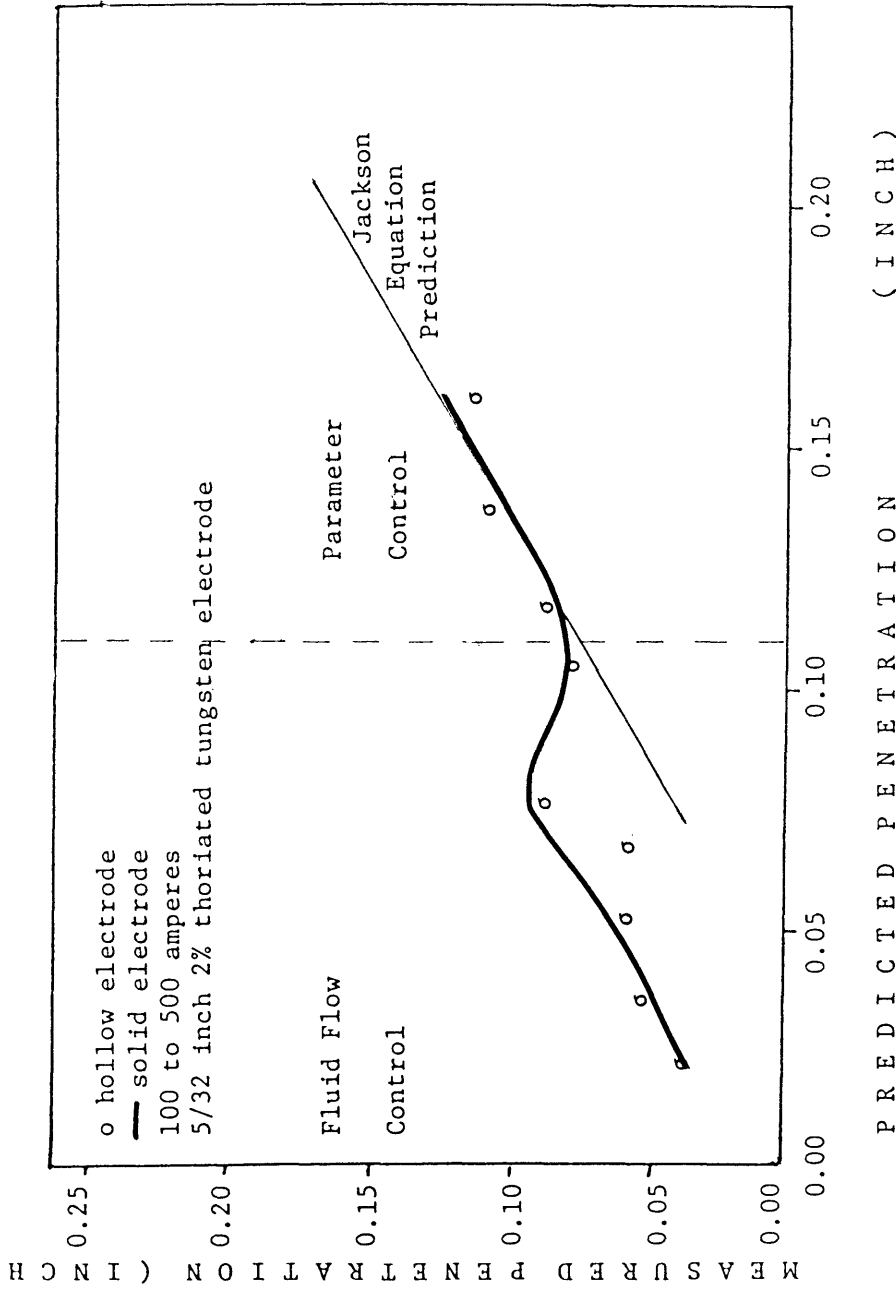


Figure 44a Measured penetration versus Jackson and Shrubbsall Functionality (35) for constant travel speed weldments utilizing 90 degree tip electrodes in 25ArHe.

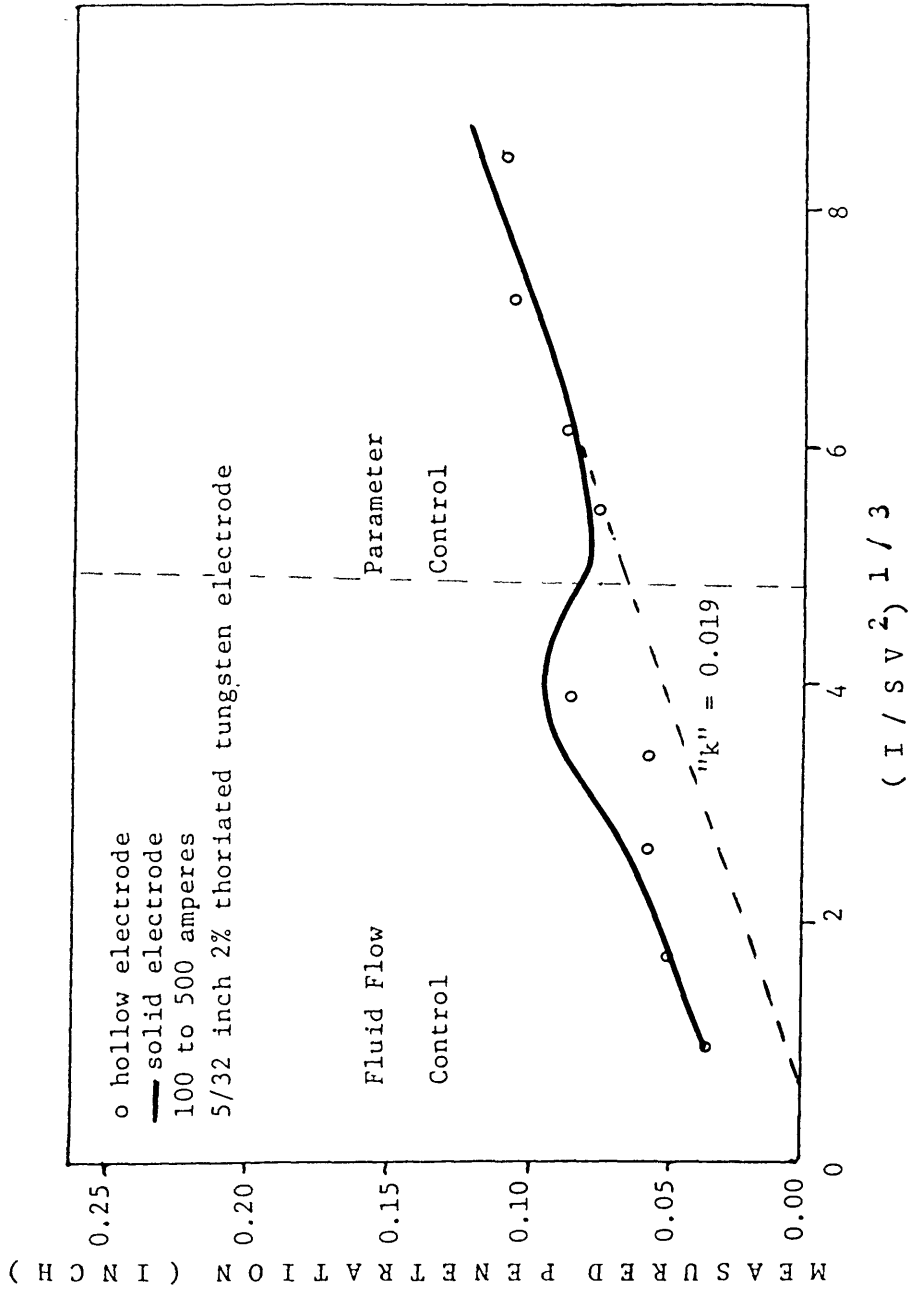


Figure 44b Predicted versus measured penetration for constant travel speed weldments utilizing 90 degree tip electrodes in 25ArHe.

It is interesting to note that shield gas and electrode tip shape have an affect on the slope of the measured versus predicted curves. Figure 45 shows the effect both of these variables had on "k". Plotted as a function of shield gas composition, it is apparent that "k" goes through a minima with a small addition of helium to the cover gas (25 percent helium addition) and appears to increase with increasing amounts of helium. While the curve is the result of only three gas compositions, the trend is seen for unshaped (180 degree) and 90 degree tip electrode weldments. This same trend is nearly non-existent for the 150 degree tip electrode.

Penetration Predictions

The Jackson and Shruballs equation (reference Table I (35)) was used to plot predicted versus measured penetration. It was found to be reasonably accurate as shown in figures 38 through 44 for both electrode types in all three shield gases. The equation holds only for the parameter control zone as shown on each of the figures. This zone occurs at approximately 250 to 350 Amperes and is the result of a characteristic change in the dominant forces of the arc and the molten weld pool.

The slope of each plot in the parameter control zone yields the "k" constant in the Jackson and Shruballs (35)

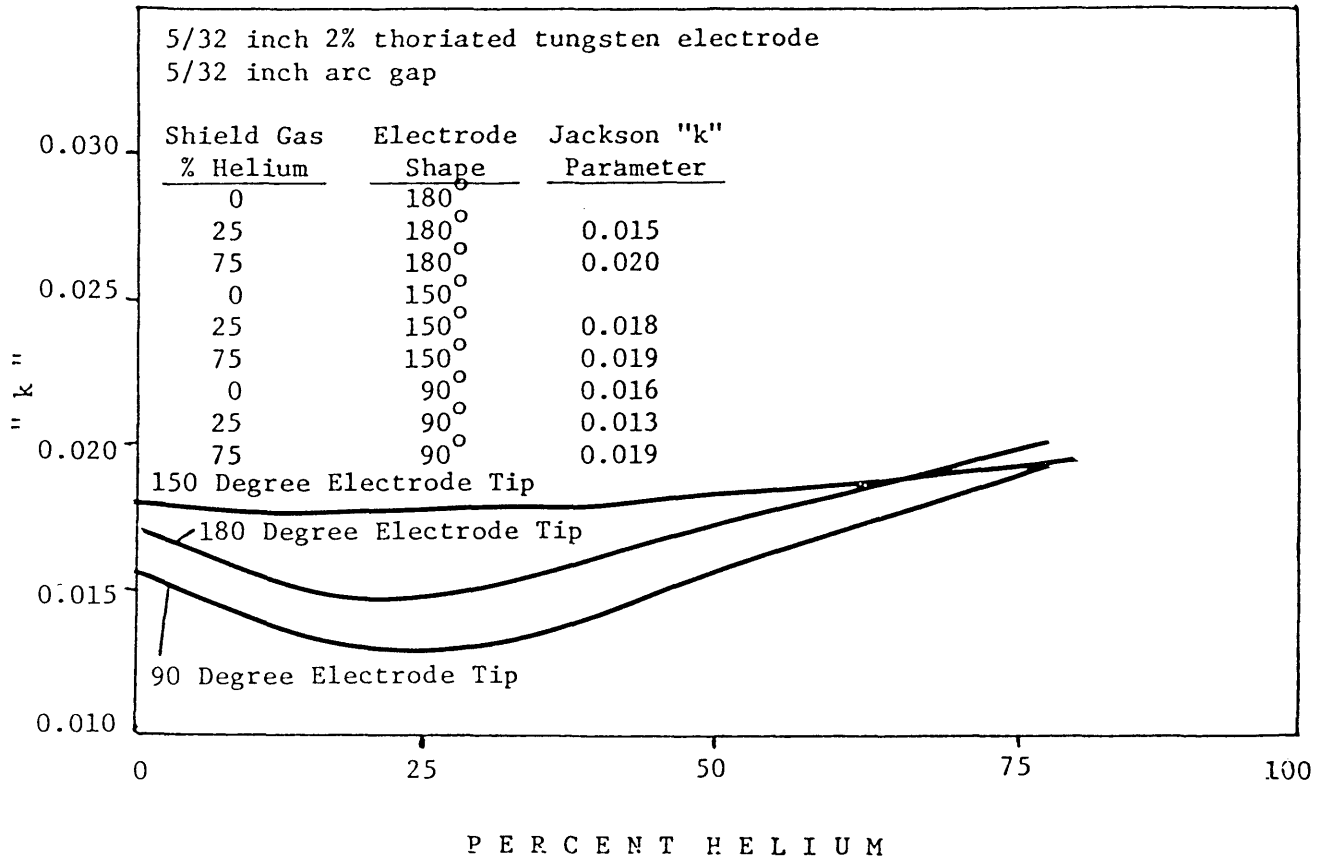


Figure 45 Plot of "k" constant in Jackson and Shrubbsall (35) Penetration Prediction equation versus shield gas composition as a function of electrode tip angle.

equation. Figure 45 shows the effect of shield gas composition and electrode tip shape on the value of "k". Once again, as seen in this figure, shield gas has a much larger affect on the arc and bead morphology than any of the other varied parameters.

Future Work Implications

One of the biggest limitations in this investigation was electrode size. In order to be able to drill the electrode to obtain the hollow electrode, a rather large electrode had to be utilized (5/32 inch (4mm) diameter). Future work with a smaller electrode and/or a larger diameter hole may indeed show that hollow electrode GTAW has some merits.

In addition, use of krypton and hydrogen in place of argon and helium as the shield gas may produce interesting results. Both gases are even farther apart physically than the gases used here and would produce a different arc field than seen here. Determining "k" from measured versus predicted penetration plots utilizing these two gases and the conditions studied here and plotting them versus hydrogen content in the shield gas should provide a better understanding of the shield gas phenomenon. Does shield gas have as large an effect on bead morphology in the normal operating current range for a given electrode diameter? This investigation indicates shield gas is a much larger factor in determining arc stability and bead morphology than the other weld variables. Is this necessarily true at current ranges pushing the limits of the electrode?

Answers to the above two questions may help us understand the factors controlling the arc and allow us a better

understanding of how to weld in space type environments as well as those environments here on Earth.

The trends seen and the transitional behavior (fluid flow to parameter control depending on current range utilized) found herein should be pursued with other anode materials. Specifically, the use of aluminum or carbon steel for the anode in studies similar to those outlined herein would prove beneficial. The use of a relatively "pure" material on the transitional behavior would also be interesting. It is known (33) how these materials behave at low currents, but how do they perform at higher currents? Do they follow the same behavior as "impure" materials and show steadily increasing penetration or p/w ratios with increasing currents (indicating at high enough current, in the parameter control region, anode chemistry has no effect on bead morphology), or does bead morphology follow another pattern.

This information will also be useful to program automatic welding systems with feedback control.

CONCLUSIONS

1. Shield gas had a much greater effect on bead morphology and arc characteristics than electrode type (solid or hollow) or shape (unshaped 180 degree) or 150 or 90 degree tip).
2. Hollow electrode GTAW is much better than solid electrode GTAW under isolated conditions only. Generally, both electrodes yielded similiar results under similiar conditions.
3. Equations of the form $P=k(I^4/SV^2)^{1/3}$ for prediction of fusion zone depth were found to be reasonable in predicting GTA weld penetration in the parameter control zone. This held true for the hollow electrode in most cases. These above equations do not apply in the fluid flow zone (less than 300 Amperes)
4. In the limited measurements made, arc stability with hollow electrodes was not different from solid electrode GTAW.

REFERENCES

1. Recommended Practices For Gas Tungsten Arc Welding; AWS C5.5-80; American Welding Society; Miami, Florida; (1980)
2. Jackson, C.E.; The Science Of Arc Welding, Parts I, II, and III; Welding Journal; 39 (4-6); pp.129-s to 140-s,177-s to 190-s, and 225-s to 230-s; (1960)
3. Danilov, V. A. and Chernyshov; On The Mechanism Of Action Of A Pulse Of Current On The Weld Pool; SVAR Prois; (1); pp. 54-56; (1974)
4. Haddad, G. N. and Farmer, A. J. D.; Temperature Measurements In Gas Tungsten Arcs; Welding Journal; 64 (12); pp. 339-s to 342-s; (1985)
5. Goldman, K.; Electric Arcs In Argon: Volt-Amp and Volt-Arc Gap Characteristics; British Welding Journal; 12 (9); pp. 430 to 434; (1965)
6. Glickstein, S. S. and Yeniscavich, W.; A Review of Minor Element Effects On The Welding Arc and Weld Penetration; WRC Bulletin 226; Welding Research Council; New York; 1977
7. Kovalev, I.M. Akulov, A.I. and Martinson, L.K.; Influence Of The Thermal Characteristics Of Arc Plumes On The Depth Of Penetration; Svar Prois; (12); pp. 19-21 1971
8. Ouden, G.D.; Physical Properties Of The Arc Column; IIW Document # 212-184-70; American Delegation to IIW; AWS; Miami, Fla
9. Heiple, C.R. and Roper, J.R.; Effect of Selenium on GTAW Fusion Zone Geometry; Welding Journal; 59 (8); pp 143-s to 145-s; (1981)
10. Nestor, O.H.; Heat Intensity and Current Density Distributions at The Anode of High Current Inert Gas Arcs; Journal of Applied Physics; 33 (5); pp. 1638-1648; (1967)
11. Quigley, M.B.C., et. al.; Heat Flow To The Workpiece From A TIG Welding Arc; Journal of Applied Physics; 39 (6); pp. 2250-2258; (1973)

12. Dinulescu, H.A. and Pfender, E.; Analysis of The Anode Boundary Layer of High Intensity Arcs; Journal of Applied Physics; 46 (6); pp. 3149-3157; (1980)
13. Jones, T.B. Kouwenhaven, W.B. and Skolnik, M.; Heat Effects In Anode Spots Of High Current Arcs; Welding Journal; 28 (10); pp 461s-465s; (1949)
14. Kouwenhoven, W.B. and Jones, T.B.; Arc Phenomena With Electrodes Moving At High Speed; Welding Journal; 27 (9) pp. 470s-475s; (1948)
15. Ludwig, H.C.; Current Density and Anode Spot Size In The Gas Tungsten Arc; Welding Journal; 47 (5) pp. 234-s to 240-s; (1968)
16. Heiple, C.R., Roper, J.R. Stagner, R.T., and Aden, R.J.; Surface Active Element Effects on the Shape of GTA, Laser; and Electron Beam Welds; Rockwell International Report #RD-178(199)-1; (1983)
17. Savage, W.F., Nippes, E.F., and Goodwin, G.M.; Effect of Minor Elements on Fusion Zone Dimensions in Inconel 600; Welding Journal; 56 (4); pp. 126-s to 132-s; (1977)
18. Heiple, C.R., Cluley, R.J., and Dixon, R.D.; Effect of Aluminum on GTA Weld Geometries in Stainless Steel; Rockwell International Report; (1979)
19. Niles, R.W. and Jackson, C.E.; Weld Thermal Efficiency of The GTAW Process; Welding Journal; 54; (1); pp. 25-s to 32-s; (1975)
20. Chihoski, R.A.; The Rationing of Power Between the Gas-Tungsten Arc and Electrode; Welding Journal; 49; (2); pp. 69s-82s; (1970)
21. Gordon, G.M., Cotter, O.A., and Parker, E.R.; Effect of Current and Atmospheres On Arc Temperatures; Welding Journal; 45 (1); pp. 109s-112s; (1966)
22. Fett, G.H.; Cathode Drop of an Arc; Welding Journal; 21 (1); pp. 27-s to 29-s; (1942)
23. Lancaster, J.F.; Energy Distribution In Argon-Shielded Welding Arcs; British Weld Journal; 1 (9); pp. 412 to 426; (1954)

24. Yamauchi, N., Taka, T. and Ohi, M.; Development And Application Of High Current TIG Process SHOLTA Welding Process; Proceedings Of International Conference On Welding Research In The 1980's; October 27-29, 1980 Osaka, Japan; Session B
25. Bukarov V.A.; On The Force Effect Of A Costricted Arc On The Welded Metal; Svar Prois; (6); pp. 5-7; (1976)
26. Selyanenkov, V.N.; Distribution Of The Pressure Of A DC Arc; Svar Prois; (7); pp. 4-6; (1974)
27. Selyanenkov, V.N., Stepanov, V.V. and Saifiev, R.Z.; The Dependence Of The Pressure Of The Welding Arc On The Parameters Of Tungsten Electrodes; Svar Prois; (5); pp. 5-7; (1980)
28. Winsor, L.P. and Turk, R.R.; A Comparative Study Of Thoriated, Zirconated And Pure Tungsten Electrodes; Welding Journal; 36 (3); pp. 113s-119s; (1957)
29. Chihoski, R.A.; The Effects of Varying Electrode Shape on Arc Operation and Quality of Welds In 2014-T6 Aluminum; Welding Journal; 47 (5); pp. 210s-222s; (1968)
30. Erokhin, A.A., et. al.; Influence Of Tungsten Cathode Geometry On Some Welding Arc Characteristics And Metal Penetration; Svar Prois; (12); pp. 17-19; (1971)
31. Savage, W.F., Strunk, S.S. and Ishikawa, Y.; The Effect Of Electrode Geometry In Gas Tungsten-Arc Welding; Welding Journal; 44 (11); pp. 489s-496s; (1965)
32. Turney, V.; The Influence of Welding Parameters and Base Metal Composition on the Bead Morphology of Gas Tungsten Arc Vanadium Welds; MS Thesis T-2546; (1982)
33. Burgardt, P. and Heiple, C. R.; Interaction Between Impurities and Welding Variables in Determining GTA Weld Shape; Welding Journal; 65 (6); pp 150-s to 155-s; (1986)
34. Shinoda, V. and Doherty; The Relationship Between Arc Welding Parameters and Weld Bead Geometry; The Welding Institute; Abington Hall; Cambridge; 1978

35. Jackson, C.E. and Shrubsall, A.E.; Control Of Penetration And Melting Ratio With Welding Technique; Welding Journal; 32 (4); pp. 172s-178s; (1953)
36. Schwemmer, D. D., Olson, D. L., and Williamson, D. L.; The Relationship of Weld Penetration To the Welding Flux; Welding Journal; 48 (5); pp. 151-s to 159-s; (1979)
37. Savage, W.F., et. al.; Minor Element Effects On Gas Tungsten Arc Weld Penetration; Interim Report to National Science Foundation for Contract MEA-8208950; Oct. 1982- Sept 1983
38. Erokhin, A. A.; Calculation of The Principal Parameters of The Pool In The Welding of Plate; Weld Production; (12); pp. 1 to 5; (1970)
39. Watanabe, M. and Satoh, L.; Prediction of Penetration In Welded Joints by Welding Conditions Parts I and II; Journal of Japan Welding Society; 24 (12) and 25 (1); pp. 512 to 519 and pp. 18 to 23; (1955) and (1956)
40. Richter, E.; Rechnerische Verfahren zum Bestimmen von Schweissparametern fur das UP-Schweissen Zismittelungen; 10 (12); pp. 1972 to 1988; (1968)
41. Sharapov, Y. A.; Width Calculation for Automatic Submerged-Arc Butt Welds; Weld Production; (3) pp. 45 to 47; (1972)
42. Bolotin, V.S. and Petrov, A.V.; Electrical Characteristics of An Arc Discharge With A Hollow Non-Consumable Electrode; Svar Prois; (7); pp. 1-4; (1976)
43. Budnik, V.N. and Letnev, A.V.; The Application Of The Method Of Experiment Planning To The Determination Of The Effective Efficiency Of Heating With An Arc Discharge With A Hollow Cathode In Vacuum; Svar Prois; (6); pp. 1-3; (1977)
44. Budnik, V.N., et. al.; Electric Operating Conditions Of An Arc Discharge With A Hollow Cathode In Vacuum; Svar Prois; (10); pp. 3-4; (1976)
45. Shiganov, N.V. et.al.; Some Special Features Of Arc Welding With A Hollow Electrode In Vacuum; Svar Prois; (9); pp. 17-19; (1973)

46. Tarasenko, E.N., et. al.; Electrostatic Phase Control Of The Arc Discharge Current With A Hollow Cathode In Welding And Surfacing In Vacuum; Svar Prois; (6); pp. 1-3; (1984)
47. Demchenko, A.D.; Mechanical Properties and Microstructure of Vanadium Alloy Welds; Svar Prois; (6); pp. 1-3; (1984)
48. Leinonen, J.I.; Some Methods For Improving TIG Weld Penetration; Stainless Steel '84; The Institute of Metals; #1 Carlton House Terrace; London SW1Y 5DB; UK; (1985)
49. Key, J.F.; Investigation of Factors Controlling GTA Weld Bead Geometry; Trends In Welding Research In the United States; American Society For Metals; Metals Park, Ohio; 1982

APPENDIX I

Constant Heat Input Raw Data and Graphs

TABLE A1-1

All values in inches unless otherwise noted

SAM- PLE#	WELD	CURRENT AMPS	TYPE	POTENTIAL VOLTS	SHIELD GAS	HOLE SIZE	ANGLE	PENETRA- TION	BEAD WIDTH	P/w	MELT AREA IN-2	TRAVEL ipm	HEAT IN- PUT kJ/in
3	1	100	DC	9.5	argon	3/32	180	0.016	0.110	0.145		2.5	22.8
49	1	150	DC	10.0	argon	3/32	180	0.056	0.247	0.227	0.208	3.5	25.7
3	2	175	DC	10.5	argon	3/32	180	0.059	0.275	0.215		4.0	27.5
49	2	200	DC	11.0	argon	3/32	180	0.063	0.305	0.207	0.220	5.5	24.0
3	3	225	DC	11.5	argon	3/32	180	0.073	0.385	0.190		6.5	23.9
49	3	250	DC	13.0	argon	3/32	180	0.079	0.390	0.203	0.212	8.0	24.4
3	4	275	DC	13.5	argon	3/32	180	0.057	0.385	0.148		9.0	24.8
9	1	290	DC	14.0	argon	3/32	180	0.065	0.400	0.137	0.222	10.0	24.4
45	1	100	DC	10.0	argon	n/a	180	0.016	0.203	0.079		3.0	20.0
9	2	150	DC	11.0	argon	n/a	180	0.049	0.302	0.162	0.168	3.5	28.3
45	2	175	DC	11.0	argon	n/a	180	0.049	0.228	0.215		4.5	25.7
9	3	200	DC	12.0	argon	n/a	180	0.059	0.335	0.176	0.236	5.5	26.2
45	3	225	DC	12.0	argon	n/a	180	0.067	0.330	0.203		6.5	25.9
60	1	250	DC	14.0	argon	n/a	180	0.059	0.400	0.147	0.242	8.0	26.3
45	4	275	DC	14.0	argon	n/a	180	0.067	0.440	0.152	0.239	9.5	24.3
60	2	290	DC	15.0	argon	n/a	180	0.075	0.427	0.176	0.295	10.5	24.9
60	3	100	AC	22.5	argon	n/a	180	0.012	0.086	0.140	0.015	5.5	24.5
18	1	150	AC	25.0	argon	n/a	180	0.036	0.258	0.140	0.031	9.0	24.0
18	2	200	AC	31.0	argon	n/a	180	0.040	0.275	0.145	0.053	15.5	25.0
18	3	230	AC	36.0	argon	n/a	180	0.045	0.267	0.169	0.084	20.0	24.8
71	1	100	AC	22.0	argon	3/32	180	0.010	0.120	0.083	0.209	5.0	26.4
71	2	150	AC	24.0	argon	3/32	180	0.031	0.205	0.151	0.261	9.0	24.0
71	3	200	AC	30.0	argon	3/32	180	0.031	0.226	0.137	0.395	15.0	24.0
33	1	230	AC	36.0	argon	3/32	180	0.041	0.255	0.161	0.445	20.0	24.8
33	2	150	DC	13.0	75ArHe	n/a	180	0.057	0.292	0.195	0.033	4.5	26.0
33	3	200	DC	14.0	75ArHe	n/a	180	0.061	0.400	0.152	0.071	7.0	24.0
24	1	250	DC	14.0	75ArHe	n/a	180	0.049	0.370	0.132	0.175	12.0	17.5
24	2	290	DC	15.0	75ArHe	n/a	180	0.054	0.396	0.136	0.231	14.5	18.0
24	3	150	AC	21.0	75ArHe	n/a	180	0.025	0.181	0.138	0.261	5.0	25.2
80	1	200	AC	24.0	75ArHe	n/a	180	0.041	0.239	0.172	0.344	9.0	24.0
80	2	250	AC	34.0	75ArHe	n/a	180	0.031	0.259	0.120	0.426	17.0	24.0
80	3	290	AC	37.0	75gArHe	n/a	180	0.053	0.352	0.151	0.602	21.0	24.3

TABLE A1-1 (continued)

SAM- PLE#	WELD	CURRENT AMPS	TYPE	POTENTIAL VOLTS	SHIELD GAS	HOLE SIZE	ANGLE	PENETRA- TION	BEAD WIDTH	P/w	MELT AREA IN-2	TRAVEL ipm	HEAT IN- PUT	kJ/in
53	1	150	DC	13.0	75ArHe	3/32	180	0.070	0.290	0.241	0.051	5.0	23.4	
53	2	200	DC	13.0	75ArHe	3/32	180	0.070	0.390	0.179	0.106	6.5	24.0	
53	3	250	DC	14.0	75ArHe	3/32	180	0.050	0.440	0.114	0.195	9.0	23.3	
14	1	290	DC	14.0	75ArHe	3/32	180	0.068	0.460	0.148	0.214	10.0	24.4	
14	2	100	AC	22.0	75ArHe	3/32	180	0.019	0.178	0.107	0.246	5.5	24.0	
14	3	150	AC	26.0	75ArHe	3/32	180	0.029	0.245	0.118	0.299	9.5	24.6	
50	1	200	AC	35.0	75ArHe	3/32	180	0.034	0.253	0.134	0.369	17.5	24.0	
50	2	100	AC	28.0	25ArHe	3/32	180	0.031	0.207					
50	3	150	AC	30.0	25ArHe	3/32	180	0.043	0.264					
79	2	200	AC	36.0	25ArHe	3/32	180	0.043	0.350					
79	3	150	DC	14.0	25ArHe	3/32	180	0.052	0.329	0.158	0.212	5.0	25.2	
35	1	200	DC	14.0	25ArHe	3/32	180	0.065	0.440	0.148	0.247	7.5	22.4	
35	2	250	DC	15.0	25ArHe	3/32	180	0.063	0.532	0.118	0.276	9.5	23.7	
35	3	290	DC	15.0	25ArHe	3/32	180	0.066	0.573	0.115	0.249	20.0	13.1	

The figures following are the actual data points used in determining the trends seen in the main section of this thesis. In all cases, the solid electrode is represented by an X and the hollow electrode is represented with a cross (+).

Units on figures where not stated are:

CURRENT - AMPERES (x-axis)
VOLTAGE - VOLTS
PENETRATION - INCH
MELT AREA - SQUARE INCHES

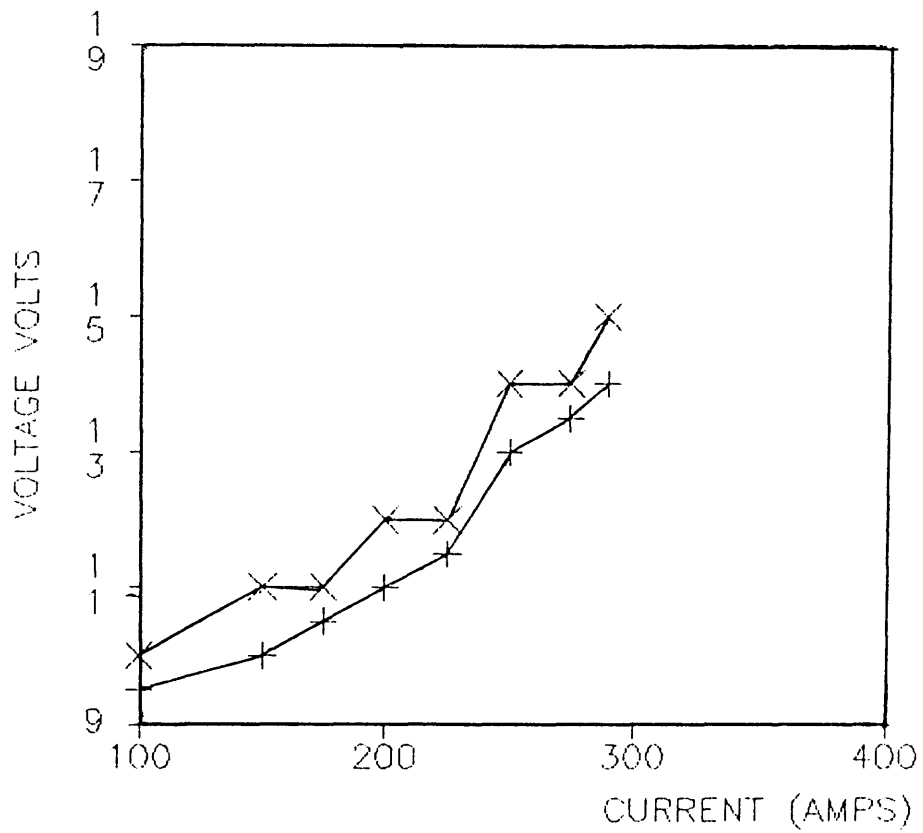


Figure A1-1

Arc Potential-Current Characteristic
Curve for DC Constant Heat Input
Welds In Argon

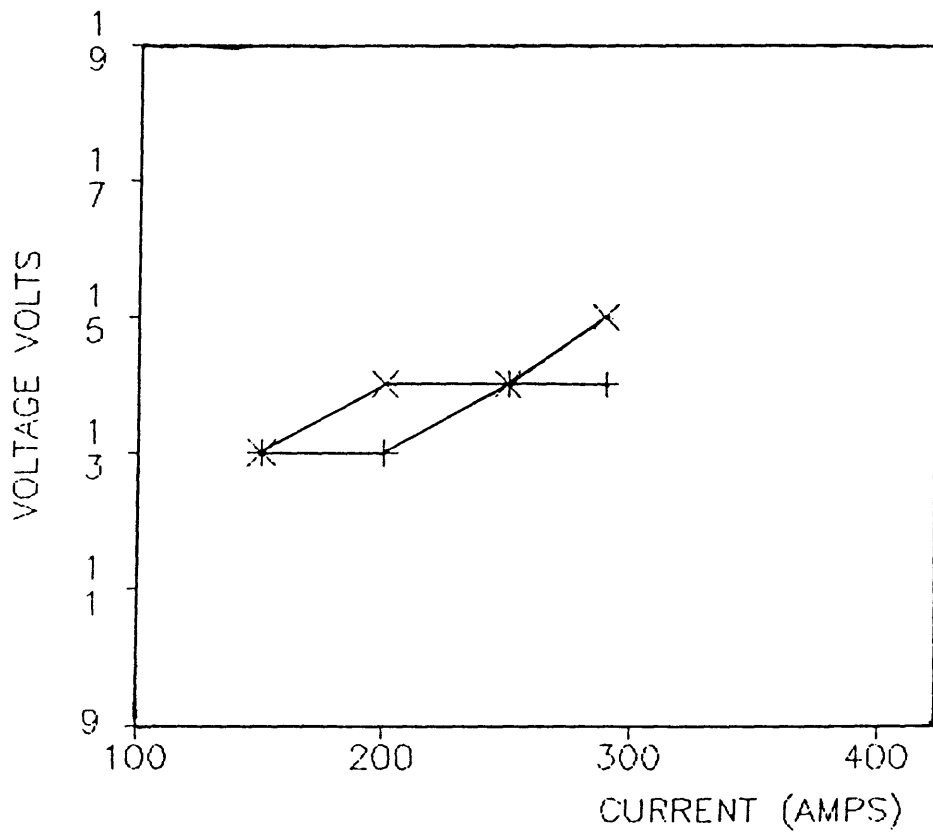


Figure A1-2 Arc Potential-Current Characteristic Curve for DC Constant Heat Input Welds In 75ArHe

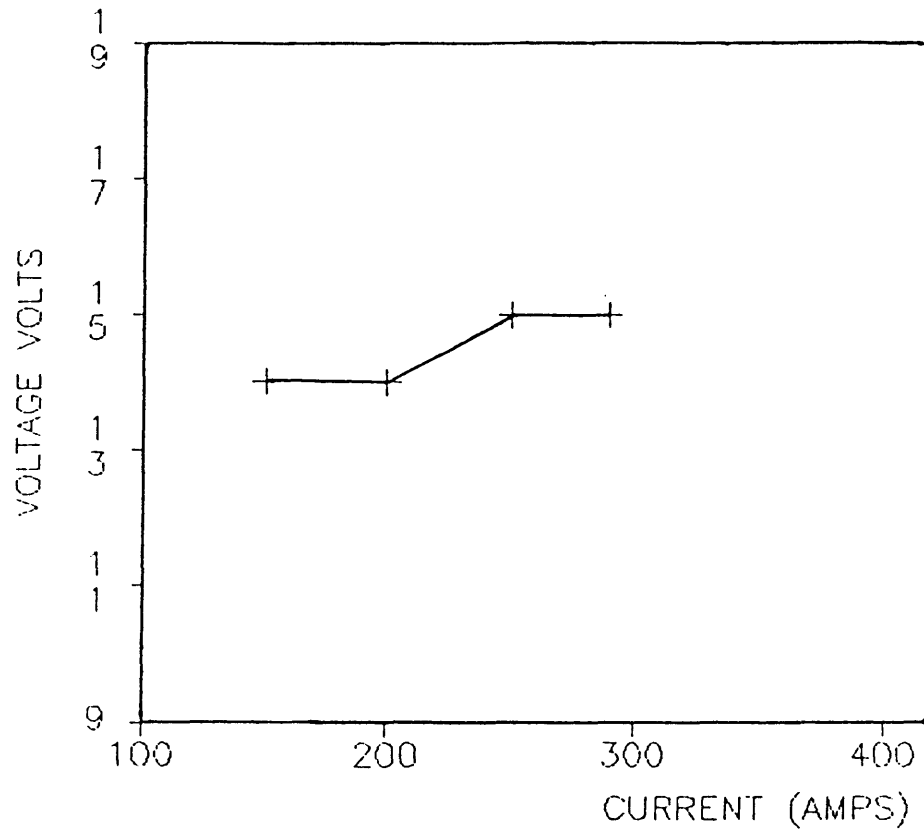


Figure A1-3 Arc Potential-Current Characteristic Curve for DC Constant Heat Input Welds In 25ArHe

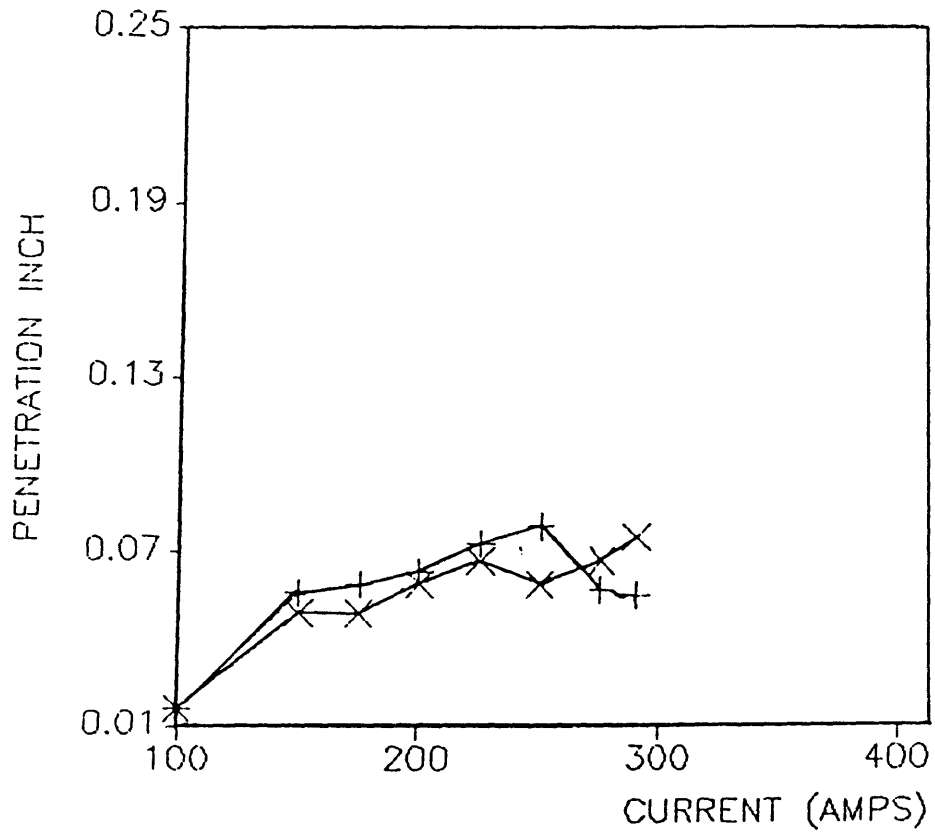


Figure A1-4 Current Versus Penetration For DC Constant Heat Input Welds In Argon

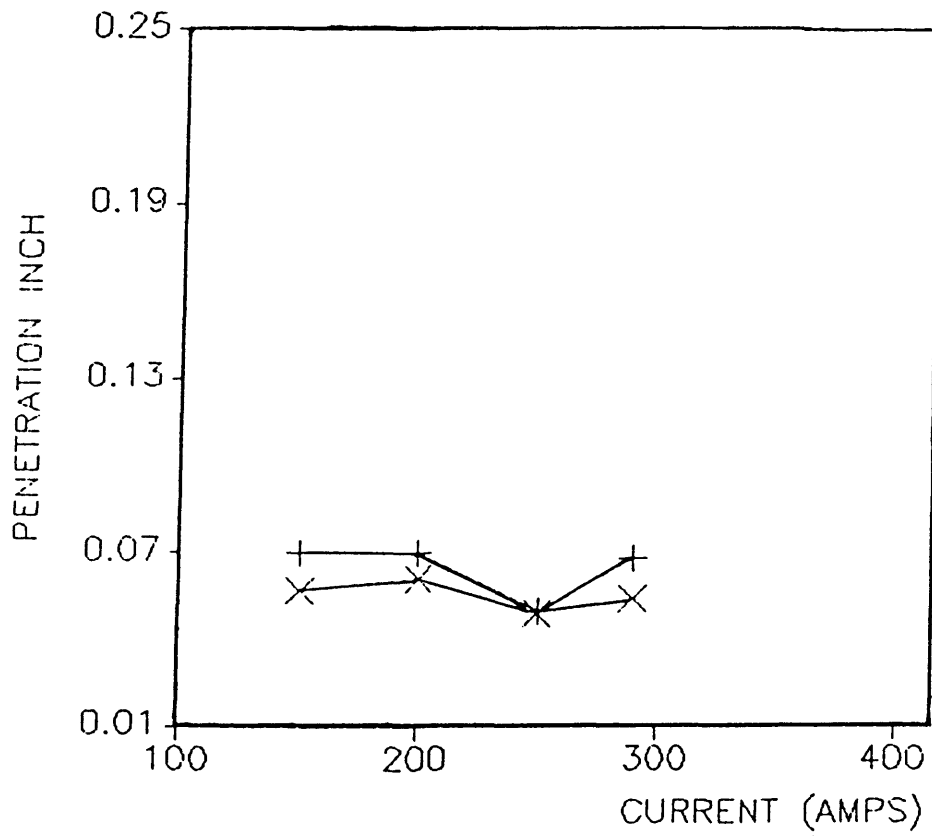


Figure A1-5 Current Versus Penetration For DC Constant Heat Input Welds In 75ArHe

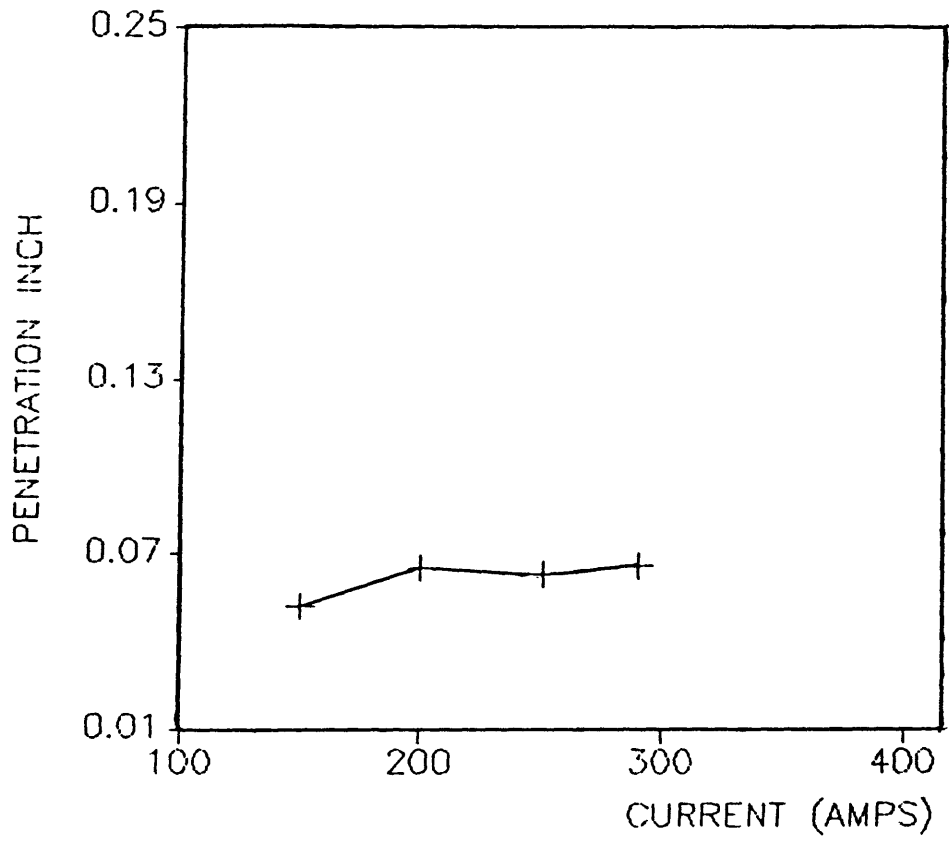


Figure A1-6 Current Versus Penetration For
DC Constant Heat Input Welds In
25ArHe

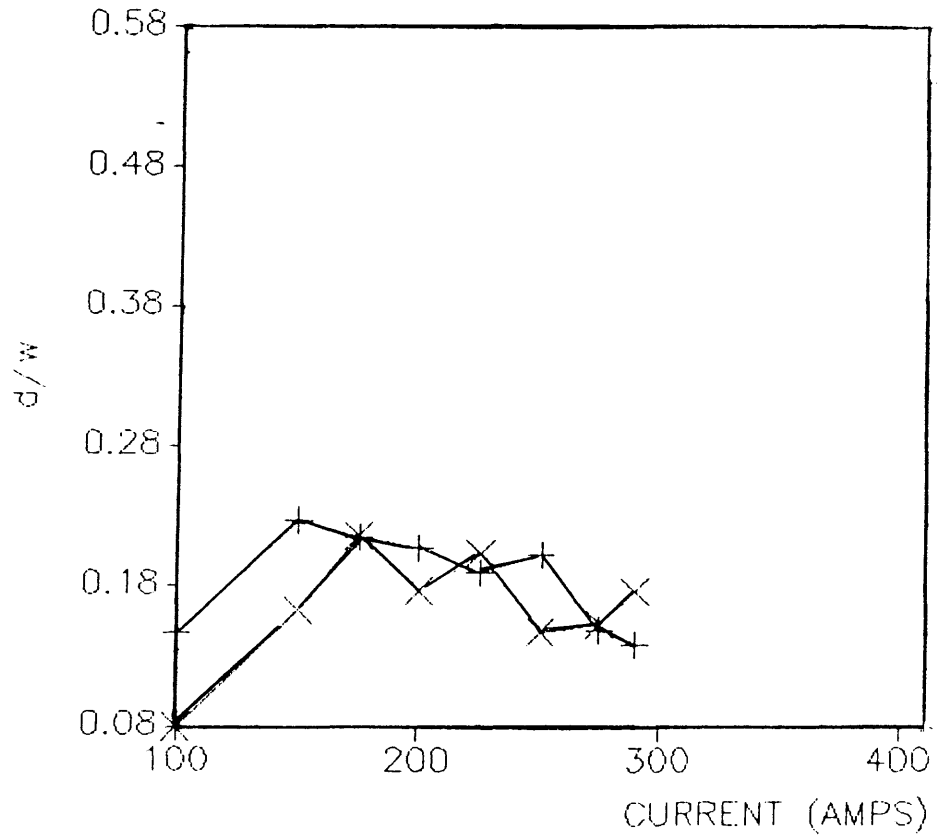


Figure A1-7 Current versus p/w For DC Constant Heat Input Welds In Argon

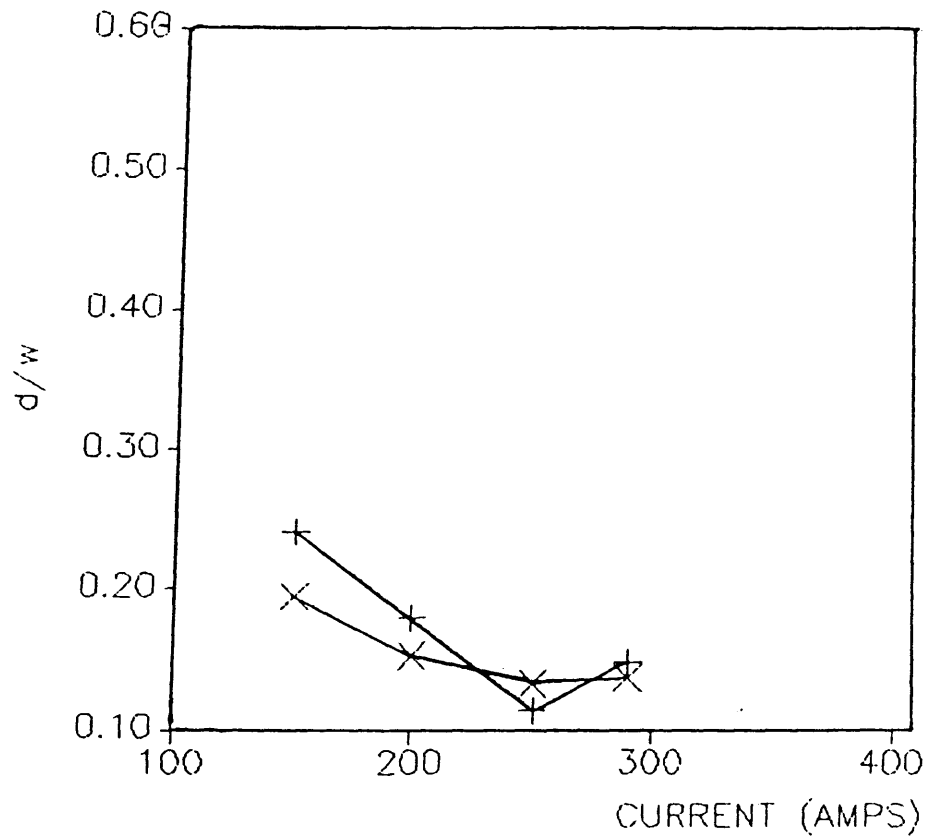


Figure A1-8 Current versus p/w For DC Constant Heat Input Welds In 75ArHe

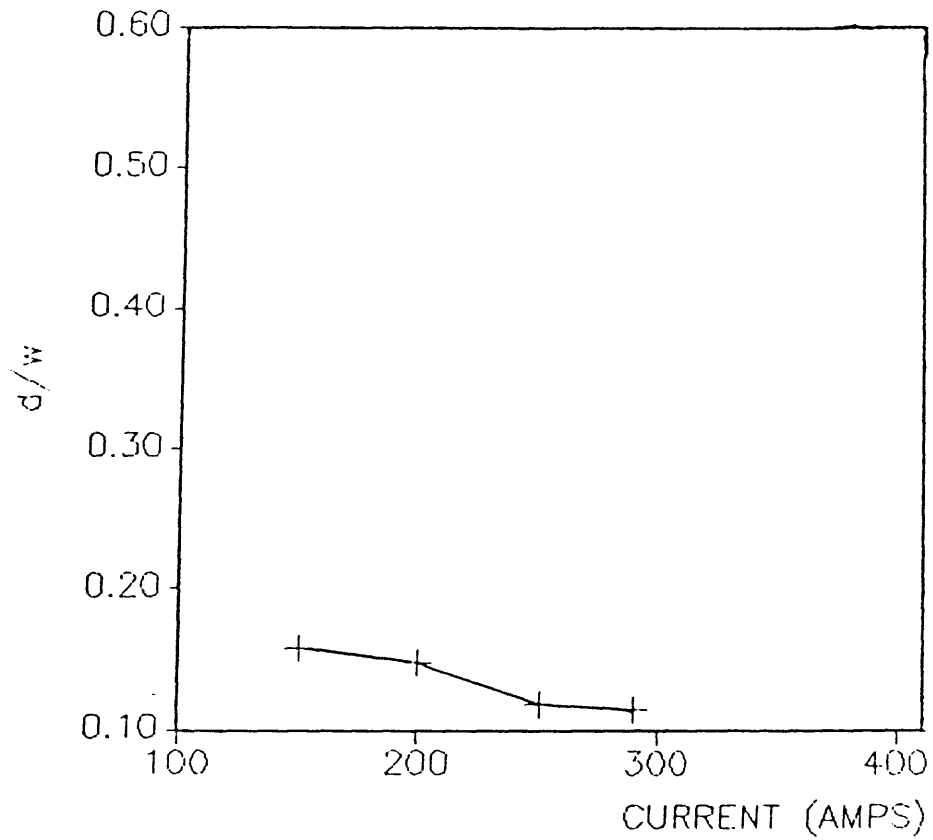


Figure A1-9 Current versus p/w For DC Constant Heat Input Welds In 25ArHe

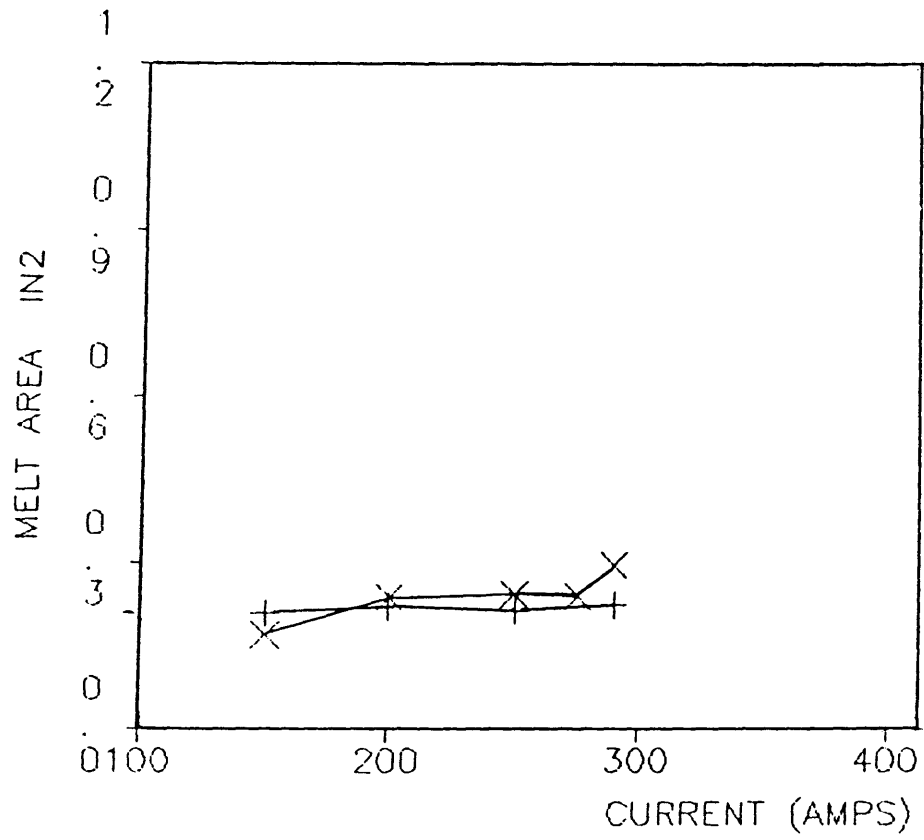


Figure A1-10 Current versus Melt Area For DC Constant Heat Input Welds In Argon

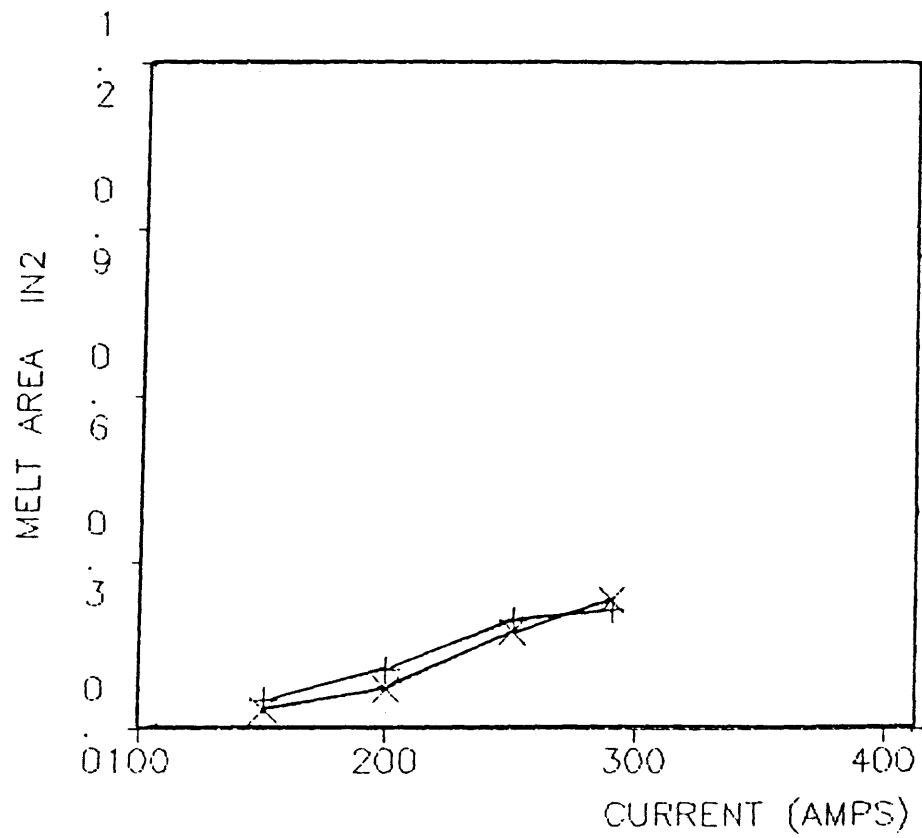


Figure A1-11 Current versus Melt Area For DC
Constant Heat Input Welds In 75ArHe

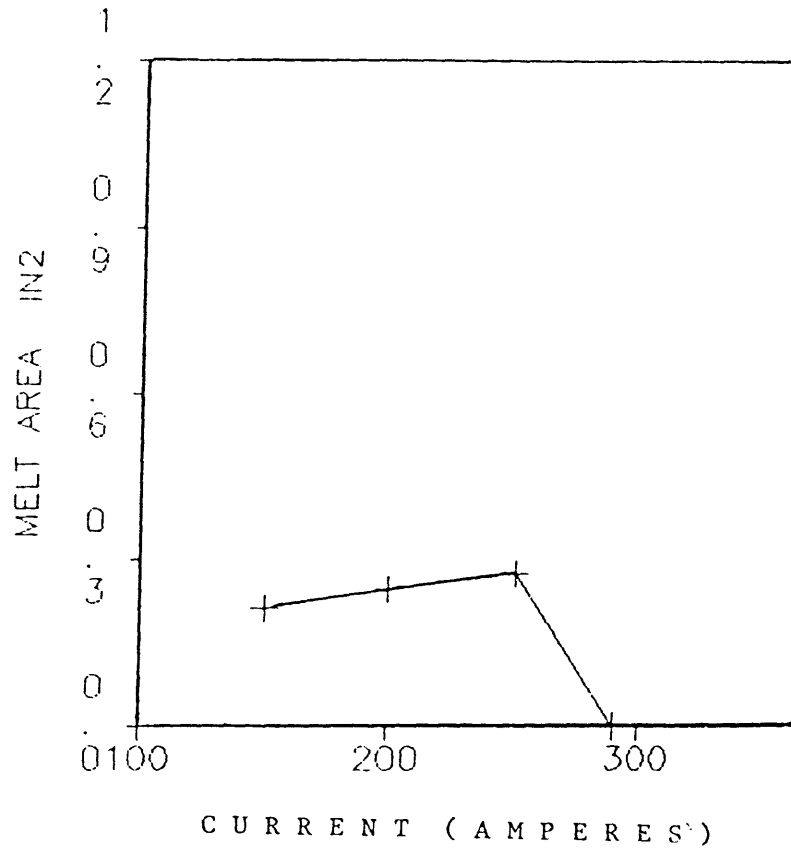


Figure A1-12 Current versus Melt Area For DC
Constant Heat Input Welds In 25ArHe

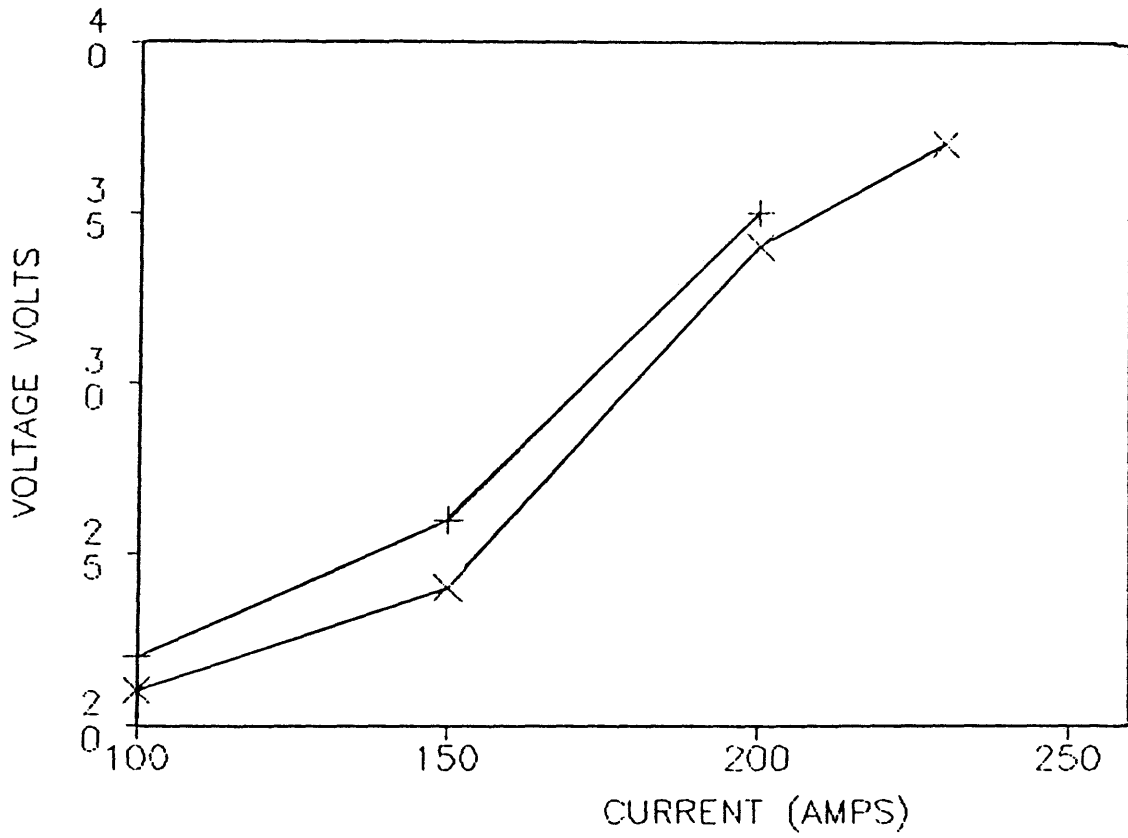


Figure A1-13 Arc Potential-Current Characteristic Curves for AC Constant Heat Input Welds In Argon

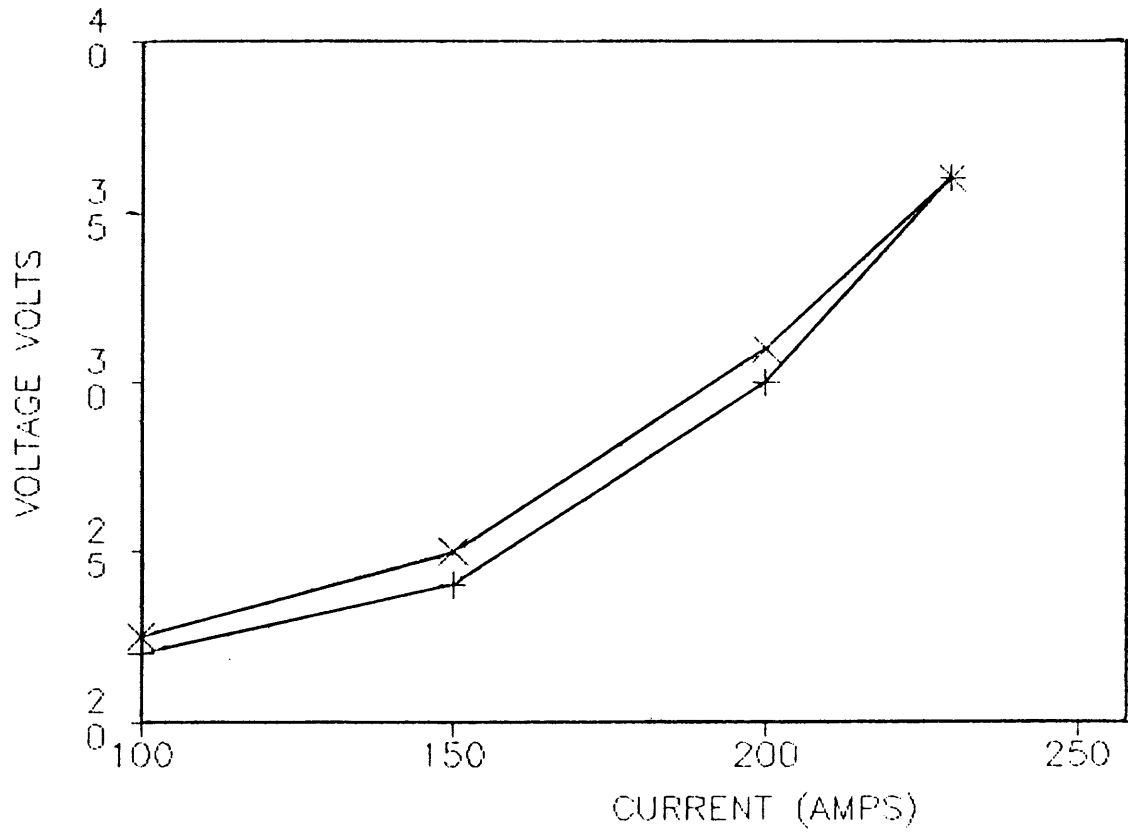


Figure A1-14 Arc Potential-Current Characteristic Curves for AC Constant Heat Input Welds In 75ArHe

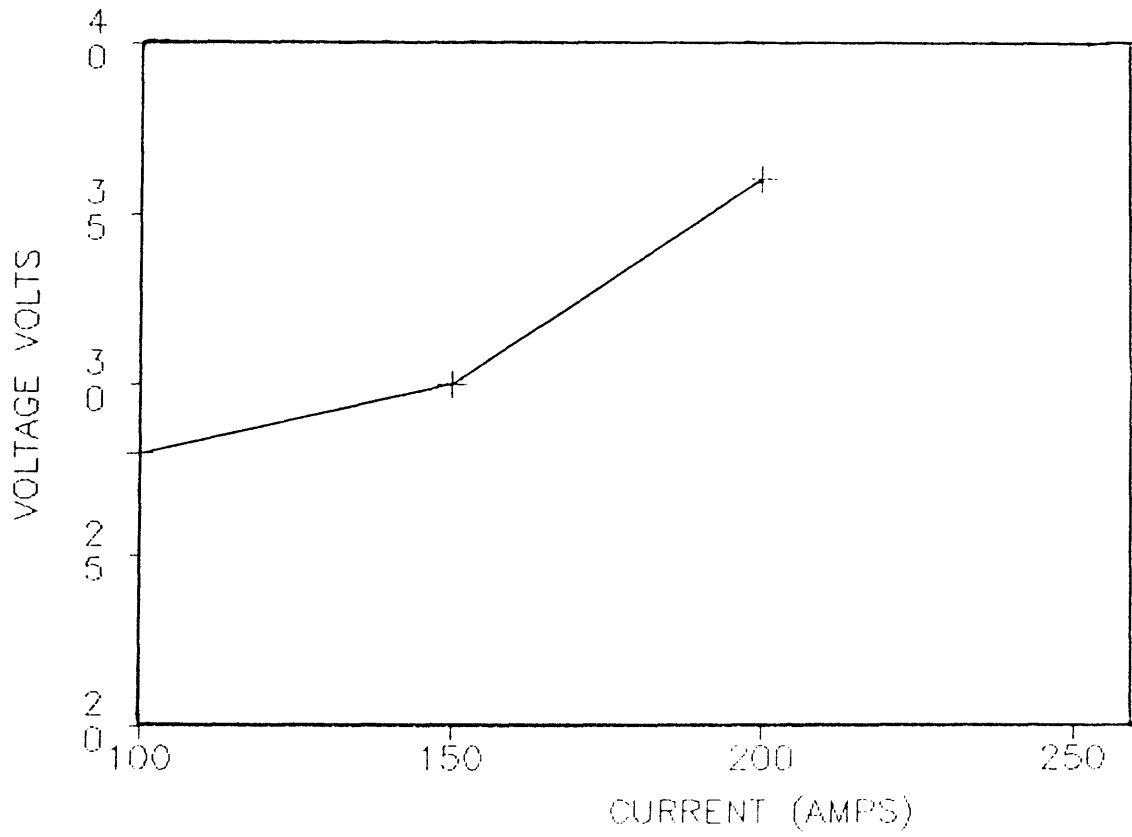


Figure A1-15 Arc Potential-Current Characteristic Curves for AC Constant Heat Input Welds In 25ArHe

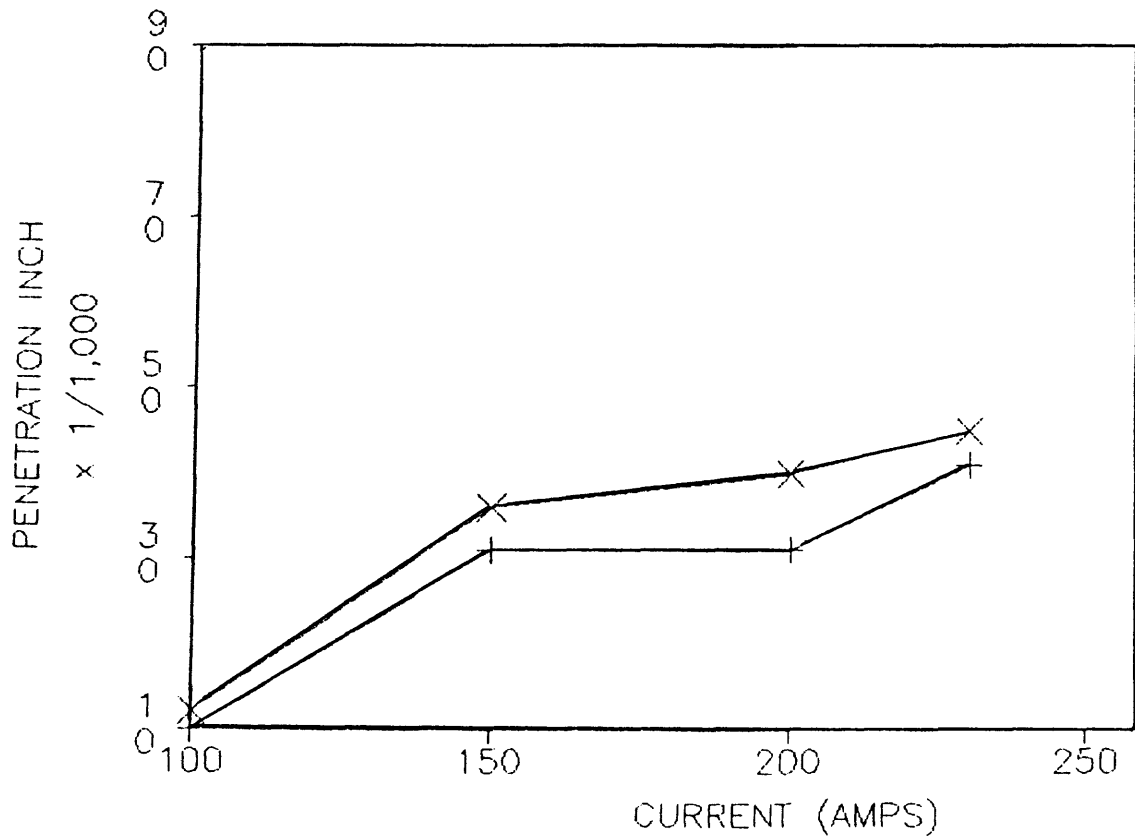


Figure A1-16 Current Versus Penetration For AC Constant Heat Input Welds In Argon

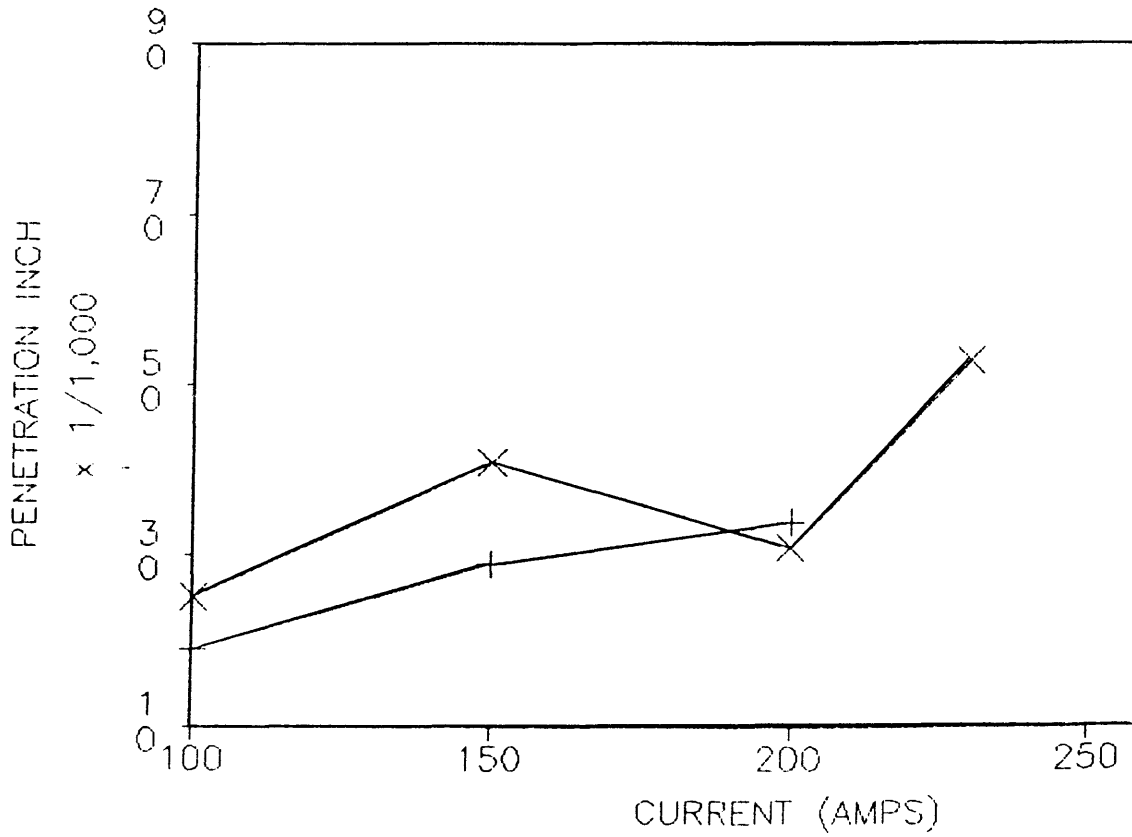


Figure A1-17 Current Versus Penetration For AC Constant Heat Input Welds In 75ArHe

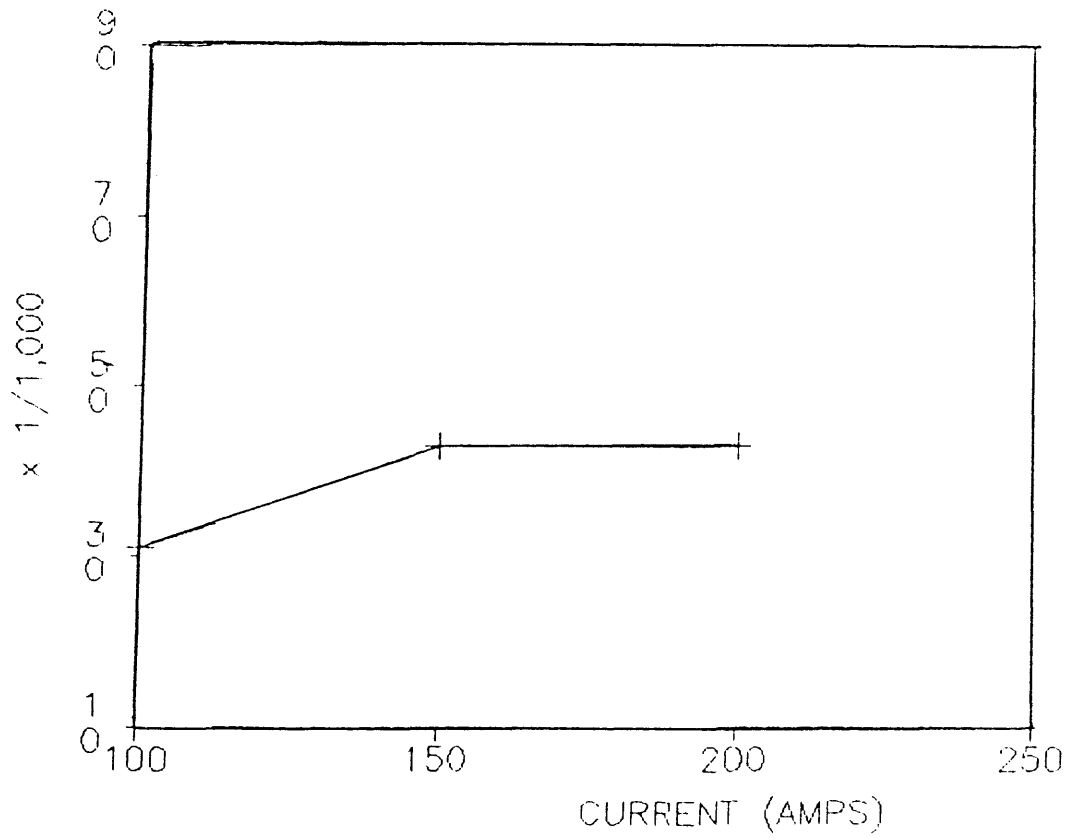


Figure A1-18 Current Versus Penetration For
AC Constant Heat Input Welds In
25ArHe

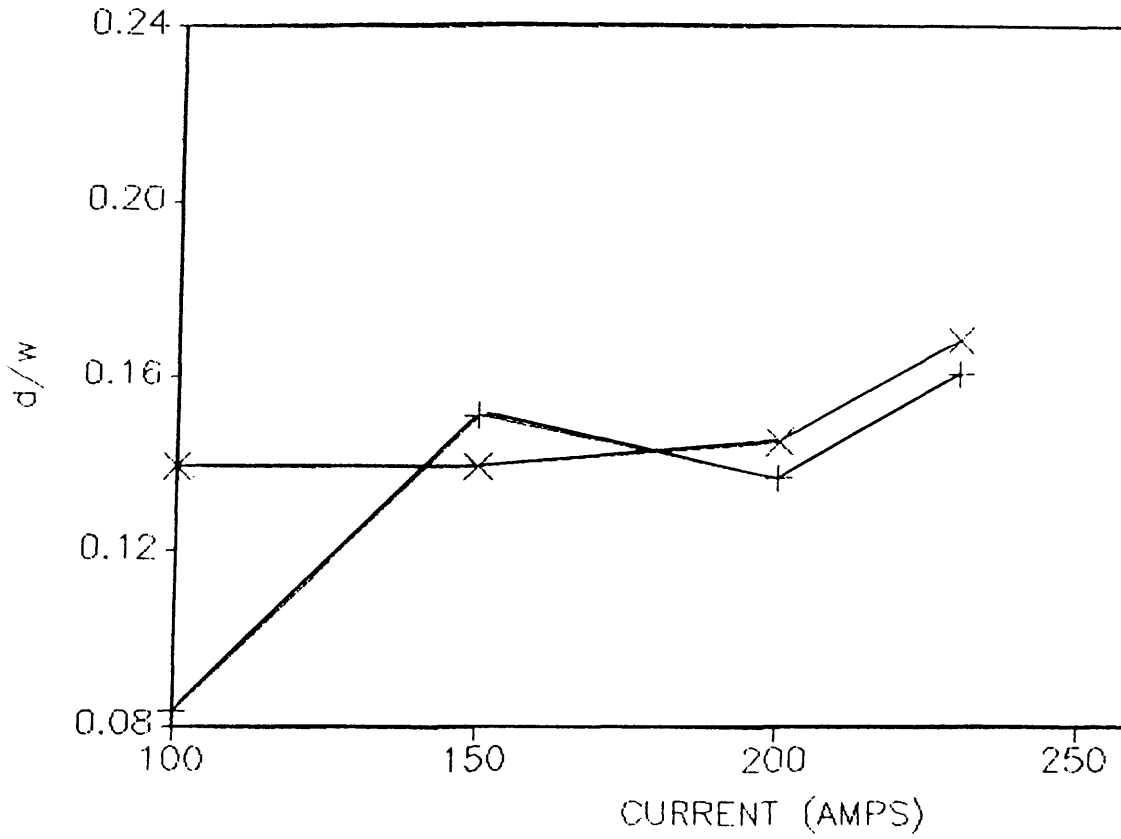


Figure A1-19 Current versus p/w For AC Constant Heat Input Welds In Argon

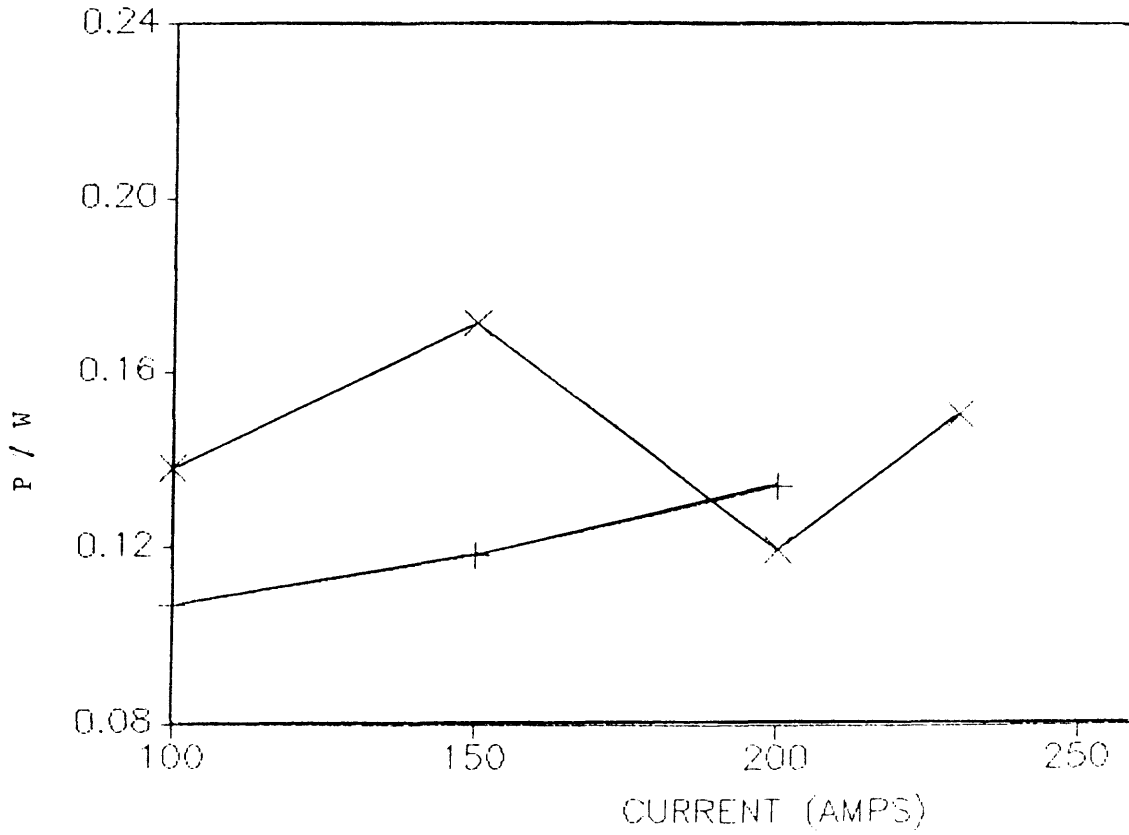


Figure A1-20 Current versus p/w For AC Constant Heat Input Welds In 75ArHe

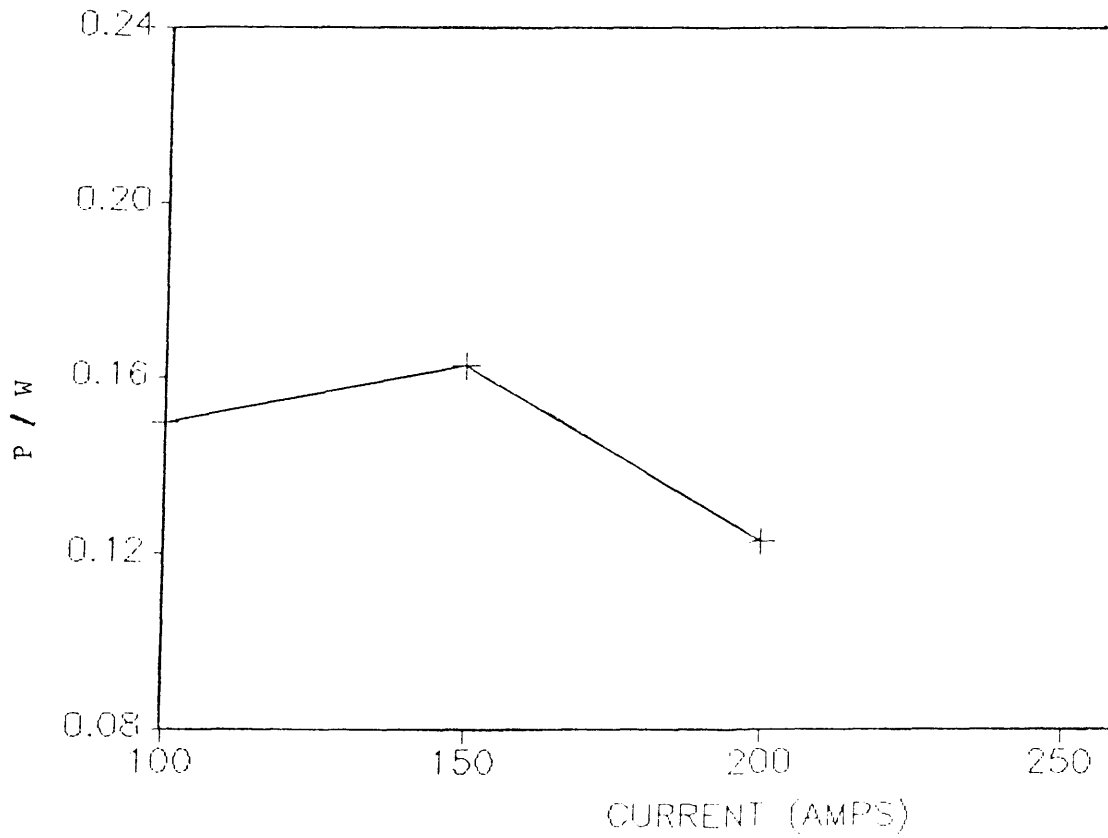


Figure A1-21 Current versus p/w For AC Constant Heat Input Welds In 25ArHe

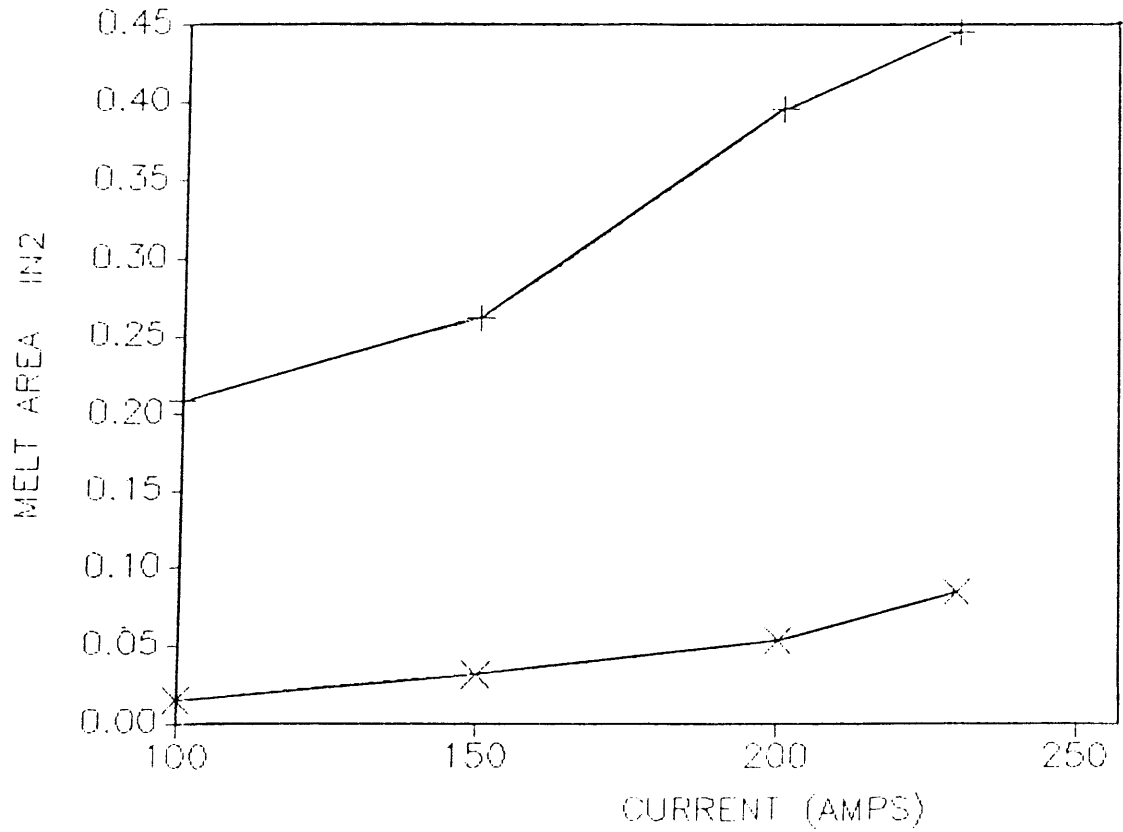


Figure A1-22 Current versus Melt Area For AC
Constant Heat Input Welds In Argon

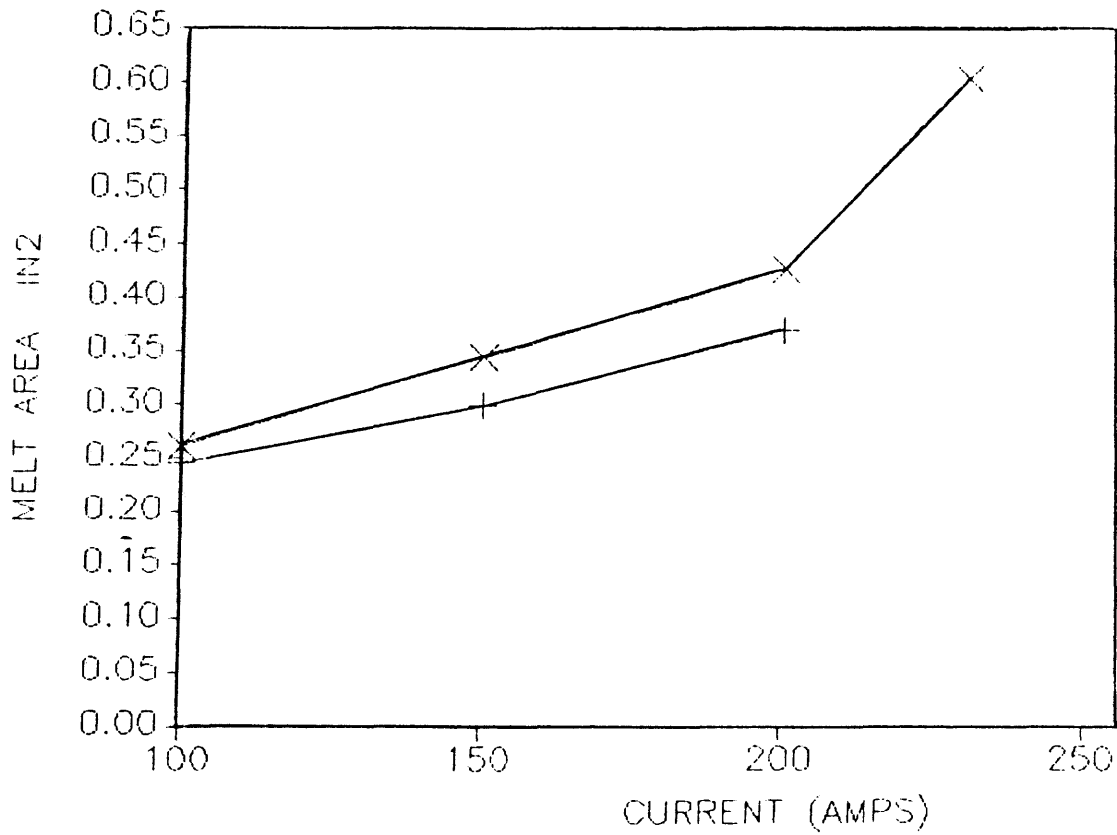


Figure A1-23 Current versus Melt Area For AC
Constant Heat Input Welds In 75ArHe

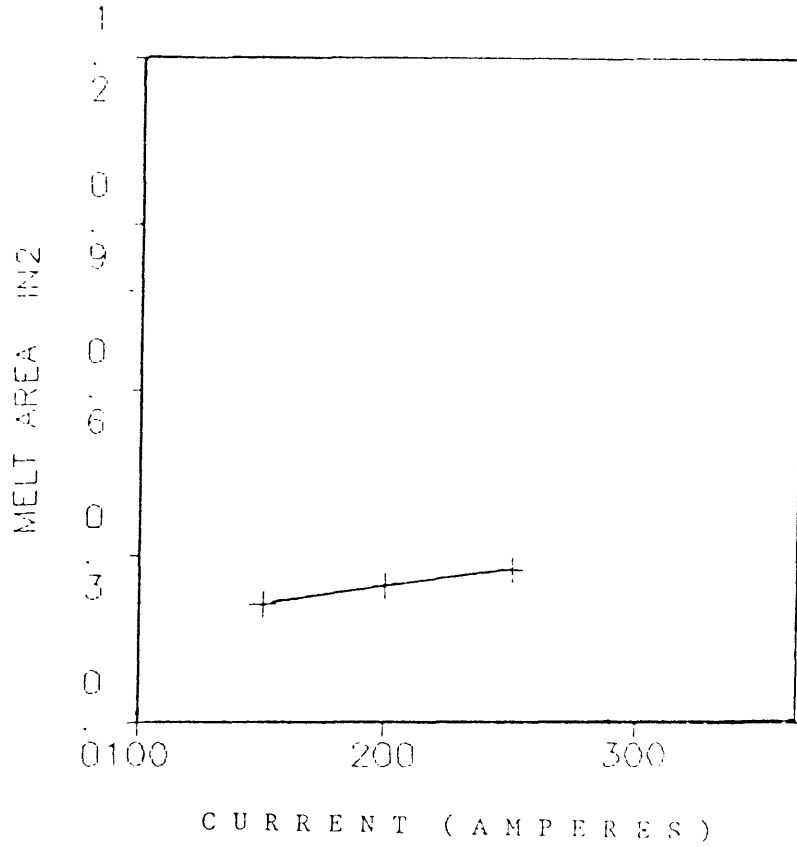


Figure A1-24 Current versus Melt Area For AC
Constant Heat Input Welds In 25ArHe

APPENDIX II

Constant Travel Speed Raw Data and Graphs

TABLE A2-1

All values in inches unless otherwise noted

SAM- PLE#	WELD	CURRENT AMPS	TYPE	POTENTIAL VOLTS	SHIELD GAS	SOLE SIZE	ANGLE	PENETRA- TION IN	BEAD WIDTH	P/w	MELT AREA IN-2	TRAVEL ipm	HEAT IN- PUT kJ/in
64	1	100	DC	12.0	75-ArHe	n/a	180	0.030	0.189	0.160	0.018	10.0	7.2
64	2	150	DC	12.0	75-ArHe	n/a	180	0.044	0.273	0.162	0.032	10.0	10.8
64	3	200	DC	13.5	75-ArHe	n/a	180	0.055	0.397	0.138	0.061	10.0	16.2
42	1	250	DC	13.0	75-ArHe	n/a	180	0.044	0.370	0.118	0.052	10.0	19.5
52	1	303	DC	14.0	75-ArHe	n/a	180	0.051	0.412	0.124	0.145	10.0	25.5
10	1	351	DC	15.0	75-ArHe	n/a	180	0.070	0.520	0.134	0.205	10.0	31.6
68	1	399	DC	15.0	75-ArHe	n/a	180	0.071	0.526	0.135	0.225	10.0	35.9
43	1	450	DC	15.0	75-ArHe	n/a	180	0.081	0.647	0.126	0.177	10.0	40.5
63	1	521	DC	16.0	75-ArHe	n/a	180	0.126	0.761	0.166	0.345	10.0	50.0
64	4	100	DC	11.5	75-ArHe	3/32	180	0.030	0.163	0.184	0.026	10.0	6.9
64	5	150	DC	12.0	75-ArHe	3/32	180	0.045	0.240	0.191	0.043	10.0	10.8
64	6	200	DC	13.0	75-ArHe	3/32	180	0.060	0.348	0.130	0.072	10.0	15.6
20	1	260	DC	13.0	75-ArHe	3/32	180	0.041	0.363	0.115	0.097	10.0	20.3
34	1	311	DC	14.0	75-ArHe	3/32	180	0.055	0.455	0.121	0.150	10.0	26.1
21	1	361	DC	14.0	75-ArHe	3/32	180	0.060	0.497	0.121	0.227	10.0	30.3
42	2	404	DC	15.0	75-ArHe	3/32	180	0.075	0.537	0.140	0.274	10.0	36.4
52	2	460	DC	16.0	75-ArHe	3/32	180	0.125	0.588	0.216	0.286	10.0	44.2
68	2	508	DC	16.0	75-ArHe	3/32	180	0.128	0.619	0.211	0.386	10.0	48.8
69	1	100	DC	13.5	25-ArHe	3/32	180	0.041	0.195	0.213	0.026	10.0	8.1
69	2	150	DC	14.0	25-ArHe	3/32	180	0.049	0.290	0.171	0.044	10.0	12.6
69	3	200	DC	15.0	25-ArHe	3/32	180	0.069	0.517	0.133	0.066	10.0	18.0
52	3	257	DC	14.7	25-ArHe	3/32	180	0.055	0.427	0.129	0.134	10.0	22.7
10	3	305	DC	14.3	25-ArHe	3/32	180	0.051	0.525	0.097	0.218	10.0	26.2
42	3	358	DC	14.2	25-ArHe	3/32	180	0.062	0.536	0.117	0.103	10.0	30.5
63	2	408	DC	16.8	25-ArHe	3/32	180	0.092	0.584	0.147	0.285	10.0	41.1
21	2	456	DC	16.2	25-ArHe	3/32	180	0.116	0.610	0.170	0.383	10.0	44.3
34	2	509	DC	17.3	25-ArHe	3/32	180	0.135	0.853	0.158	0.488	10.0	52.8
69	4	100	DC	14.0	25-ArHe	n/a	180	0.048	0.230	0.208	0.029	10.0	8.4
69	5	150	DC	14.5	25-ArHe	n/a	180	0.050	0.323	0.157	0.058	10.0	13.1
69	6	200	DC	15.0	25-ArHe	n/a	180	0.078	0.530	0.147	0.080	10.0	18.0
20	2	255	DC	14.0	25-ArHe	n/a	180	0.048	0.405	0.117	0.107	10.0	21.4
43	2	307	DC	14.2	25-ArHe	n/a	180	0.057	0.490	0.117	0.124	10.0	26.1
68	3	360	DC	14.1	25-ArHe	n/a	180	0.068	0.537	0.125	0.214	10.0	30.5
21	3	406	DC	17.0	25-ArHe	n/a	180	0.088	0.675	0.130	0.251	10.0	41.4
20	3	454	DC	17.5	25-ArHe	n/a	180	0.101	0.728	0.139	0.305	10.0	47.7
43	3	506	DC	17.3	25-ArHe	n/a	180	0.112	0.735	0.153	0.552	10.0	52.5

TABLE A2-1 (continued)

SAM- PLE#	WELD	CURRENT AMPS	TYPE	POTENTIAL VOLTS	SHIELD GAS	HOLE SIZE	ANGLE	PENETRA- TION IN	BEAD WIDTH	p/w	MELT AREA IN-2	TRAVEL ipm	HEAT IN- PUT kJ/in
5	5	100	DC	12.0	argon	n/a	90	0.023	0.152	0.151	0.040	10.0	7.2
5	6	150	DC	12.0	argon	n/a	90	0.038	0.277	0.137	0.079	10.0	10.8
36	1	200	DC	13.5	argon	n/a	90	0.048	0.322	0.149	0.053	10.0	16.2
36	2	250	DC	14.0	argon	n/a	90	0.064	0.402	0.159	0.085	10.0	21.0
36	3	285	DC	15.0	argon	n/a	90	0.073	0.445	0.164	0.109	10.0	25.7
6	3	350	DC	13.6	argon	n/a	90	0.064	0.477	0.134	0.198	10.0	28.6
39	3	397	DC	14.0	argon	n/a	90	0.074	0.520	0.162	0.277	10.0	33.3
6	4	449	DC	16.3	argon	n/a	90	0.129	0.555	0.232	0.385	10.0	43.9
39	4	501	DC	17.2	argon	n/a	90	0.164	0.525	0.312	0.583	10.0	51.7
36	4	100	DC	11.5	argon	3/32	90	0.030	0.189	0.159	0.034	10.0	6.9
36	5	150	DC	11.0	argon	3/32	90	0.031	0.190	0.163	0.068	10.0	9.9
62	1	200	DC	11.5	argon	3/32	90	0.040	0.297	0.135	0.060	10.0	13.8
62	2	250	DC	12.0	argon	3/32	90	0.048	0.358	0.134	0.084	10.0	18.0
62	3	385	DC	13.0	argon	3/32	90	0.057	0.440	0.130	0.117	10.0	22.2
6	1	352	DC	13.3	argon	3/32	90	0.066	0.447	0.148	0.206	10.0	28.1
39	1	399	DC	14.0	argon	3/32	90	0.072	0.500	0.144	0.239	10.0	33.5
6	2	450	DC	15.7	argon	3/32	90	0.112	0.497	0.225	0.357	10.0	42.4
39	2	502	DC	15.8	argon	3/32	90	0.107	0.520	0.206	0.412	10.0	47.6
51	1	100	DC	12.0	75-ArHe	n/a	150	0.030	0.178	0.169	0.015	10.0	7.2
51	2	150	DC	12.5	75-ArHe	n/a	150	0.043	0.260	0.165	0.031	10.0	11.3
51	3	200	DC	13.0	75-ArHe	n/a	150	0.054	0.340	0.159	0.053	10.0	15.6
51	4	250	DC	14.0	75-ArHe	n/a	150	0.071	0.417	0.170	0.084	10.0	21.0
51	5	285	DC	14.5	75-ArHe	n/a	150	0.077	0.520	0.148	0.122	10.0	24.8
13	1	358	DC	13.3	75-ArHe	n/a	150	0.067	0.490	0.137	0.209	10.0	28.6
16	1	403	DC	14.6	75-ArHe	n/a	150	0.069	0.530	0.149	0.261	10.0	35.3
19	1	455	DC	14.9	75-ArHe	n/a	150	0.095	0.603	0.158	0.395	10.0	40.7
22	1	507	DC	14.8	75-ArHe	n/a	150	0.110	0.650	0.169	0.445	10.0	45.0
23	2	100	DC	12.0	75-ArHe	3/32	150	0.023	0.157	0.146	0.033	10.0	7.2
23	3	150	DC	12.0	75-ArHe	3/32	150	0.043	0.220	0.150	0.071	10.0	10.8
23	4	200	DC	13.0	75-ArHe	3/32	150	0.042	0.333	0.126	0.175	10.0	15.6
23	5	250	DC	14.0	75-ArHe	3/32	150	0.050	0.420	0.119	0.231	10.0	21.0
23	6	285	DC	14.5	75-ArHe	3/32	150	0.064	0.492	0.130	0.242	10.0	24.8
13	4	360	DC	14.2	75-ArHe	3/32	150	0.076	0.540	0.141	0.261	10.0	30.7
16	4	400	DC	14.5	75-ArHe	3/32	150	0.092	0.635	0.145	0.344	10.0	34.8
19	4	450	DC	15.3	75-ArHe	3/32	150	0.128	0.647	0.198	0.426	10.0	41.3
22	4	503	DC	16.6	75-ArHe	3/32	150	0.220	0.517	0.426	0.602	10.0	50.1

TABLE A2-1 (continued)

SAM- PLE#	WELD	CURRENT AMPS	TYPE	POTENTIAL VOLTS	SHIELD GAS	HOLE SIZE	ANGLE	PENETRA- TION IN	BEAD WIDTH	p/w	MELT AREA IN-2	TRAVEL ipm	HEAT IN- PUT kJ/in
51	6	100	DC	12.0	75-ArHe 3/32	3/32	90	0.033	0.170	0.194	0.051	10.0	7.2
5	1	150	DC	13.0	75-ArHe 3/32	3/32	90	0.040	0.295	0.136	0.106	10.0	11.7
5	2	200	DC	14.0	75-ArHe 3/32	3/32	90	0.048	0.327	0.147	0.195	10.0	16.8
5	3	250	DC	14.5	75-ArHe 3/32	3/32	90	0.061	0.447	0.136	0.214	10.0	21.8
5	4	285	DC	14.0	75-ArHe 3/32	3/32	90	0.076	0.532	0.143	0.252	10.0	23.9
29	1	352	DC	13.4	75-ArHe 3/32	3/32	90	0.068	0.375	0.181	0.246	10.0	28.3
44	1	400	DC	14.0	75-ArHe 3/32	3/32	90	0.074	0.568	0.130	0.299	10.0	33.6
75	1	450	DC	15.5	75-ArHe 3/32	3/32	90	0.081	0.588	0.138	0.369	10.0	41.9
8	1	506	DC	16.5	75-ArHe 3/32	3/32	90	0.102	0.693	0.147	0.463	10.0	50.1
15	3	100	DC	12.0	75-ArHe n/a	n/a	90	0.027	0.185	0.146	0.029	10.0	7.2
15	4	150	DC	12.0	75-ArHe n/a	n/a	90	0.045	0.282	0.160	0.088	10.0	10.8
15	5	200	DC	12.5	75-ArHe n/a	n/a	90	0.059	0.377	0.156	0.119	10.0	15.0
15	6	250	DC	13.5	75-ArHe n/a	n/a	90	0.063	0.432	0.146	0.212	10.0	20.3
23	1	285	DC	14.0	75-ArHe n/a	n/a	90	0.058	0.447	0.130	0.247	10.0	23.9
29	4	355	DC	13.0	75-ArHe n/a	n/a	90	0.075	0.515	0.146	0.276	10.0	27.7
44	4	399	DC	14.0	75-ArHe n/a	n/a	90	0.076	0.565	0.135	0.698	10.0	33.5
75	4	449	DC	14.0	75-ArHe n/a	n/a	90	0.097	0.603	0.161	0.875	10.0	37.7
8	4	503	DC	14.7	75-ArHe n/a	n/a	90	0.110	0.740	0.149	1.130	10.0	44.4
66	5	100	DC	15.0	25-ArHe n/a	n/a	150	0.039	0.215	0.181	0.024	10.0	9.0
66	6	150	DC	15.5	25-ArHe n/a	n/a	150	0.048	0.292	0.164	0.045	10.0	14.0
26	1	200	DC	15.0	25-ArHe n/a	n/a	150	0.047	0.378	0.124	0.052	10.0	18.0
26	2	250	DC	15.5	25-ArHe n/a	n/a	150	0.060	0.490	0.122	0.098	10.0	23.3
26	3	285	DC	16.0	25-ArHe n/a	n/a	150	0.071	0.557	0.127	0.130	10.0	27.4
13	3	353	DC	17.2	25-ArHe n/a	n/a	150	0.075	0.610	0.123	0.642	10.0	36.4
16	3	400	DC	16.3	25-ArHe n/a	n/a	150	0.094	0.657	0.143	0.790	10.0	39.1
19	3	451	DC	16.4	25-ArHe n/a	n/a	150	0.126	0.737	0.171	0.993	10.0	44.4
22	3	506	DC	16.2	25-ArHe n/a	n/a	150	0.136	0.743	0.183	1.147	10.0	49.2
58	1	100	DC	14.5	25-ArHe 3/32	3/32	150	0.034	0.205	0.166	0.029	10.0	8.7
58	2	150	DC	14.5	25-ArHe 3/32	3/32	150	0.040	0.300	0.133	0.041	10.0	13.1
58	3	200	DC	15.0	25-ArHe 3/32	3/32	150	0.044	0.365	0.121	0.062	10.0	18.0
58	4	250	DC	15.0	25-ArHe 3/32	3/32	150	0.057	0.465	0.123	0.140	10.0	22.3
58	5	285	DC	16.0	25-ArHe 3/32	3/32	150	0.071	0.593	0.120	0.218	10.0	27.4
13	2	355	DC	15.2	25-ArHe 3/32	3/32	150	0.074	0.595	0.124	0.581	10.0	32.4
16	2	402	DC	16.6	25-ArHe 3/32	3/32	150	0.096	0.660	0.145	0.842	10.0	40.0
19	2	452	DC	16.7	25-ArHe 3/32	3/32	150	0.105	0.690	0.152	0.875	10.0	45.3
22	2	505	DC	18.2	25-ArHe 3/32	3/32	150	0.121	0.700	0.173	1.127	10.0	55.1

TABLE A2-1 (continued)

SAM- PLE#	WELD	CURRENT AMPS	TYPE	POTENTIAL VOLTS	SHIELD GAS	HOLE SIZE	ANGLE	PENETRA- TION IN	BEAD WIDTH	P/w	MELT AREA IN-2	TRAVEL ipm	HEAT IN- PUT kJ/in
26	4	100	DC	14.5	25-ArHe	n/a	90	0.035	0.220	0.159	0.029	10.0	8.7
26	5	150	DC	14.5	25-ArHe	n/a	90	0.050	0.300	0.167	0.058	10.0	13.1
26	6	200	DC	14.0	25-ArHe	n/a	90	0.057	0.363	0.157	0.080	10.0	16.8
15	1	250	DC	15.0	25-ArHe	n/a	90	0.056	0.462	0.121	0.107	10.0	22.5
15	2	285	DC	16.0	25-ArHe	n/a	90	0.085	0.557	0.153	0.382	10.0	27.4
29	3	353	DC	14.9	25-ArHe	n/a	90	0.076	0.585	0.130	0.334	10.0	31.6
44	3	399	DC	16.1	25-ArHe	n/a	90	0.084	0.646	0.130	0.518	10.0	38.5
75	3	450	DC	16.0	25-ArHe	n/a	90	0.104	0.662	0.157	0.755	10.0	43.2
8	3	503	DC	15.9	25-ArHe	n/a	90	0.110	0.740	0.149	1.192	10.0	48.0
58	6	100	DC	13.5	25-ArHe	3/32	90	0.037	0.210	0.176	0.029	10.0	8.1
66	1	150	DC	14.0	25-ArHe	3/32	90	0.049	0.285	0.172	0.044	10.0	12.6
66	2	200	DC	16.0	25-ArHe	3/32	90	0.061	0.372	0.164	0.070	10.0	19.2
66	3	250	DC	16.5	25-ArHe	3/32	90	0.070	0.442	0.158	0.128	10.0	24.8
66	4	285	DC	16.5	25-ArHe	3/32	90	0.104	0.563	0.185	0.140	10.0	28.2
29	2	356	DC	15.2	25-ArHe	3/32	90	0.074	0.593	0.125	0.336	10.0	32.5
44	2	399	DC	16.2	25-ArHe	3/32	90	0.095	0.672	0.141	0.518	10.0	38.8
75	2	449	DC	16.0	25-ArHe	3/32	90	0.104	0.715	0.145	0.655	10.0	43.1
8	2	502	DC	16.0	25-ArHe	3/32	90	0.122	0.563	0.217	0.812	10.0	48.2

The figures following are the actual data points used in determining the trends seen in the main section of this thesis. In all cases, the solid electrode is represented by an X and the hollow electrode is represented with a cross (+).

Units on figures where not stated are:

CURRENT - AMPERES (x-axis)
VOLTAGE - VOLTS
PENETRATION - INCH
MELT AREA - SQUARE INCHES

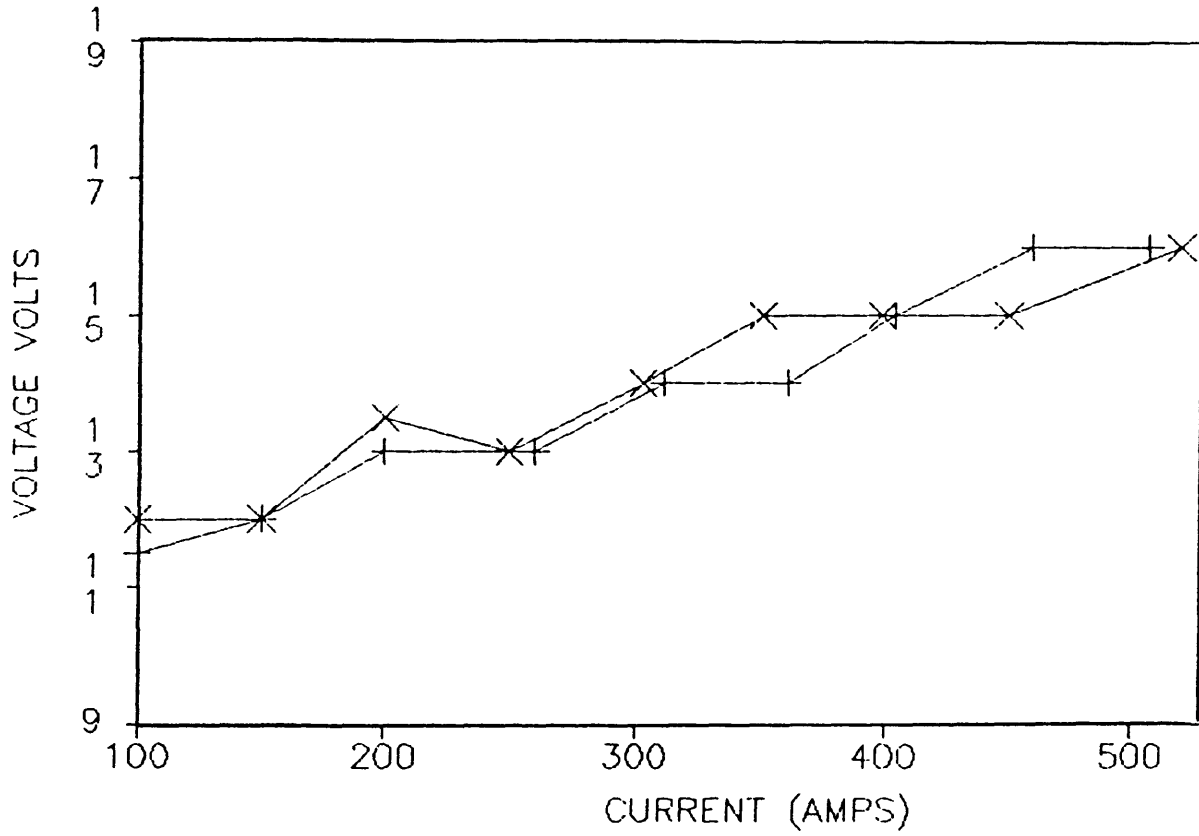


Figure A2-1 Arc Potential-Current Characteristic Curves for Constant Travel Speed Welds Unshaped Electrode In 75ArHe

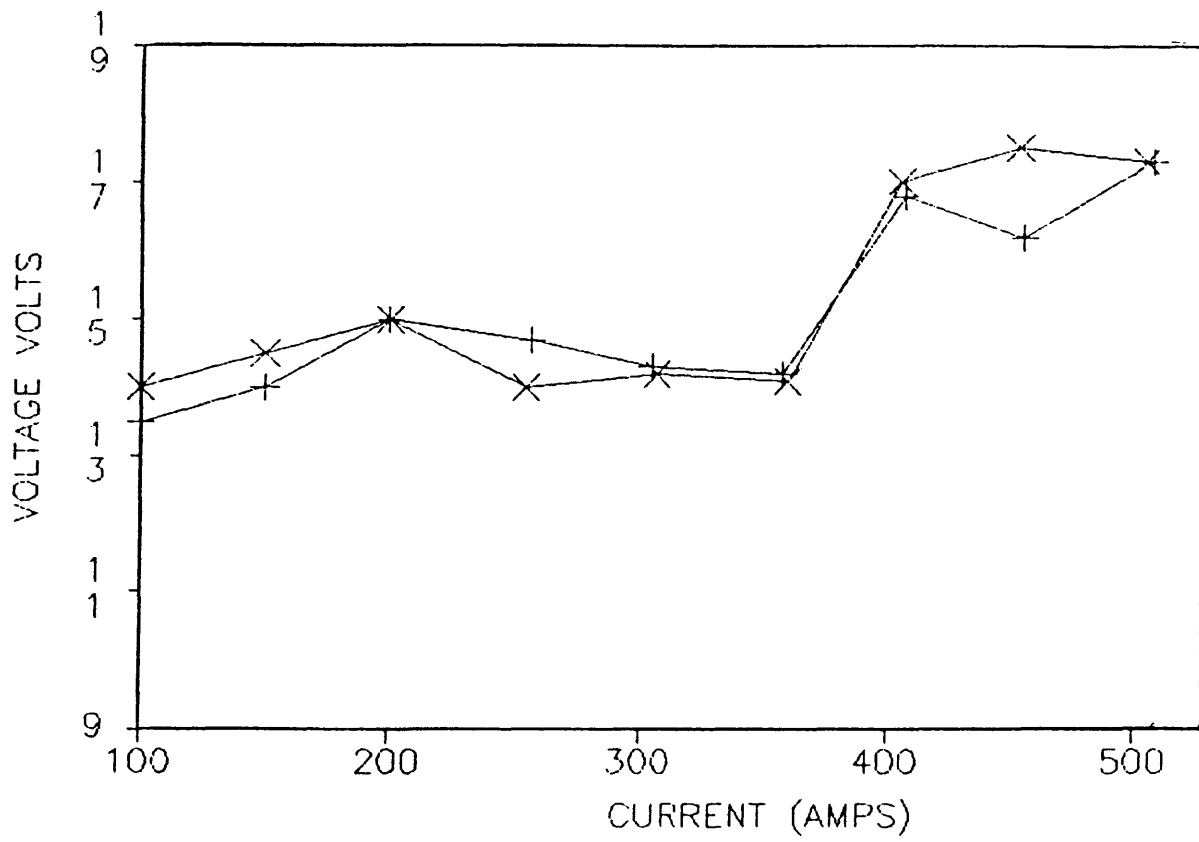


Figure A2-2 Arc Potential-Current Characteristic Curves for Constant Travel Speed Welds Unshaped Electrode In 25ArHe

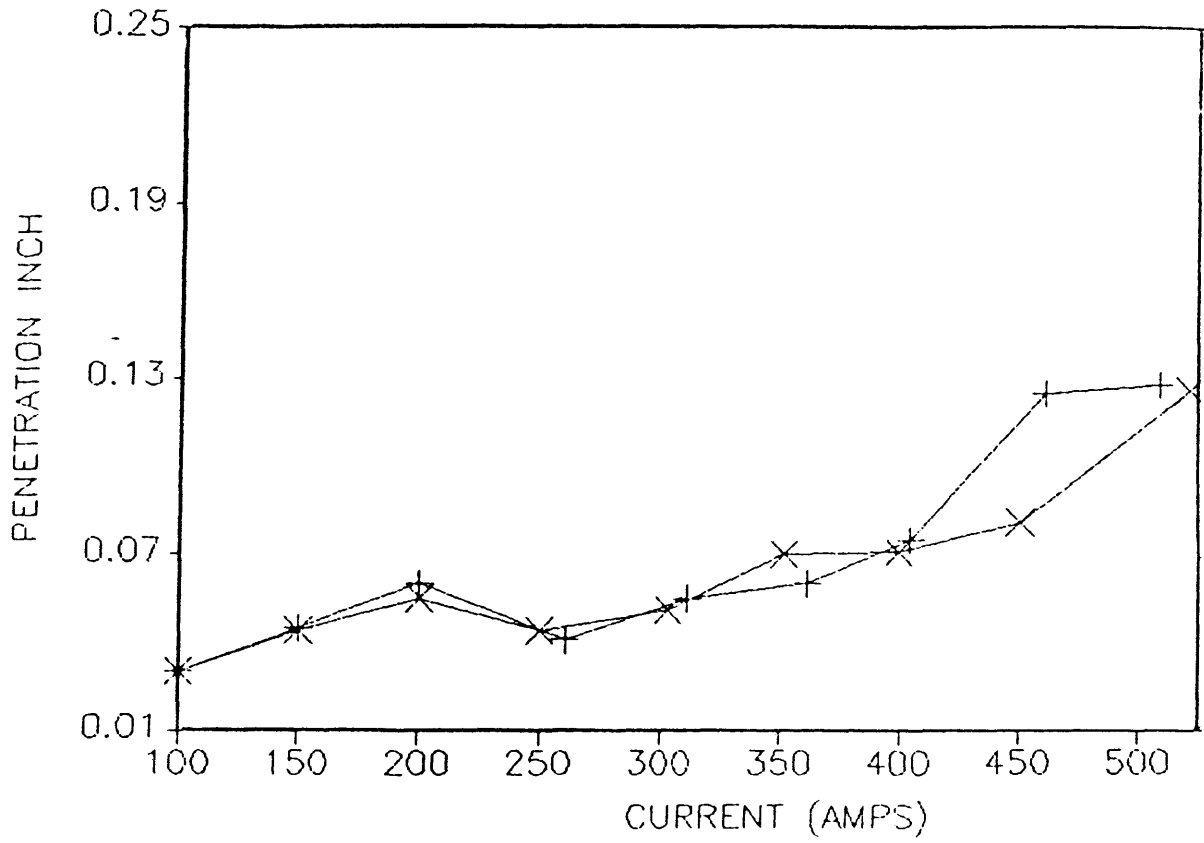


Figure A2-3 Current Versus Penetration For
Constant Travel Speed Welds
Unshaped Electrode In 75ArHe

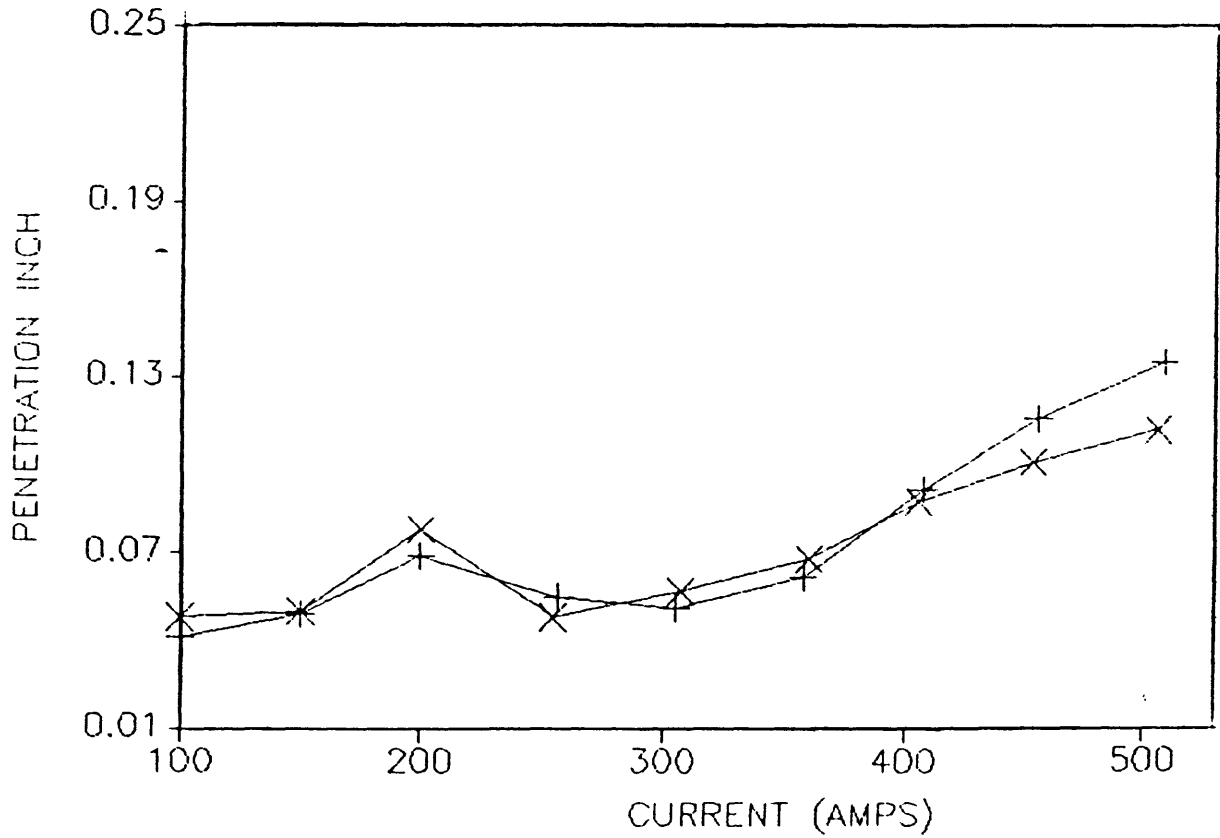


Figure A2-4 Current Versus Penetration For
Constant Travel Speed Welds
Unshaped Electrode In 25ArHe

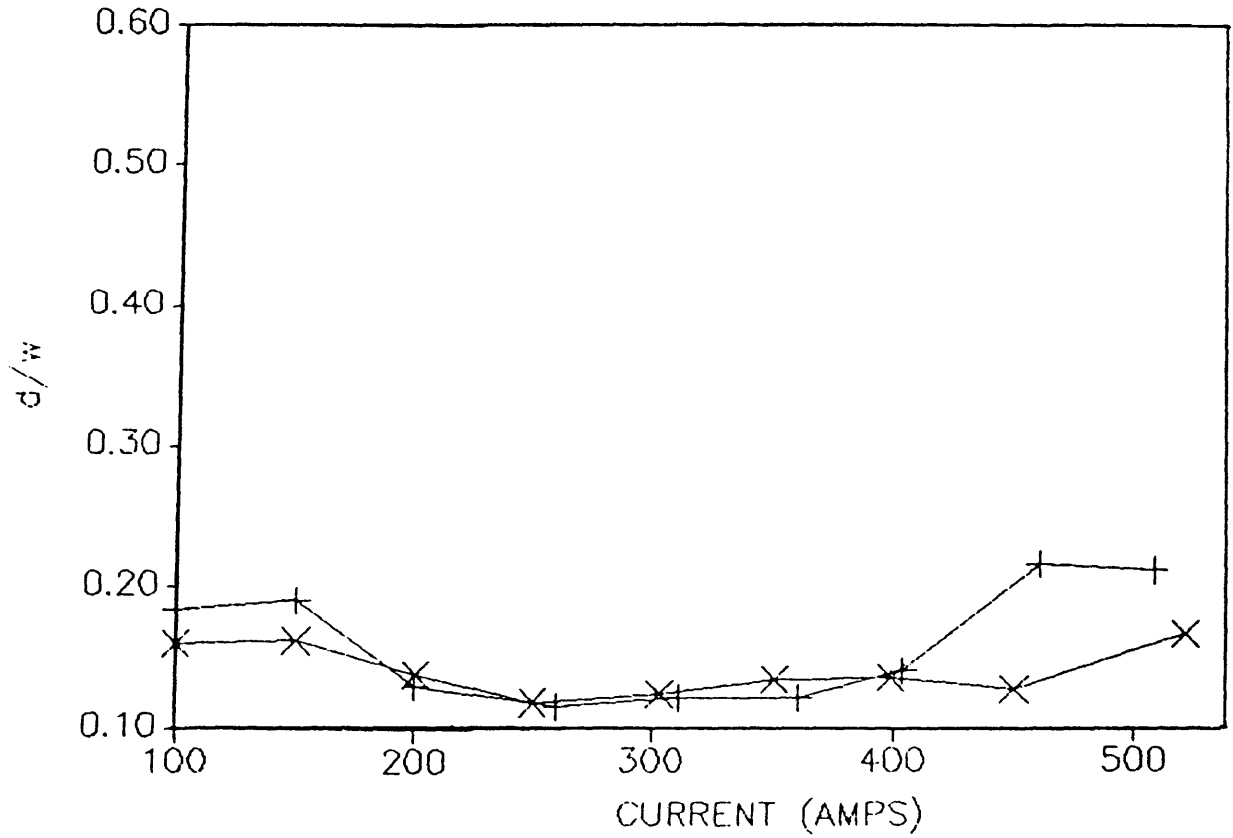


Figure A2-5 Current versus p/w For Constant Travel Speed Welds Unshaped Electrode In 75ArHe

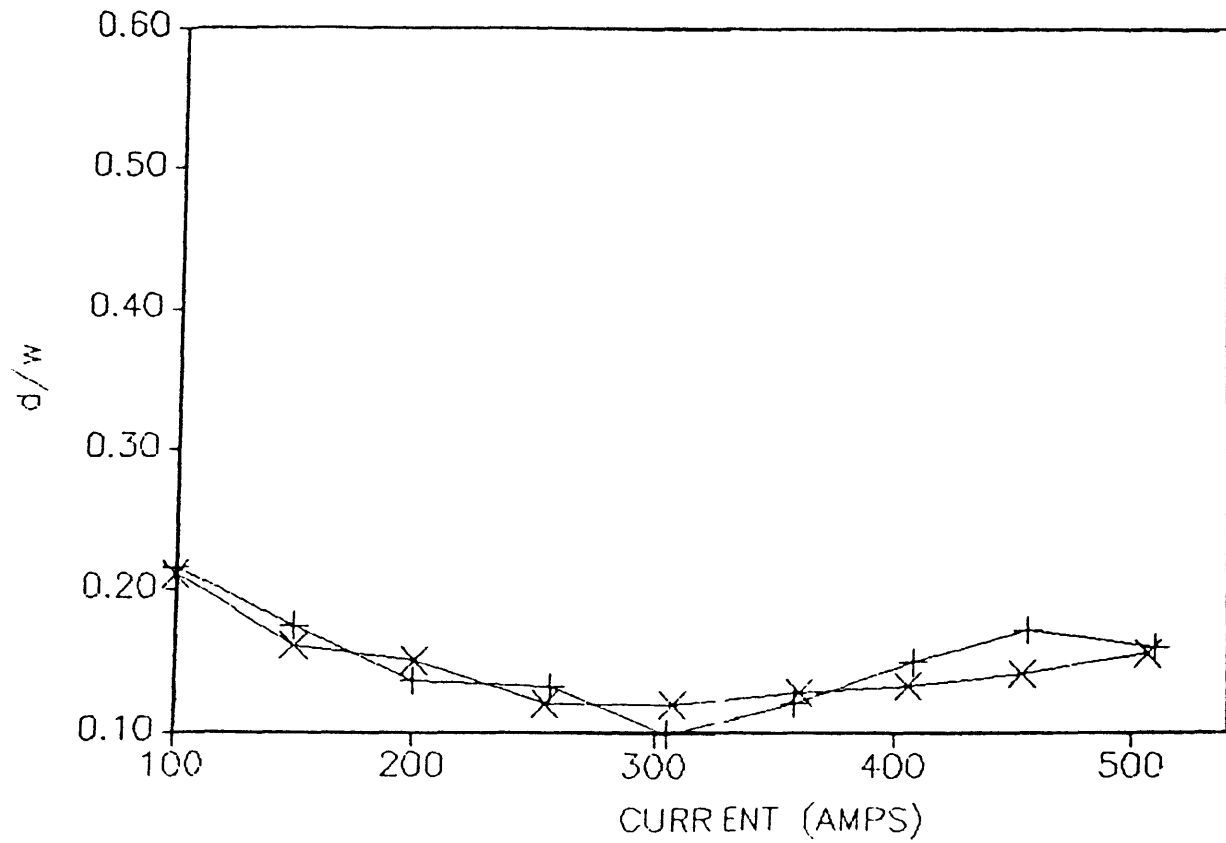


Figure A2-6 Current versus p/w For Constant Travel Speed Welds Unshaped Electrode In 25ArHe

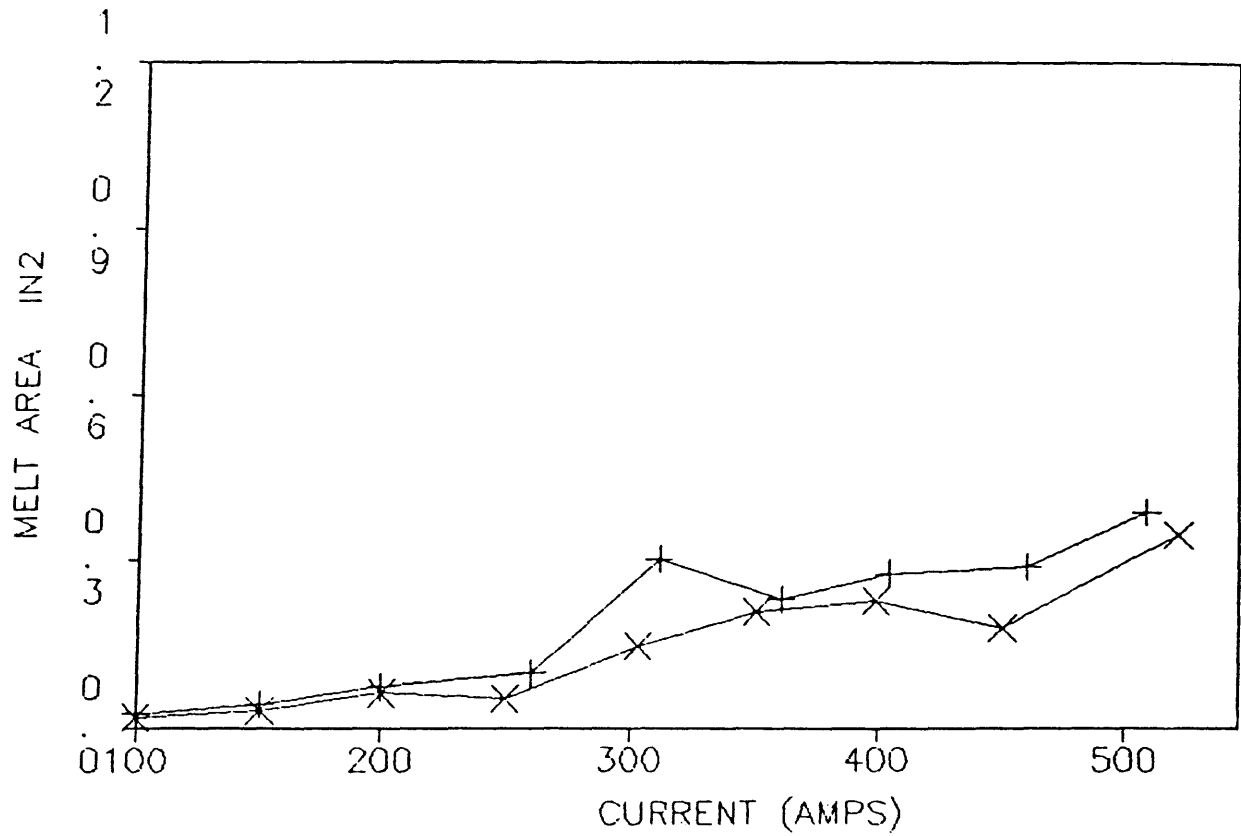


Figure A2-7 Current versus Melt Area For Constant Travel Speed Welds Unshaped Electrode In 75ArHe

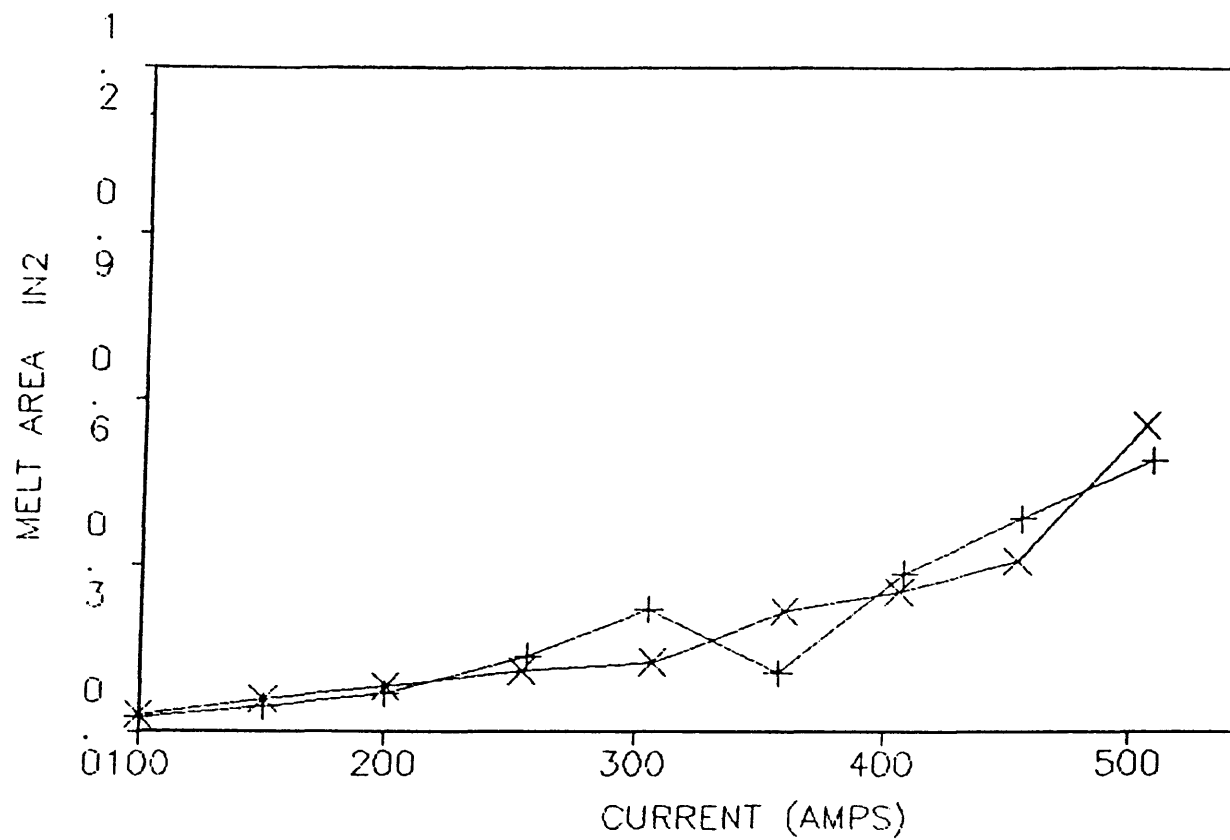


Figure A2-8 Current versus Melt Area For Constant Travel Speed Welds Unshaped Electrode In 25ArHe

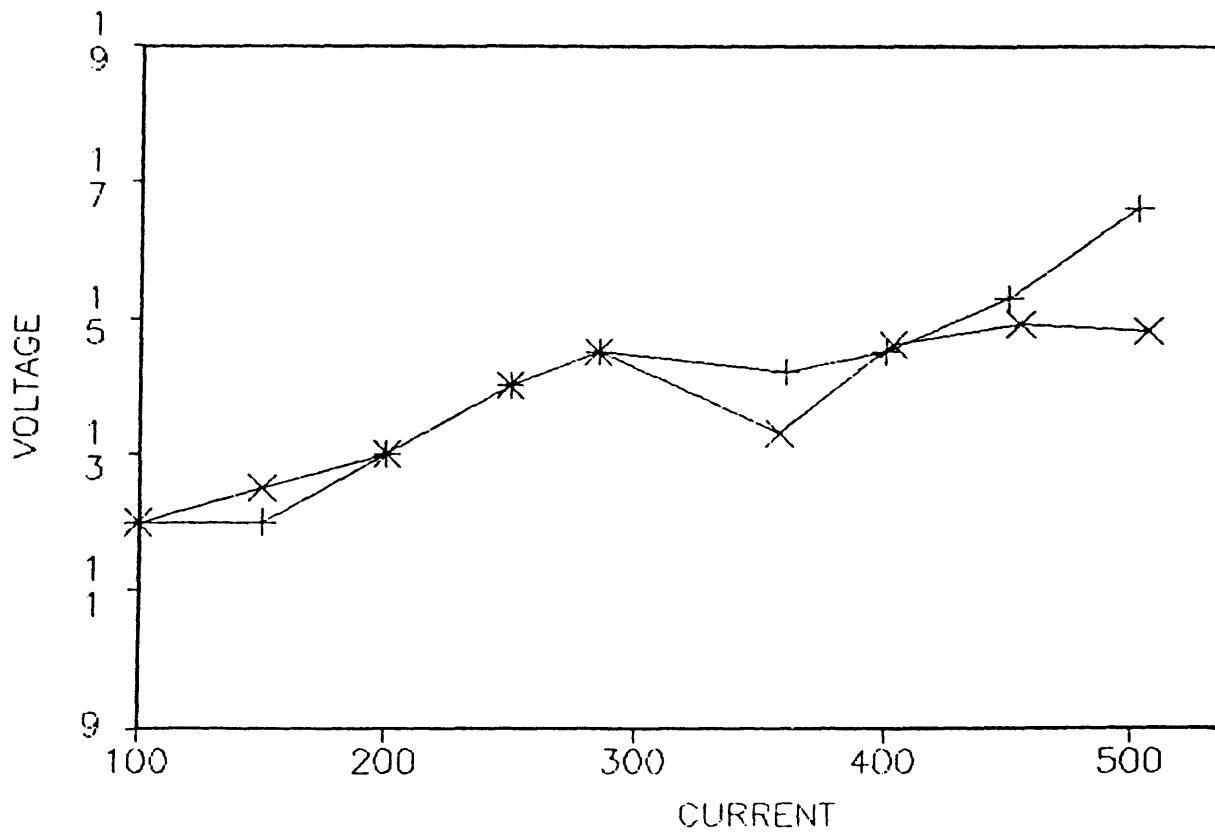


Figure A2-9 Arc Potential-Current Characteristic Curves for Constant Travel Speed Welds 150 Degree Tip Angle In 75ArHe

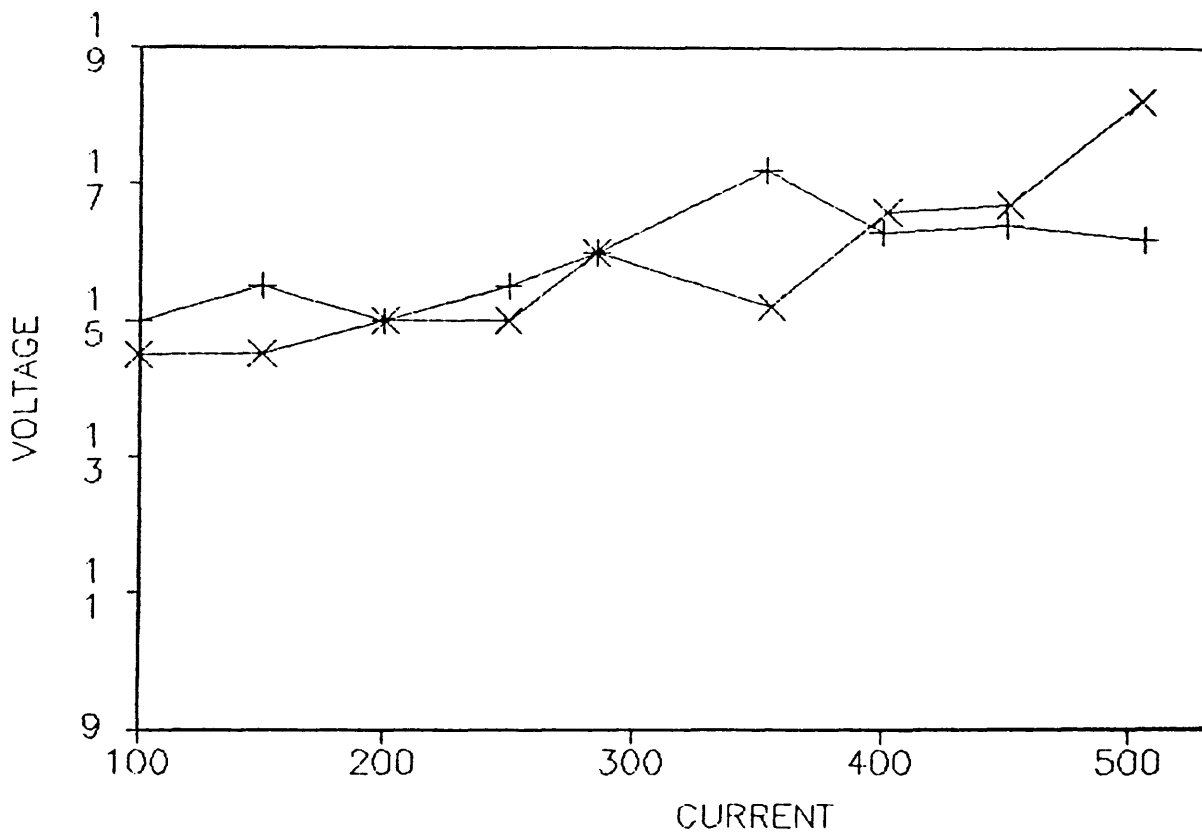


Figure A2-10 Arc Potential-Current Characteristic Curves for Constant Travel Speed Welds 150-Degree Tip Angle In 25ArHe

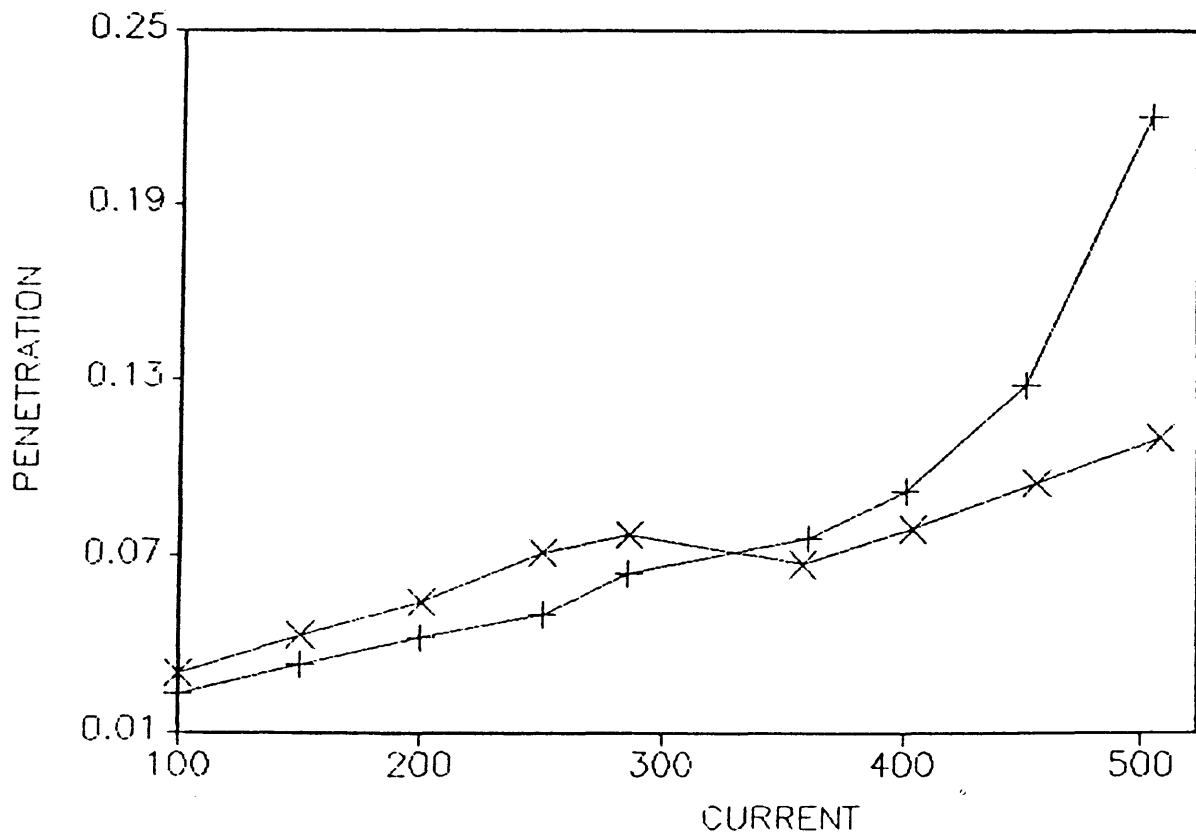


Figure A2-11 Current Versus Penetration For
Constant Travel Speed Welds
150 Degree Tip Angle In 75ArHe

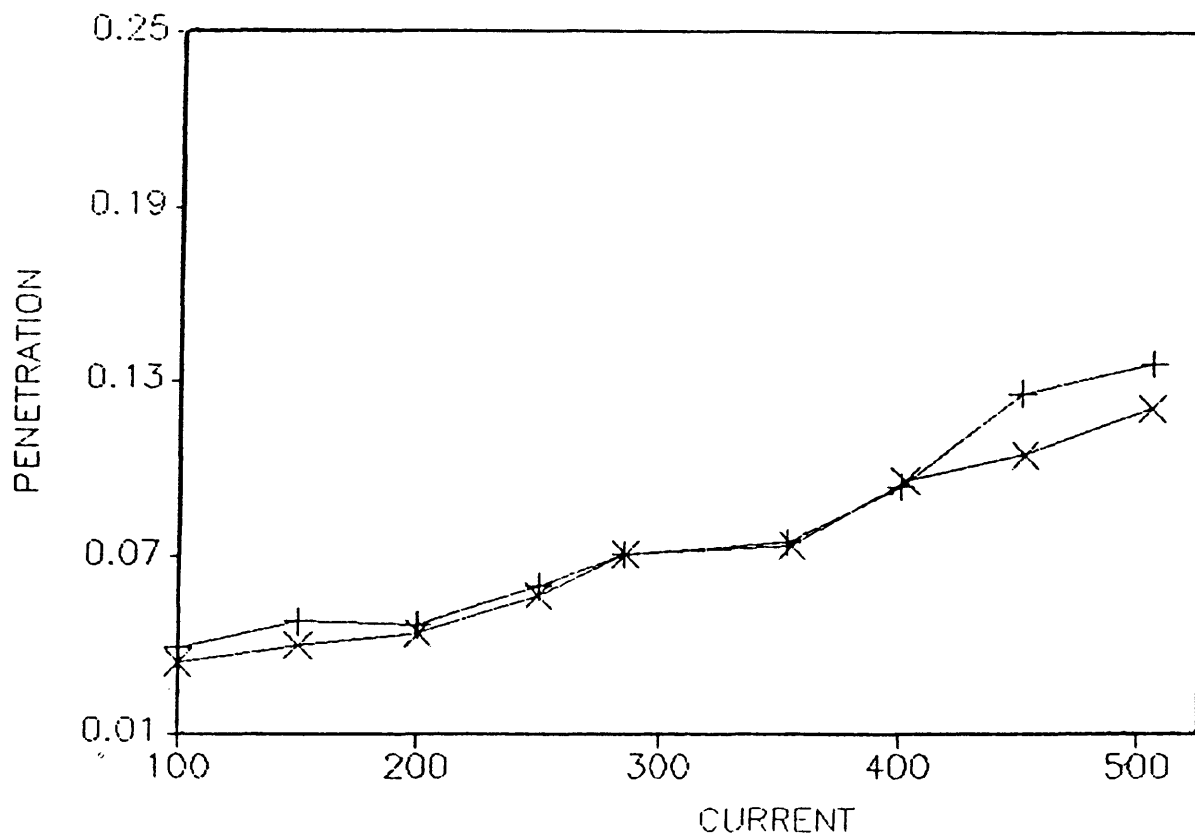


Figure A2-12 Current Versus Penetration For
Constant Travel Speed Welds
150 Degree Tip Angle In 25ArHe

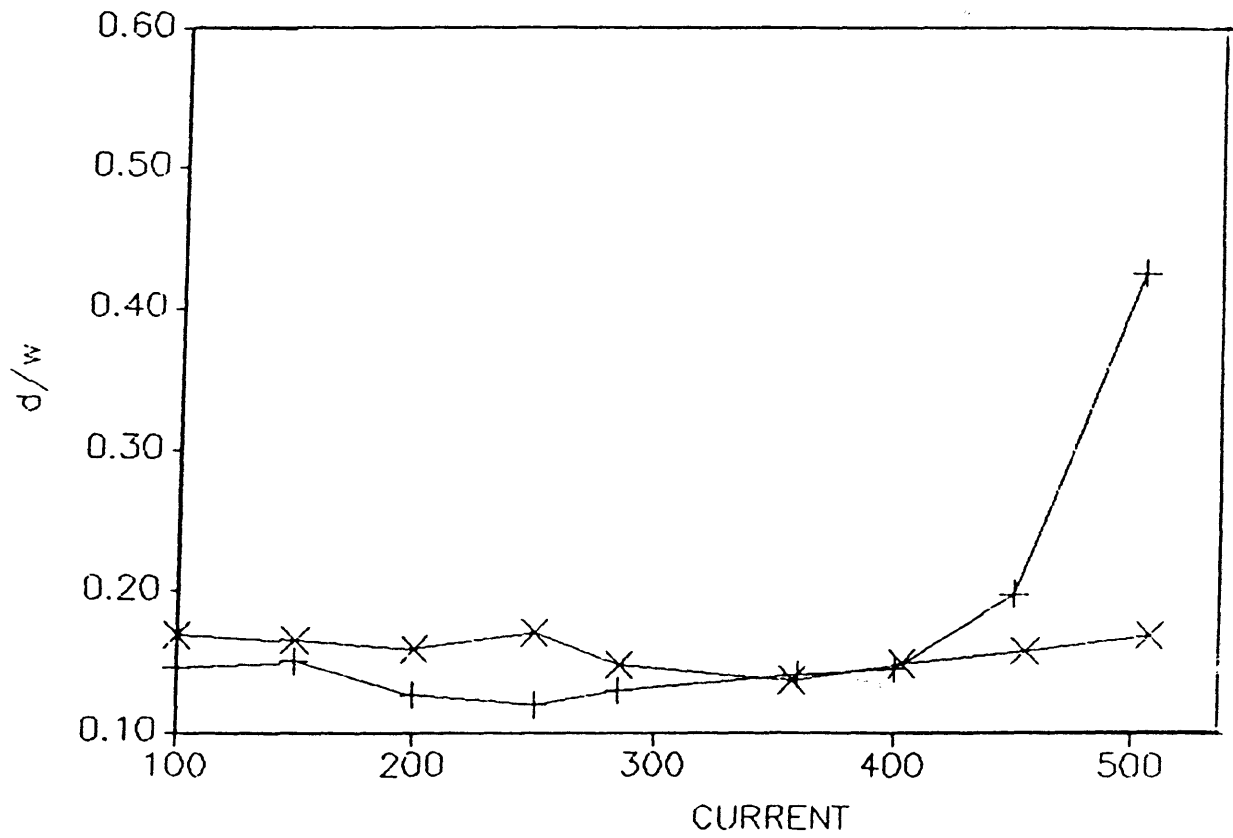


Figure A2-13 Current versus p/w For Constant Travel Speed Welds 150 Degree Tip Angle In 75ArHe

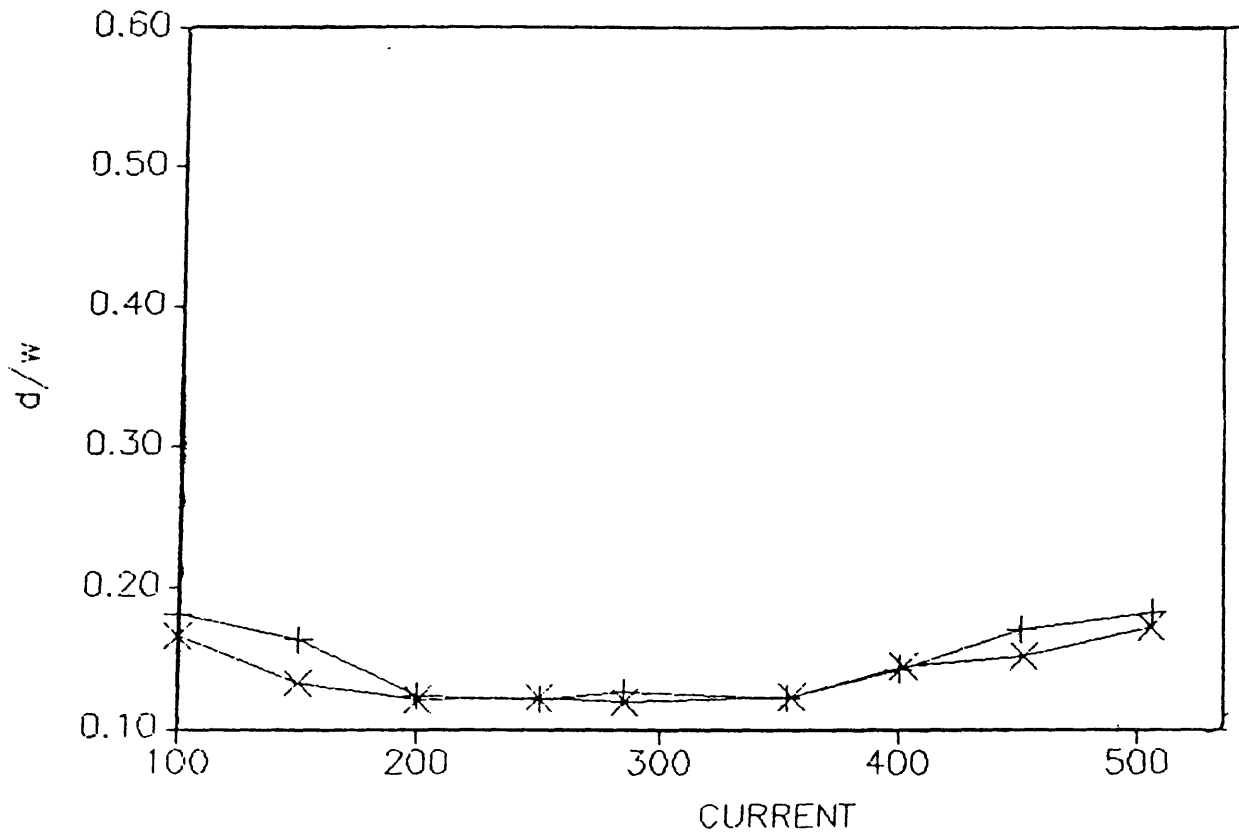


Figure A2-14 Current versus p/w For Constant Travel Speed Welds 150 Degree Tip Angle In 25ArHe

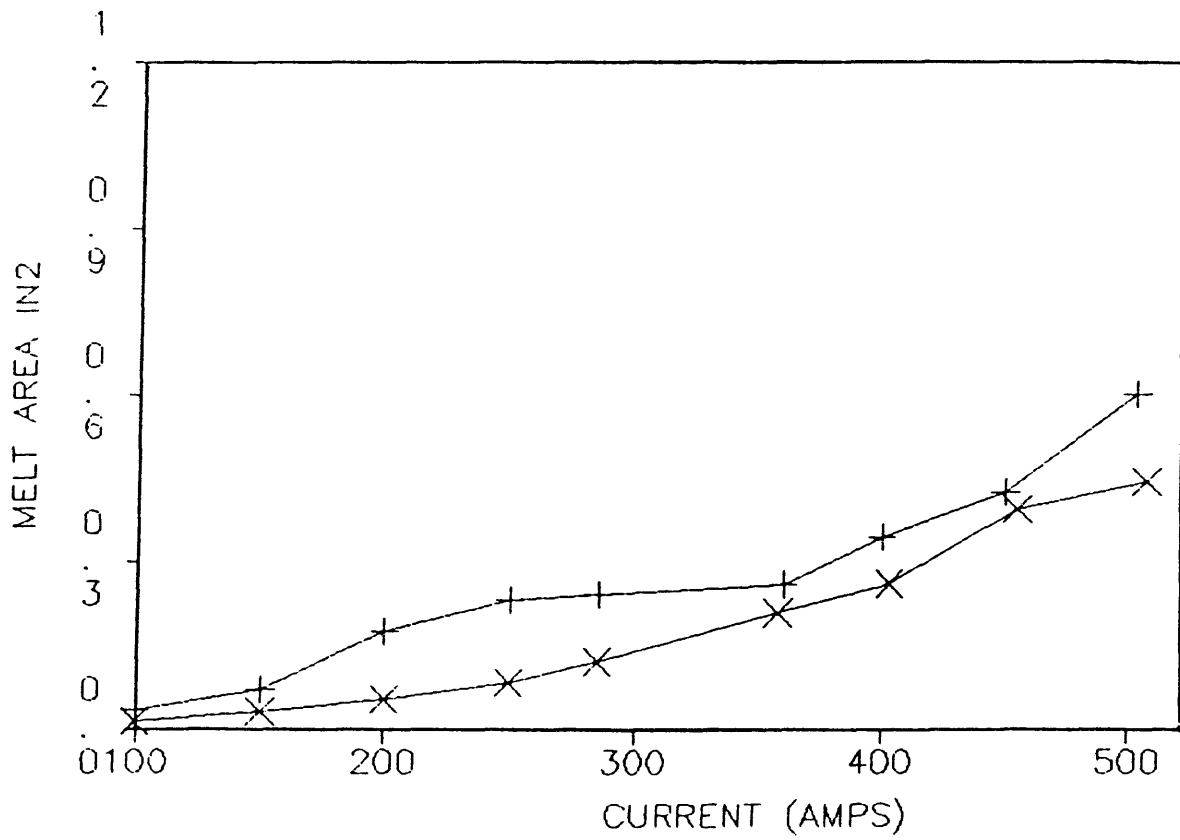


Figure A2-15 Current versus Melt Area For Constant Travel Speed Welds 150 Degree Tip Angle In 75ArHe

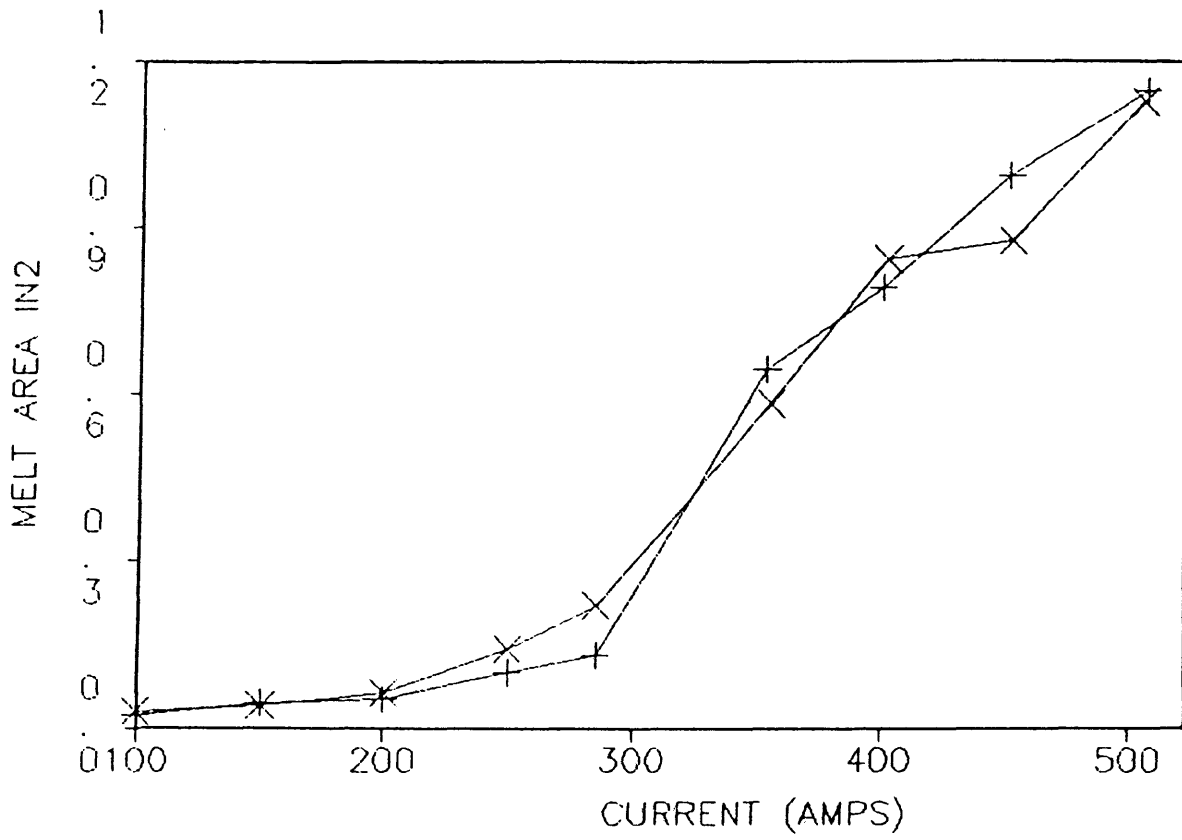


Figure A2-16 Current versus Melt Area For Constant Travel Speed Welds 150 Degree Tip Angle In 25ArHe

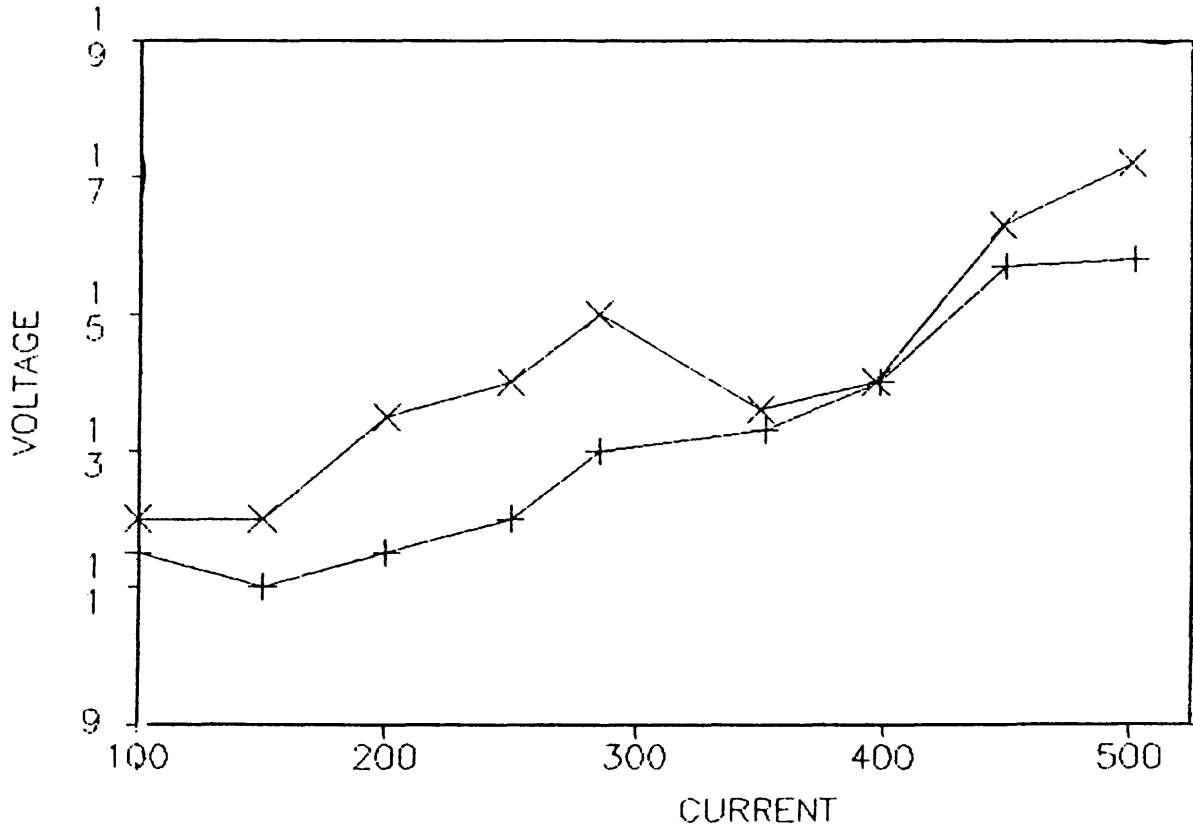


Figure A2-17 Arc Potential-Current Characteristic Curves for Constant Travel Speed Welds 90 Degree Tip Angle In Argon

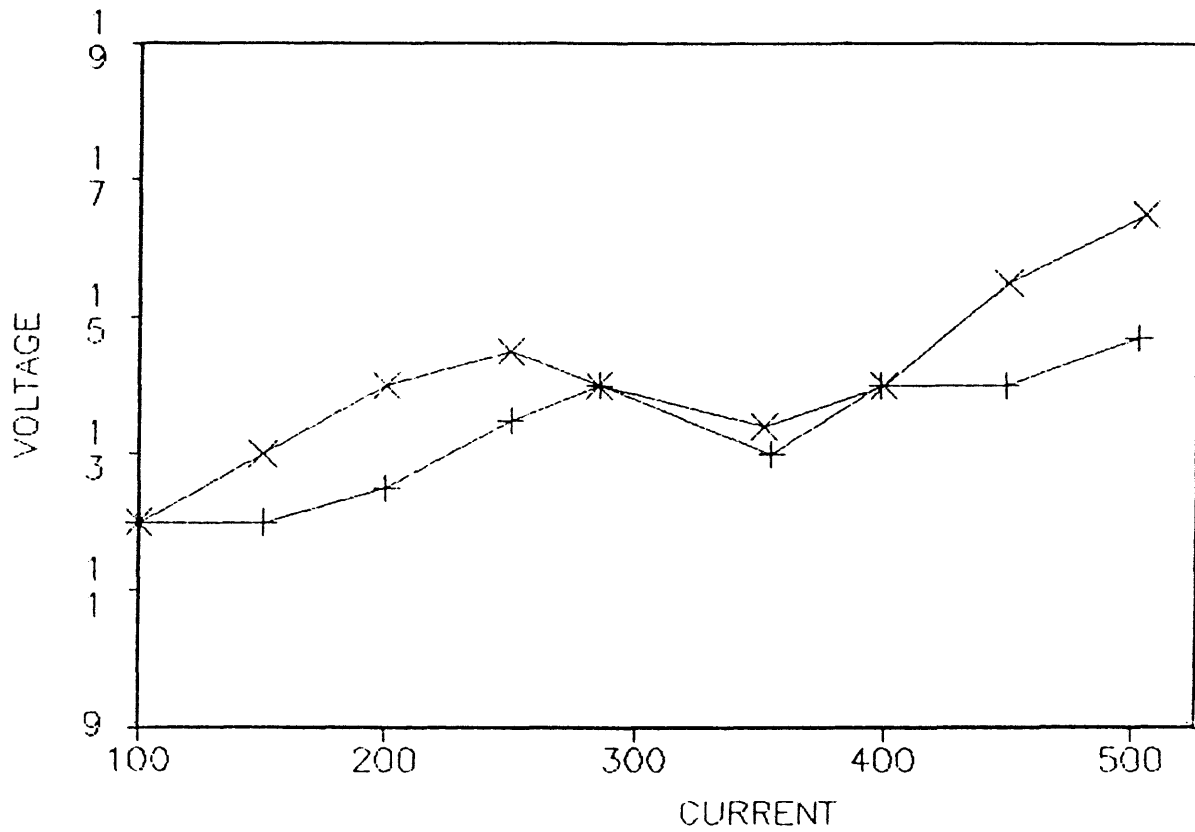


Figure A2-18 Arc Potential-Current Characteristic Curves for Constant Travel Speed Welds 90 Degree Tip Angle In 75ArHe

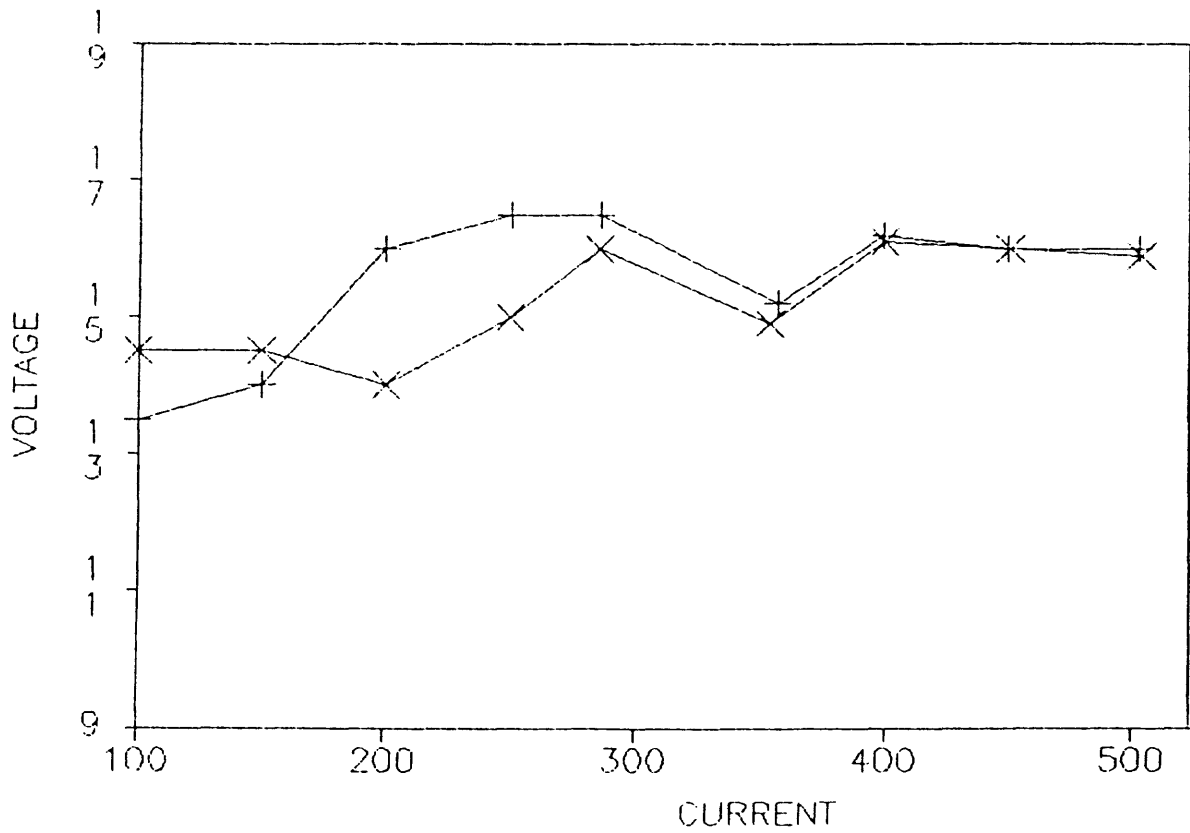


Figure A2-19 Arc Potential-Current Characteristic Curves for Constant Travel Speed Welds 90 Degree Tip Angle In 25ArHe

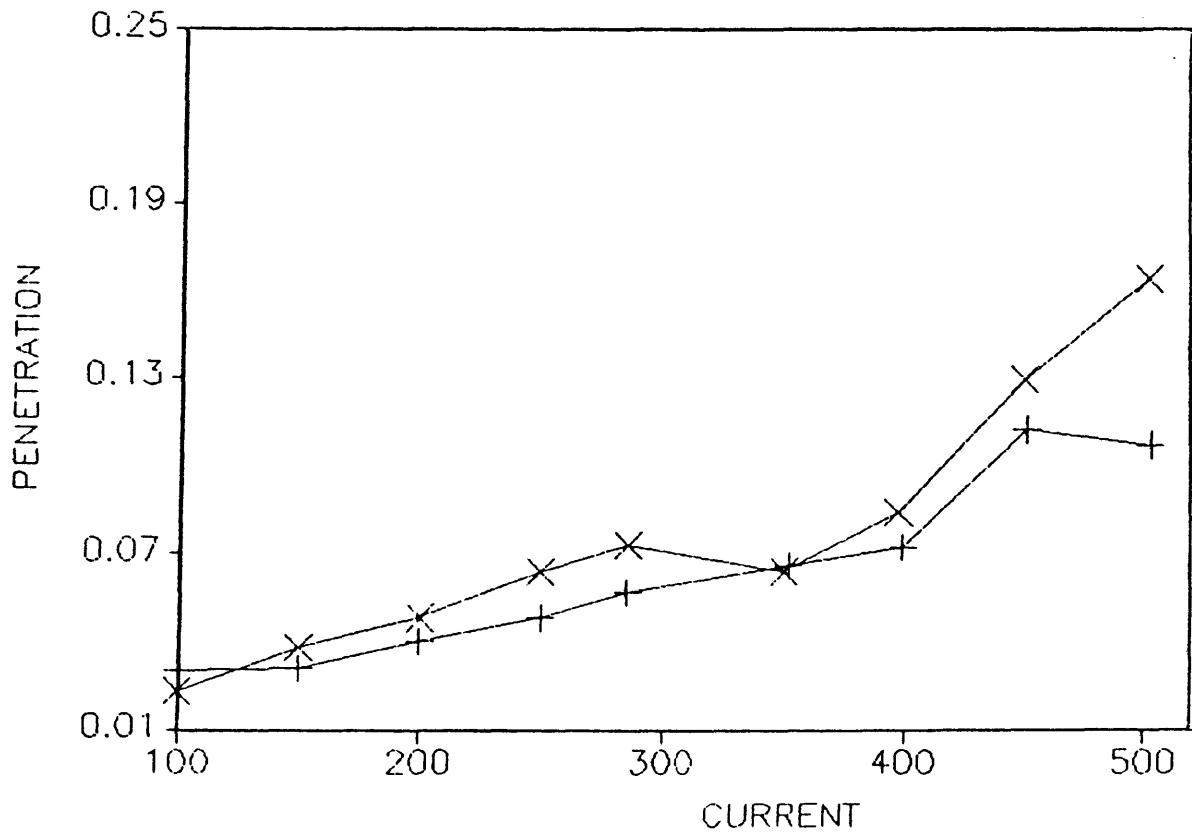


Figure A2-20 Current Versus Penetration For
Constant Travel Speed Welds
90 Degree Tip Angle In Argon

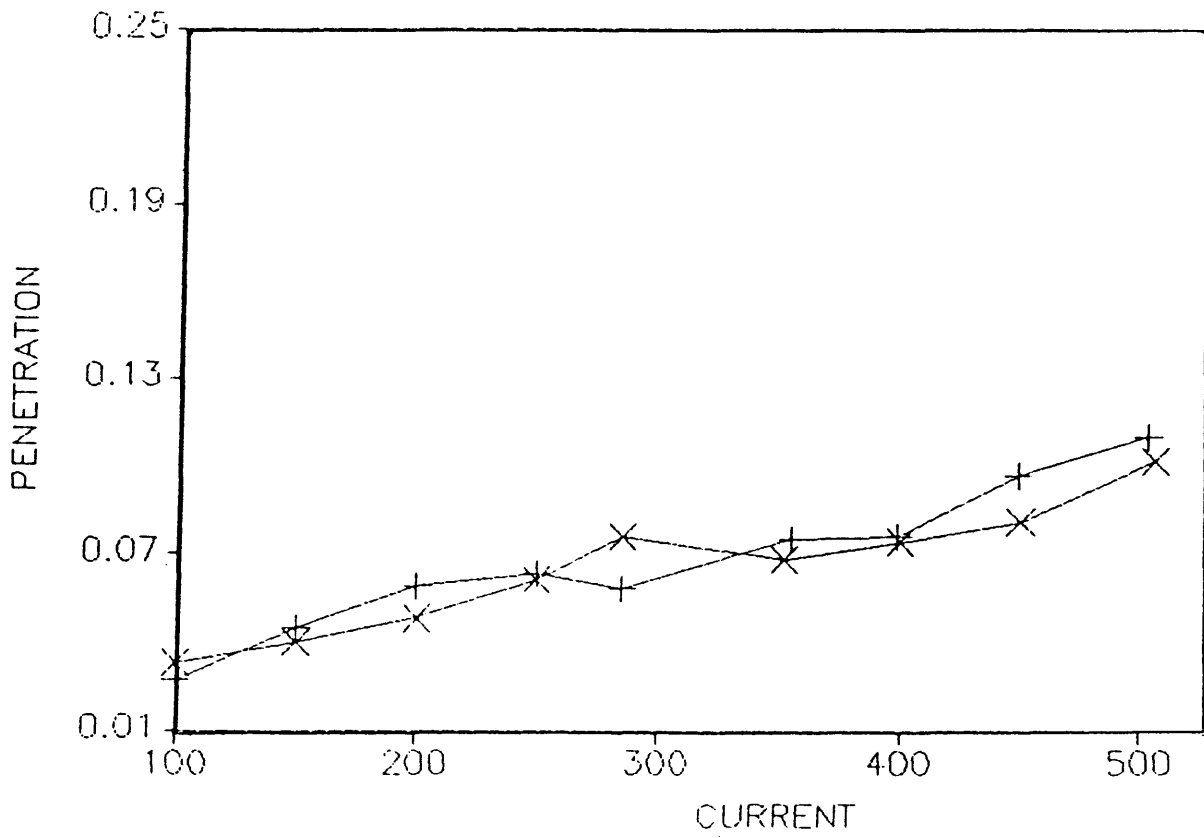


Figure A2-21 Current Versus Penetration For
Constant Travel Speed Welds
90 Degree Tip Angle In 75ArHe

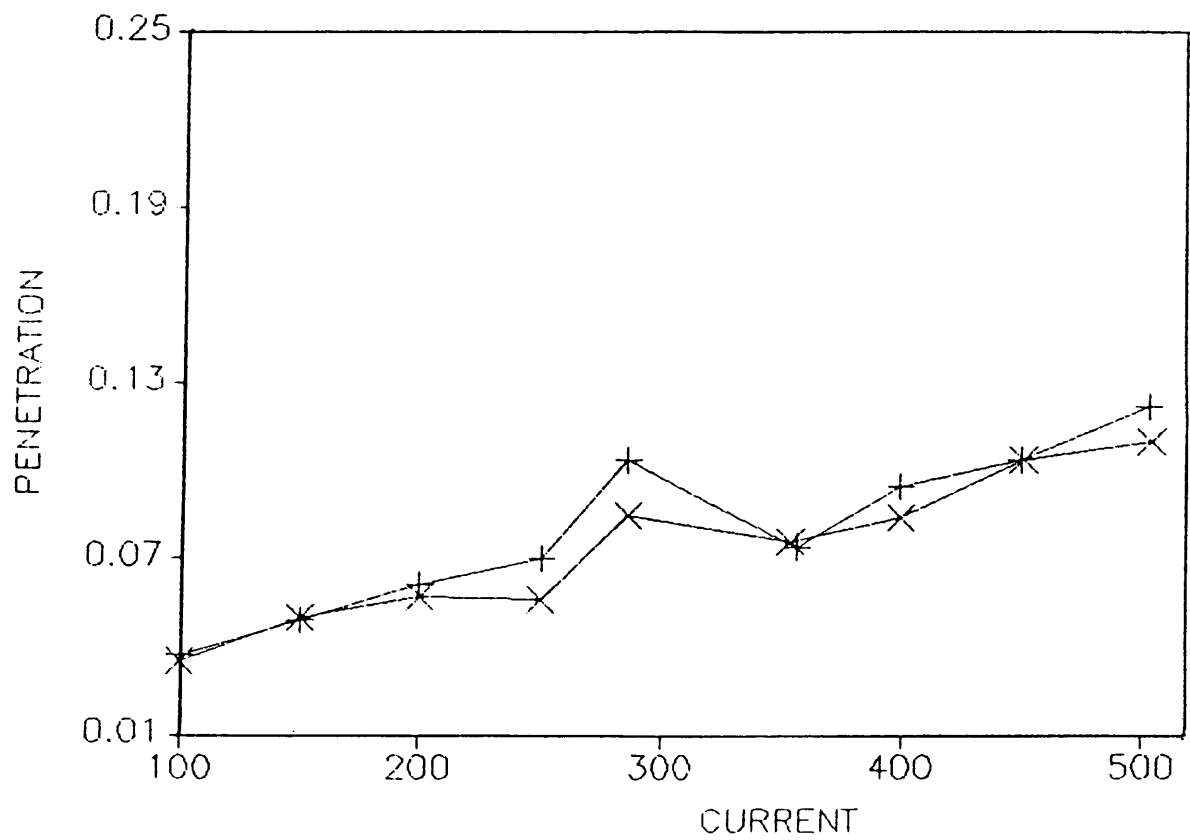


Figure A2-22 Current Versus Penetration For
Constant Travel Speed Welds
90 Degree Tip Angle In 25ArHe

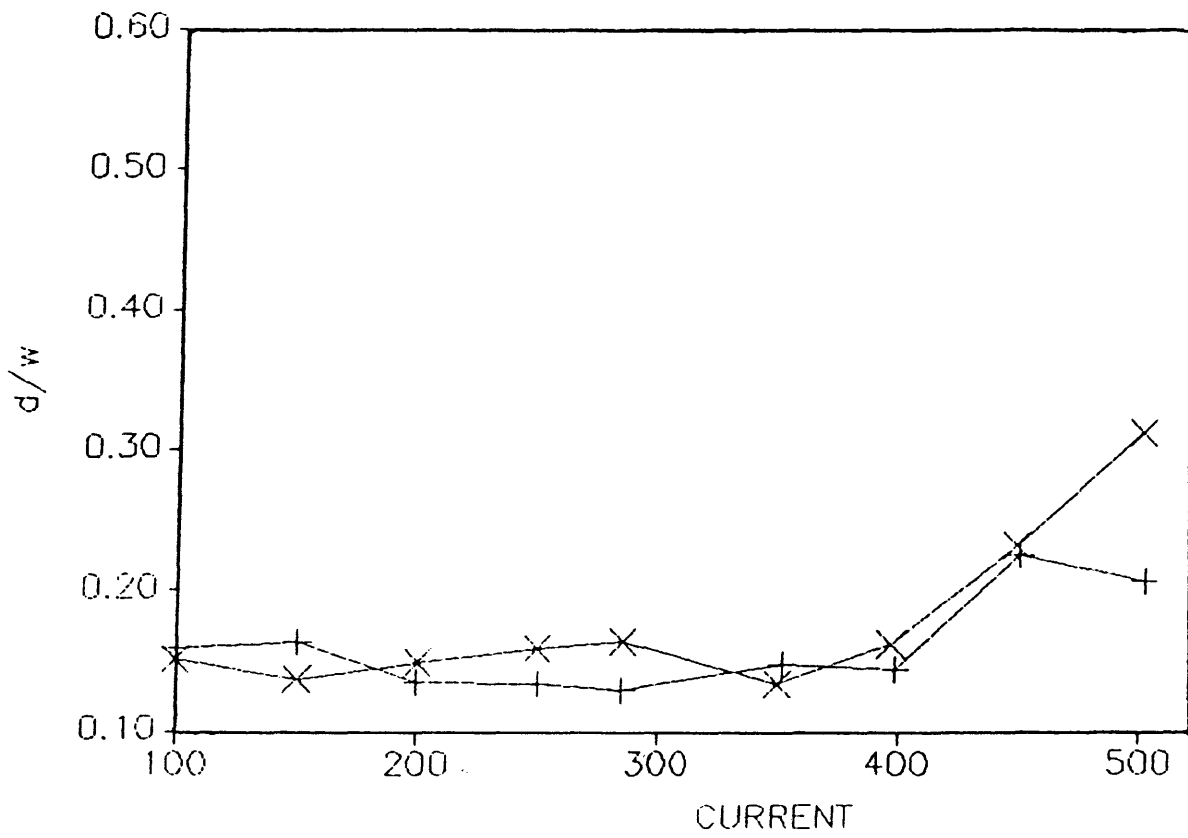


Figure A2-23 Current versus p/w For Constant Travel Speed Welds 90 Degree Tip Angle In Argon

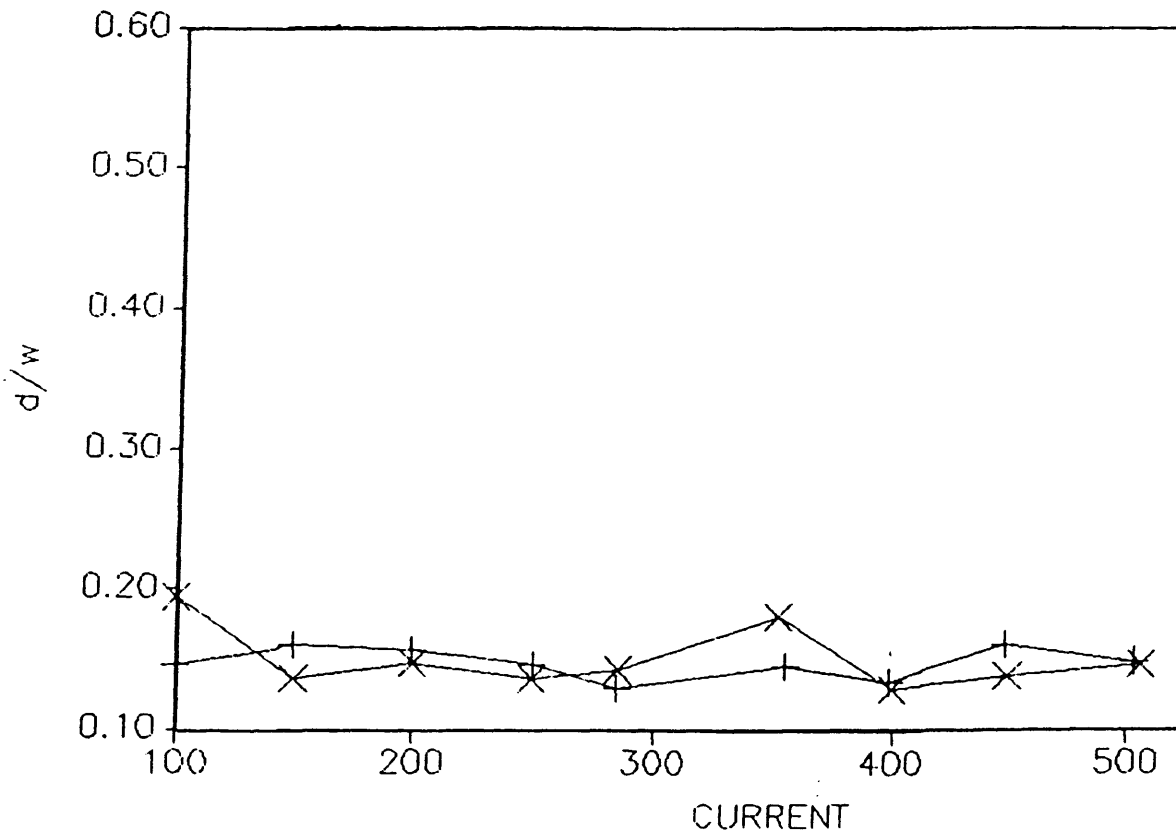


Figure A2-24 Current versus p/w For Constant Travel Speed Welds 90 Degree Tip Angle In 75ArHe

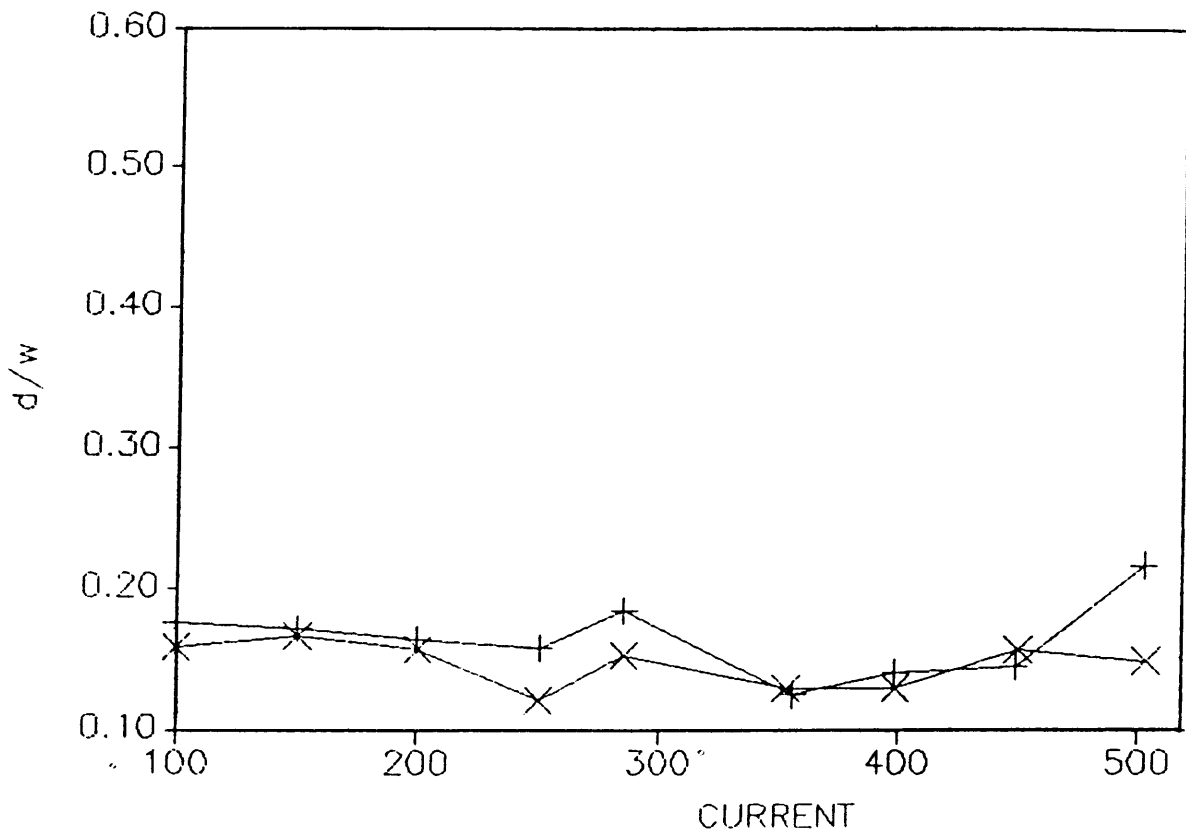


Figure A2-25 Current versus p/w For Constant Travel Speed Welds 90 Degree Tip Angle In 25ArHe

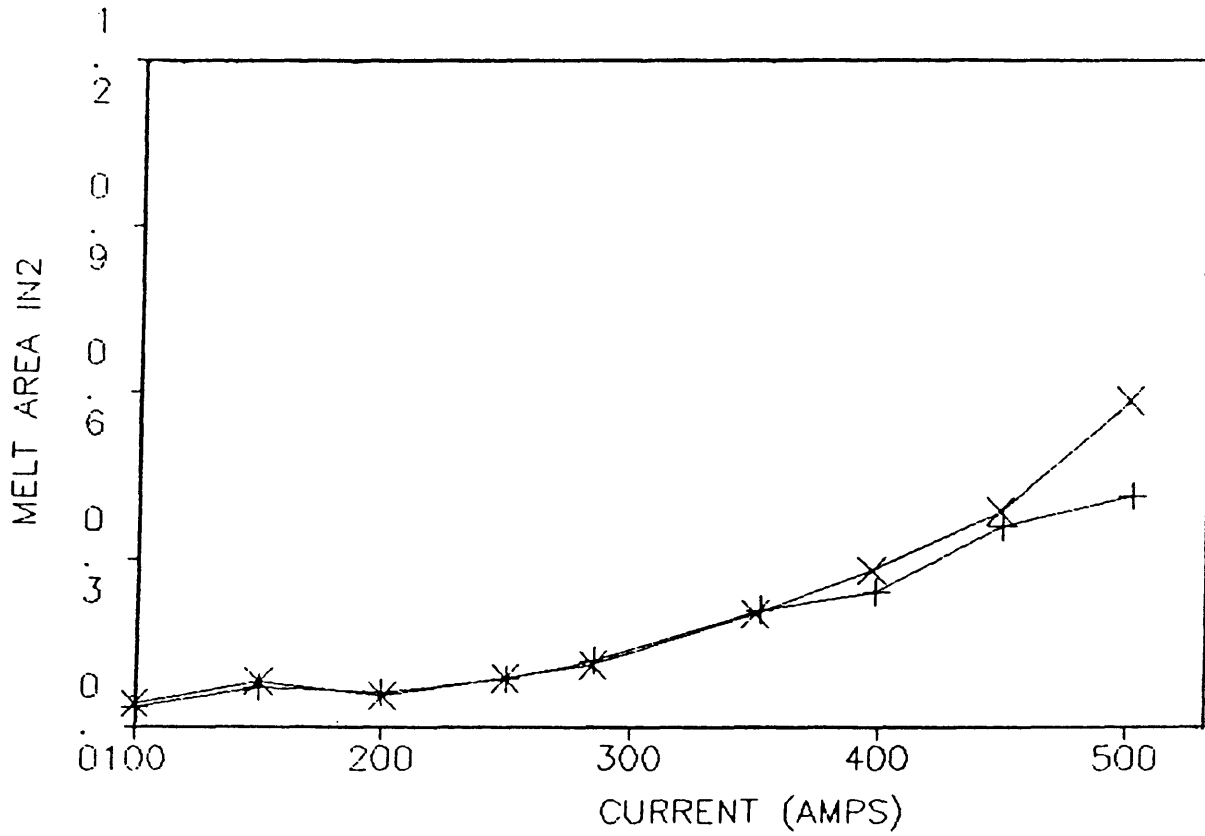


Figure A2-26 Current versus Melt Area For Constant Travel Speed Welds 90 Degree Tip Angle In Argon

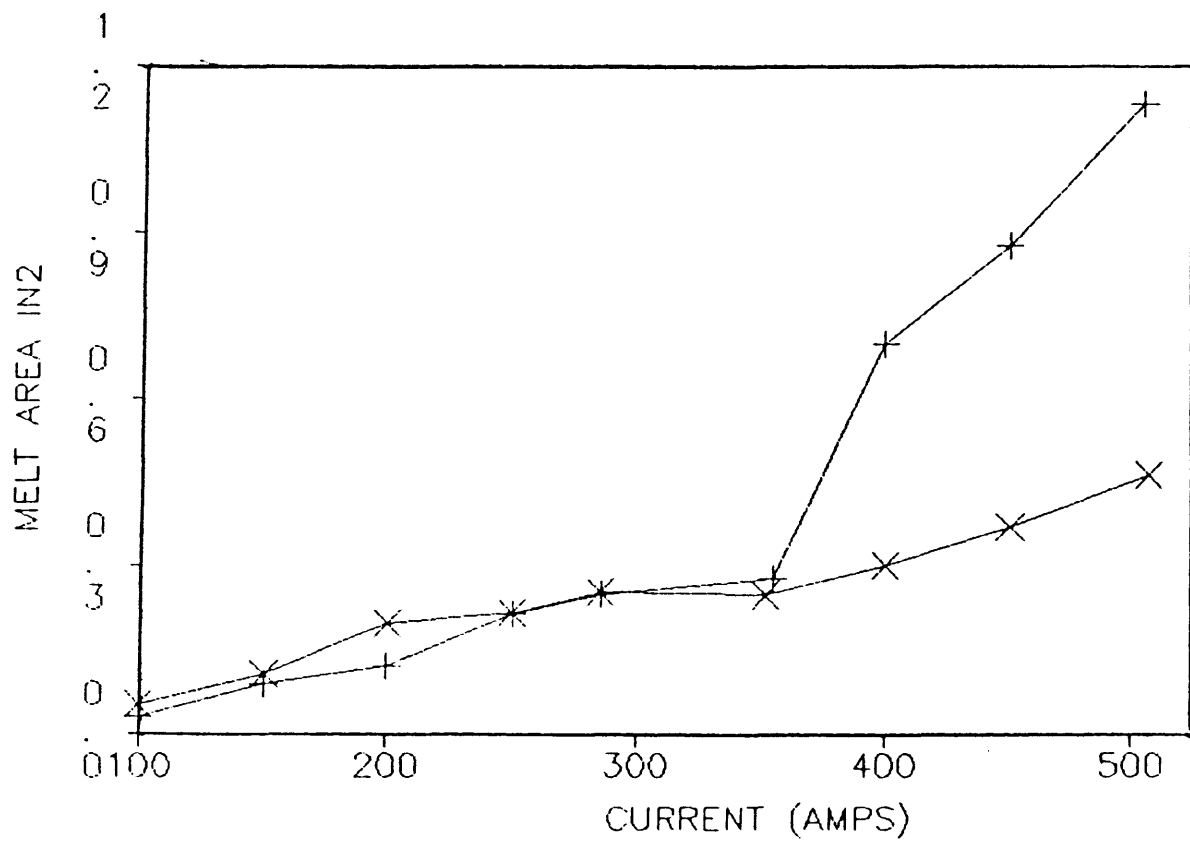


Figure A2-27 Current versus Melt Area For Constant
Travel Speed Welds 90 Degree Tip Angle
In 75ArHe

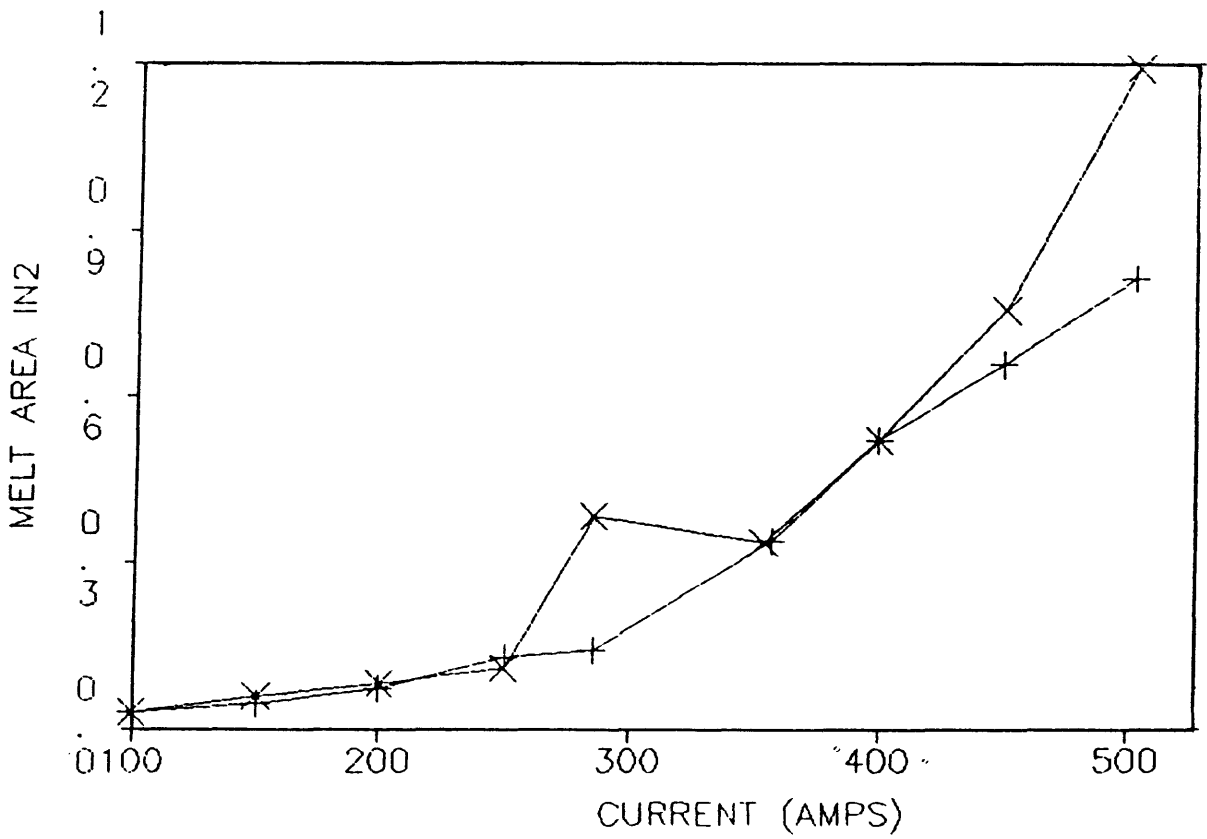


Figure A2-28 Current versus Melt Area For Constant Travel Speed Welds 90 Degree Tip Angle In 25ArHe

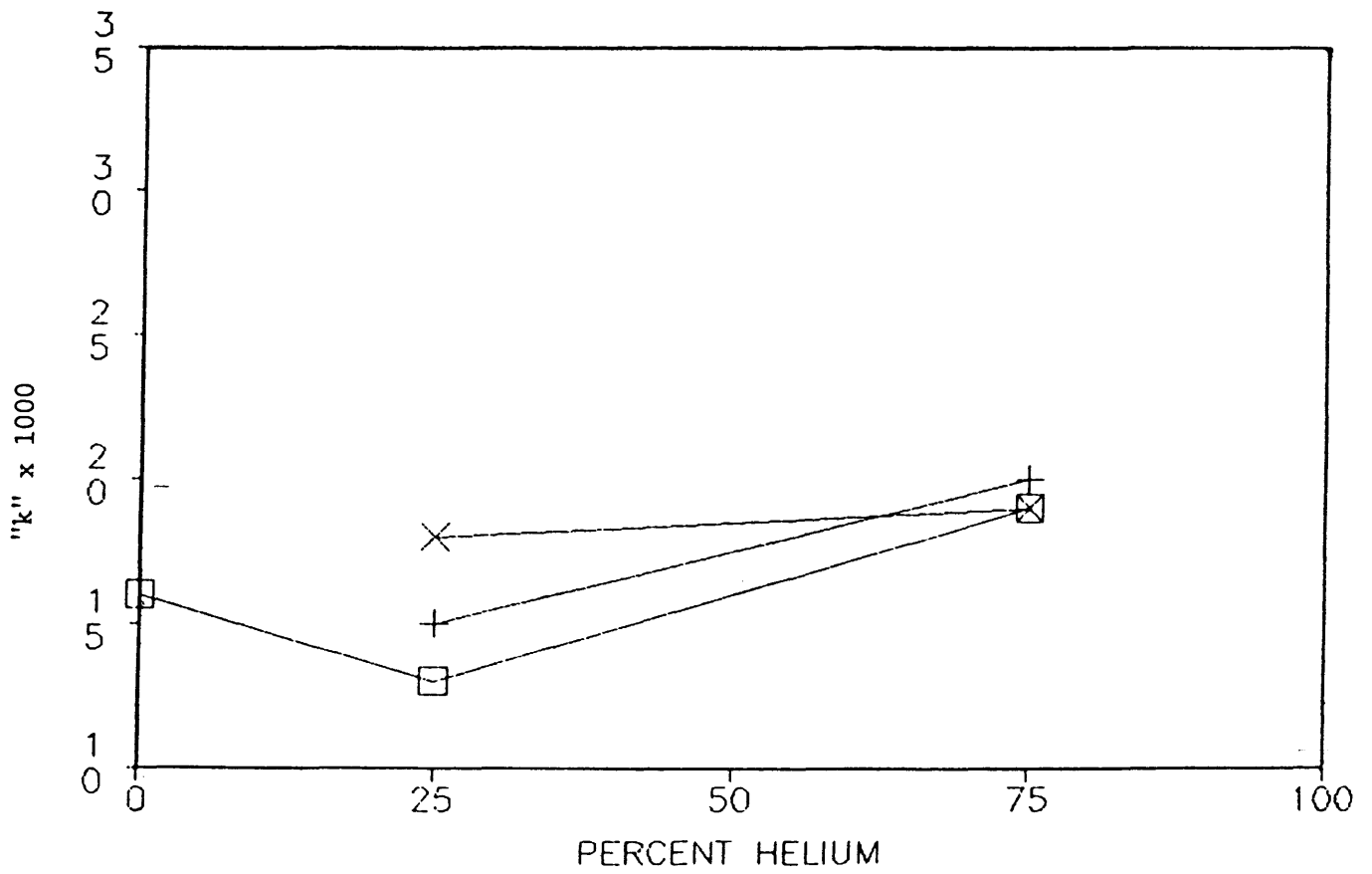


Figure A2-29 Effect of Shield Gas and Electrode Shape On "k" In Jackson and Shrubbsall Penetration Prediction Equation

Appendix III Melt Area Prediction Results

The results of plotting actual melt area versus that predicted by the Jackson and Shrubbsall equation (35) are shown in figures A3-1 and A3-2 for unshaped (180 degree) electrodes, in 75ArHe and 25ArHe respectively.

Figures A3-3 and A3-4 show the results of plotting predicted versus measured melt area, respectively for weldments using 150 degree tip electrodes in 75ArHe and 25ArHe.

Figures A3-5, A3-6, and A3-7 show the results of plotting predicted versus measured melt area, respectively for weldments using 90 degree tip electrodes in argon, 75ArHe, and 25ArHe.

Figures A3-1 thru A3-7 illustrate the validity of a melt area prediction equation in predicting melt area as a function of current, arc voltage, and travel speed. The equation was developed by Jackson and Shrubbsall (35). In general, the equation was not accurate in predicting melt area, except at lower currents (in the fluid flow control region). As can be seen in figures A3-1 through A3-7, the actual melt area is greater than that predicted by the Jackson and Shrubbsall (35) equation. This difference increases with increasing current and increasing helium content in the shield gas.

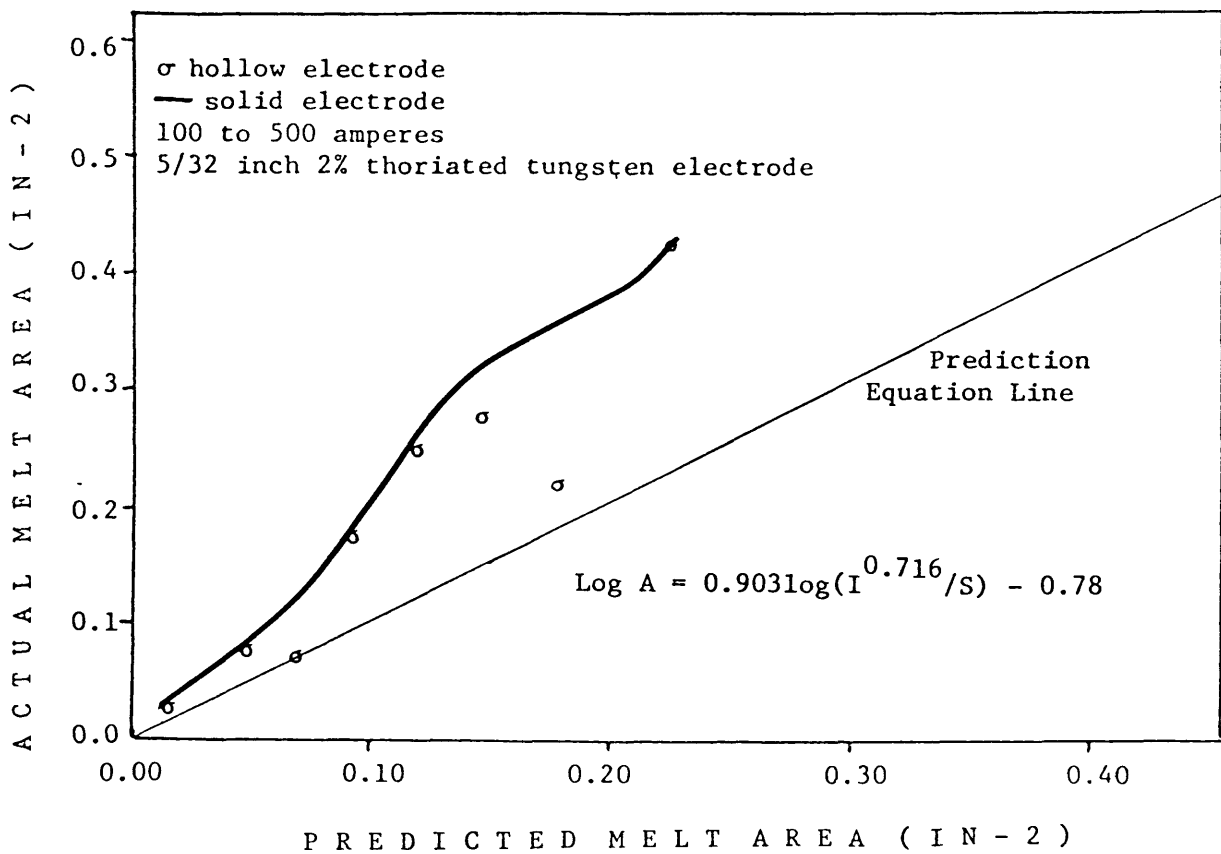


Figure A3-1 Measured versus predicted melt area for constant travel speed weldments utilizing 75ArHe with unshaped electrodes.

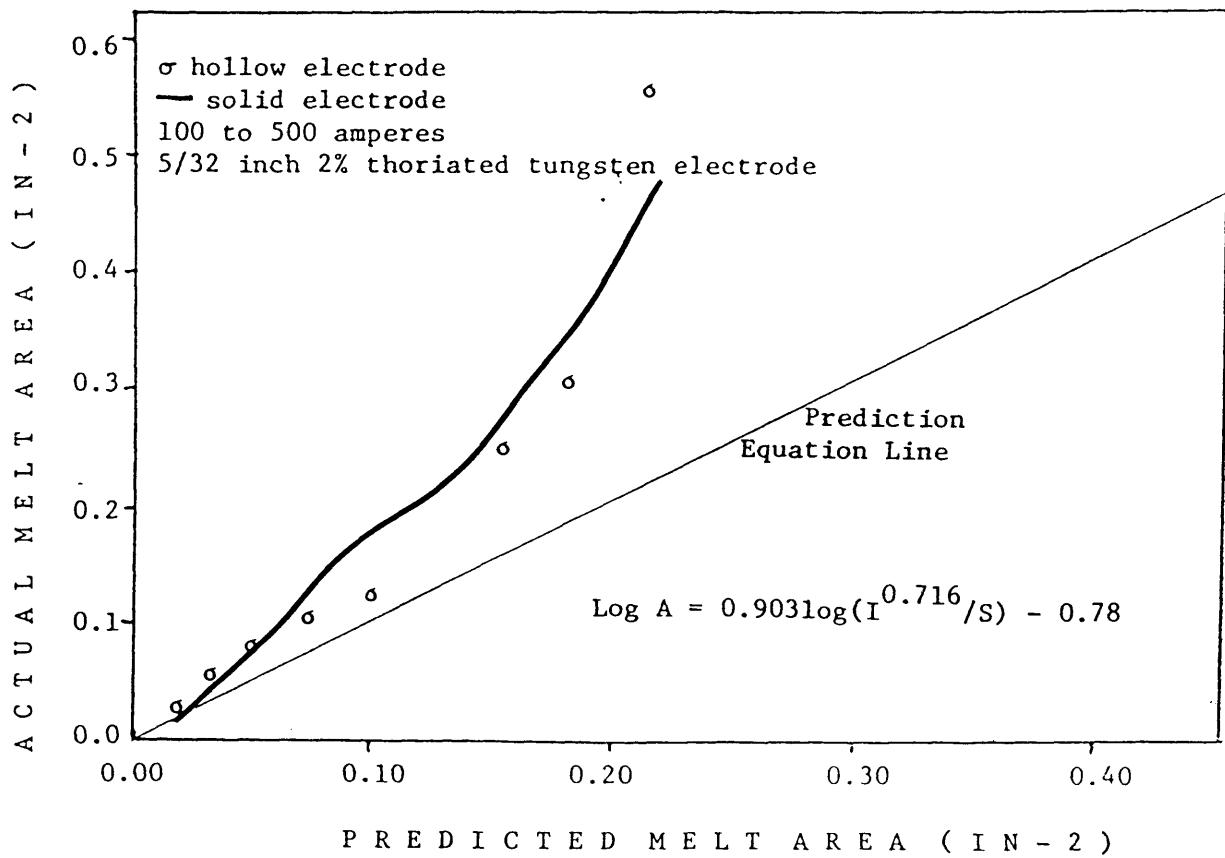


Figure A3-2 Measured versus predicted melt area for constant travel speed weldments utilizing 25ArHe with unshaped electrodes.

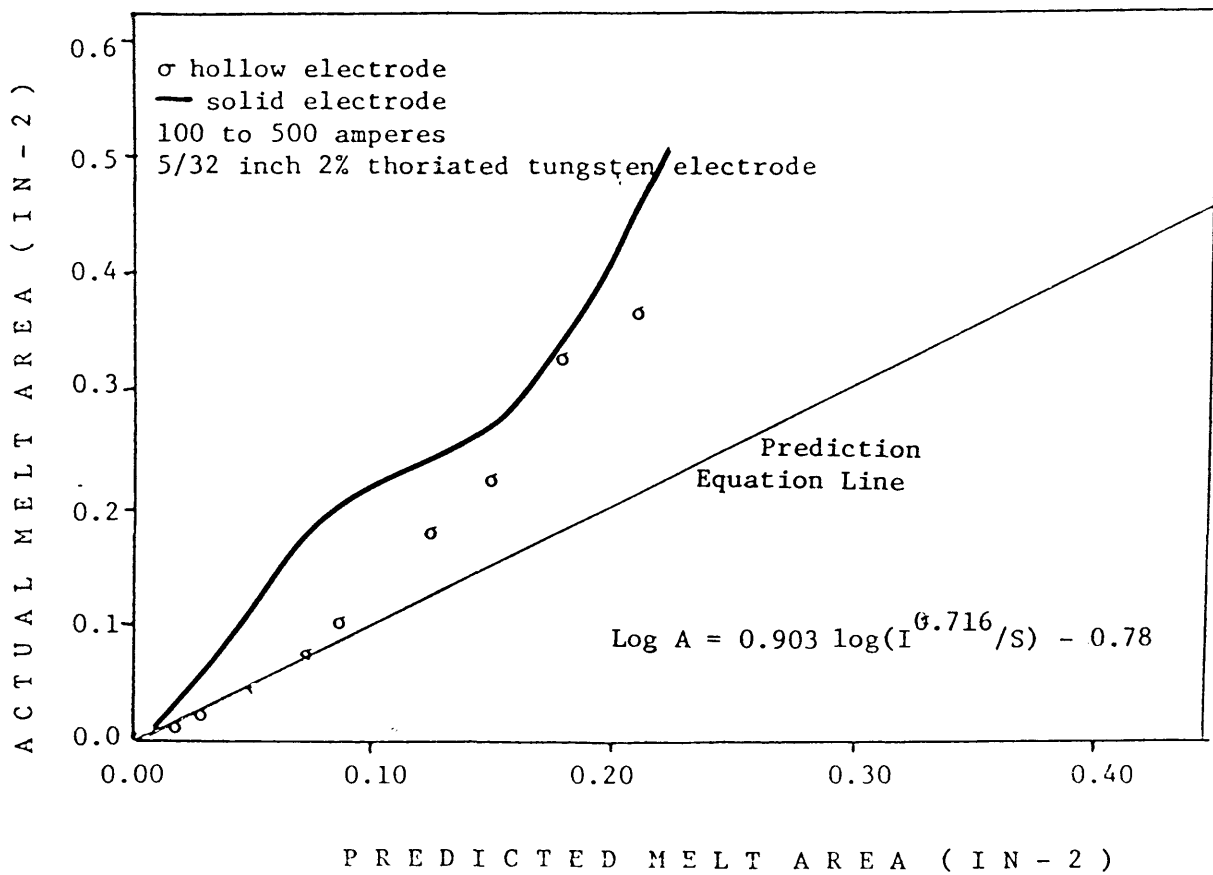


Figure A3-3 Measured versus predicted melt area for constant travel speed weldments utilizing 75ArHe with 150 degree tip electrodes.

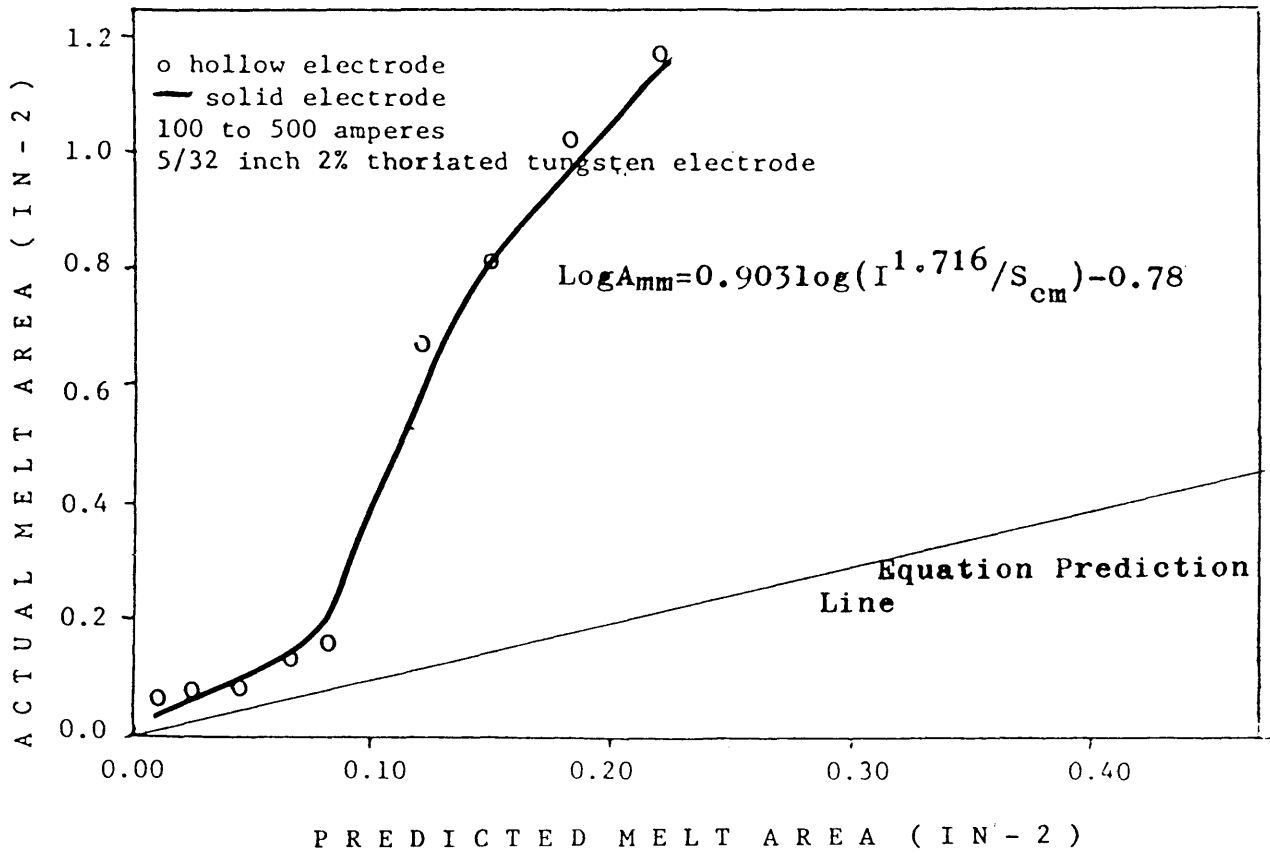


Figure A3-4 Measured versus predicted melt area for constant travel speed weldments utilizing 25ArHe with 150 degree tip electrodes.

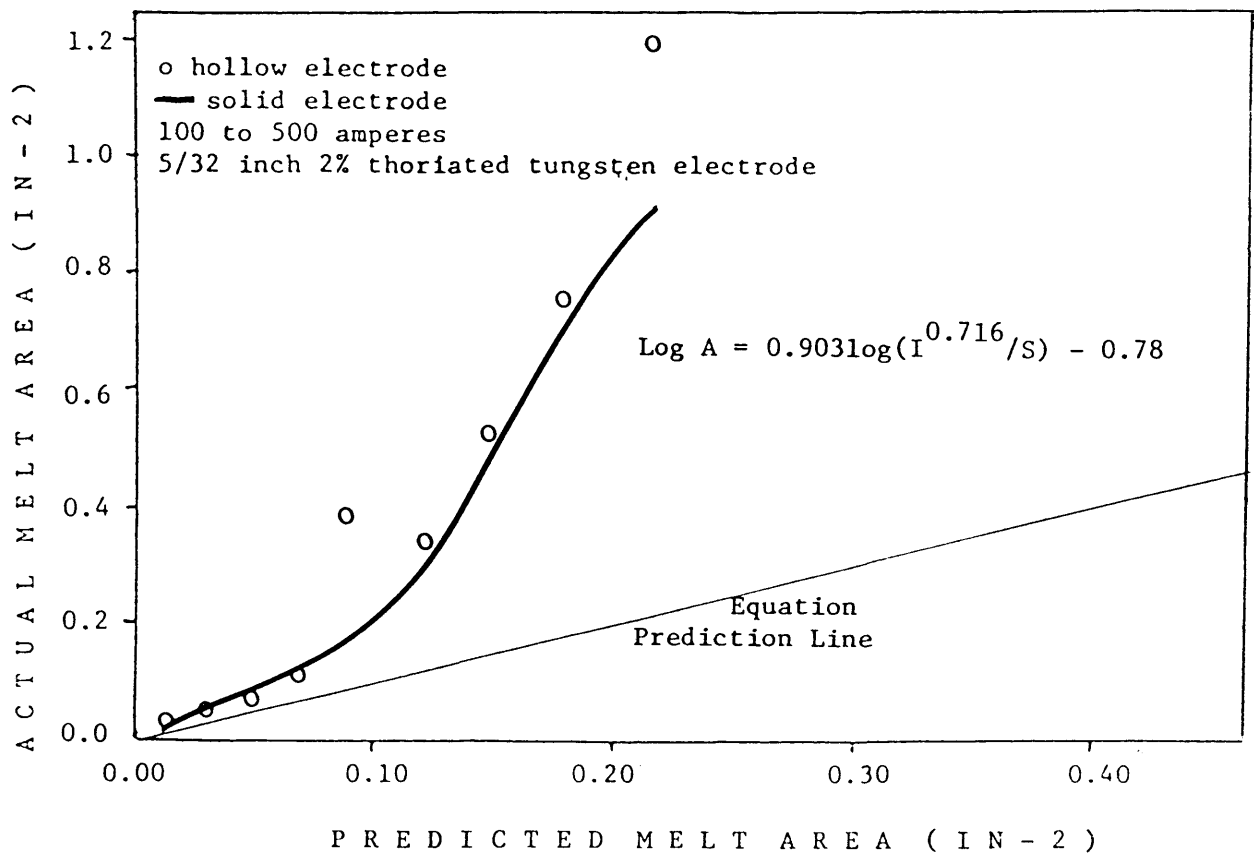


Figure A3-5 Measured versus predicted melt area for constant travel speed weldments utilizing argon with 90 degree tip electrodes.

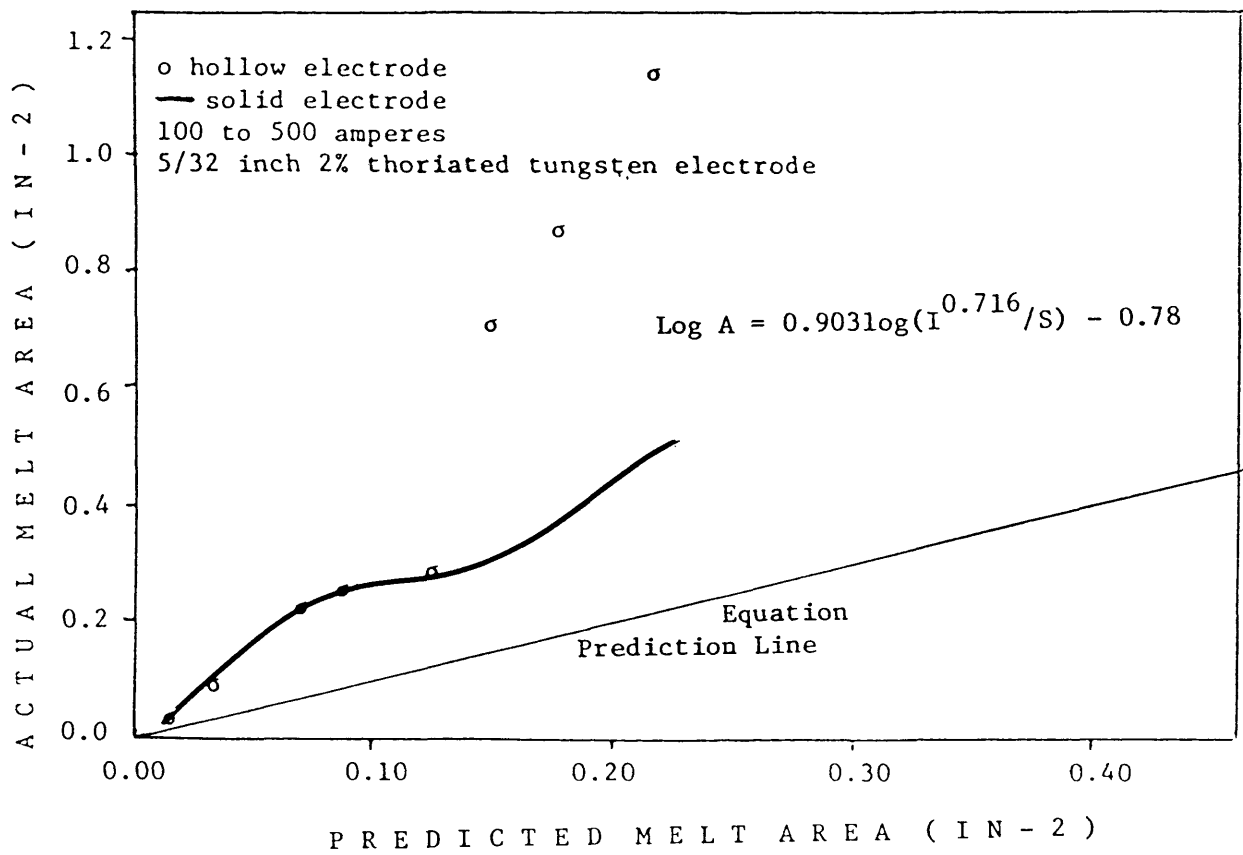


Figure A3-6 Measured versus predicted melt area for constant travel speed weldments utilizing 75ArHe with 90 degree tip electrodes.

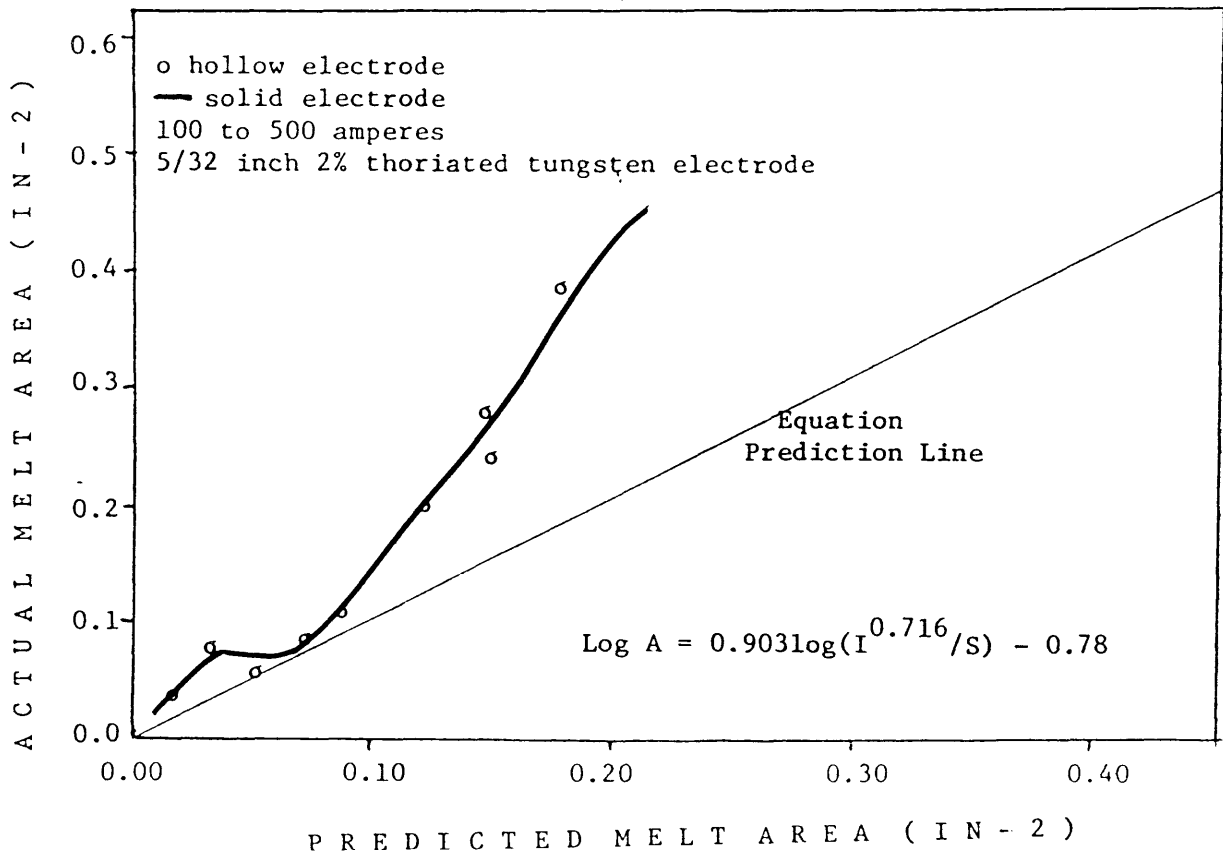


Figure A3-7 Measured versus predicted melt area for constant travel speed weldments utilizing 25ArHe with 90 degree tip electrodes.

Appendix IV Arc Stability Measurements for Constant
Travel Speed Weldments

<u>SAM- PLE</u>	<u>CURRENT AMPERES</u>	<u>POTENTIAL VOLTS</u>	<u>SHIELD GAS</u>	<u>ELECTRODE TYPE</u>	<u>ELECT ANGLE</u>	<u>DELTA I AMPERES</u>	<u>DELTA V VOLTS</u>
6	350	13.6	ARGON	SOLID	90		2.9
39	397	14.0	ARGON	SOLID	90		3.5
6	449	16.3	ARGON	SOLID	90		2.0
39	501	17.2	ARGON	SOLID	90	3.0	1.5
6	352	13.3	ARGON	HOLLOW	90		2.5
39	399	14.0	ARGON	HOLLOW	90		2.0
6	450	15.7	ARGON	HOLLOW	90		2.0
39	502	15.8	ARGON	HOLLOW	90	2.5	1.1
13	358	13.3	75ArHe	SOLID	150		2.8
16	403	14.6	75ArHe	SOLID	150		2.6
19	455	14.9	75ArHe	SOLID	150		2.6
22	507	14.8	75ArHe	SOLID	150	3.0	1.9
13	360	14.2	75ArHe	HOLLOW	150		2.6
16	400	14.5	75ArHe	HOLLOW	150		1.9
19	450	15.3	75ArHe	HOLLOW	150		2.0
22	503	16.6	75ArHe	HOLLOW	150	2.7	3.8
29	358	13.3	75ArHe	SOLID	90		2.7
44	403	14.6	75ArHe	SOLID	90		3.1
75	455	14.9	75ArHe	SOLID	90		2.7
8	507	14.8	75ArHe	SOLID	90	3.5	1.9
29	352	13.4	75ArHe	HOLLOW	90		2.7
44	400	14.0	75ArHe	HOLLOW	90		2.4
75	450	15.5	75ArHe	HOLLOW	90		3.7
8	506	16.5	75ArHe	HOLLOW	90	5.0	2.4
13	353	17.2	25ArHe	SOLID	150		2.8
16	400	16.3	25ArHe	SOLID	150		2.0
19	451	16.4	25ArHe	SOLID	150		1.4
22	506	16.2	25ArHe	SOLID	150	2.0	1.7
13	355	15.2	25ArHe	HOLLOW	150		1.0
16	402	16.6	25ArHe	HOLLOW	150		0.7
19	452	16.7	25ArHe	HOLLOW	150		1.4
22	505	18.2	25ArHe	HOLLOW	150	3.0	1.5
29	353	14.9	25ArHe	SOLID	90		2.5
44	399	16.1	25ArHe	SOLID	90		1.9
75	450	16.0	25ArHe	SOLID	90		2.1
8	503	15.9	25ArHe	SOLID	90	3.0	1.6
29	356	15.2	25ArHe	HOLLOW	90		2.1
44	399	16.2	25ArHe	HOLLOW	90		1.6
75	449	16.0	25ArHe	HOLLOW	90		3.0
8	502	16.0	25ArHe	HOLLOW	90	3.0	1.7